Assessment Procedures for Structural Wrought Iron

A thesis submitted to The University of Manchester for the degree of PhD

in the Faculty of Engineering and Physical Sciences

2013

Matthew O'Sullivan

School of Mechanical, Aerospace and Civil Engineering

CONTENTS

Word count for thesis: 58143

List of Tables

List of Figures

Abstract

The main objective of this research project was to develop a new methodology for the assessment of wrought iron structures using a more informed knowledge of the material.

A database of tensile test data for wrought iron across the range of all types of structural elements was compiled and analysed to establish the characteristic yield strength for comparison with the value of 220N/mm^2 quoted by the UK Highway Standard BD21. It was found that the characteristic yield strength of bar iron is 151N/mm^2 and that of plate iron is 187N/mm^2.

Bending tests of wrought iron beams were conducted to investigate the potential for brittle fracture under static loads, which was observed, and further investigated by conducting Charpy impact tests, where it was found the that ductile to brittle transition temperature of the metal lies in the range 20 to 80^{o}C, whereas that of mild steel, is typically in the range -30 to 10 ^{o}C.

A new assessment method was proposed that incorporates a 'quality factor' and a 'component significance factor' into the definition of design yield strength. Comparative studies using the proposed method and the existing method were conducted on a trussed highway bridge, a long span iron roof to a railway station and the Clifton Suspension Bridge. The newly obtained lower values of characteristic yield strength tend to dominate the final design strength value of a component, but this may be improved by the expansion of the database. Furthermore, the inclusion of the quality and significance factors offset this effect and their inclusion was validated by proving that a safe yet not overly conservative design yield strength may be established by application of the proposed method.

Declaration

No portion of the work referred to in the thesis has been submitted in support of an application for another degree or qualification of this or any other university or other institute of learning.

Copyright Statement

Acknowledgments

I would like to thank all of those individuals who have helped me during the course of this research. In particular my supervisors Tom Swailes and Dr. Adrian Bell for their guidance and assistance throughout my research. My gratitude to the exceptionally helpful technical staff at the University of Manchester Structures Laboratory, including Paul Nedwell and Peter Hassell, for their technical advice and help. I would also like to thank Archivist Carol Morgan at the Institution of Civil Engineers who was very gracious in providing access to the Institution's archives.

Chapter 1 Introduction

1.1 Background to project and layout of report

Wrought-iron was the dominant structural framing material from 1850 to 1890. With similar properties to early mild steel, it is more variable, creating uncertainty in the assessment of existing structures where sampling and testing opportunities are limited. The principal aim of this project is to supplement existing knowledge about the mechanical properties of wrought iron so that a better informed assessment of wrought iron structures may be undertaken. The objective is to establish an assessment methodology that may be employed when dealing with wrought iron structures. Although wrought iron has not been used to build structures since before the 20th century, knowledge of its mechanical properties is necessary because of the many wrought iron bridges and other structures still in use today.

For most of the 19th century engineering quantities such as yield stress and modulus of elasticity were not measurable. Furthermore, quality of material varied considerably. The need for better understanding of the properties of iron became ever more important as engineers and architects designed structures of greater span and complexity. This prompted the spread of material testing in many countries. A sufficient volume of both historical and modern test data on wrought iron has been collected as part of this research project to furnish a clear understanding of its structural capacity and behaviour.

The introductory chapter of this report begins with a description of the manufacture of wrought iron, because its mechanical properties depend upon how it was made. Following this is a brief discussion of the development of structural wrought iron, with particular focus on its use as a material for suspension bridges and for long span girders. The physical properties of wrought iron are then discussed in detail in the remainder of this Chapter.

In Chapter 2 the sources of historical tensile test data are discussed and the present knowledge of the mechanical properties of the metal are summarised. The issues with the current method of assessing wrought iron structures are also discussed.

Chapters 3 and 4 are concerned with the methods and results of material testing conducted as part of this research project. Chapter 3 is about the testing of wrought iron beams under static load, and Chapter 4 is about the testing of small metal samples extracted from the beams. These include tensile tests, testing of rivets in shear, Charpy impact tests, and examination by microscope.

In Chapter 5 the issues involved in assessing the quality of wrought iron using tensile test data are examined. Also, a new method of assessing wrought iron structures is proposed that is based on a detailed examination of a database of tensile test results collected as part of this research project.

In Chapters 6 to 8 the results of comparative studies using the proposed method and the existing method when applied to three different structures are presented. These structures include a trussed highway bridge (Chapter 6), Clifton Suspension Bridge (Chapter 7), and a long span iron roof to a railway station (Chapter 8).

Chapter 9 is a discussion of the proposed assessment method in relation to the case studies of Chapters 6 to 8.

Finally Chapter 10 is a presentation of the findings and conclusions of the research project.

1.2 Early production of wrought iron

Iron, the fourth most abundant element in the earth's crust is found in nature in oxide form, in the ores hematite (Fe_2O_3), magnetite (Fe_3O_4), and siderite ($FeCO_3$). (Ebbing 1996). The extraction of iron from its ore has been practiced since about 2000 BC and essentially consists of heating the ore in the presence of carbon. Iron has a strong attraction for oxygen, hence the existence of the oxide ores and the ease with which iron rusts, but carbon has an even stronger attraction for oxygen in the heat of a furnace. Therefore, in the high temperature conditions of a furnace, and in the presence of carbon, iron oxides will give up their oxygen to the carbon to form carbon monoxide and leave the iron as the free metallic element. The chemical reaction that takes place in the furnace is as follows: (Ebbing 1996)

$$\underset{\substack{\text{hematite}\\\text{(iron ore)}}}{Fe_2O_3(s)} + \underset{\substack{\text{carbon}\\\text{(charcoal)}}}{3C(s)} \rightarrow \underset{\text{iron}}{2Fe(s)} + \underset{\text{carbon monoxide}}{3CO(g)}$$

It is possible to produce wrought iron directly from the ore in a *bloomery*, which was a small scale craft furnace that contained charcoal as the fuel. Iron ore was dropped through the furnace chimney onto the hot charcoal. More charcoal was fed into the furnace as required and heat was maintained by blowing air into the furnace at its base using bellows. The heat was maintained for a few hours, after which time, a small spongy lump or *bloom* of iron and slag had formed at the base of the furnace. (Den Ouden 1981). It was this bloom which was usually only about the size of a man's fist that gave the furnace its name. These bloomeries did not generate sufficient heat to form a molten iron product. That is, the reaction was a solid state reaction, although the reactants were considerably softened during the reduction process. This was the only means of producing wrought iron prior to about the year 1400, when the blast furnace was developed. Using an air blast from water powered bellows temperatures of about 1150^{o}C could be achieved, which was sufficient to melt the reactants and produce a crude form of iron that was cast into blocks known as

pigs. To produce wrought iron these blocks of pig iron were heated with charcoal in a hearth called a *finery*. (Den Ouden 1981). A blast of air was blown over the heated blocks which remained in the solid state. The oxygen in the air reacted with the carbon in the pig iron to form carbon monoxide which burned away, thereby removing most of the carbon and leaving behind the softer and workable wrought iron. The chemical reaction is as follows (Den Ouden 1981)

$$2C(s) + O_2(g) = 2CO(g)$$

carbon monoxide

Because the objective was to produce wrought iron, but involved the production of cast iron as a first step, this method of iron production was known as the *indirect method*. (Den Ouden 1981). The wrought iron was then taken to another charcoal hearth called a *chafery* where it was reheated, but this time without the air blast. (Den Ouden 1981). It was heated to a temperature sufficient to allow it to be worked or wrought into whatever shape was desired. The finery and chafery workshop where wrought iron was produced were known as *the forge.* (Den Ouden 1981). Figure 1.1 shows a 1772 painting by Joseph Wright of Derby (1734-97) that depicts a typical scene from a blacksmiths forge where wrought iron is being worked by a tilt hammer.

Figure 1.1 *An Iron Forge*, 1772 by Joseph Wright of Derby (www.tate.org.uk accessed 2012)

1.3 Industrial production of wrought iron

The production of wrought iron prior to the 19th century depended upon the supply of charcoal for both the blast furnace and the finery. Although it is a rich source of carbon, coal could not be used in it's natural state in the blast furnace, as it contains impurities, principally, phosphorus and sulphur, which have a deleterious effect on the wrought iron produced. In 1709 Abraham Darby used coke, which is a purified form of coal, to successfully smelt iron in his blast furnace at Coalbrookdale, Shropshire, and produce a reasonably good quality cast iron. However, the iron was still unsuitable for the production of wrought iron, probably because of a high phosphorus content. (Trinder 1974). High phosphorus content results in wrought iron being brittle at normal temperatures. This condition is known as *coldshort* or *bloodshot* wrought iron. It is most likely that this is the reason why iron smelting using coke did not become popular immediately. In fact in many of the places where it was attempted it was found that they had to revert back to charcoal in order to make iron of suitable quality. (Gale 1977)

It was not until Abraham Darby's son, also called Abraham, that the production of wrought iron using coke was finally achieved. Abraham Darby II became involved in the running of the ironworks in 1728 at the age of 17. (Trinder 1974). During the late 1740's and early 1750's he experimented with the process of smelting iron until he achieved a pig iron that was suitable for making into wrought iron (Trinder 1974). It was from this time on that the use of coke for iron smelting spread rapidly.

The problem of the dependence on charcoal for smelting had been solved but charcoal was still needed to convert pig iron into wrought iron. The next major development in iron making was the invention of the *puddling process* by Henry Cort in 1784. (Gale 1977). This process effectively ended the dependence of the industry on charcoal. (Gale 1977).

In Henry Cort's puddling process coal, in its mined form, was used as the fuel in a reverberatory furnace to convert pig iron into wrought iron. The reverberatory furnace had already been in use for other purposes, but Cort was the first to successfully use it to make

wrought iron (Gale 1966). An early reverberatory furnace is shown in Figure 1.2. It consists of two regions separated by a firebridge, which is a wall that rises part way up the interior of the furnace, creating two chambers. A coal fire burns on a grate in the right hand chamber, labelled (b) in Figure 1.2. The hot gases rising from the fire are carried by chimney draught over the top of the firebridge and are deflected by the shape of the furnace roof onto the iron in the left hand chamber. It is this action of reflecting the heat and hot air that gave the furnace its name.

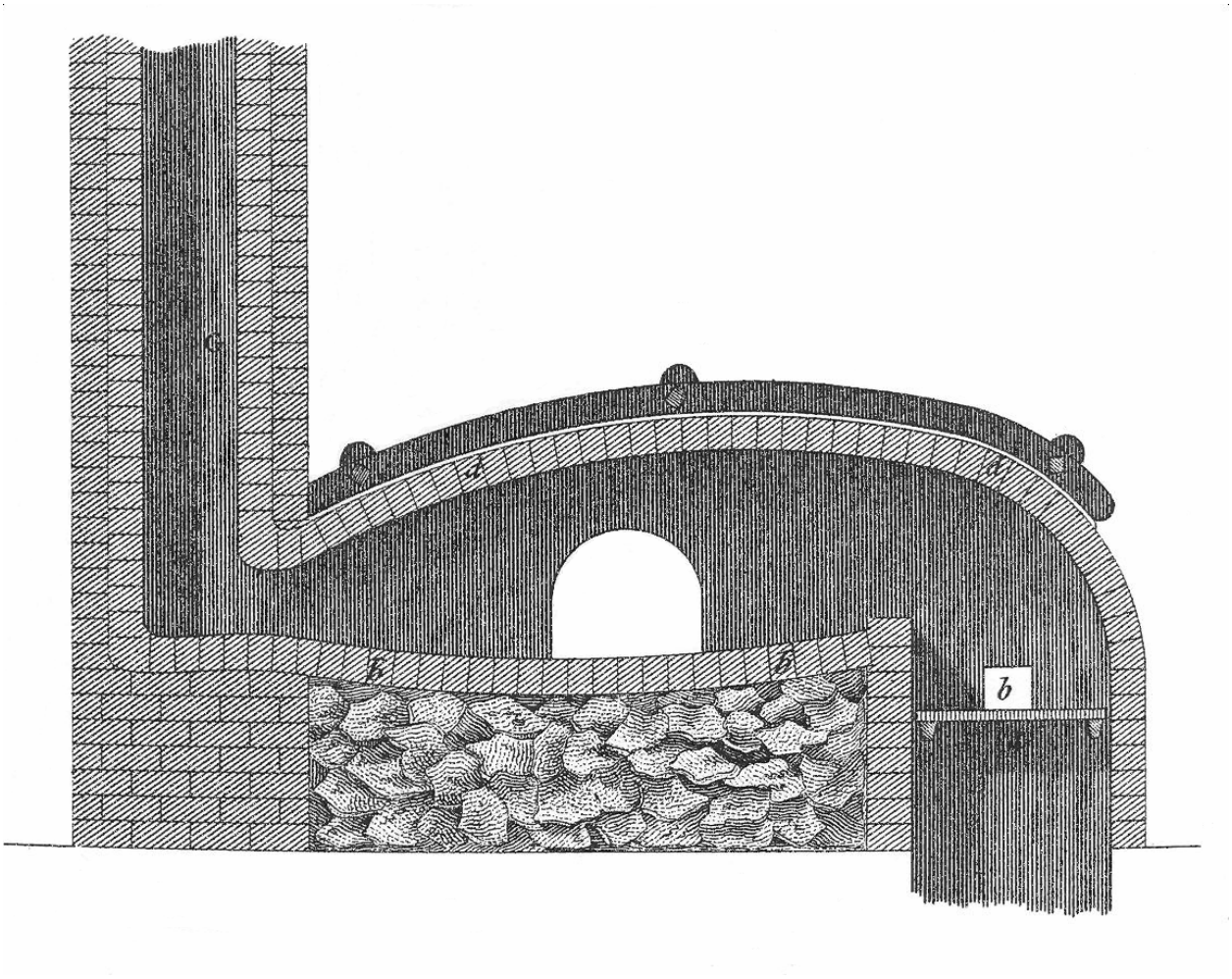

Figure 1.2 Reverberatory furnace circa 1800 (Engraving by Wilson Lowry from Longman & Rees Encyclopaedia 1811)

The heat from the hot gases and adjacent coal fire melt the pig iron. The chamber containing the iron has a concave or dished base that serves to contain the molten iron. As the hot gases, which contain oxygen, pass over the molten iron, the carbon in the iron combines with the oxygen to form carbon monoxide which burns away, and thus decarburises the iron. During this time the puddle of molten iron is stirred to expose as

much of the iron to the hot air as possible. It was this pool of molten iron which gave the process its name. The firebridge served to prevent the coal from contaminating the molten iron. As the carbon content of the molten iron reduced the melting point of the iron increased, so that the metal gradually solidified into a spongy lump that was taken from the furnace and hammered to expel much of the slag that was still present. The slag was essentially molten iron silicate. The iron itself was now almost pure ferrite. and so was quite malleable, and could be worked into whatever shape was required.

Although Cort's process was a major breakthrough, in that it dispensed with the need for charcoal, the process had one major limitation. The only source of oxygen for the decarburisation of the iron was the hot air passing over it. This was found to be unsatisfactory for ordinary grey iron. The process only worked for cast iron that was already low in carbon and silicon, namely *white iron* (Turner 1908). Thus, grey cast iron had to be refined prior to use in the puddling process. This was carried out in a furnace called a *refinery* or *running-out fire*, where the iron was melted and subjected to an air blast (Turner 1908). This oxidised some of the carbon and much of the silicon migrated into the slag, which formed in the process. (Turner 1908). The iron and slag were then run out of the fire in a molten state where the slag floated on top of the iron and was easily separated. (Gale 1969) The white cast iron that solidified was brittle and was known as *refined iron, plate metal, fine metal* or *finer's metal* and it was then ready for the puddling process. (Gale 1969)

Thus in practice, Cort's method was a two step process. The first step was the refining of grey cast iron to make white iron and the second was the puddling process itself. At any step in a refining process some portion of the desired metal is inevitably lost in the slag removed. In the refining of grey cast iron to make white iron the loss of iron was estimated to be about 10% (Turner 1908). Not only was the making of white iron wasteful of iron it

consumed fuel in the form of coke and was labour intensive. Another problem with the method was that iron oxide in the molten metal readily formed a slag with silica from the sand lining the bottom of the puddling furnace (Gale 1963). Thus the sand added to the volume of slag with a consequent loss in iron in the form of iron oxide dissolved in the slag. The loss in iron during puddling was estimated to be about 20%. (Hall 1927)

The puddling process was greatly improved when the sand lining of the bottom of the furnace was replaced with iron oxide in the form of mill scale or furnace cinder (Gale 1963). Experimentation by Joseph Hall of Tipton, in the period 1811 to 1830, led to the understanding that by the addition of substances rich in iron oxides, grey pig iron could be decarburised in the puddling furnace to produce a wrought iron of good quality and with a much higher yield of iron than with Cort's method. (Gale 1969) "Halls process used about 21 cwt. (1067 kg) of pig iron to make a ton of wrought iron, against 40 cwt. (2032 kg) with the older method" (Gale 1969). Furthermore, "while Cort's process removed mainly the silicon and carbon, Hall's method also reduced the phosphorus and sulphur content, giving a much superior material" (Hall 1927).

Because Hall's method used ordinary grey cast iron, more molten slag was present than in Cort's method.. The presence of slag imparts the property of fluidity to the molten mixture. Because of this and because of the appearance of a boiling effect during decarburisation due to a more rapid and vigorous reaction, Halls method was known a *wet puddling* to distinguish it from Cort's slower more viscous method, which took the name *dry puddling*. (Gale 1966). Hall's method which was also known as *pig boiling* was quickly adopted and remained in use right up until wrought iron was replaced by mild steel in the latter half of the 19th century (Gale 1966).

James Whitham's patented puddling furnace is shown in Figure 1.3, and is a typical example of a furnace from the Victorian period. It is of cast iron construction with interior fire brick, and consists of two chambers, just as in the earlier form of reverberatory furnace. A coal fire burns in the chamber on the left, which is most clearly shown in the plan view of the interior of the furnace, labelled *Fig 3* of Figure 1.3. In this particular furnace the iron can be worked from opposite sides by means of the suspended hook-ended bars known as *rabbles*, that penetrate a hole known as the *stopper hole*, at the bottom of the furnace doors. (Gale 1963)

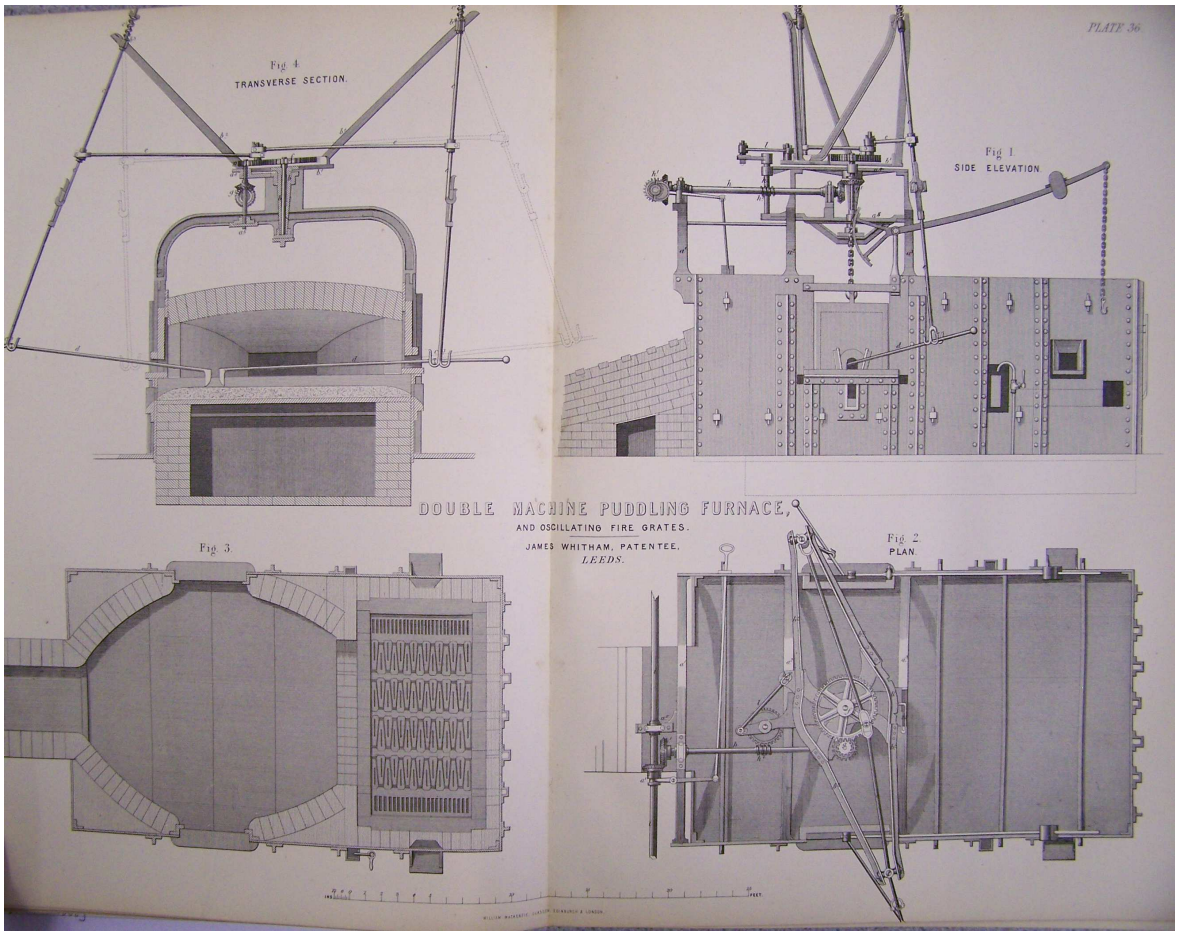

Figure 1.3 James Whitham's patented puddling furnace (Kohn circa 1868)

A cross section through the working part or bowl of the furnace is shown in *Fig 4* of Figure 1.3. When the cast iron pigs were added to the puddling furnace they melted down, which took about 30 minutes. (Gale 1963). Then the molten iron was stirred to exposed as much of it to the oxide lining as possible. (Gale 1963) The carbon monoxide produced, burned

with a blue flame, known as '*puddlers' candles'*. (Gale 1963). As the process continued the carbon content reduced and the mix became more viscous. Eventually the puddlers' candles went out, indicating that all the carbon was out of the iron, and the iron was said to have '*come to nature'*. (Gale 1963) The puddler then gathered together balls of what was now a spongy mass of iron and slag. Four of five balls each weighing about 50 kg could be obtained from one puddling charge. (Gale 1963). When the ball of iron was removed from the furnace it was necessary to hammer it quickly while it was still at welding temperature. in order to consolidate the metal and expel excess molten slag. This hammering action was known as *shingling* and was done by the *shingling hammer*. (Gale 1963).

James Nasmyth's invention of the steam hammer in 1843 replaced the helve hammer for shingling iron and greatly improved the control and capacity of the shingling hammer. It was the necessity of forging the 30in diameter paddle-shaft of the SS-Great Britain that led Nasmyth, of the Bridgewater foundry in Manchester, to develop a large capacity and powerful steam hammer. As Nasmyth put it, existing hammers were unsuitable "*simply because of their want of compass, of range and fall, as well as their want of power of blow"*, (Nasmyth 1883). Nasmyth's first hammer was of the single-acting type and was built in the early part of 1843 (Cantrell 1985). It was a manually controlled machine, where each blow was controlled by the operator. However, iron forgers at that time were used to helve hammers that would stroke continuously, that is, operate on a self acting basis. The first potential customers of the steam hammer wanted a hammer with a self-acting mechanism. (Cantrell 1985). Although Nasmyth's patent included a self acting mechanism it was not a workable design and was not included in the first Nasmyth hammer (Cantrell 1985). It was Robert Wilson, then general works manager at the Bridgewater foundry and later to become managing partner, who in April 1843 independently designed a self-acting apparatus for the steam hammer (Cantrell 1985). In the same year the steam hammer was also made double acting. The new machine could stroke continuously using its self-acting

apparatus or it could be operated on entirely manual control (Gale 1969). These features created a machine of immense usefulness, being capable of delivering blows as light or as heavy as required with exceptional control over the movement of the hammer head. In particular, the double acting mechanism meant that the operator had control over the balance of pressure on either side of the piston. This control was often demonstrated by cracking an egg using a hammer of several tons yet stopping it short of crushing the egg. (Gale 1969). According to Nasmyth "there was no want of orders when the valuable qualities of the steam hammer came to be seen and experienced", (Nasmyth 1883). The first hammer that the Bridgewater foundry supplied for sale had "a hammer block of 5 tons weight and a clear fall of 5 feet", (Nasmyth 1883).

Figure 1.4 James Nasmyth with his steam hammer in 1855. (Photograph by J.B. Dancer, obtained from Manchester Central Library 2007).

1.4 The rolling of wrought iron

The shingling hammer consolidated the iron into a rectangular block. The iron block was then taken to the first rolling mill known as the *forge train*. (Gale 1963). In the ironworks of the 19th century, the part of the works containing the puddling furnaces and hammers was known as the *forge*. (Gale 1963) The part of the works where iron was rolled was known as the *mill*. (Gale 1963) The forge and mill were generally treated as separated areas and often had different managers (Gale 1963). However, because of the need to consolidate the iron quickly the forge had one rolling mill. This first rolling mill was the forge train and consisted of a pair of cast iron rolls, one above the other, which rotated in opposite directions so that the iron block could be fed between them and deformed into a thinner and longer piece of iron. When only two rolls are present the arrangement is known as a *two-high mill*. (Gale 1977) In foundry terminology, a pair of rolls and the supporting frame and mechanism was referred to as a *train* (Scoffern 1866).

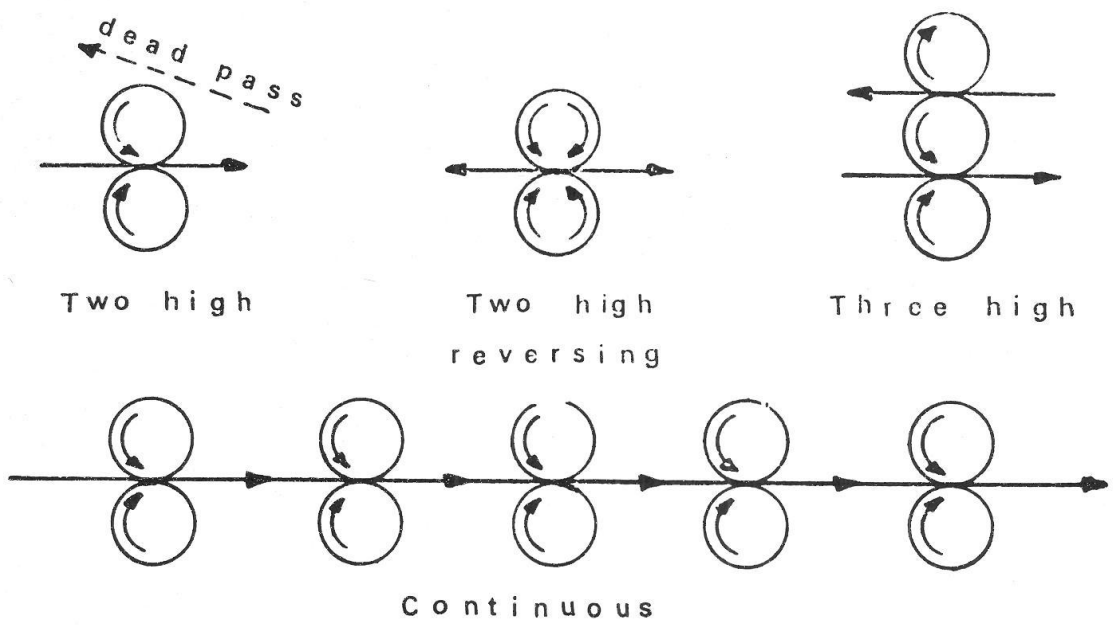

Four basic types of rolling mill are shown here diagrammatically. The earliest (two-high) dates from the sixteenth century, the two-high reversing from 1866, the three-high from about 1815 and the continuous from 1862. All four types – and modifications of them – are still in use.

Figure 1.5 Various types of rolling arrangements. (Gale 2002 but originally 1981)

1.5 (a) Operations in the forge.

The forge train was a two-high, non reversing mill and when the iron emerged from the rolls it was lifted and passed back into another pair of rolls of closer spacing. (Gale 1963). Thus the iron was reduced in thickness until it was the required size. At this stage the iron had been reduced to a flat rectangular cross section of up to about 1in x 6in and about 15ft long, and was referred to as *puddled bar*, *rough flats*, or *muck bar* (Gale 1963). Muck bar was an intermediate product in the making of wrought iron and was never sold as a finished product because it contained coarse slag inclusions and was generally of unreliable strength and quality. The muck bar was allowed to cool before being passed to the mill part of the ironworks for further working. (Gale 1963). The sequence of operations in rolling a length of wrought-iron in the forge are shown in Figures 1.6 to 1.9. The pictures were taken at the iron works at Blist's Hill Victorian Town, which is part of the Ironbridge Gorge World Heritage Site in Shropshire.

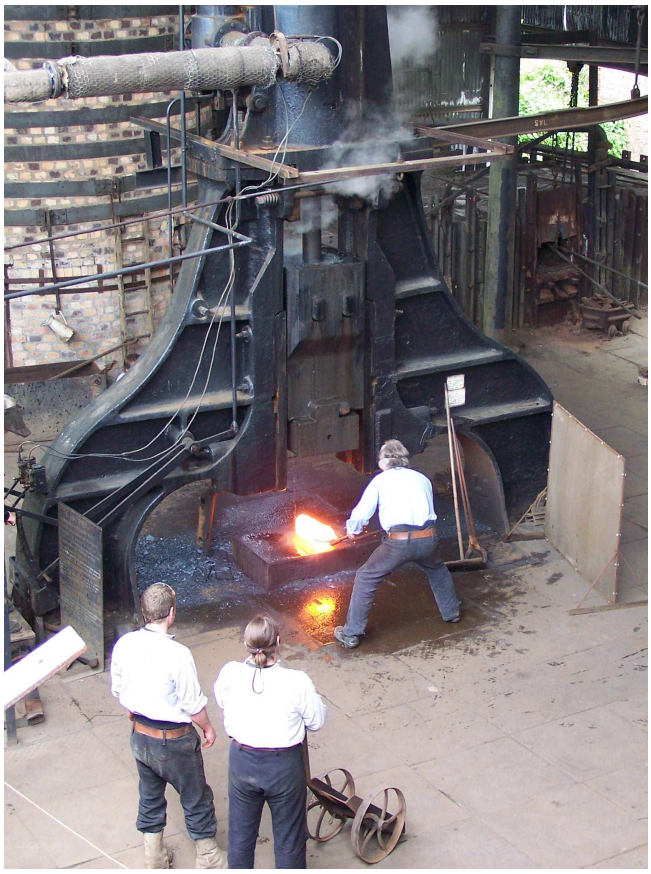

Figure 1.6 Shingling the iron billet before rolling. **Figure 1.7** Inserting the billet for the first rolling (Photos by M.O'Sullivan at iron works of Blists Hill Victorian Town, Ironbridge Gorge, Shropshire 2008)

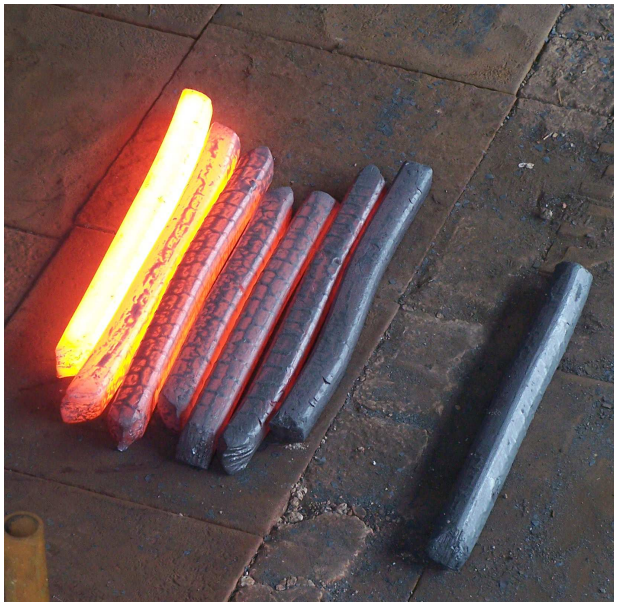

Figure 1.8 Passing the bar back (a dead pass) **Figure 1.9** The bar lengthens as it is repeatedly rolled. (Photos by M.O'Sullivan at iron works of Blists Hill Victorian Town, Ironbridge Gorge, Shropshire 2008)

1.5 (b) Operations in the mill.

The muck bar was first cut up into equal lengths by a power driven shears and was then piled as shown in Figure 1.10.

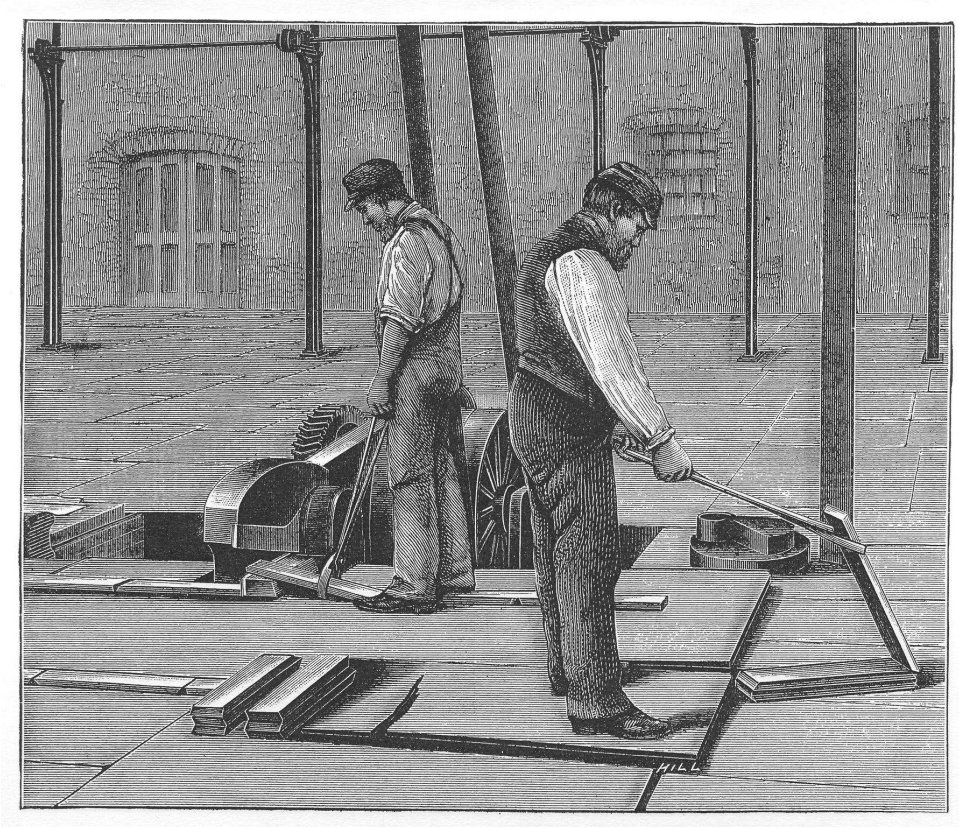

Figure 1.10 Bars being piled or stacked (The Engineer 1890)

The piled bars were then taken to the heating furnace as shown in Figure 1.11 where they were reheated to welding temperature. They were then re-rolled to form what was called "*common*", "*merchant*" or "*crown*" iron (Gale 1964).

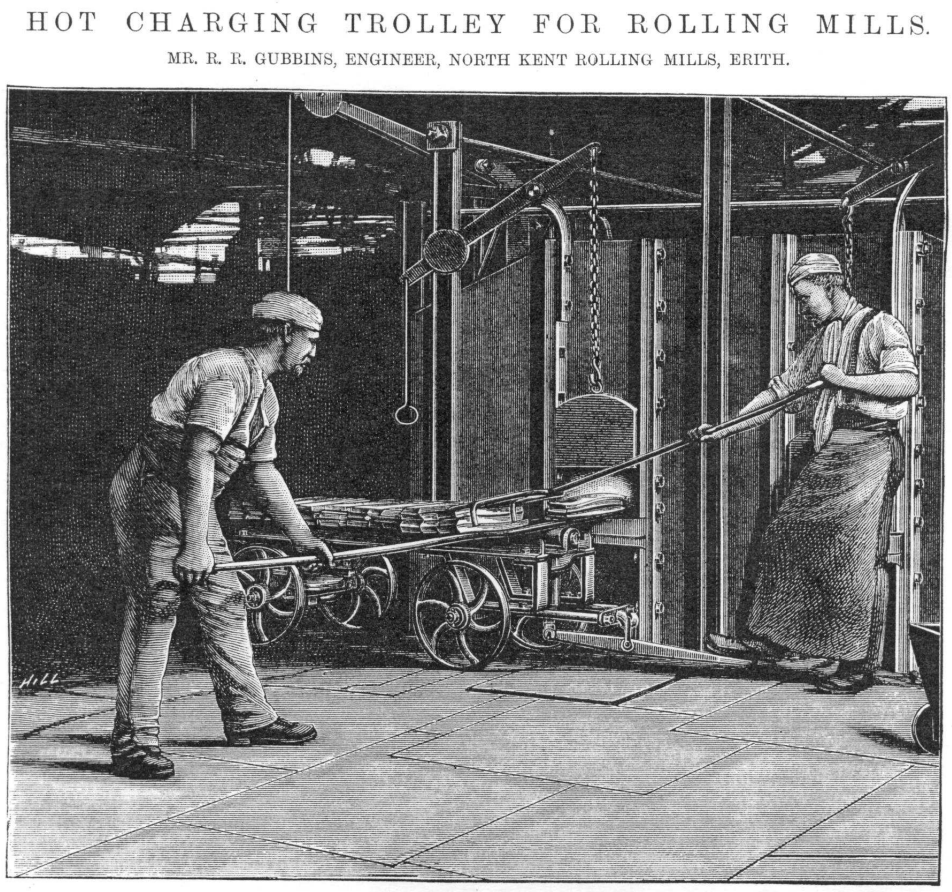

Figure 1.11 Placing piled iron into the heating furnace. Method of work practiced at the North Kent Rolling Mill, Erith (The Engineer 1890).

Merchant iron was so called because it was the grade that was mostly stocked by iron merchants (Gale 1964). Repeating the process of piling and rolling produced "Best" iron and repeating the process a further time produced "Best, Best" iron or "BB" iron. Repeating the process one more time produced "Best, Best, Best" iron or "BBB" iron which was the highest grade of iron available. (Gale 1964). Subjecting the iron to repeated workings caused the slag inclusions to be refined. The slag inclusions were made smaller, shorter and more evenly dispersed with a consequent improvement in the mechanical properties of the iron. It was shown by experiment that the benefits of repeated workings reached a peak at about the 6^{th} working (Turner 1908). However it was not economical to repeat the process beyond "BBB" grade. (Gale 1964). Some firms produced a special grade

of iron known as 'Best Yorkshire' notably the firms, Lowmoor, Farnley, Monkbridge and Taylors. Best Yorkshire iron was prized for its toughness. Its high quality was not derived from further reworking but was due to the use of refined iron (i.e. white iron) in the puddling furnace. (Gale 1964).

The rolling of wrought-iron caused elongation of the slag inclusions and resulted in greater strength in a direction parallel to the direction of rolling than perpendicular to the rolling direction. An effective means of equalising the strength in both directions was cross-piling in which the bars were piled in alternating directions as shown in Figures 1.12 and 1.13. Plate iron was made in this way, as it was important for the plate iron used in steam boilers to have equal strength in all directions.

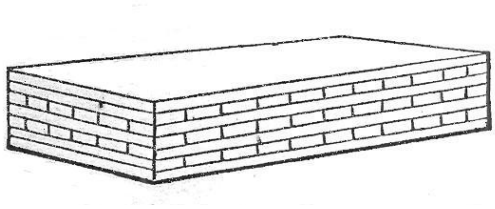

Figure 1.12 Cross-piling to form plate-iron. (Hutchinson 1879)

Figure 1.13 Cross-piling of wrought iron bars. (M.O'Sullivan 2008)

Although wrought-iron is no longer manufactured, some companies rework old iron to make new products such as railings and gates. An example is the iron works of Chris Topp in North Yorkshire whose workshop is shown in Figures 1.14 and 1.15.

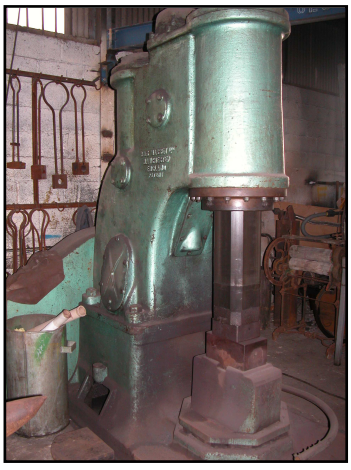

Figure 1.14 Modern forge hammer (photo by T. Swailes 2006)

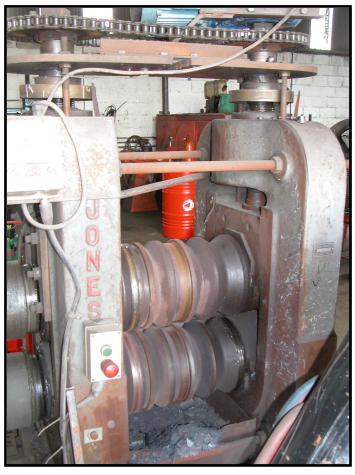

Figure 1.15 Modern two-high rolling mill (photo by T. Swailes 2006)

Having processed the iron to satisfactory quality the next step was to roll it to the desired finished shape. In the early part of the 19th century only relatively simple and small sectional forms could be rolled. The first rolled structural sections were angles and Tees. The shape of rolls needed to form a tee section is shown in Figure 1.16.

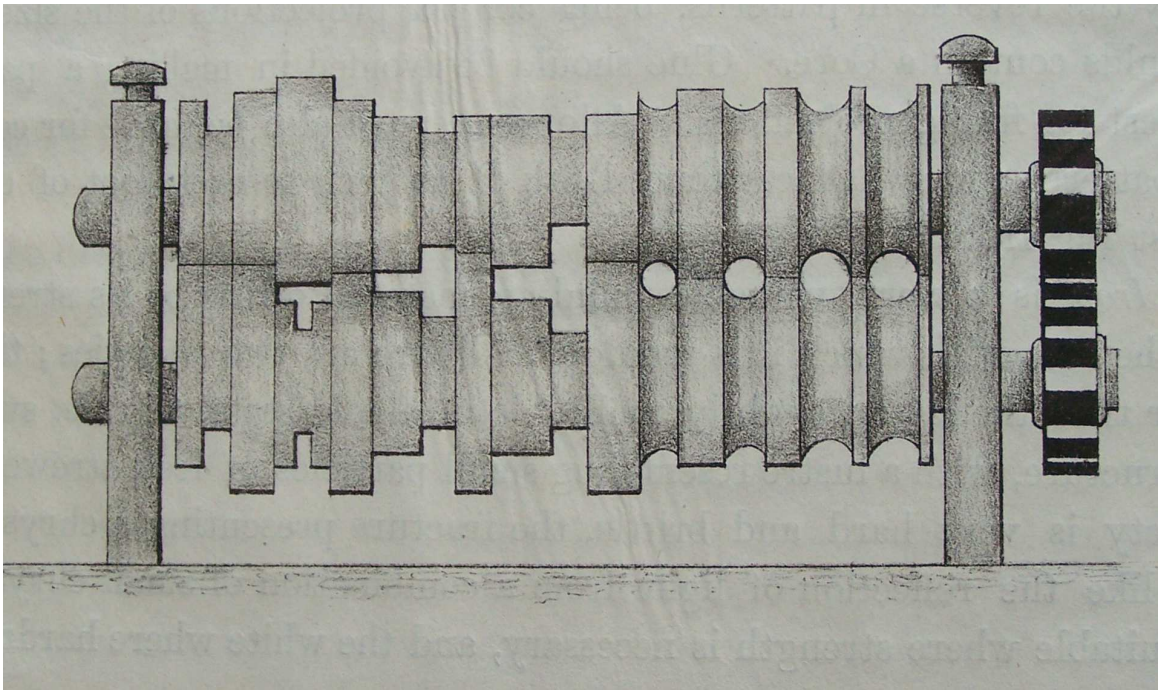

Figure 1.16 Two-high mill for rolling T-sections and round bars. (Goodwyn 1844)

Rolling of a structural section began by passing the iron through the larger aperture first, and as the shape became more accurately formed and the bar elongated, rolling progressed to the smallest aperture of final dimensions. For the rolling of large structural sections the bars had to be stacked in the form roughly resembling the desired section as shown in Figures 1.17

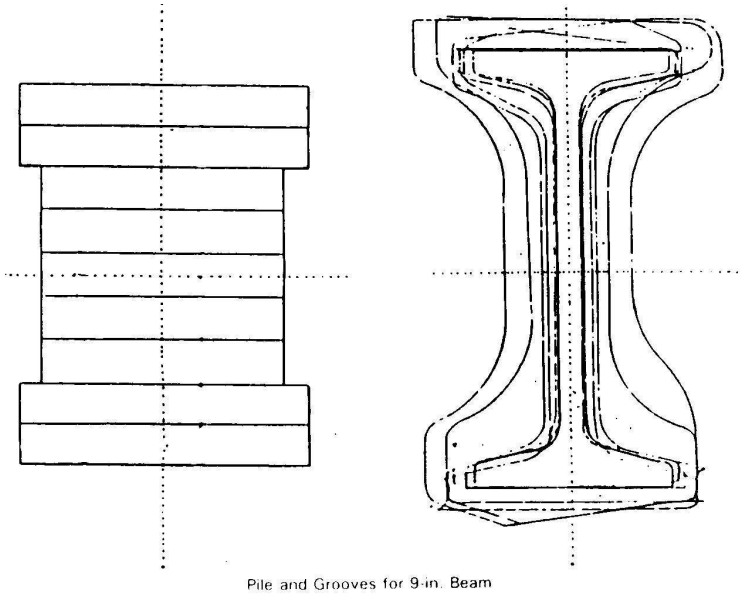

Figure 1.17 Cross sectional change occurring in hot-rolled 9 inch high wrought-iron I-beam (Elban 1998, originally Weissenborn 1861)

The cast iron I-beam was developed in the early part of the 19th century and used extensively in fireproof mill buildings. The wrought-iron I-beam however did not emerge until the 1840's. The reason for this later arrival is firstly due to the dominance of cast iron as a framing material in the early part of the nineteenth century but also due to the lack of powerful rolling mills strong enough to handle this difficult form. The first cases where wrought iron was rolled into an I shaped form were in the 1820's and 30's for use as rail track.

Then in 1844 James Kennedy and Thomas Vernon of Liverpool, patented a structural I form for use as deck beams in ships (Diestelkamp 1982). It was in 1844 that the earliest significant structural use of Kennedy and Vernon's wrought iron I form took place. This was for the construction of the Palm House in the Royal Botanic Gardens at Kew, built 1844-49 by Architect Decimus Burton and ironwork manufacturer Richard Turner. (see Figure 1.18).

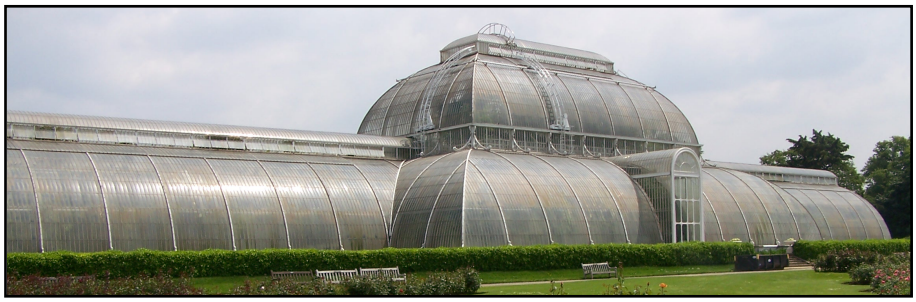

Figure 1.18
Palm House at Kew Gardens (Photo by M.O'Sullivan 2006)

The 9 inch deep cross section of one of the main ribs of the Palm House at Kew Gardens is shown in Figure 1.19. Despite the success of the I-section form in the Palm House at Kew Gardens it was several years before rolled wrought-iron I-beams were produced commercially. Developments in I-beam manufacture also took place in France and America around this time. In France the first I-beams were made in 1849 and used in the floors of a house in Paris (No. 18 Boulevard des Filles-du-Calvaire) and by the early 1850's I-beams were being made by a number of mills in various sizes (Peterson 1980).

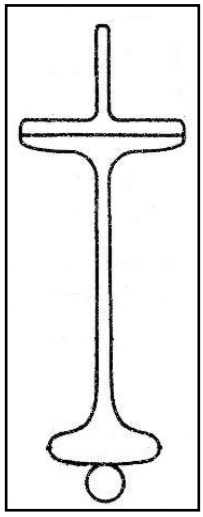

Figure 1.19 Cross section of main rib of Palm House, at Kew Gardens (Diestelkamp 1982).

A number of ways of piling wrought iron bars to achieve a rolled I section, are shown in Figure 1.20.

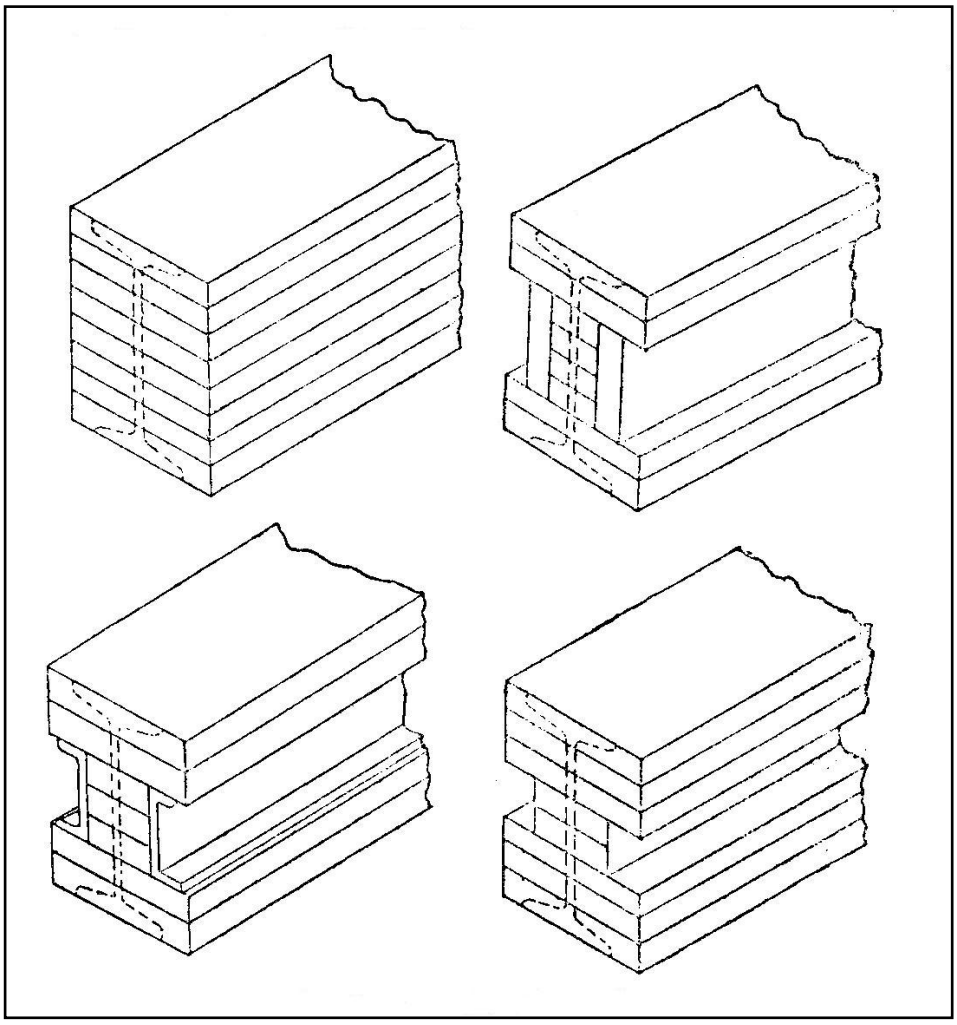

Figure 1.20 Modes of piling to achieve an I-beam. (Twelvetrees 1900)

1.6 Development of the plate and angle girder

For the first half of the 19th century the only means of spanning significant distances was through the use of a suspension bridge. Cast iron beams were limited by casting and handling techniques to spans of 60ft (Sutherland 1964). During the 1830's iron trusses were constructed with cast iron acting as compression members and wrought iron as tension members, but by the end of the 1840's trusses were built entirely of wrought iron. There was a period in the 1830's and 40's where greater distances were spanned using cast iron beams with straps of wrought iron fixed to them, to form what was called a *trussed girder*. This was an unsafe form of construction which abruptly ended with the collapse of the Dee Bridge in 1847 and the subsequent Royal Commission to Inquire into the Application of Iron to Railway Structures. It was also around this time that the great spanning capabilities of wrought iron in the form of riveted plate and angle tubes were demonstrated by the construction of the Britannia and Conway Bridges over the Menai Straits. The clear span of both of these bridges is over 400ft and both were designed by Robert Stevenson with preliminary consultation work undertaken by William Fairbairn and Eaton Hodgkinson.

Small tubular beams built up from wrought-iron plates and angles as in Figure 1.21 were in use since the early 1830’s. According to Rankine the first time this form of beam was used in a railway bridge was around 1832 for a bridge on the Pollok and Govan Railway (Rankine 1895). Smith put the date of this bridge as 1840, but said that similar beams had been in use for several years at the ironworks of William Dixon, fabricator of the bridge in question. (Smith 1992).

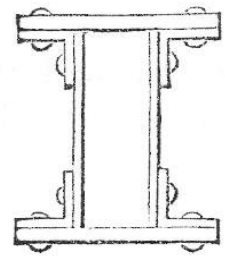

Figure 1.21 Plate iron tubular beam (Rankine 1864)

William Fairbairn, an ironwork manufacturer in Manchester was also known to have made this form of beam for use in ships in the early 1840's (Smith 1992). In 1847 he completed two wrought iron hollow girder bridges for the Blackburn & Bolton Railway. (Sutherland

1964). His involvement in the proposed bridge project for crossing the Menai Straits consisted of preliminary testing of tubular beams and the construction of one-sixth scale test models. (Smith 1992).

The Britannia Bridge was completed in 1850, and although it succeeded as a working railway bridge this type of giant tubular bridge fell out of favour within a few years due to factors such as the build-up of smoke from the steam trains that passed through the tube, corrosion from condensation, and the uneconomical use of material. (Smith 1992). The last bridge of this type was the Great Victoria Bridge in Canada completed in 1859. (Smith 1992). William Fairbairn went on to promote the use of tubular beams such as those shown in Figure 1.22. However, eventually even small tubular beams also fell out of favour because of inaccessibility for painting of the interior of the tube and because of the generally perceived excessive use of material. (Smith 1992). Tubular beams were largely a British and European style of bridge form and were never really a popular method of bridge construction in America. Pin connected truss bridges were much more popular in America. This was largely due to the competitive system of bridge construction there, and due to the established use of timber trusses which merged into iron trusses with time.

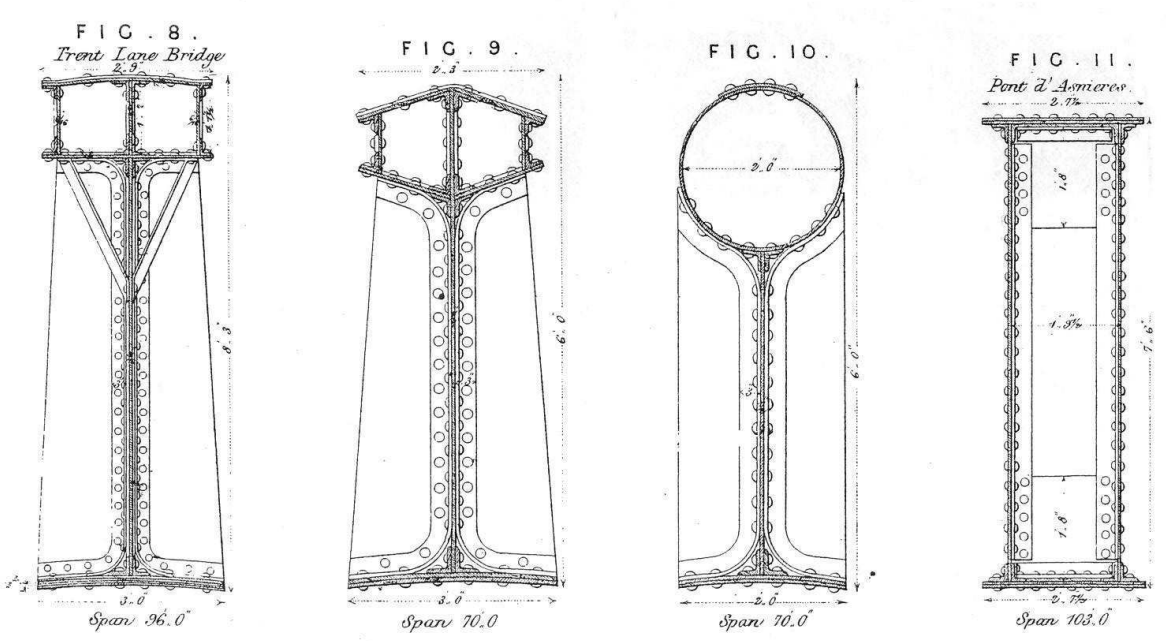

Figure 1.22 Examples of various types of plate girder (Humber 1870)

1.7 Development of suspension bridges in Britain

As it is a structural form which relies on tensile strength and ductility early suspension bridges could be possible only with wrought iron. What may be regarded as the first modern suspension bridge was built by James Finley in 1801 over Jacob's Creek in Pennsylvania. It had a span of 70 ft and width of 12.5 ft. and is shown in Figure 1.23. (Kemp 1979).

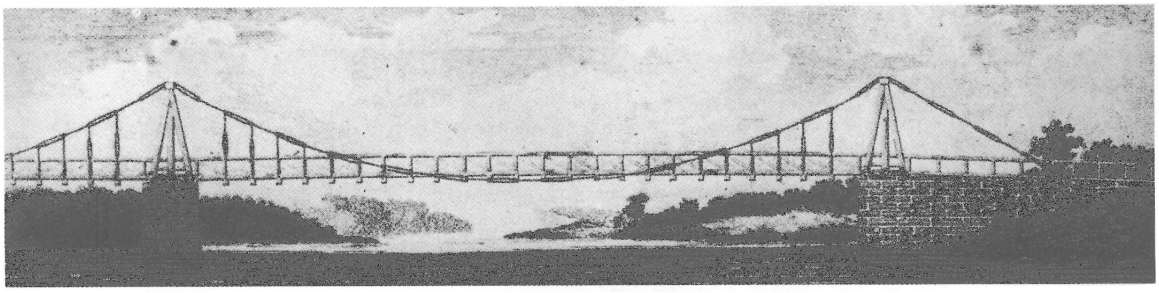

Figure 1.23 Jacob's Creek Bridge, Pennsylvania, 1801, from James Finley's paper of 1810. (Kemp 1979)

In Britain two of the main engineers involved in early 19th century suspension bridge development were Captain Samuel Brown and Thomas Telford. Their work led to a number of British suspension bridges including Union bridge (1820) and Menai Bridge (1826). Union bridge was the first of Samuel Brown's and was built in 1820 over the river Tweed near Berwick-upon-Tweed. It is the worlds oldest suspension bridge that still carries public road traffic, although now only one car at a time. (Miller 2006). At the time of its construction it was the first suspension bridge in Britain built to carry loaded carriages and with a deck length of 367 ft. it was also the world's longest suspension bridge (Miller 2006).

Figure 1.24
Union Bridge (Photo from bbc.co.uk accessed July 2012)

During his time in the navy, Samuel Brown had successfully demonstrated the use of iron chains as a replacement for the hemp ropes used for the anchor cables of ships. From the very beginning of his iron chain developments Brown had engaged in experiments on the strength of wrought-iron. As early as 1808 Brown had carried out strength tests on iron bolts, bars and chains and in 1816 he installed a testing machine of his own design at his Millwall works (Jones 1981). The significance of Browns influence on suspension bridge development is his use of linked straight bars instead of looped chain links for the main chains of a suspension bridge. Brown's bar-chains with coupling links are shown in Figure 1.25, with a close up of the coupling link of Union bridge in Figure 1.26. "Although not unique, Brown's preference for straight eye-bar links did not follow the generally established practice of using ordinary chains or even specially long-linked chains as the main suspension cables" (Day 1983)

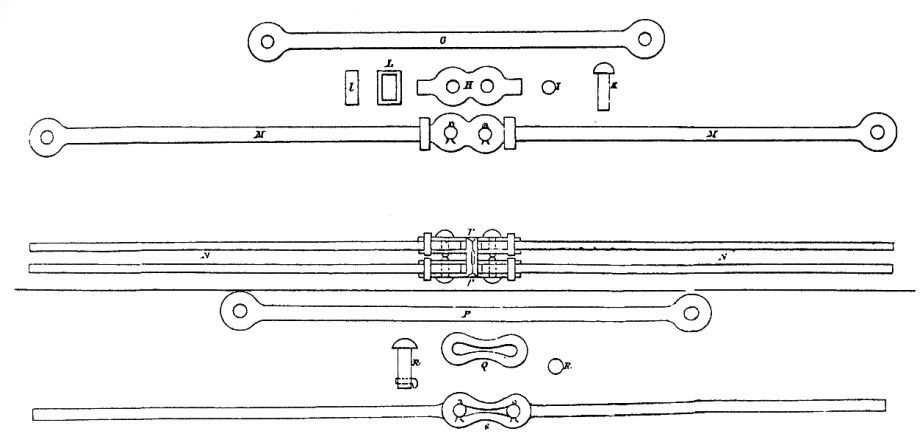

Figure 1.25 Samuel Brown's bar-chains and coupling links (Day 1983)

Figure 1.26
Coupling link in suspension chain of Union Bridge (Photo from bbc.co.uk accessed July 2012)

In 1814 it was proposed that a bridge be constructed across the Mersey at Runcorn Gap, as part of a road scheme linking Liverpool and London. (Paxton 1978). This bridge was never built, due to lack of funds, but the scheme is important in the development of suspension bridges in Britain, as it led Thomas Telford to submit a suspension bridge design based on investigations on the strength of wrought iron and on the means of constructing such a bridge. In 1814 Telford conducted over 200 tests on wrought iron bars which led to his adoption, at that time, of a design strength of 15 tons/in^2 (232 N/mm^2) for "stretching limit" and 27 tons/in^2 (417 N/mm^2) for "breaking limit". (Paxton 1978). "Telford's investigations into chain strength confirmed that the small link chain was not the most appropriate for application to the suspension principle. For this purpose he required that the metal should be kept as far as practicable in straight lines and also have few joinings". (Paxton 1978).

In 1817 Telford was asked to report on the practicality of constructing a suspension bridge across the Menai Strait. "The suggestion of a suspension bridge probably resulted from the publication of Telford's Runcorn Bridge reports in 1817." (Paxton 1978) Telford's Menai Suspension Bridge was built in the period 1818 - 1826 and spanned 570ft. Its construction was considerably more substantial than Brown's Union Bridge, with the main chains consisting of rectangular cross section eyebars interleaved with each other. The original iron chains of Menai Bridge were replaced with steel chains in 1938-41. As engineers developed greater confidence in using wrought iron, and in the suspension bridge principle, greater spans were attempted. Only a few years after the completion of the Menai bridge, the construction of Clifton Suspension Bridge was commenced, the details of which are described in Chapter 7.

1.8 19th Century engineers understanding of the strength of wrought iron

The 19th century was a very experimental time for the iron and steel making industry, and in the latter half of the 19th century particularly, metallurgy became more scientific.

However, for wrought iron, which was used on a large scale as a structural material only since the 1840's, there was a high degree of variability in quality between the various iron manufacturers. Iron makers did not work to a universal national standard of quality such as the modern day British Standard or Eurocode. In fact the first attempt at a national standard on the subject was in 1906 and referred to the quality of structural steel (Bussell 1997). By this time iron had been replaced by mild steel for structural purposes and so it was never subjected to a national quality standard.

Yet the absence of a national standard of quality for wrought iron did not mean that there was no system of quality control. As discussed in section 2.1 of this report there was a system in use in the 19th century which graded iron on its quality and was based on a number of qualitative foundry tests and on the number of times the iron was processed. But in general quality of iron was dependent on the individual manufacturing firm and on this basis a firm's reputation could be made or lost. In addition, many engineers required that the iron and sometimes the finished structural component, such as an eye-bar, was subjected to tensile tests prior to use.

For the proposed suspension bridge across the Mersey at Runcorn in 1814 Thomas Telford specified a maximum working stress of 4 ton/in^2 (62 N/mm^2) and for his Menai Suspension Bridge of 1826 he specified a value of 5.25 ton/in^2 (81 N/mm^2), (Day 1983). However, Samuel Brown adopted the less conservative value of 10 ton/in^2 (155 N/mm^2) as a standard value for the bar chains of his suspension bridges (Day 1983)

By the 1860's the Board of Trade in Britain imposed a value of 5 ton/in^2 (77 N/mm^2) as the maximum design stress for members in railway bridges. This value applied equally to situations of tensile and compressive stress as it was used for the designing of both the top and bottom chords of wrought-iron girders (Colburn 1863). French engineers worked to a

value of 3.8 ton/in^2 (59N/mm^2) as the maximum design stress for members in railway bridges, (The Engineer 1863).

For many years prior to the 1860's the yielding of a sample of iron under a sufficiently large stress was observed, but it was in assigning a value for the working stress sufficiently low to avoid a permanent set of the metal that was the greatest problem. Regarding the "*question of safe working strength much difference of opinion exists among engineers, the permanent supporting power of iron being variously estimated at from four-tenths down to one -tenth of its breaking strength*" (Colburn 1863)

In 1862 David Kirkaldy presented the results of his extensive series of tests which he had conducted at the Napier Works 1858-61 on iron and steel. Kirkaldy had only measured ultimate strength and ductility. In a discussion of the results W.J.M. Rankine proposed that the best measure of strength was the stress at which elongation of the specimen was no longer proportional to the applied load as seen on a graph of load versus elongation.

"*He thought that the point where the change in the curve of elongation occurred was that at which the strength of the material had been overcome",* (Rankine 1863). And further stated that: "*If they could only make experiments so precisely as to measure the area of the bar at the instant of that change, and compare it with the load, and take the corresponding load per square inch, they would get at the true strength of the material*." (Rankine 1863)

This appears to be one of the first instances of a change in opinion in the established method of using ultimate strength as the design reference quantity. Within a few years sufficiently accurate strain measuring devices were invented that made measurements of elastic limit possible. During the 1860's and 70's materials testing became more routine as various laboratories were set up throughout Europe and America. David Kirkaldy set up the first independent testing laboratory in Britain in 1865.

1.9 Composition and texture of wrought iron

The classification of ferrous metals is principally based on their carbon content and in this respect wrought iron can be considered as almost pure iron, as its carbon content is generally less than 0.2%. An examination of the iron-carbon phase diagram (Figure 1.27) will show that iron exists as ferrite (or α iron) with a BCC crystal structure and is placed on the left-hand side of the diagram. The low carbon content means that wrought iron is ductile, and malleable when red hot, in fact, in some of the older literature wrought iron is sometimes referred to as *malleable iron*. Cast iron which is hard and relatively brittle due to its higher carbon content of about 5%, would be placed toward the right-hand side of the iron-carbon phase diagram. Steel has carbon content in the range 0.2-1.0% which is not very different from wrought iron, yet the microstructure and texture of wrought iron and steel are quite different, and this results in distinctly different material properties.

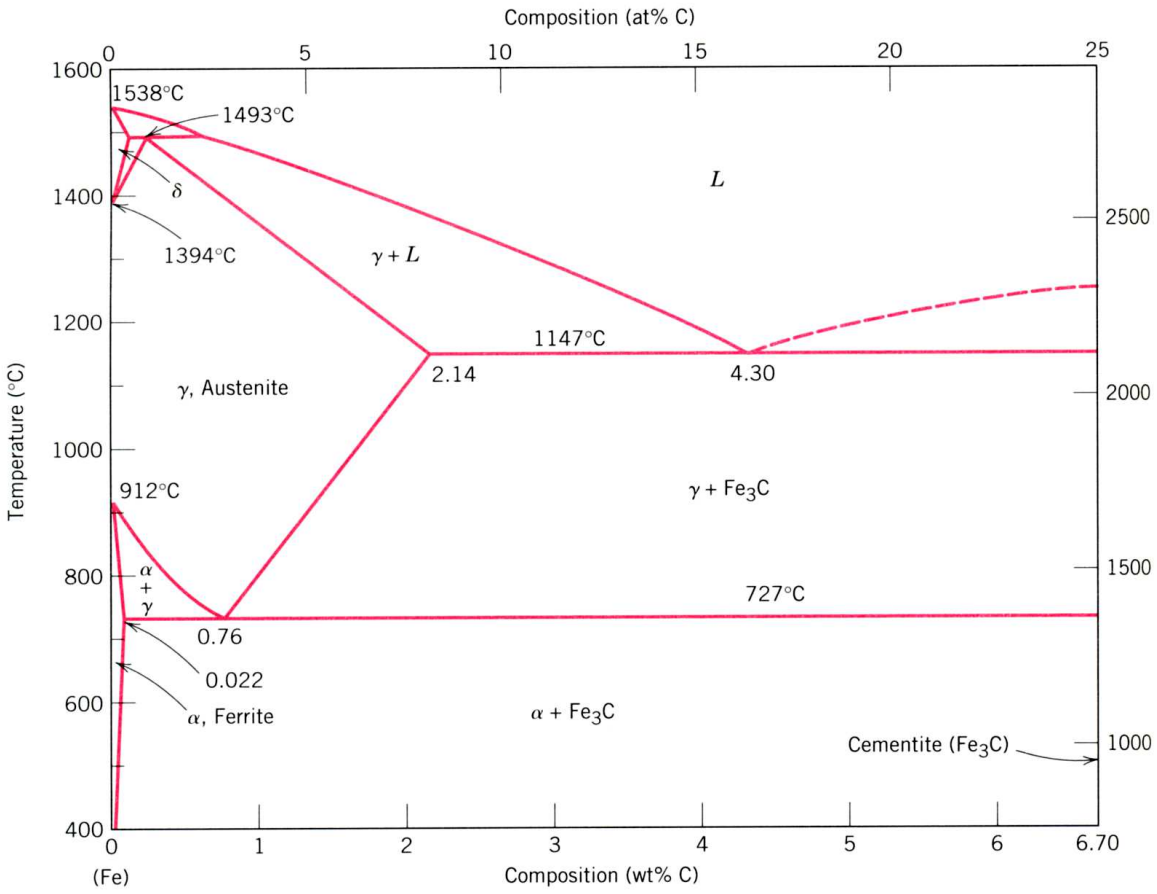

Figure 1.27 Iron-carbon phase diagram (Callister 2000)

In addition to carbon, some of the other elements present in wrought iron are silicon, phosphorus, copper, sulphur and manganese. An excessive sulphur content renders the wrought iron *red short*, a condition in which there is a lack of cohesion when the metal is red-hot. The metal cracks or crumbles when being hot worked and results from the iron not being sufficiently purified in the puddling furnace. (Skelton 1924). Sulphur is present in wrought-iron as iron sulphide (FeS) but it tends to segregate from the ferrite at the grain boundaries. (Johnson 1939). Because iron sulphide has a low melting point it causes a lack of cohesion between the grains when the iron is heated to red-hot (Johnson 1939). Sections rolled from red-short iron are likely to have rough edges (Johnson 1939). *Cold short* iron is the condition of low ductility at normal temperatures due to an excess of phosphorus or copper.

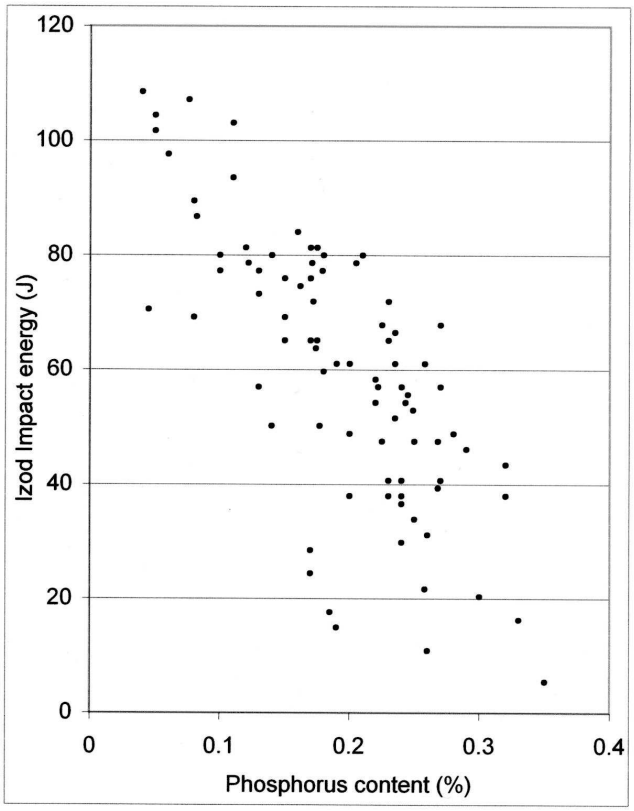

Figure 1.28 Effect of phosphorus on Izod impact energy of wrought iron. (Jeffrey 1959)

"A good wrought-iron would have a maximum sulphur content of 0.05% and a maximum phosphorus content of 0.16%. The manganese content should be less than 0.1% and silicon content less than 0.2%. The puddling process largely eliminates manganese so that amounts greater than 0.1% suggest adulteration of the product with steel scrap" (Jeffrey 1959). Of all the impurity elements phosphorus has the most significant effect on mechanical properties. Elevated phosphorus content causes higher yield strength and ultimate strength but causes a sharp fall in ductility and impact resistance, as shown in Figure 1.28

Wrought iron may be regarded as a composite material as it is composed of two phases, one being ferrite-iron and the other slag. The slag does not enhance the strength of the iron and is not well bonded to it, and therefore it is not a structural composite. The slag inclusions appear as narrow elongated strands or streaks and are given this shape by rolling the iron in a particular direction while the iron and slag are still hot and soft enough to be deformed. Thus wrought iron can be described as having a macroscopic grain. “The amount of slag in wrought iron can be up to 3 wt% of the total. (Walker 2002). It is relatively inert, glass like and consists of iron silicate and iron oxide” (Walker 2002). The thickness of the slag inclusions can range from microscopic size to 3mm. The composite nature of wrought iron is shown in Figure 1.29.

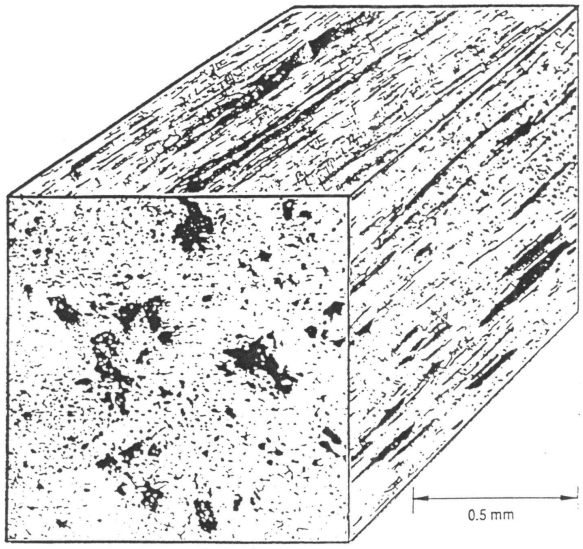

Figure 1.29 Composite texture and ‘grain’ of wrought iron. (Morgan 1999)

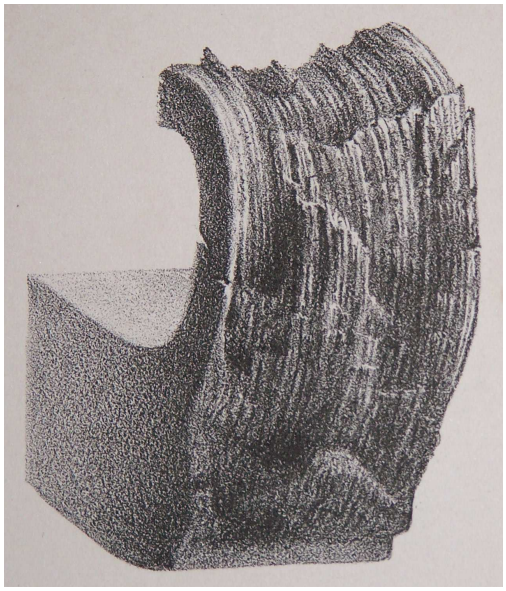

Figure 1.30 Fibrous texture of wrought-iron revealed by tearing open a bar in a nick-bend test. (Thorneycroft 1850)

The elongated slag inclusions divide the metal into strands or columns of ferrite and give it a fibrous appearance like wood. This fibrous texture is more clearly seen when a nicked bar is bent backwards tearing open the metal, as shown in the drawing of Figure 1.30. This was the most popular way of testing the quality of wrought iron in the foundry. Good quality iron exhibited significant fibrous texture while poor quality, harder iron showed a greater degree of granular texture.

1.10 Effect of slag inclusions on ductility and strength

Wrought iron has both greater tensile strength and ductility in a direction parallel to the direction of rolling than perpendicular to the direction of rolling. This is due to the directionality of the slag inclusions. Tensile strength is greater along the grain because, when loaded in this direction, there is a greater cross sectional area of more continuous ferrite which can carry the tensile load. When loaded perpendicular to the grain, the strand-like inclusions of slag disrupt the continuity of the ferrite across the load path and hence inhibit the ability of the ferrite to carry the tensile load. In test samples loaded perpendicular to the grain direction failure occurs by means of an internal rupture surface which passed preferentially through the slag (Gordon 1988). Tests conducted by Gordon showed that "if the ferrite has not been embrittled by phosphorus the ductility of wrought iron is mainly controlled by the distribution of slag in it" (Gordon 1988). This can be explained in terms of the microstructure of the composite. The size, shape and distribution of the slag inclusions in wrought iron vary greatly. In general, the slag inclusions are elongated because of rolling. In cases where there is a high degree of elongation of the slag inclusions the ferrite matrix is divided into columns. (Gordon 1988). When a tensile load is applied to a wrought iron sample in this condition the ferrite columns elongate, but the brittle slag inclusions cannot (because they are glass-like) and undergo transverse cracking. (Gordon 1988). Internally, various ferrite columns undergo plastic deformation and begin to neck and fail forming a localised internal rupture surface which spreads across the specimen (Gordon 1988). This quickly leads to failure of the specimen with little reduction in cross sectional area at failure. In other words, low ductility is measured in the tensile test. This is why an over abundance of long slag inclusions reduces the ductility of wrought iron even though the ferrite is ductile (Gordon 1988).

Equally bad, are tiny, globular slag inclusions which result from excessive working of wrought-iron. An iron with such a microstructure "lacks the fibrous texture, typical of good wrought-iron, and behaves like a dirty low-carbon steel; it tends to be brittle and has

poor fatigue properties." (Jeffrey 1959). That is why wrought-iron exhibits improved mechanical properties up to about the 6th working and thereafter the mechanical properties deteriorate with further working. (Turner 1908).

The effect of grain direction on tensile strength is further discussed in Chapter 2 with the conclusion that plate iron is on average about 15% stronger in the direction of the dominant grain.

1.11 The effects of cold work

It is important that the metal is kept hot during working, particularly during the final stages of working into a finished shape, so as to avoid strain hardening the metal by cold rolling. This can sometimes be difficult, particularly with the rolling of long bars of small diameter, because the smaller or thinner the section the faster it loses heat. Annealing removes the effects of cold work. In a number of the historical testing programs which provided data for this report the samples were annealed before tensile testing. This was done because the mechanical history of some of the specimens was unknown. By first annealing the metal the 'natural' strength and ductility could be determined as opposed to measuring the strength of a strain hardened sample. Shearing and punching iron strain hardens the area around the cut or hole. "M. Barba showed that drilling out a ring 1/8 inch wide round a punched hole, or annealing the plate, entirely removed the prejudicial effect of punching" (Unwin 1910). Drilling holes for rivets did not strain harden the metal but was slower and more expensive than punching. Kirkaldy found that punched plates experienced a 50% loss in ductility compared with plates that were drilled. (Kirkaldy 1876).

1.12 Compressive strength of wrought iron

Tests conducted by Marshall in 1887 and Kirkaldy in 1866 showed that for practical purposes the tensile and compressive strengths of wrought-iron can be taken as the same.

However, Gordon has proposed that in cases where the slag inclusions are excessively elongated test samples can exhibit lower compressive strengths due to the ferrite matrix being divided into columns, which can buckle prior to yielding of the ferrite. (Gordon 1988). Such buckling at the microscopic level, is detected by the test machine as initial compressive yielding even though the ferrite has not yet yielded. Buckling of the ferrite columns occurs because the slag is weak, brittle and non-cohesive with the ferrite, so it offers little support to it. (Gordon 1988). Gordon's tests showed that the average compressive yield strength, along the grain, was about 20% lower than that of similar specimens pulled in tension along the grain. (Gordon 1988). Given that this result can be attributed to excessive elongation of slag inclusions it is reasonable to conclude that the more refined the iron is, the closer is the equality of compressive and tensile strength, as the ferrite will then not be divided into slender columns. When loaded across the grain this relationship is reversed as it is dominated by the weakness in tension caused by the slag inclusions in that orientation. (Gordon 1988). Across the grain the yield strength in compression was higher than that in tension. (Gordon 1988). In conducting compressive tests on iron it is important to size the specimen so that buckling of the sample is avoided. Gordon states that specimens longer than about 3 diameters usually buckle before the test has progressed to the point where compressive yield strength and modulus of elasticity can be measured. (Gordon 1988). Gordon also states that the compressive yield strength is independent of specimen shape as long as the length is greater than twice the diameter (Gordon 1988).

1.13 Impact resistance and fatigue of wrought iron

In terms of fatigue failure the fatigue limit of wrought iron may be taken to be about one-third of the ultimate tensile strength (Cullimore 1967). Lack of toughness rather than strength has been attributed to various failures of structural elements. Wrought iron from the S.S. Great Britain (Morgan 1996) and Walnut Street Bridge in the U.S.A (Green 1999) showed a high ductile-to-brittle transition temperature indicating that wrought-iron is

potentially prone to brittle fracture at normal temperatures, (See Figure 1.31). This was confirmed by tests conducted as part of the present research project where it was found that the ductile-to-brittle transition temperature most likely lies in the range 40 to 60^{o}C. Impact test data indicates that the toughness of wrought is quite variable. Charpy values for wrought-iron from an American truss bridge were in the range 34-144 Joules (Sparks 1998) while Charpy values for Walnut Street Bridge (See Figure 1.31) were in the range 10-60 Joules. (Green 1999). For a rolled wrought-iron beam taken from the Royal Albert Hall and tested at UMIST at room temperature the average Charpy values were quite low, 10 Joules for the flanges and 23 Joules for the web (Steude 2000).

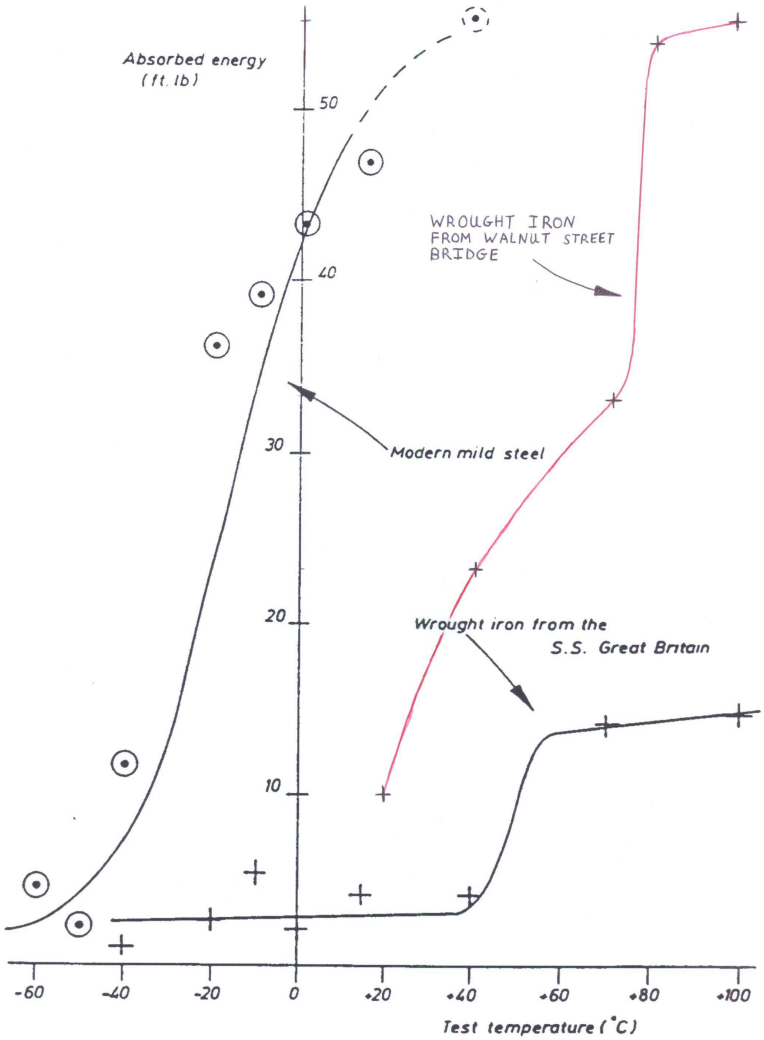

Figure 1.31 Impact Energy – Temperature curve for the wrought-iron of the S.S. Great Britain (Morgan 1996) with similar impact data from Walnut Street Bridge (Green 1999).

This beam material was tested again as part of the present research project and compared with material taken from a plate-and-angle beam from Edinburgh GPO. The Albert Hall beam material gave similar results to those stated above but the Edinburgh GPO beam gave Charpy values in the range 20J to 40 J, and based on this and other tests the Edinburgh GPO wrought iron was considered to be of better quality. However, Charpy data is so variable, particularly in wrought iron, that it is not a reliable means of assessing resistance to impact and can only serve as rough guide in comparing different wrought irons.

It is shown in Chapter 3 with reference to a bending test of the Albert Hall joist mentioned above that brittle fracture can occur in wrought iron under static loads. The cause of brittleness in wrought iron is most likely due to high phosphorus content or strain hardening caused by cold rolling. In the absence of these factors wrought iron can be expected to offer good resistance to suddenly applied loads.

The behaviour of wrought iron in a fire is likely to be very similar to that of steel, as like steel, its strength falls sharply above about 400^{o}C. (Sutherland 1992). The coefficient of linear expansion of wrought iron is similar to that of steel, being generally between 10×10^{-6} and 12×10^{-6} per ^{o}C at normal working temperatures. (Sutherland 1992).

1.14 Working with wrought iron - repair and preservation

A summary of the physical properties of wrought iron in comparison to those of mild steel and cast iron is given in Table 1.1. In general, wrought iron is slightly more resistant to corrosion than steel. (Wallis 2008). This may be due to a layer of millscale, which is a tough layer of hardened and compressed slag and iron oxide. The lack of slag in steel, and thus the absence of iron silicate in steel millscale, may render it a less effective barrier to moisture, with consequent greater ease of corrosion. Effective corrosion protection of wrought iron is achieved by painting. When repainting wrought iron the millscale should not be removed if it is adhering. (Wallis 2008).

Cast iron	Wrought iron	Mild steel
1.8–5%C	Almost pure iron (<0.1% C, silicate slag content up to 4%)	0.1–0.4 %C
Crystalline structure	Fibrous wood-like structure (thin 'laminae' or layers of slag alternating with iron)	Crystalline structure
Brittle, poor resistance to mechanical or thermal shock	Ductile, malleable (forgeable)	Ductile, malleable
Good in compression,weak in tension	Good in tension and compression	Good in tension and compression
Difficult to weld	Readily forge-welded	Readily welded
Good corrosion resistance	Better resistance than steel	Corrodible
Can chill hard in the mould; brittle	Ductile	Ductile, tough
Formed by casting in mould	Rolled or hammered to shape	Rolled to shape

Table 1.1. Comparative properties of cast and wrought iron and mild steel (Wallis 2008)

"Loosely adhering millscale, rust and paint can be removed by hand tool cleaning - wire brushing, scraping, and chipping - but these methods will not remove tightly adhering material. Wire brushing tends to polish rather than remove adhering rust, reducing the adhesion of subsequent paintwork. Power tool cleaning - sanding, needle gunning and descaling chisels - is more effective, but is more likely to cause damage. Flame cleaning, being non-abrasive, is particularly suitable for the soft surface of wrought iron, and is effective in dislodging rust packed between joined components". (Wallis 2008)

(See Figure 1.33)

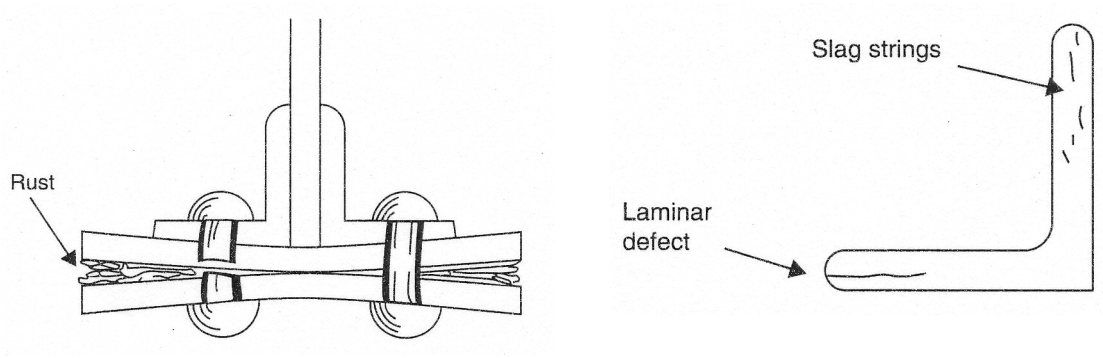

Figure 1.33 Typical hidden flaws in wrought iron work (Wallis 2008)

Cathodic protection may be used to prevent corrosion of wrought iron and has been used successfully to protect wrought iron cramps buried within stonework. (Wallis 2008).

Typical hidden flaws in wrought ironwork are broken rivets and delamination of the metal due to large slag inclusions. Defective rivets can often be detected by hammering as they emit a duller sound than sound rivets. (Wallis 2008).

Electric arc welding such as MMA or MIG techniques can be used to join wrought iron components. Although the traditional means of joining wrought iron was forge welding this would be impractical for making repairs to a structure on site. "Wrought iron should preferably be welded with a full or partial penetration butt weld over its cross section, as an alternative to fillet-welding of the metal surface, which can be ineffective owing to the laminar nature of wrought iron."(Wallis 2008). When wrought iron is welded by either of the electric arc techniques mentioned above the best results will be obtained if the welding speed is decreased slightly below that used for the same thickness of mild steel. (Marine 1937). The reason for this is that with reduced speed the pool of molten metal immediately following the arc is maintained in a molten condition for a longer period of time, thus allowing the slag the opportunity to float out of the weld metal and to allow a more complete elimination of the gases. (Marine 1937). Furthermore, with the electric arc processes it is desirable to use a slightly lower current value than that used for the same thickness of mild steel. (Marine 1937). This is of importance when thin sections are being

joined, since there is the possibility of burning through the material using the slower welding speed. (Marine 1937). However, as a general rule wrought iron should be worked hotter than steel to produce a good weld. (Marine 1937). This is possible because the high purity of the ferrite in wrought iron, particularly with respect to carbon, manganese and silicon reduces the possibility of burning. (Marine 1937). The ferrite component of wrought iron melts at about 1500^{o}C which is somewhat higher than that for low and medium carbon steels, while the slag melts at the lower temperature of 1200^{o}C. (Marine 1937). Melting of the slag gives the surface of the metal a greasy appearance which should not be mistaken for actual melting of the base metal. In general it is advisable to use an electrode rod which has a yield strength near that of wrought iron and to avoid rods containing high carbon or alloys intended to increase the yield strength. (Marine 1937). Flux coated mild steel rods are suitable. A guide to welding procedures for wrought iron is given in Tables 1.2 and 1.3.

Plate thickness (mm)	6	9	12	15	19	22	25
No. of passes	3	4	5	6	8	9	10
Diameter or electrode rod (mm)	5	5	5	5	5	5	5
Current (Amperes) (approx)	170	170	180	180	180	180	180

Table 1.2 Manual Metal Arc (MMA) welding procedure guide for wrought iron. (Marine 1937)

Plate thickness (mm)	6	9	12	15	19	22	25
First layer - first side (V side)	200	200	175	175	175	150	150
Intermediate layers - first side (V side)	125	125	125	125	125	125	125
Last layer - first side (V side)	125	125	100	100	100	100	100
First layer - second side	125*	125*	100*	100*	100*	150	150
Intermediate layers - second side	---	---	---	---	---	125	125
Last layer - second side	---	---	---	---	---	100	100

*Not used unless a double weld is specified.

Table 1.3 Recommended rate of travel of electrode in mm per minute for Manual Metal Arc (MMA) welding of wrought iron plates flat and butt edge-to-edge with V joint. (Marine 1937)

The essential guidance conveyed by the data in Table 1.8 is that the first layer of weld metal should be applied a little faster than subsequent layers. This may be to prevent burning through the thin metal at the bottom of the V groove on the first pass. As more layers of weld metal are laid down, there is less possibility of burning through the plate so a slower rate of welding may be employed. In 1938 Marine Engineering and Shipping Review reported on tensile and bending tests conducted on wrought iron plates welded edge-to-edge and flat, with the edges to be welded forming a V groove. In all of the tests fracture occurred away from the weld zone and it was concluded that the welds were stronger that the wrought iron plate. (Marine 1938). In addition, stretching during bending was more pronounced in the wrought iron parent metal than in the weld metal due to the greater strength of the latter. (Marine 1938). Although arc welding of wrought iron structures is possible forge welding is generally preferred as it results in a more uniform component both compositionally and mechanically.

Chapter 2 Review of past and current assessment methods for wrought iron

2.1 Assessing the quality of wrought iron in the 19th century ironworks

In the early days of wrought iron manufacture the only way of assessing the quality of the finished metal was to subject it to a variety of destructive tests performed by hand. These tests normally consisted of bending, tearing, twisting or punching the metal to see how it responded to ill-treatment. Such tests quickly showed whether the iron was good or bad. Even with the introduction of regular tensile tests performed by machine the simple foundry tests performed by the blacksmith were never abandoned during the entire time of wrought-iron manufacture. Shown in Figure 2.1 is a picture taken from a catalogue of the New British Iron Company depicting the various foundry tests used to determine the quality of the iron.

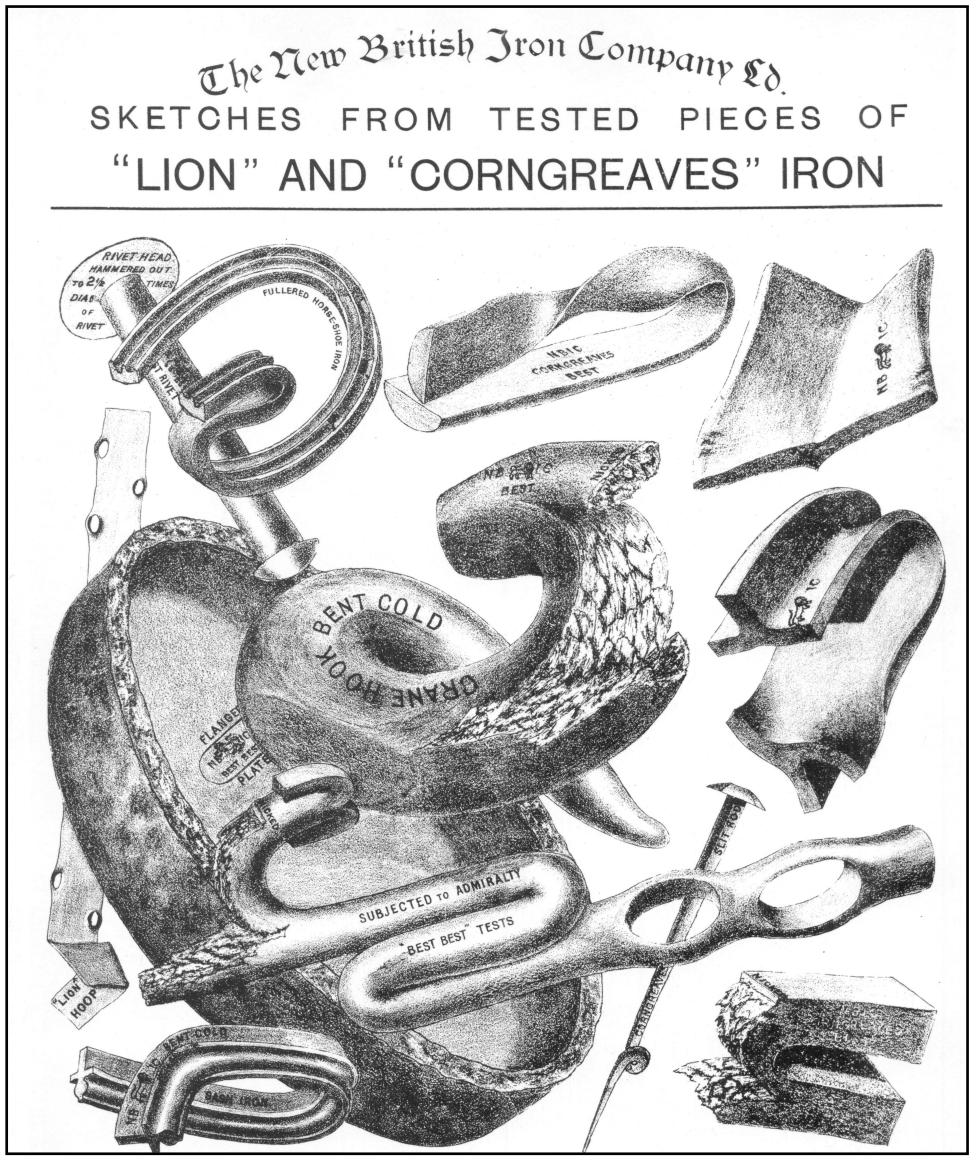

Figure 2.1 The New British Iron Company foundry tests for wrought-iron (Gale 1977)

Probably the most widely used test was the nick-bend test shown in the bottom right-hand corner of Figure 2.1. The nick-bend test was included in nearly all specifications for wrought iron (Rawdon 1924). It consisted of making a small transverse nick across the bar to be tested and then the bar was bent backward by striking with a hammer on the edge of the smiths anvil, tearing open the bar and exposing the fibrous texture or otherwise of the iron. The following description illustrates the blacksmiths interpretation of what he saw when examining the freshly broken fracture.

"Long, silky fibres adhering together like a bundle of hempen strands make him believe that his iron is of a tough, soft quality, easy to forge and shape, but hard to break. A coarse granular fracture indicates a harsh, brittle iron, subject to 'cold shortness' or to being easily broken when in use. A 'red-short' iron is generally denoted by the appearance of numerous cracks on the edges of the bar." (The Engineer 1863)

By definition red-shortness is detected when the iron is hot. If after heating a bar to a red heat, cracks developed along the edges, and when bent the piece broke easily, then the iron was red-short. (Skelton 1924) This indicated that the iron had not been purified sufficiently in the puddling furnace and contained an excess of phosphorus (Skelton 1924).

When the steam hammer was first introduced many iron workers disliked it as they believed that it prevented the early identification of red-short iron. The reason is that in the days prior to the steam hammer the helve hammer was used which delivered a constant and relatively heavy blow. Under a heavy blow red-short iron would simply crumble and so would be sent back to the puddling furnace. However, with the much greater control of the steam hammer and its variable force of impact, red-short iron could be 'nursed' under gentle blows in order to form a cohesive mass. (Gale 1966). Thus bad iron could be produced and remain undetected until much further along in the manufacturing process.

For this reason some foundries never adopted the steam hammer and chose instead to use steam powered helve hammers. (Gale 1966). However, most foundries did adopt the steam hammer and with care and experience the iron workers learned how to identify bad iron, so that these foundries were still able to produce iron of equal quality to those who chose not to use the steam hammer (Gale 1966).

Various hot and cold foundry tests were applied to the iron depending on the grade of iron being produced. The highest quality grade of iron in British practice was called Best-Yorkshire iron and was produced in the Leeds and Bradford areas of West Yorkshire. Some of the firms that made Best Yorkshire iron were Lowmoor, Farnley, Monkbridge, and Taylors. For this grade of iron the 1913 British Standard specification included the following clause relating to foundry tests on bar iron.

Test pieces shall be lightly and evenly nicked on one side with a sharp cutting tool and bent back at this point through an angle of 180^{o} by pressure in a press or by a succession of light blows, when they shall show a fibrous fracture free from slag or dirt. The same test pieces when nicked all round and broken off short shall show a fine uniform crystalline fracture. (Rawdon 1924)

For rivet iron the foundry test of quality was to bend a 24 in length into the form shown in Figure 2.2. The iron was considered to be of good quality if there were no signs of fracture on the outside of the bent portions.

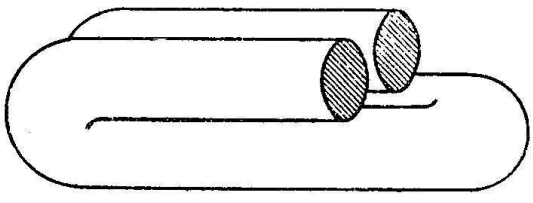

Figure 2.2 Cold bend test for rivet iron (Skelton 1924)

With regard to regularity of foundry testing the relevant British Standard clause was as follows:

One cold and two nick-bend tests and two fracture tests shall be taken from each three tons of material (Skelton 1924). For rivet iron the tests had to be performed on every ton of metal produced.

For grade 'A' iron, which was the next level of quality under 'Best Yorkshire', the iron was subjected to the foundry test shown in Figure 2.3. The description of the test is a follows:

Specimens of the bars as rolled shall be punched at full red heat with a punch one-third the diameter or width of the bar, at a distance from the end of the bar equal to 1.5 times the diameter or width (Fig. 1). The hole shall then be drifted out 1.25 times the diameter or width of the bar (Fig. 2). The end of the bar up to the hole shall then be split, and the ends must admit of turning back without fracture (Fig. 3). (Skelton 1924).

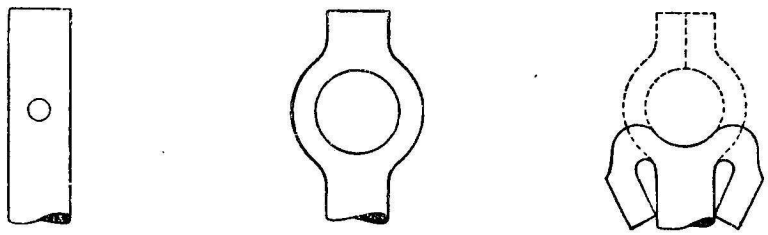

Figure 2.3 Hot forge test for wrought iron (Skelton 1924)

The above descriptions of foundry tests of quality are just a small number of the types of tests performed. The tests described were taken from the 1913 British Standard, however it should be remembered that in the hey-day of wrought iron manufacture, i.e. 1850 -1890, there was no British standard relating to foundry tests and individual foundries could assess the quality by whatever means they liked, as indicated in Figure 2.1. However, many foundry tests were maintained by tradition and engineers expected to see quality demonstrated by means of certain well known tests.

As an example of a foundry test prior to the British Standard, Matheson describes the bending of iron through a certain distance as the measure of quality. “A plate 0.5 in. thick, bent to an angle of 35^{o} without damage, will, if it possesses sufficient breaking strength, afford, for ordinary purposes, a satisfactory proof of its elasticity. Of course, the thicker the plate, the more acute should be the angle by which it is tried." (Matheson 1873). Matheson also states that iron from which rivets are made should be of a better quality than ordinary bars, and its ductility should be such that it will bend double when cold without cracking. (Matheson 1873). This would explain why in the British Standard rivet iron was tested more often than bar iron.

2.2 Development of tensile testing of wrought iron

In the early half of the 19^{th} century tensile testing was not conducted in a standardised way, nor was it routinely performed. At that time tensile testing was generally carried out when needed for a particular structure. However, by the middle of the 19^{th} century, when wrought iron began to surpass cast iron and when long span roofs and other slender structures were developed, there emerged a greater need for better knowledge of material strength and reliability.

When David Kirkaldy conducted his investigation into the properties or wrought-iron and steel in 1858-61 at the Napier shipbuilding firm, his instruments could not measure elastic limit. When Napier and Sons discontinued Kirkaldy’s testing program he resigned his position with the firm so that he could devote his entire time to materials testing. He designed a new form of testing machine and set up Britain’s first commercial testing works in 1865 (Smith 1980). Records of his tests conducted in 1866 show that by this time Kirkaldy was able to measure elastic limit.

The development of accurate strain measuring devices in the 1860’s made reliable measurements of elastic limit possible. During the 1860’s and 70’s materials testing became more routine as various laboratories were set up throughout Europe and America.

From 1863 Knut Styffe as director of the Royal Technological Institute in Stockholm conducted tests on iron and steel as part of a commission set up to investigate iron and steel for railway purposes. August Wöhler and Johan Bauschinger did much to establish and standardise materials testing in Germany. Various government owned laboratories were set up in German universities; the first was in 1871 at the Polytechnical Institute of Munich with Bauschinger as its director (Timoshenko 1953). In 1878 A.B.W. Kennedy set up the first British university engineering laboratory at University College London.

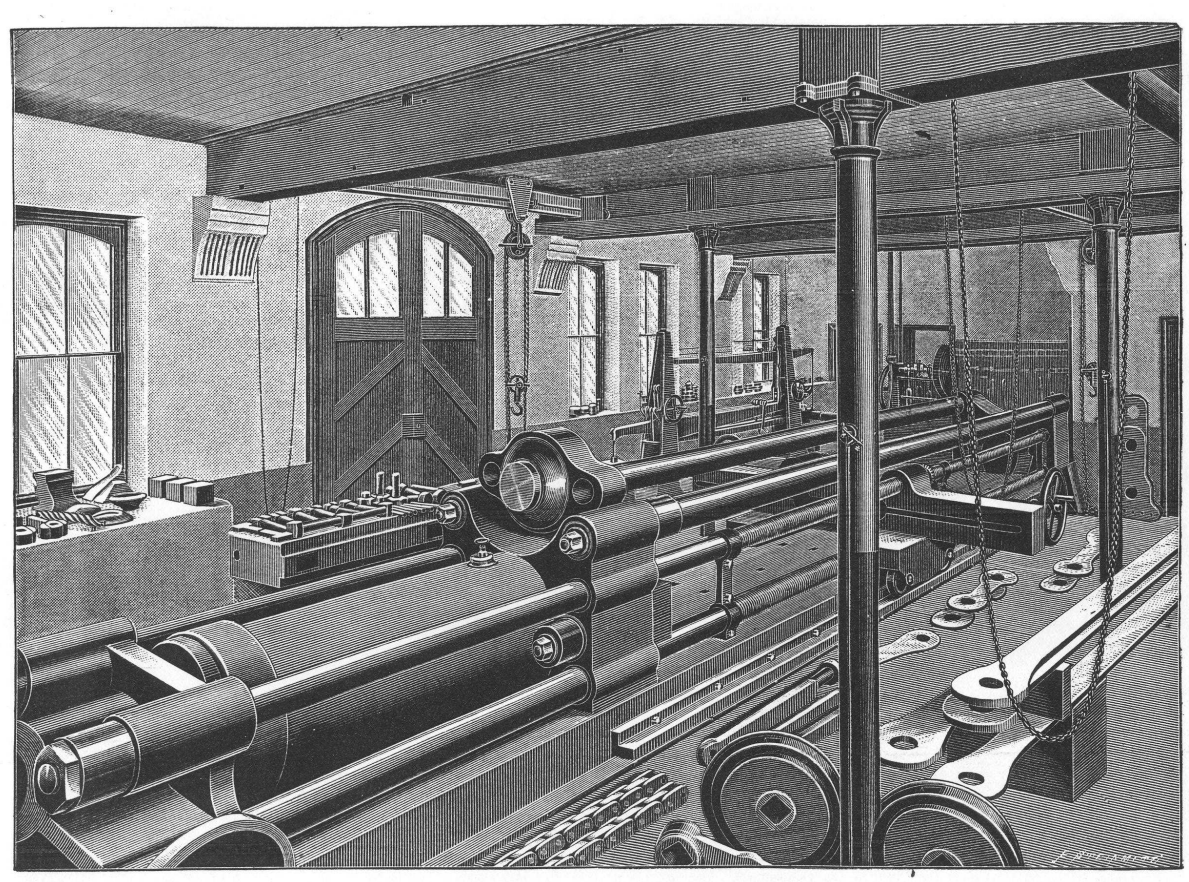

Figure 2.4 Testing room of David Kirkaldy's Experimental and Testing Works at 99 Southwark Street, London. The drawing shows the testing machine which Kirkaldy designed himself. (Kirkaldy 1891)

In America the desire for better understanding of the mechanical properties of iron was probably greater than anywhere else, because at that time many American engineers viewed themselves as being too reliant on foreign experimental work for knowledge about the mechanical properties of iron and steel (Pugsley 1944). The U.S. Government created a Board in 1874 to provide a national facility for testing materials. (Gordon 1996).

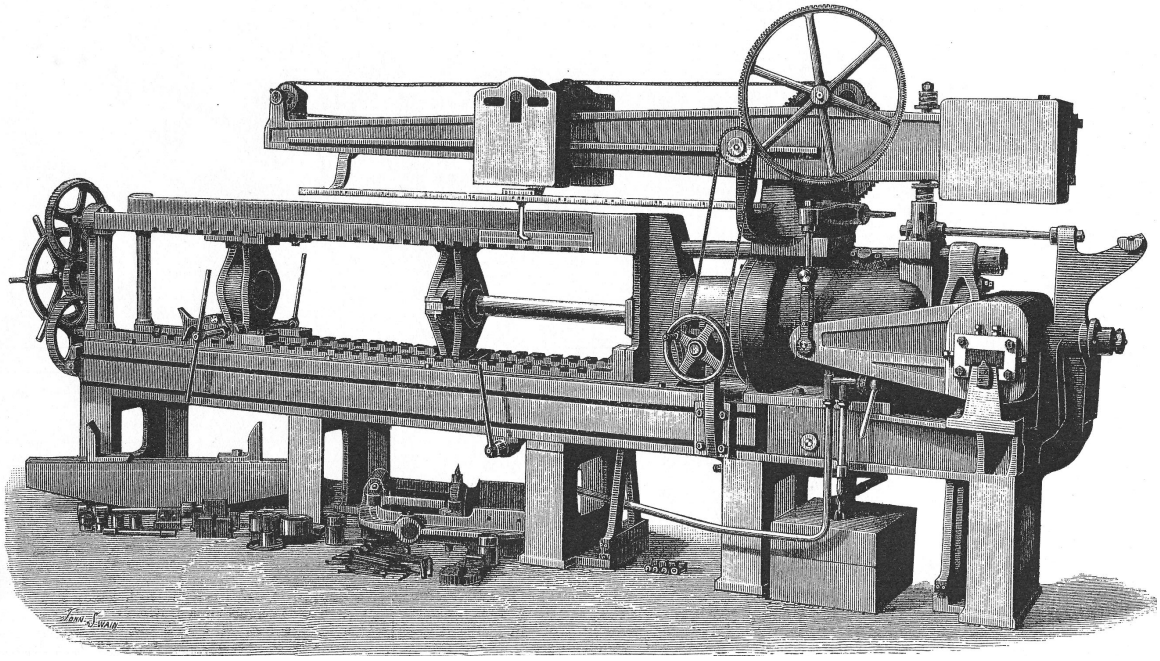

Figure 2.5 Professor Alexander Kennedy's testing machine at University College London. (The Engineer 1890)

Congress allocated $75,000 to the Board and in June 1875 a contract was made with Albert H. Emery to design a precision testing machine (Gibbons 1934). The machine was completed and installed at Watertown Arsenal, Watertown, Massachusetts in 1879 (The Engineer 1888). An extensive program of testing began which was reported on an annual basis. The testing machine at Watertown Arsenal, which became known as the 'United States Testing Machine', was a significant achievement as it was one of the largest and most precise testing machines in the world. America was now in a position to make significant contributions to the field of materials testing.

As in Britain and Europe the American universities also set up their own materials testing laboratories. One in particular was that at the Massachusetts Institute of Technology. This particular university is of interest in the present context because of the meticulous records of tests on wrought-iron that were made there in the 1880's and 90's. In 1883 Gaetano Lanza was put in charge of the department of mechanical engineering and immediately began a considerable expansion of the mechanical engineering laboratories. He was particularly interested in the testing of full size structural members (Lanza 1912).

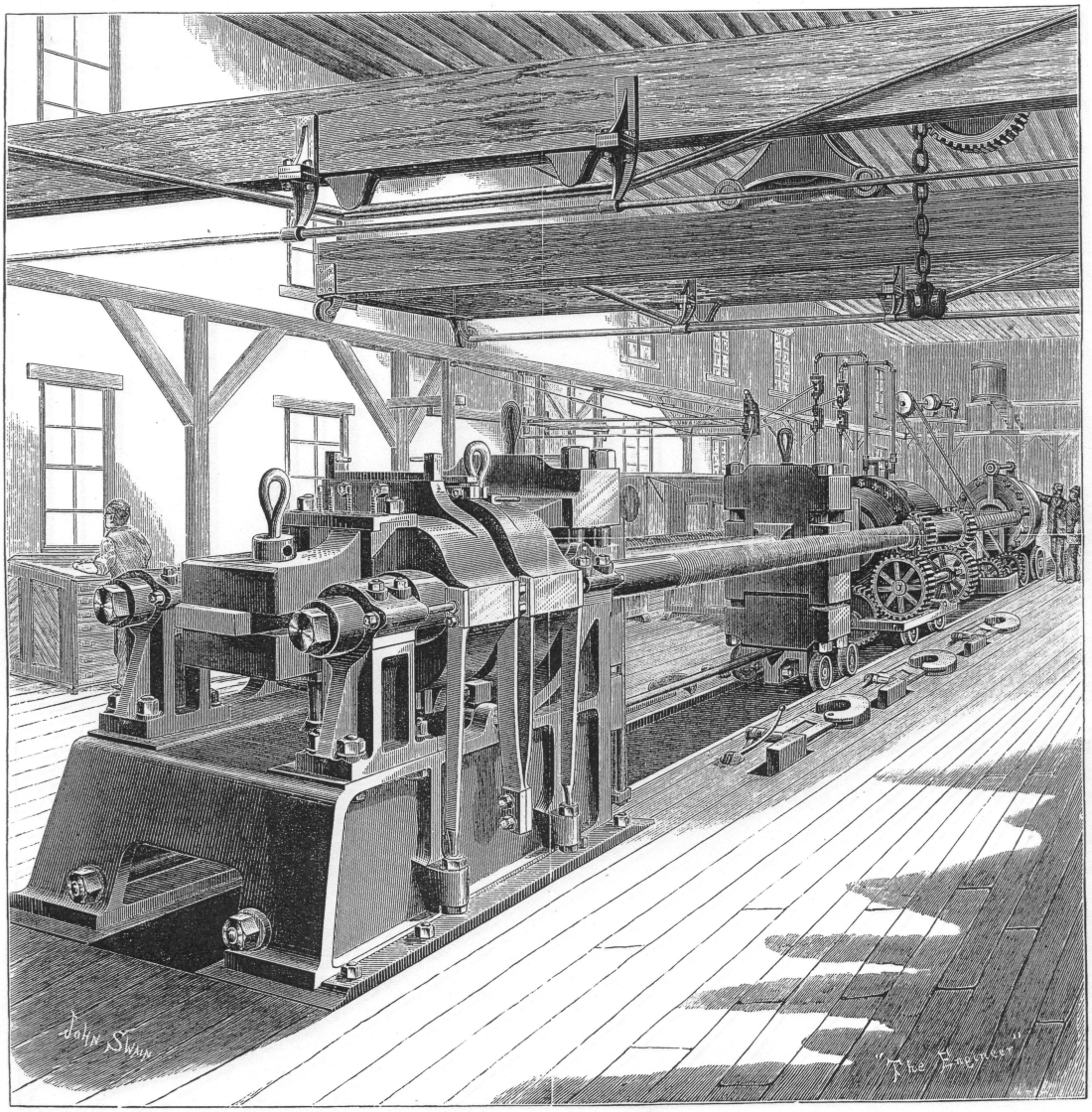

Figure 2.6 United States Testing Machine at Watertown Arsenal (The Engineer 1888)

At M.I.T. Lanza had a Fairbanks testing machine of 50,000 lbs capacity which besides being used for making tensile tests on iron and wire rope, could be adapted in such a way as to enable full size beams to be tested for transverse strength and deflection. The allowable spans were up to 25 feet. (Lanza 1887). Lanza retired from M.I.T in 1911 but for a number of years after this he was associated with the Baldwin Locomotive works in Philadelphia, where his expertise in full size mechanical testing was required. (The Tech 1925). M.I.T.'s test records were used in the present research on wrought-iron. By the end of the 19th century, steel had eclipsed wrought iron as the dominant structural material, and as a consequence, there was a reduction in the volume of tests on wrought iron. Therefore, the period of most abundant and reliable tensile test records is between 1860 and 1900. In

the 20th century tests on wrought iron were usually conducted when an old iron structure was demolished or refurbished.

When wrought iron was used as a structural material it was never subject to a design standard. The earliest publication of a structural design standard in the UK was in 1906 when what became known as BS 15 was introduced. (Bussell 1997). This was the British Standard for structural steel for bridges and general building construction, but it only applied to steel and not wrought iron. (Bussell 1997). It was the first attempt to introduce a national standard for steel and thus avoid the use of the traditional steel 'grade' system, which had been in place since the time of wrought iron. (Bussell 1997). This was followed by the 1909 London act which specified loads, stress and design methods for structural steelwork. (Bussell 1997).

2.3 Present knowledge of wrought iron material properties

Although there are a number of books about the assessment of existing iron structures the only current standard in the UK which applies to wrought iron is BD21/01 The Assessment of Highway Bridges and Structures. In this standard the characteristic yield strength of wrought iron is given as 220 N/mm^2. However it was found during the course of this research that any body of tensile test data will generally give a lower value of characteristic yield strength than that quoted by BD21/01.

In a recent study conducted for Network Rail by Cass Hayward Consulting Engineers, a large number of tensile test records on wrought iron were collected. The data was primarily for plate iron but some angle and tee iron data was also gathered. The results of a statistical analysis of this data are summarised in Tables 2.1 to 2.4. and represents the most recent published study of wrought iron material properties. These records, together with those collected as part of the present research project, have been used to produce a database of tensile test records, the assessment of which is the subject of much of the remainder of this chapter.

With-grain tension specimens: mean values

Nominal plate thickness: mm	Nominal plate width: mm	Number of specimens	Elastic modulus, E: kN/mm^2	0·2% proof stress: N/mm^2	Ultimate tensile strength: (N/mm^2	Elongation: %
13	450	6	201	276	347	6·3
10	565	10	212	277	337	6·6
10	234	6	214	250	365	18·4
6	570	5	190	232	295	7·3
11	–	6	237	216	328	4·4

Table 2.1 Tensile test results for loading parallel to grain direction (Moy 2009)

Cross-grain tension specimens: mean values

Nominal plate thickness: mm	Nominal plate width: mm	Number of specimens	Elastic modulus, E: kN/mm^2	0·2% proof stress: N/mm^2	Ultimate tensile strength: (N/mm^2	Elongation: %
13	450	6	228	285	301	1·6
10	565	10	241	277	290	2·0
10	234	6	255	244	260	1·4
6	570	5	191	223	277	6·3

Table 2.2 Tensile test results for loading perpendicular to grain direction (Moy 2009)

With-grain specimens – mean values

Nominal plate thickness: mm	Nominal plate width: mm	Number of specimens*	Elastic modulus, E: kN/mm^2	0·2% proof stress: N/mm^2	Ultimate compressive strength: N/mm^2
13	450	9 (4)	176	239	553
10	565	10 (6)	180	204	443
10	234	12 (4)	153	184	485

Table 2.3 Compression test results for loading parallel to grain direction (Moy 2009)
* Values in brackets indicate number of elastic modulus specimens.

	Mean	Standard deviation	Lowest credible value	Characteristic value*	No. of tests
Yield stress in tension: (N/mm^2)					
With grain	250	29	190	198	329
Across grain	234	39	154	153	48
Ultimate tensile strength: (N/mm^2)					
With grain	348	36	232	283	329
Across grain	285	27	243	221	22
Elastic modulus in tension: (kN/mm^2)					
With grain	210	35	167	-	22
Across grain	241	35	151	-	22
Elongation at failure: (%)					
With grain	15.0	7.0	4.0	-	329
Across grain	1.36	0.76	0.38	-	22
Yield stress in compression: (N/mm^2)					
With grain	208	17	152	161	12
Elastic modulus in compression: (kN/mm^2)					
With grain	171	26	138	-	14

Table 2.4 Summary of tensile test results for plate wrought iron (Moy 2009)
* The Characteristic Value is given by: CV = x - ks where x is the mean and s is the standard deviation of the set of test results, and k = 4.21 for 5 results, k = 2.91 for 10 results, k = 2.57 for 15 results, k = 2.22 for 30 results, and k = 1.64 for an infinite number of results. (Moy 2009).

From Table 2.4 it appears that the modulus of elasticity is greater across the grain than parallel to the grain. The reason for this is unknown and may require further research.

2.3 (a) Modulus of elasticity of wrought iron

Tensile tests on various American, British and Norwegian wrought-irons were compiled to produce the histogram of values for modulus of elasticity shown in Figure 2.7. The mean value is 197 kN/mm^2, which is close to the BD21 Highway Standard value of 200 kN/mm^2. Outlying values are probably a consequence of experimental measurement error.

Samples tested along grain. No. of tests: 242	
	Modulus of elasticity
	kN/mm^2
Range	124 - 253
Mean	197
Standard deviation	13

Table 2.5. Numerical summary of modulus of elasticity data represented in Figure 1.32. (O'Sullivan 2007).

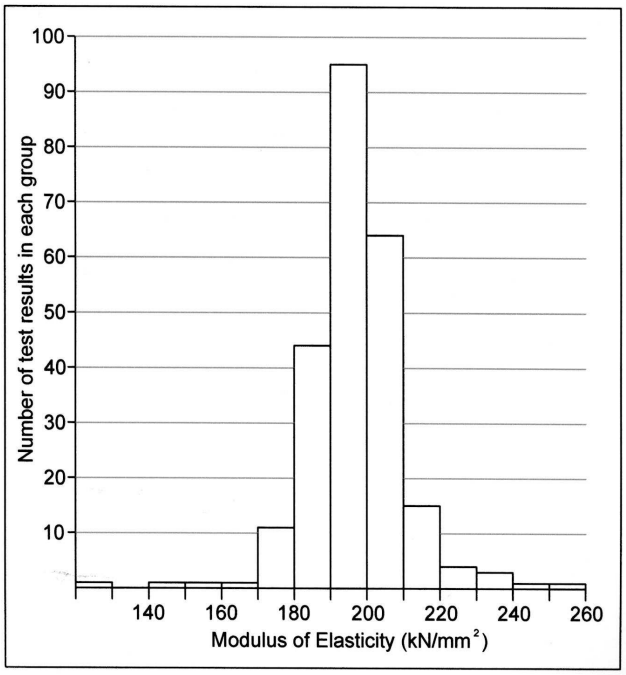

Figure 2.7 Modulus of elasticity of bar wrought-iron (O'Sullivan 2007)

Popplewell stated that the modulus of elasticity is 190-207 kN/mm^2 (Popplewell 1901).

Bussell gave the modulus of elasticity as 154-220 kN/mm^2 (Bussell 1997).

The Department of Transport Highway Standard BD21 specifies 200 kN/mm^2 for modulus of elasticity. A search has revealed nothing published on the origins of the BD21 data and thus it is not known what data set was used to generate the characteristic values given in BD21.

2.3 (b) Tensile strength of plate iron

As previously mentioned, for plate iron, an effective means of equalising the strength parallel and perpendicular to the direction of the grain was cross-piling, in which the bars were piled in alternating directions, as shown in Figure 1.12, before being rolled into a thin plate. However, sometimes the plates were formed with the outer layers in the same direction possibly resulting in greater strength in that direction.

Furthermore, the direction of final rolling may have given some dominance to the grain in that direction. In the results summarised in Figure 2.8 the grain direction of the plate refers to the dominant grain direction.

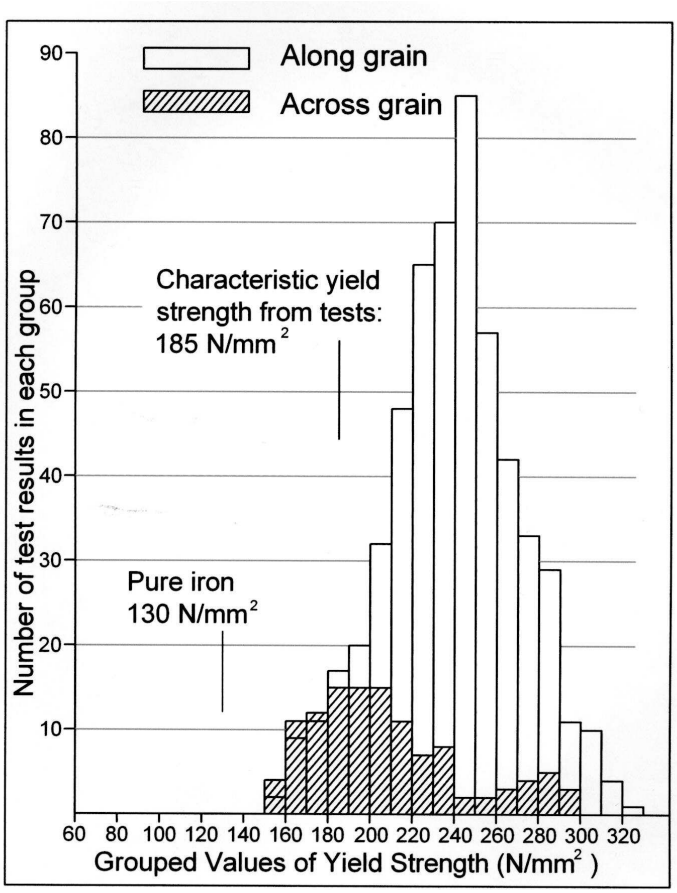

Figure 2.8 Yield strength of plate iron tested along and across grain direction. (O'Sullivan 2008).

It can be seen from the collection of about 550 tensile tests results along the grain (Table 2.6) and about 115 tests perpendicular to the grain (Table 2.7) that plate iron is on average about 15% stronger in the direction of the dominant grain. It is because of this, that plate girders were constructed with the grain of the plate along the longitudinal direction of the girder. From these test results the characteristic yield strength along the grain is 187 N/mm^2 which is lower than the value given in the Highway Standard BD21, which states 220 N/mm^2.

Table 2.6 Summary of data represented in Figures 2.8 and 2.9.

Plate iron. Tested parallel to grain. Number of tests: 550			
	Yield strength	Ultimate strength	Elongation at failure
	N/mm^2	N/mm^2	%
Range	160 - 363	232 - 470	1 - 36
Mean	240	345	15
Standard deviation	32	35	7

Table 2.7 Summary of test data for plate iron tested perpendicular to grain. Yield strength values are represented in Figure 2.8 only.

Plate iron. Tested perpendicular to grain. No. of tests: 115			
	Yield strength	Ultimate strength	Elongation at failure
	N/mm^2	N/mm^2	%
Range	154 - 298	183 - 389	0.1 - 29.2
Mean	208	296	8
Standard deviation	36	39	7

In Figure 2.9 the yield strength and ultimate strength of plate iron is plotted against elongation at failure (i.e. ductility). Generally, the image shows the considerable variability in the material, both in terms of strength and ductility.

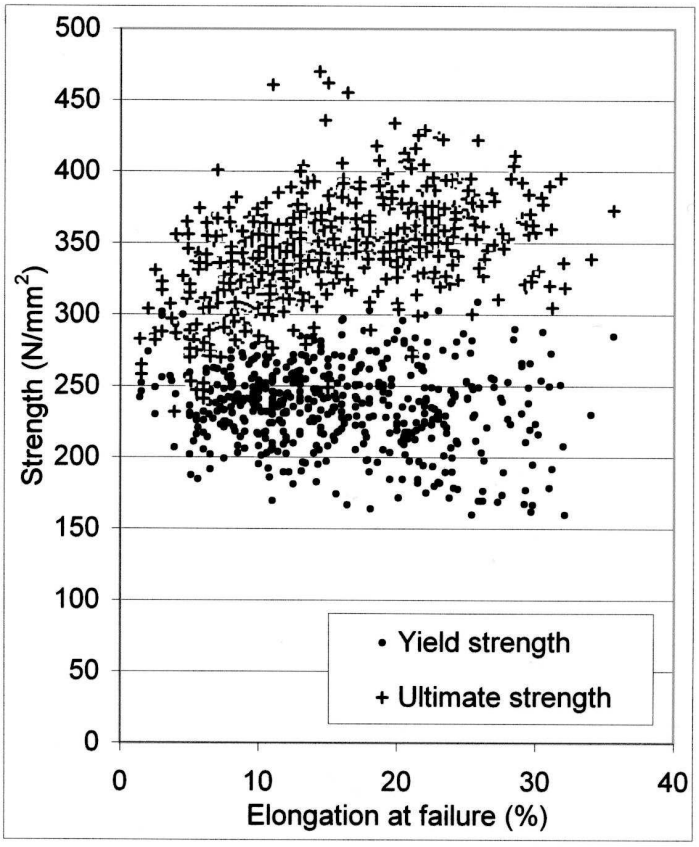

Figure 2.9. Strength of plate iron tested along grain direction. Vertical pairs of data points are from the same tensile test. (O'Sullivan 2008).

2.3 (c) Assessing normality of plate iron tensile strength data

The comparison of the actual frequency of yield strength with the normal distribution is shown in Figure 2.10. From this diagram the yield strength appears to follow a normal distribution and this can be confirmed by computing the Kolmogorov-Smirnov statistic which is given in Table 2.8. A non-significant result (Sig. value of more than 0.05) indicates normality. (Pallant 2010). In this case the Sig. value is 0.067, which confirms that the yield strength data along the grain direction follows a normal distribution.

	Kolmogorov-Smirnov		
	Statistic	df	Sig.
yield_stress	.037	549	.067

Table 2.8 Results of test for normality of yield strength data

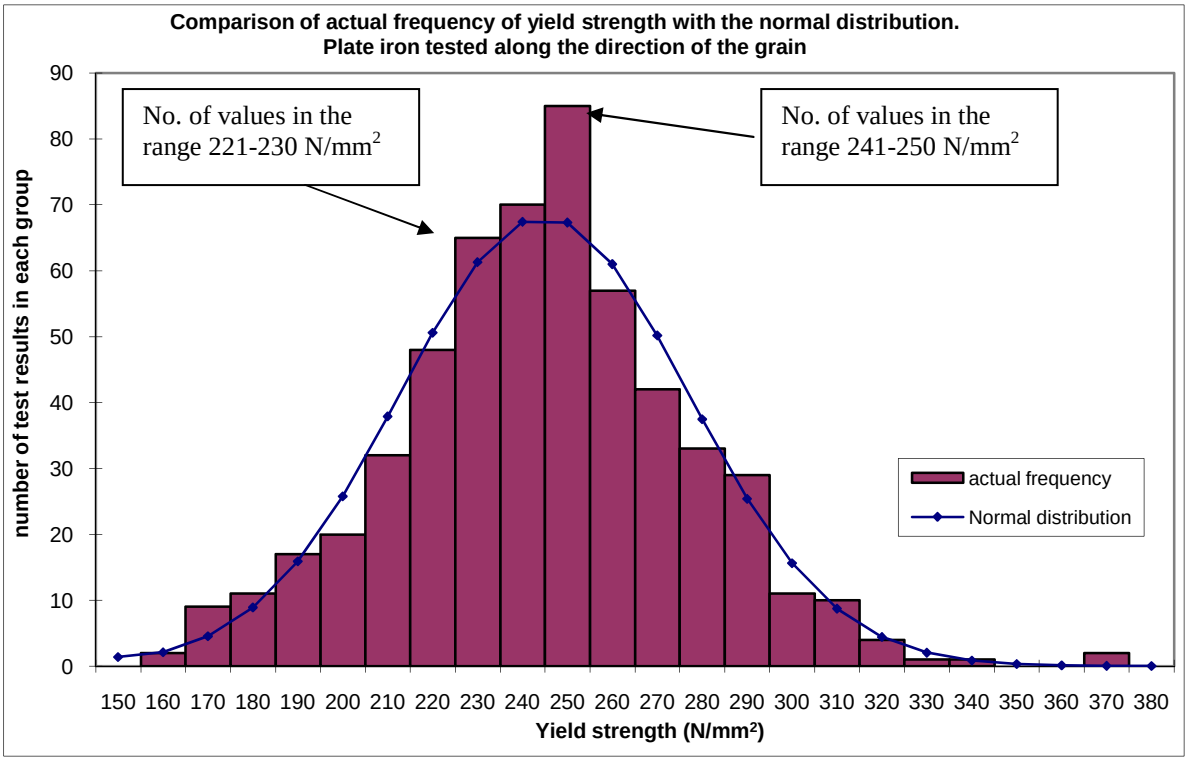

Figure 2.10 Comparison of actual frequency of yield strength with the normal distribution for plate iron tested along the grain direction. (O'Sullivan 2012).

This is also supported by an inspection of the normal probability plot (labeled Normal Q-Q Plot). In this plot, the measured yield strength for each test is plotted against the expected value from the normal distribution. A reasonably straight line suggests a normal distribution, which is the case, as shown in Figure 2.11.

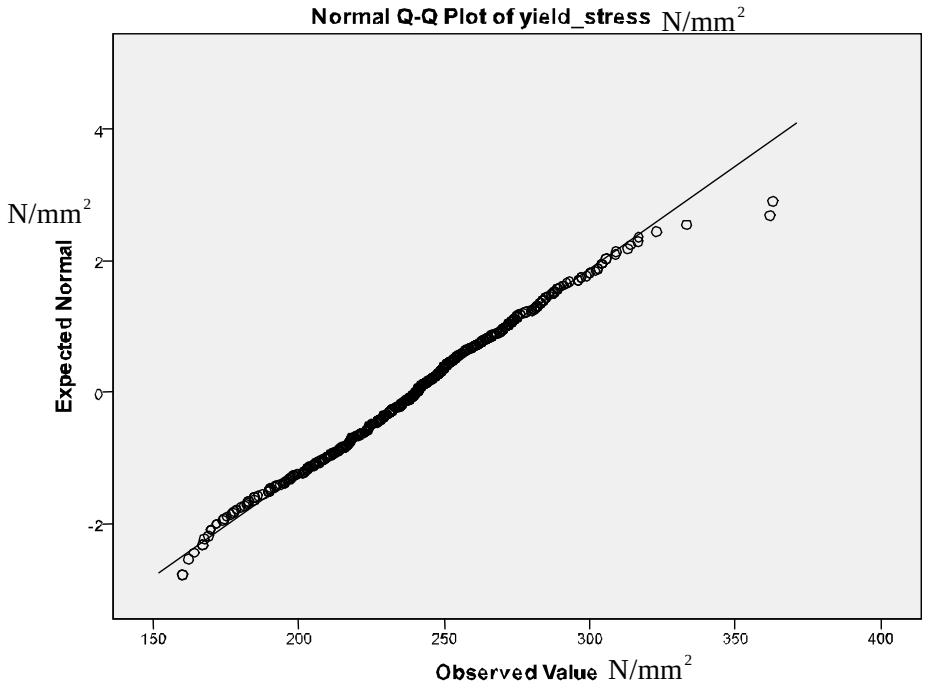

Figure 2.11 Plot of measured yield strength against expected value from the normal distribution. Plate iron along grain direction. (O'Sullivan 2012).

The Detrended Normal Q-Q Plot shown in Figure 2.12 is related to the Normal Q-Q plot of Figure 2.11, in that it is a plot of the actual deviation of the measured yield strength results from the Normal straight line. If normality exists then there should be no real clustering of points away from the zero line, with most collecting around the zero line.

In all representations comparing the yield strength data to the normal distribution given here, there appears to be a number of outlying values at the high end of the strength scale. These values which consist of just two in number, may be classified as outliers as they are not representative of the majority of strength values.

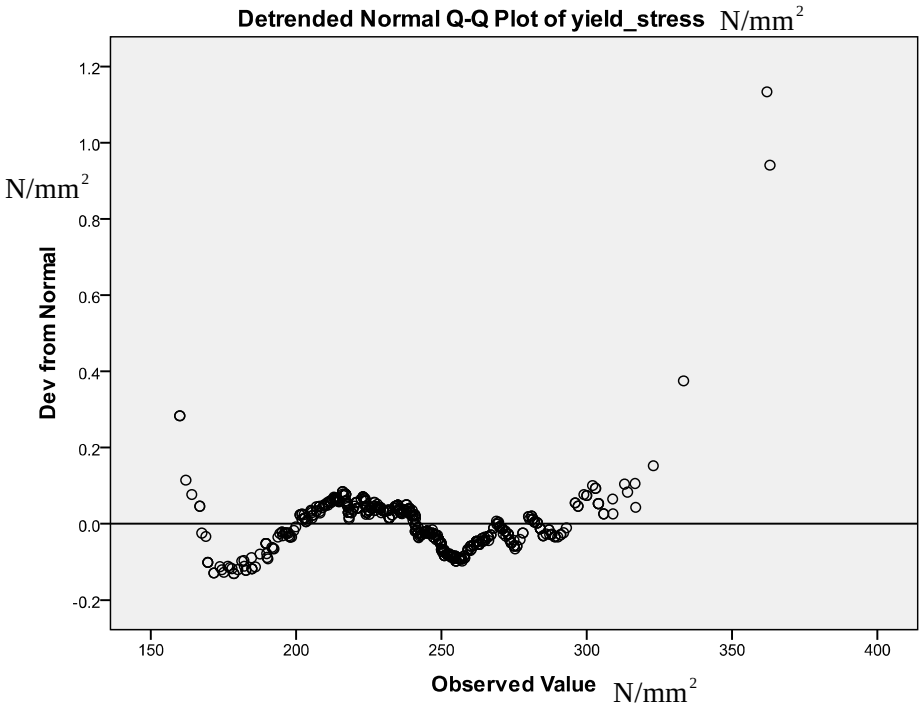

Figure 2.12 Detrended Normal Q-Q Plot. Yield strength data along grain direction (O'Sullivan 2012).

A boxplot of the distribution of yield strength test results is shown in Figure 2.13. The rectangle represents 50% of the test results, with the whiskers (the lines protruding from the box) going out to the smallest and largest values. The additional circles outside this range are the outliers. The line inside the rectangle is the median value.

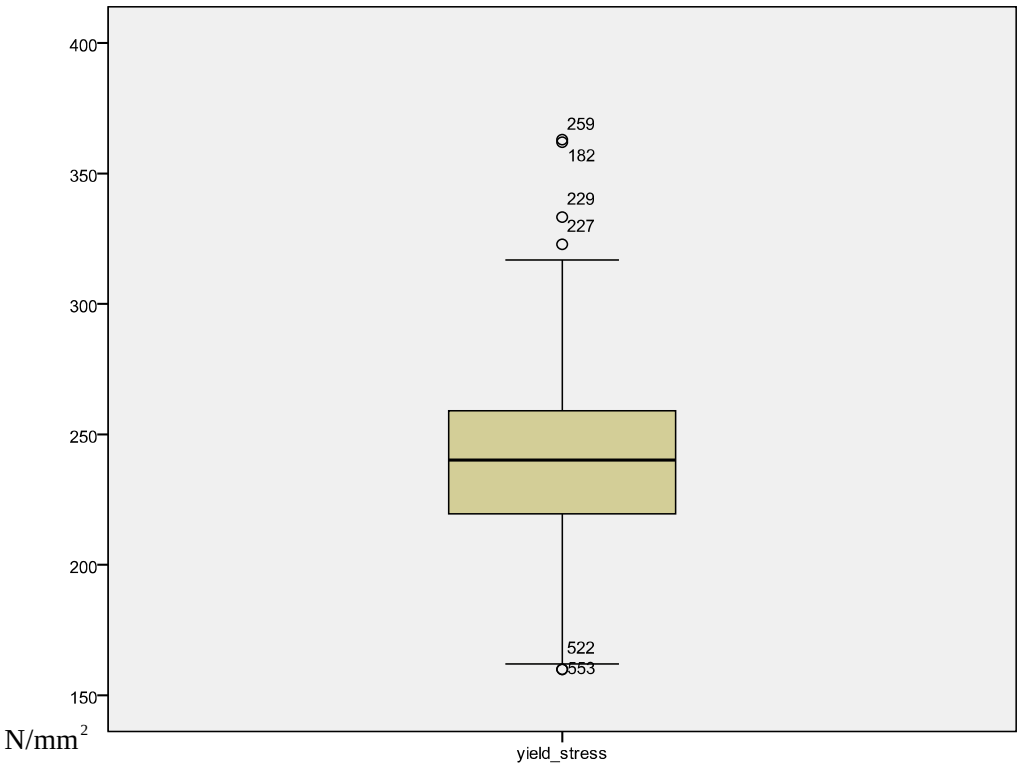

Figure 2.13 Boxplot of yield strength test data, along grain direction (O'Sullivan 2012).

2.3 (d) Effect of plate thickness on mechanical properties

The data indicates that there is no relationship between mechanical properties and plate thickness. This is illustrated in Figure 2.14 in the case of yield strength. The zero thickness data points in Figure 2.14 should be ignored as these values correspond to tensile tests in which the plate thickness was unknown. Considering a plate thickness of 10mm it is clear that the yield strength values vary widely. This is in contrast to the case of round bars illustrated in Figure 2.15 where thinner bars showed greater strength. In Figure 2.15 a series of bars of the same material but with diameters ranging from 50mm down to 10mm were tested in tension. The stress-strain graphs are staggered to show more clearly the reduction in yield strength with increasing diameter. The thinner bars have greater strength possibly because they experienced a greater amount of hot rolling which makes the ferrite grain sizes smaller and may also cause greater cohesion between grains (Johnson 1939)

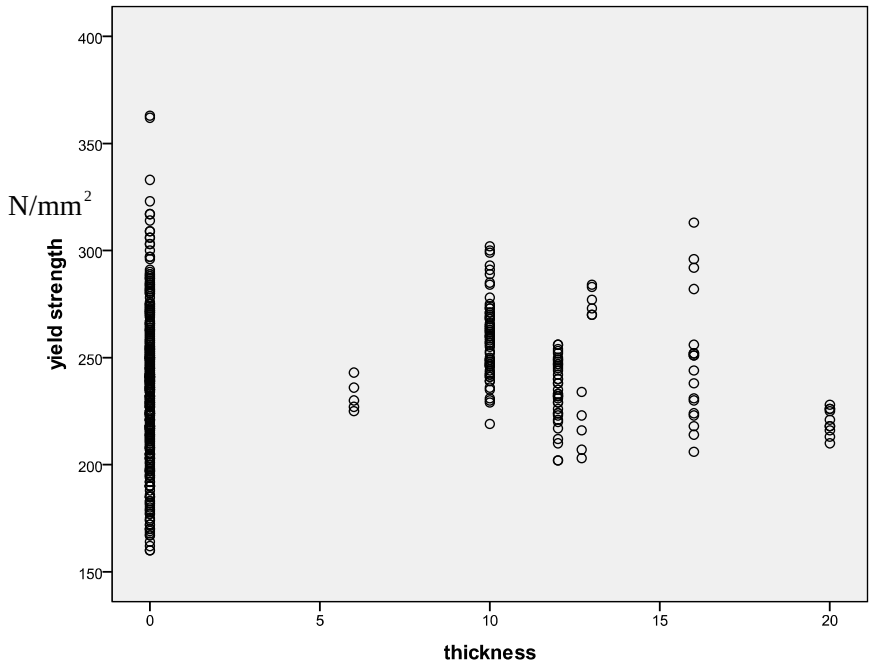

Figure 2.14 Plot of yield strength values against plate thickness for plate iron tested along grain direction (O'Sullivan 2012).

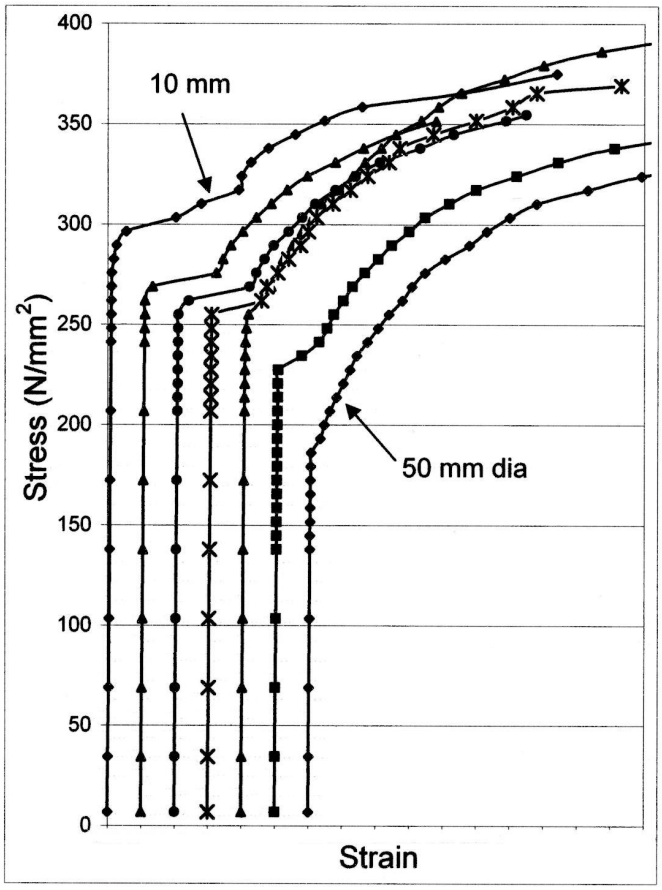

Figure 2.15 Stress-strain graph of 7 round bars with diameters 10mm, 13mm, 17mm, 23mm, 26mm, 39mm, and 50mm (Watertown Arsenal 1888)

2.4 Current assessment method for structural wrought iron

In the UK Highway Standard BD21/01 the partial factor of safety for material strength is given as γ_m =1.2. Therefore the assessment yield strength or assessment resistance, as it is referred to in BD21, is given by:

$$R^* = F_c.\frac{f_k}{\gamma_m} = \text{condition factor}.\frac{\text{characteristic yield strength}}{\text{material safety factor}} = F_c\,\frac{220\text{N/mm}^2}{1.2} = F_c(183\text{N/mm}^2)$$

One of the main problems with the current assessment method for wrought iron structures is that it applies a single strength value to a material which is known to have a highly variable strength. Wrought iron was manufactured to different grades and higher grades would have higher strength values. In addition, unlike steel, which followed a larger scale and more industrial manufacturing process, resulting in a more uniform product, wrought iron was made by hand using a craft scale process, which was more prone to greater variability of quality.

When assessing a structure often the origin of the iron is unknown, so that the grade and quality are unknown factors. As part of an assessment one may consider taking samples from the structure to provide information about that particular structure. The problem with this approach, apart from the obvious fact that some element of the historic structure must be sacrificed to provide the test material, is that the results cannot be relied upon to represent the entire structure, because wrought iron is such a variable material. In the absence of any sampling, under the current assessment method one is forced to apply a uniform characteristic strength of 220 N/mm^2 to the metal, as no adjustment to the material strength is provided, based on the component type or function of the component. This may lead to underestimating the strength of certain components with the consequence that they are judged to be unsafe.

Furthermore, by the examination of a body of test data, the characteristic yield strength value of 220 N/mm^2 given by BD21/01 can sometimes be found to be too high a value as was the case for the plate iron data examined by Cass Hayward. (See Table 2.4, where the characteristic yield strength for plate iron is given as 198 N/mm^2).

Data about the buckling resistance of wrought iron is rather limited, and so, engineers are forced to use strut curve data for steel to estimate the buckling resistance of wrought iron components. Tests on the compressive resistance of full size wrought iron columns were carried out at Watertown Arsenal in 1883 and 1884. (Cooper 1889 and Watertown Arsenal 1883-1893). These columns were of various form and built up from riveted angle, plate, and channel section.

As an assessment method plastic analysis of a structure is deemed unsafe for wrought iron due to the sometimes low ductility of the metal. This limits the choice of assessment methods to elastic analysis which may lead to further underestimation of the robustness of wrought iron structures.

Chapter 3 Testing wrought iron beams

3.1 Introduction

In total three beams were tested. The first was a rolled I-beam, made circa 1868, which had been used as part of the fireproof floor of the Royal Albert Hall (Steude 2000). It is shown in Figure 3.1. The second and third beams tested, were from the floor structure of the old Edinburgh Post Office, completed in 1866. These beams were of riveted plate and angle construction (see Figure 3.2). The Edinburgh beams had timber planks bolted onto the sides of the webs, which provided housing for timber floor joists. One of the Edinburgh beams was first tested with the timber attached and then tested again without timber.

.

Figure 3.1 Rolled beam segments from Royal Albert Hall (Photo by M.O'Sullivan 2008)

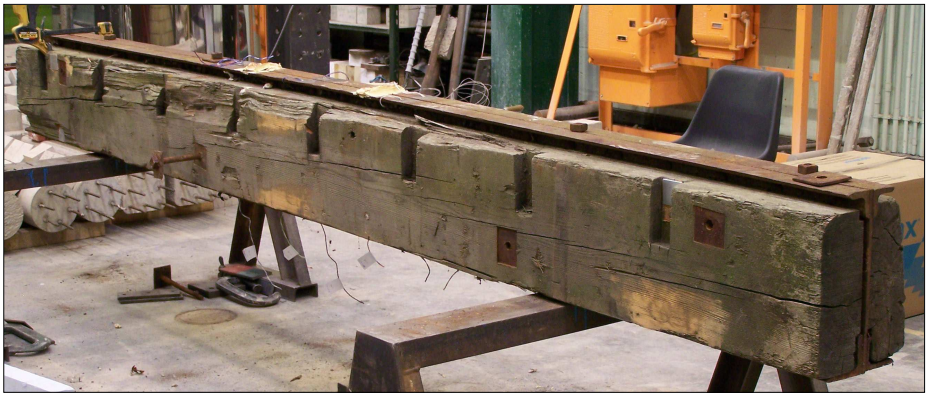

Figure 3.2 Built-up plate and angle flitch beam from Edinburgh Post Office. (Photo by M.O'Sullivan 2008).

3.2 Beam testing under a 4-point loading arrangement

The decision to employ a 4-point bending arrangement for both beams stemmed from the advantage of having two points of lateral frictional restraint of the top flange, as opposed to having only one in the case of a 3-point bend test. It was hoped that a greater degree of lateral restraint would hold off buckling of the top flange long enough to achieve yielding of the metal, and thus provide a more informative test of the beams behaviour under load. In a 4-point loading arrangement, the central region between load points experiences no shear force, and so, is in a state of pure bending, as shown in Figure 3.3. The principal tensile and compressive stress trajectories for a rectangular beam under this loading arrangement are shown at the bottom of Figure 3.3.

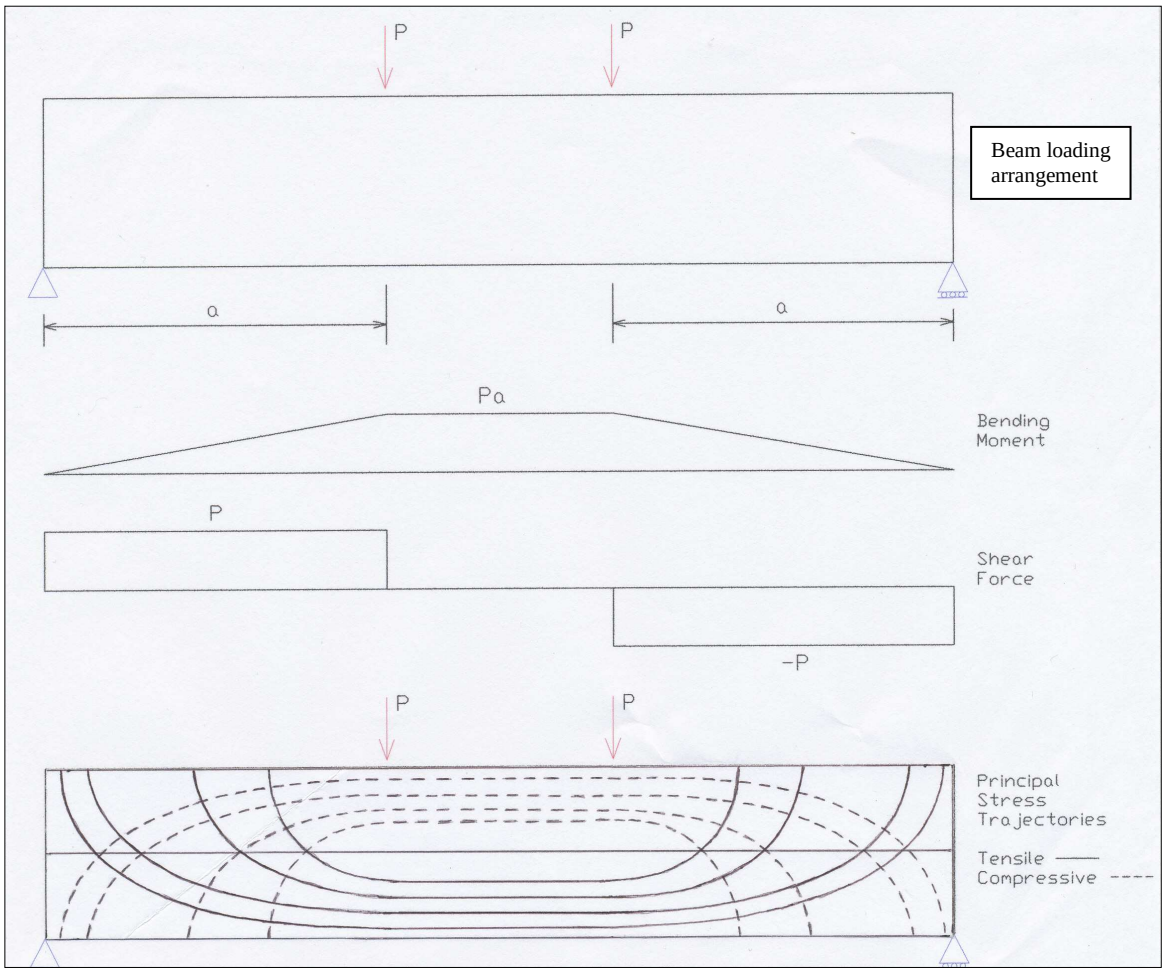

Figure 3.3 Stress trajectory diagrams for a rectangular beam (M.O'Sullivan 2009)

3.3 Beam testing equipment

The machine used to test the beams was a 2500kN Avery universal testing machine, shown in Figure 3.4. The loading plate (A) of the machine is fixed in position by locking it into 3 vertical posts. The machine operates by raising the base (B) at a constant rate so that when the beam encounters the loading plate it experiences load. The tests were conducted under displacement control, which means that the base of the machine and everything it carries rises at a constant rate regardless of whatever fluctuations in load occur between the beam and the loading plate. Sudden load fluctuations can occur during testing, when parts of the beam fail or at yielding of the material. Displacement control allows such load fluctuations to be measured and is particularly important when attempting to identify the yield point of the beam. In all the tests conducted the lifting rate was 0.03mm/s.

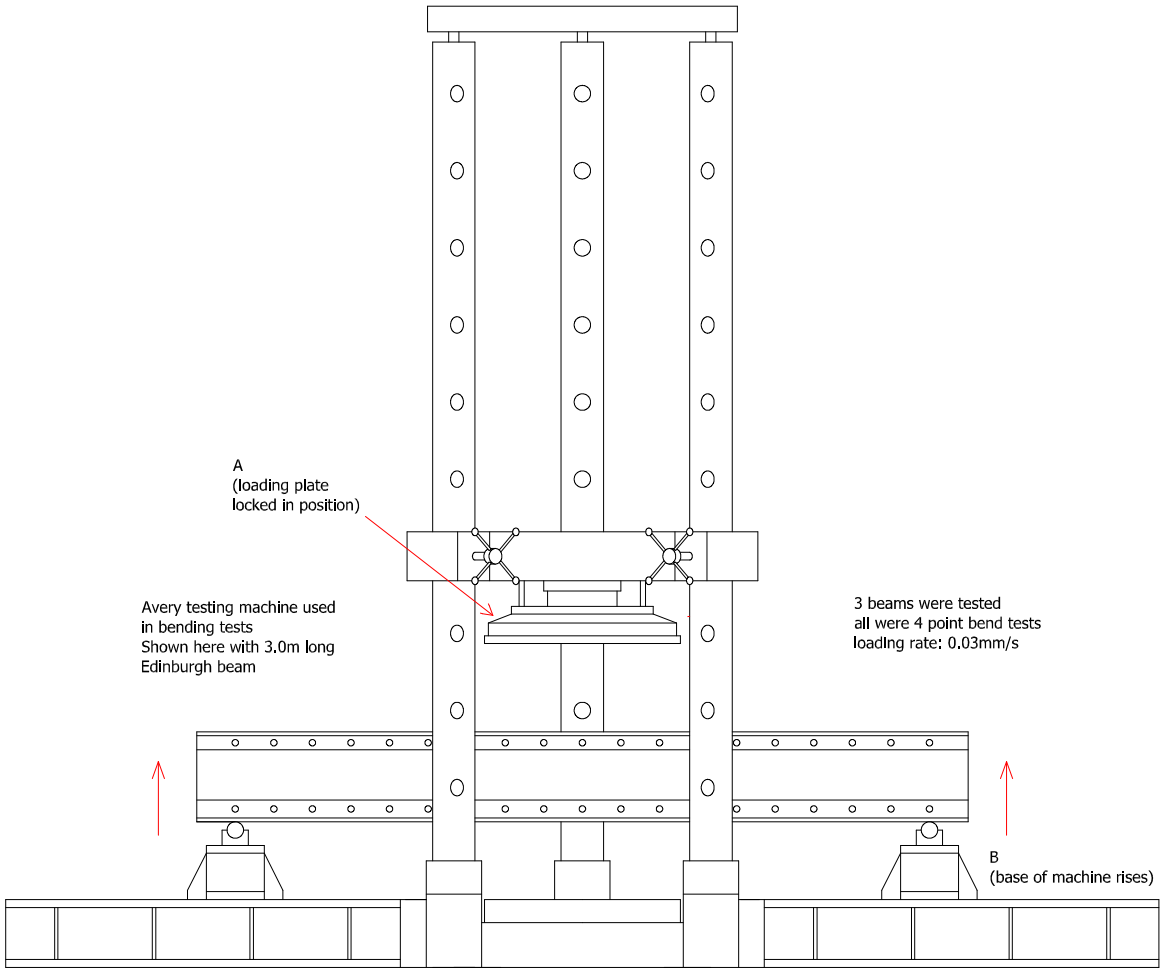

Figure 3.4 Avery Testing Machine used in beam tests. (M.O'Sullivan 2009)

3.4 Testing the Royal Albert Hall beam – Objectives

One of the Royal Albert Hall beams was tested by Steude as part of an earlier research project (see Steude 2000) and another beam of the same dimensions and source was tested as part of the present research project. It was decided to repeat the test performed during the previous research project using the same loading and span but with the exception of having a deliberate flaw in the beam. The flaw was a rounded notch at mid-span across the bottom flange, which was cut using a grinding wheel. The details of the notch are show in Figure 3.5. Such a blunt flaw can occur in structures, for example, by careless use of an angle grinder during refurbishment work. However, placement of the notch across the bottom flange, at mid-span, was chosen in order to encourage failure at this critical section. Therefore, the objective of the test was to investigate the effect of a flaw on strength and behaviour. The significance of the flaw is best seen by direct comparison with the results for the un-notched beam. Test results are compared in section 3.6.

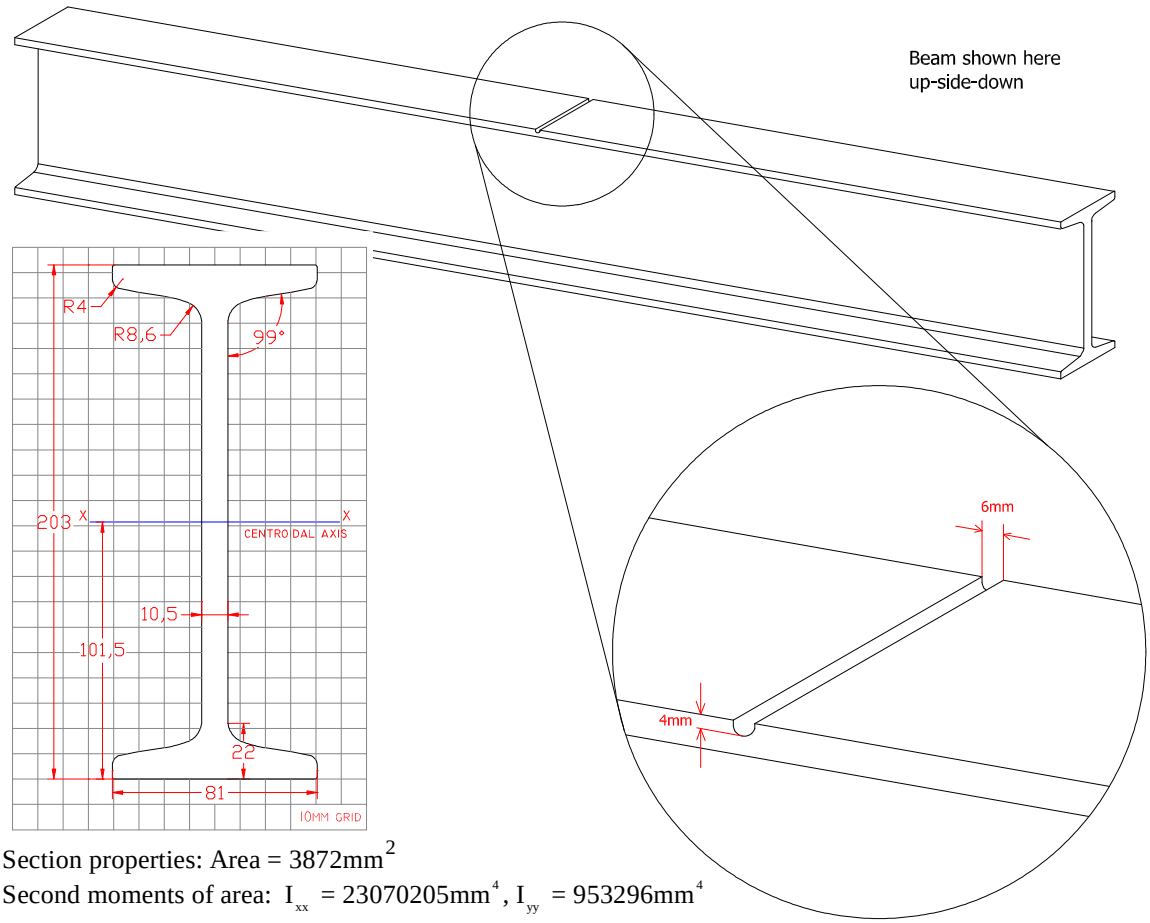

Section properties: Area = 3872mm^2
Second moments of area: I_{xx} = 23070205mm^4, I_{yy} = 953296mm^4

Figure 3.5 Albert Hall beam with machined notch across bottom flange. Shown here with beam up-side-down. Also section properties of intact beam section. All dimensions in mm.

Two tests were conducted. In the first the beam was loaded up to 90kN and then unloaded. In the second test the beam was loaded to failure. The purpose of the first test was simply to investigate the behaviour of the beam during loading within the elastic range.

Because the beam has an I shaped cross section the actual stress trajectories were somewhat more complicated than those depicted for the rectangular beam of Figure 3.3. Nevertheless, the stress trajectories shown in Figure 3.3 gave a starting point for the choice and arrangement of strain gauges. In order to determine the direction and magnitude of the principal stresses in regions of the beam experiencing both bending moment and shear force a rosette of 3 strain gauges was necessary. A calculation example of how this was done is given in section 3.10. For the region in pure bending, where the principal stresses are horizontal, a single horizontal strain gauge is all that was required. Deflection gauges were also placed at various points against the beam as shown in Figures 3.6 and 3.7. These deflection gauges are also known as linear potentiometers.

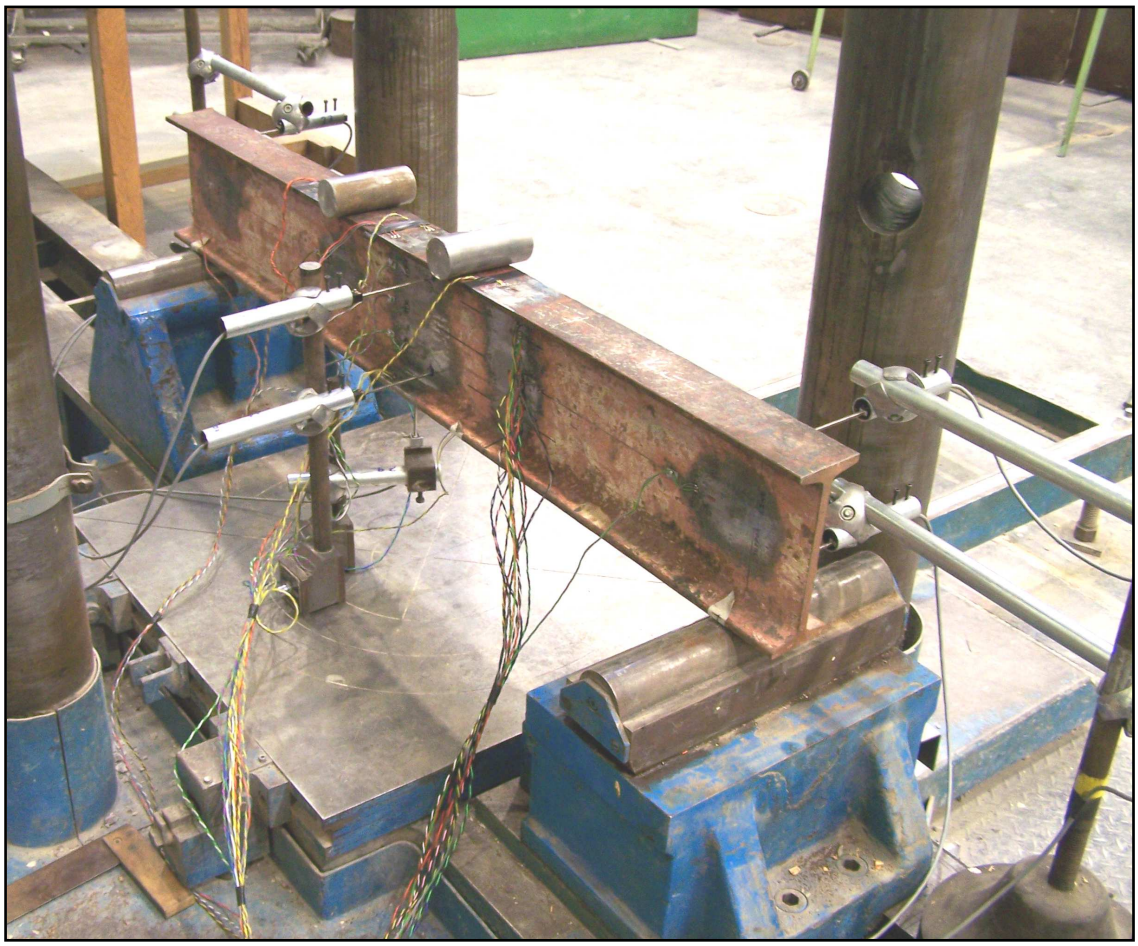

Figure 3.6 Loading and gauge arrangement for Albert Hall beam test. This picture shows the back elevation of the beam and can be compared directly with Figure 3.7. (Photo by M.O'Sullivan 2008)

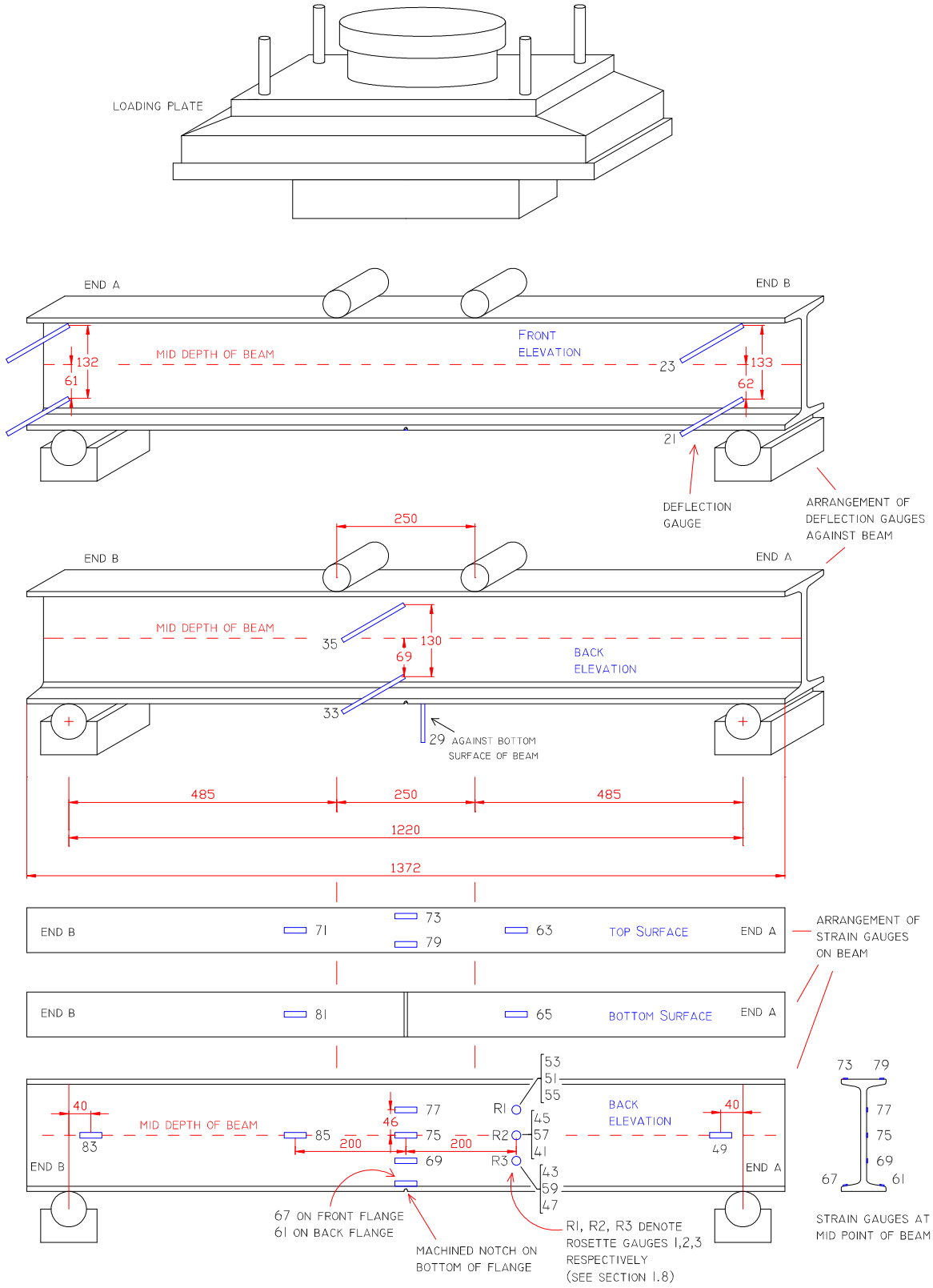

Figure 3.7 Loading and gauge arrangement for Albert Hall beam test. Numbers in black indicate gauge numbers. All dimensions in mm.

3.5 Results of bending test of Albert Hall beam – deflection behaviour

The first test of the beam involved loading it up to 90kN, which kept the beam within the elastic range. The load / vertical deflection diagram at mid-span is shown in Figure 3.8. The graph for the notched beam shows that it returned to its original position with no permanent strain. This confirms that the loading remained within the elastic range.

The un-notched beam also returned to its original position even thought the graph may indicate otherwise. The non-zero displacement value at the end of the unloading part of the graph for the un-notched beam was due to machine component settlement. The vertical displacement of the un-notched beam was recorded using machine displacement, whereas the displacement of the notched beam was measured directly with a deflection gauge placed against the underside of the middle of the beam. (i.e. gauge 29).

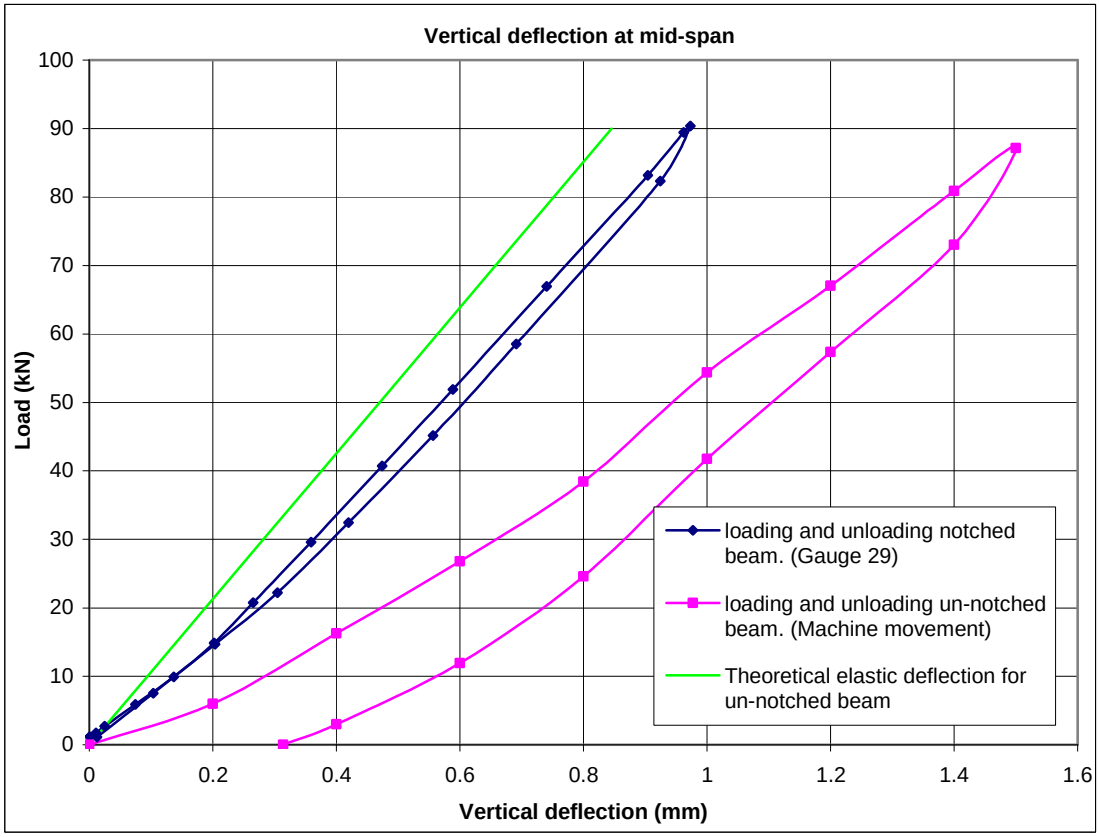

Figure 3.8 Vertical deflection of the middle of the beam (O'Sullivan 2008 & *Steude 2000)

The lateral deflections of the notched beam are summarised in Figures 3.9 and 3.10. The deflections were too small to be of visual significance. At the locations of the loading points there was considerable friction between the contact surfaces, which caused

resistance to lateral movement. This is demonstrated in Figure 3.9, where the maximum deflections are written onto the picture. For example, at end A the roller support restricted lateral movement of the lower part of the beam to only 0.1mm whereas the free upper part of the beam, at the same cross section, moved 2.0 mm laterally. The beam as a whole, exhibited a slight amount of twist but it was so small that to the naked eye the bending appeared to occur in the vertical plane.

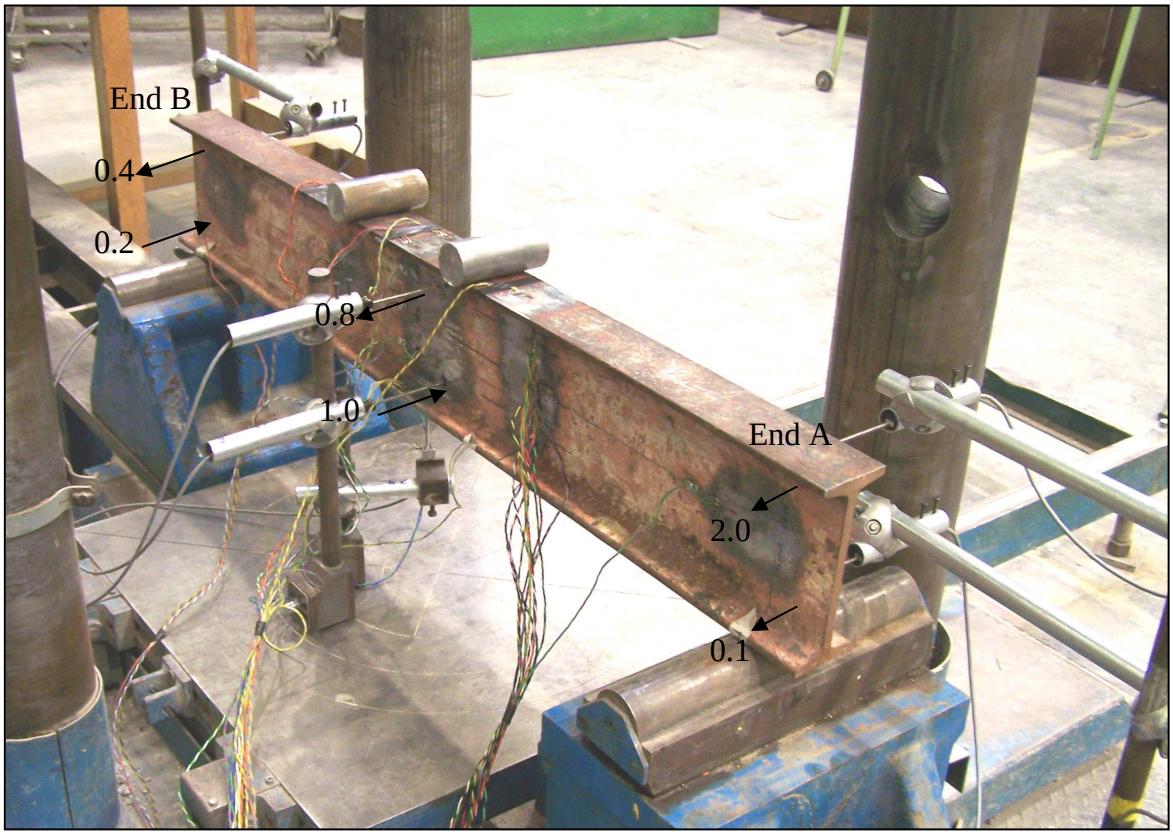

Figure 3.9 Loading arrangement of the Albert Hall beam test. Deflections noted are in mm and occurred under a load of 90kN.

In the present discussion, let the back elevation of the beam, which is shown in Figure 3.9, also be known as the left side of the beam. In Figure 3.10 deflections with a negative sign indicate movement toward the left. A positive deflection value means movement toward the right.

In the second test the beam was loaded all the way to failure. The load / vertical deflection diagram for this test is shown in Figure 3.11. Elastic behaviour was exhibited up to a load

of about 260kN, at point E in Figure 3.11. After that, the graph deviated from a straight line as the beam began to yield.

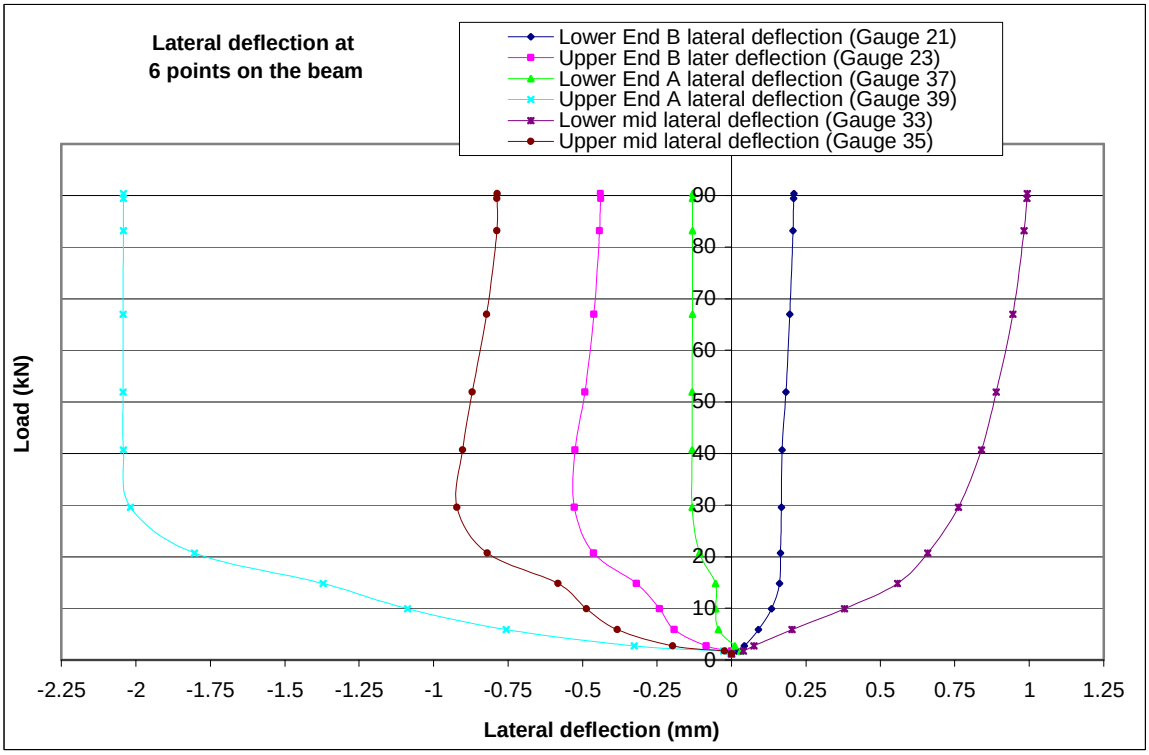

Figure 3.10 Lateral deflection readings for loading up to 90kN. (Loading within elastic range – Test 1)

However, quiet cracking sounds were heard from point E onward so it is unclear whether the metal was yielding or undergoing micro cracking. At point C, a very loud bang resembling a snapping sound occurred and a large crack was immediately apparent.

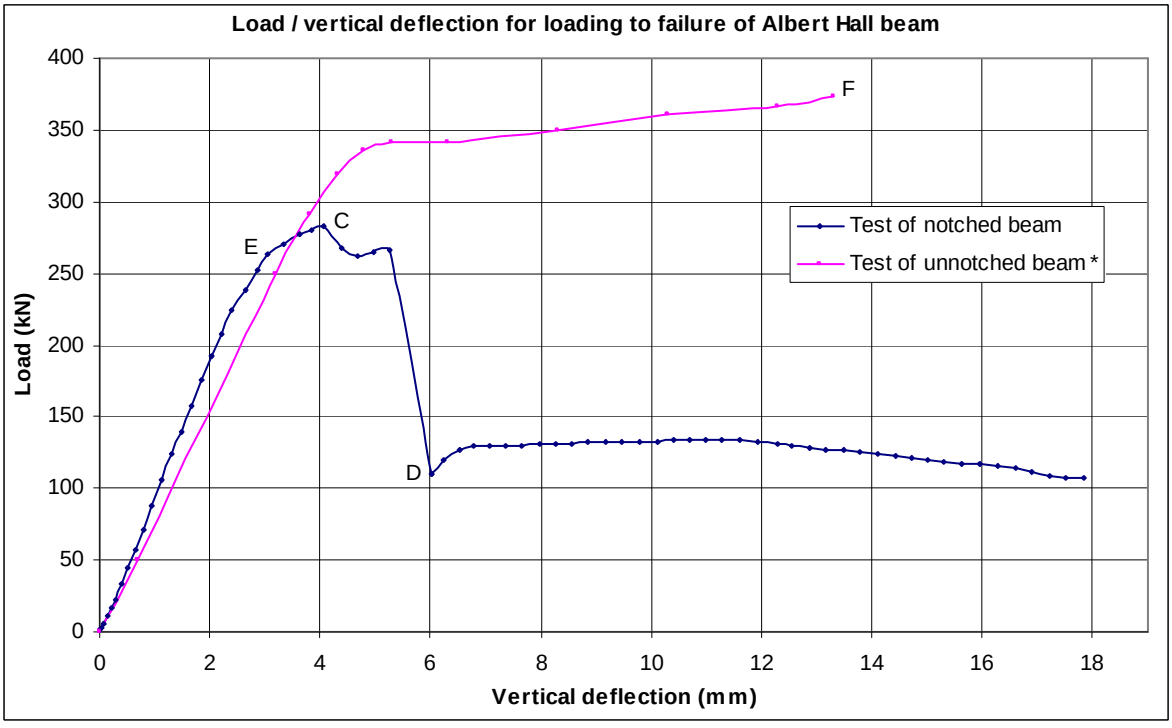

Figure 3.11 Vertical deflection of the middle of the beam (O'Sullivan 2008 & *Steude 2000)

The sharp fall in the graph at point C corresponds to the sudden cracking of the beam. At this point in the test, loading was halted so that the beam could be examined safely. The load at point C was 283kN, and may be taken as the ultimate breaking load for the notched beam. The collapse load for the un-notched beam was 373kN at point F in Figure 3.11. Thus, the effect of a 4mm deep blunt notch across the bottom flange was to reduce the beams ultimate load carrying capacity by 90kN. In addition, the un-notched beam exhibited linear elastic behaviour up to a load of about 320kN, some 60kN higher than the notched beam.

The crack in the notched beam, which appeared at point C, extended about 60mm up from the notch in the bottom flange, as shown in Figure 3.13. It is not known what arrested the crack. When the test was resumed (at point D in Figure 3.11), the beam began to carry an increasing load for a while. However, this behaviour was short lived as the crack slowly and steadily grew up through the web of the beam.

It is clear from the sudden cracking of the beam, under a slowly applied load, that the beam was quite brittle. However, the load-deflection graph for the un-notched beam suggests that beam possessed some degree of ductility. The reasons for brittleness in wrought iron are discussed in Chapter 1. One main possibility is rolling of the iron without being sufficiently hot, such that strain hardening occurs at the time of manufacture. The second possibility is chemical composition. Excessive quantities of phosphorus or carbon in iron cause brittleness.

For the second test of the notched beam the lateral deflection gauges at the ends of the beam were removed because they would yield little useful information, and it was likely that they would be damaged upon failure of the beam. The lateral deflection gauges at the middle of the beam were left in place for the test to failure and the results are illustrated in Figure 3.14.

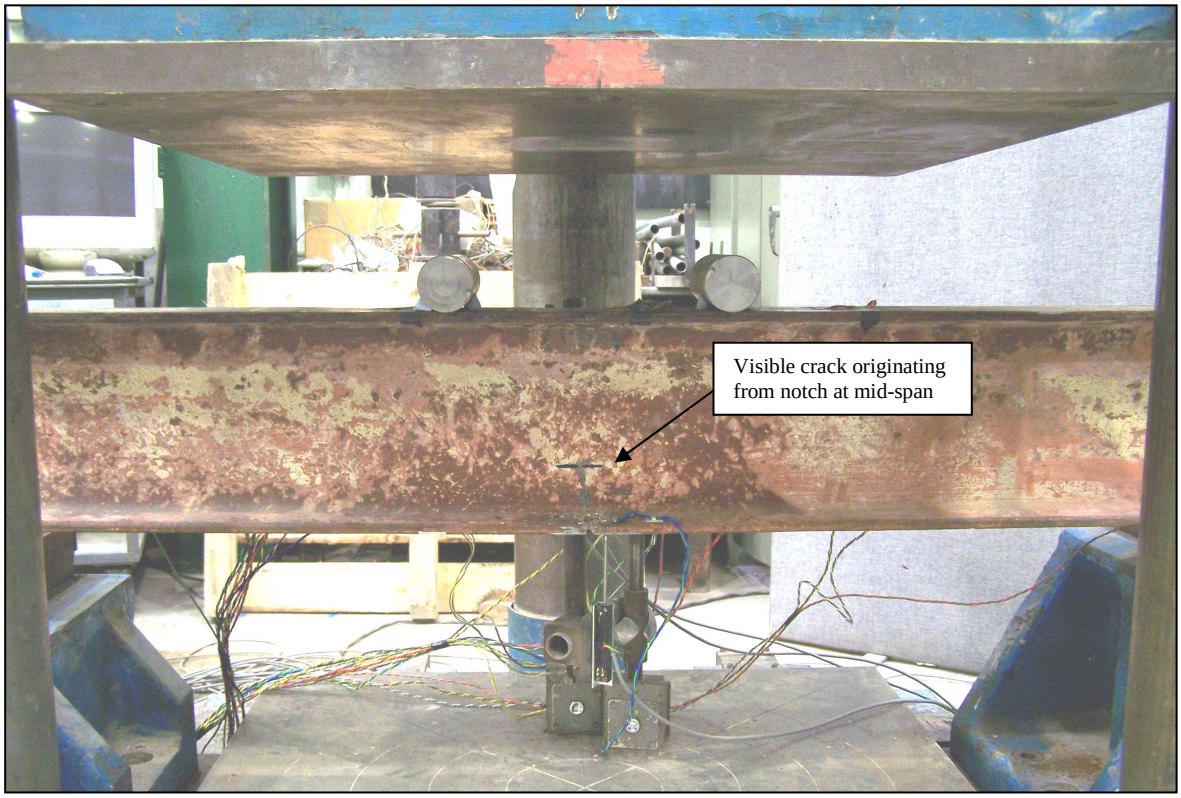

Figure 3.12 Notched beam after unloading following initial cracking at point C in Figure 3.11 (Photo by M.O'Sullivan 2008)

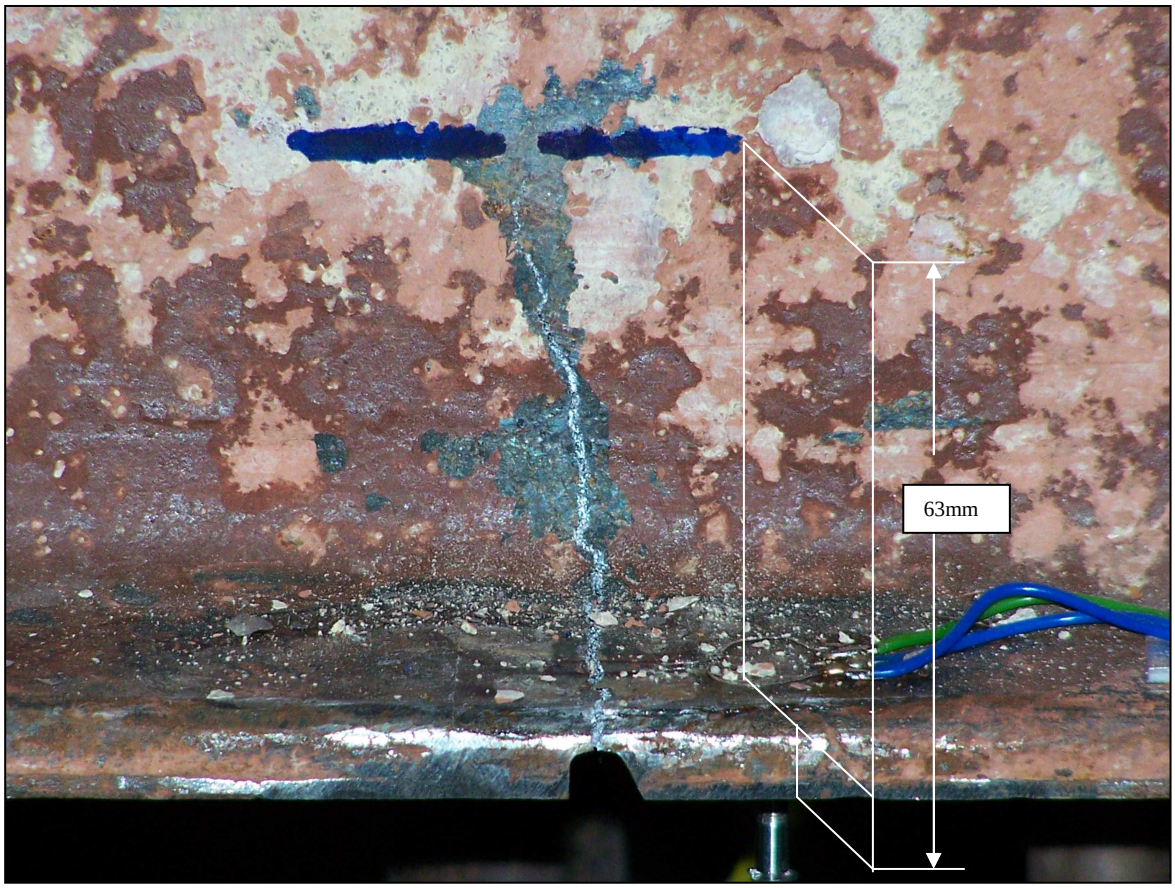

Figure 3.13 Close-up of crack in beam originating from blunt notch. (Photo by M.O'Sullivan 2008)

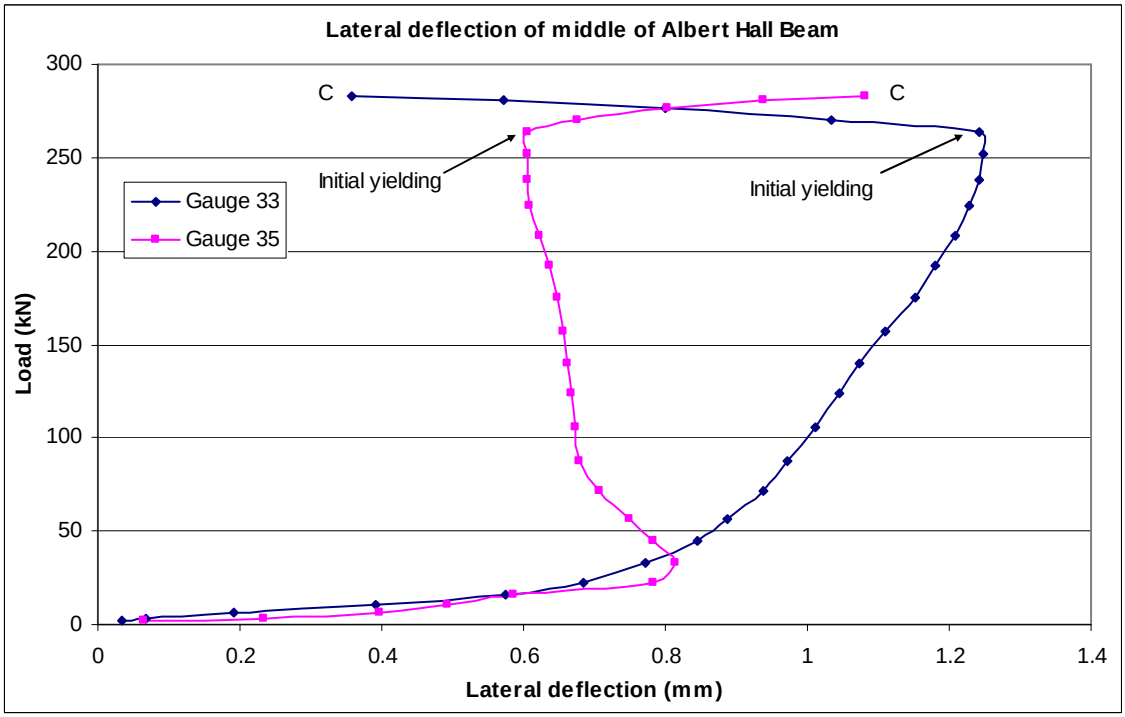

Figure 3.14 Lateral deflection of the middle of the beam up to the point of sudden cracking at point C.

The graph in Figure 3.14 shows the lateral movements of the middle of the beam up to the point at which the beam suddenly cracked at point C. Both the upper and lower parts of the beam moved to the right, which means that there was little or no twist. At this cross section the free lower part of the beam moved outward slightly more than the upper part, which was partially restrained by the two nearby roller load points in contact with the upper flange. A maximum outward movement of 1.2mm occurred at the point of initial yielding, and the beam moved back as yielding progressed. It is clear that these lateral deflections were quite insignificant and loading to failure occurred within the vertical plane. Sighting the beam along its length during the test confirmed this.

3.6 Results of bending test of Albert Hall beam – strain measurements

Four strain gauges were fixed to the flanges of the beam at mid-span. These are shown in Figure 3.15. Two strain gauges were placed on the outer top surface of the beam and two gauges were fixed to the lower flange just above the notch. For the test to failure the load / strain diagram for these gauges is shown in Figure 3.16.

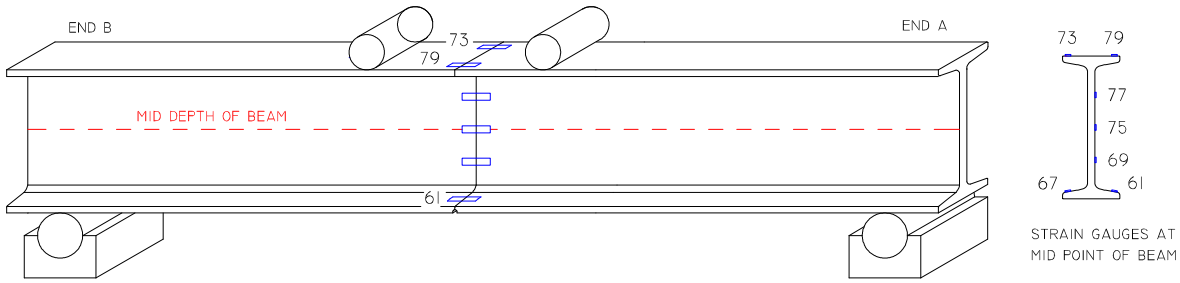

Figure 3.15 Back of beam showing placement of strain gauges. Gauges are numbered as shown. The load / strain diagrams for these gauges are shown in Figure 7.16 (M.O'Sullivan 2009)

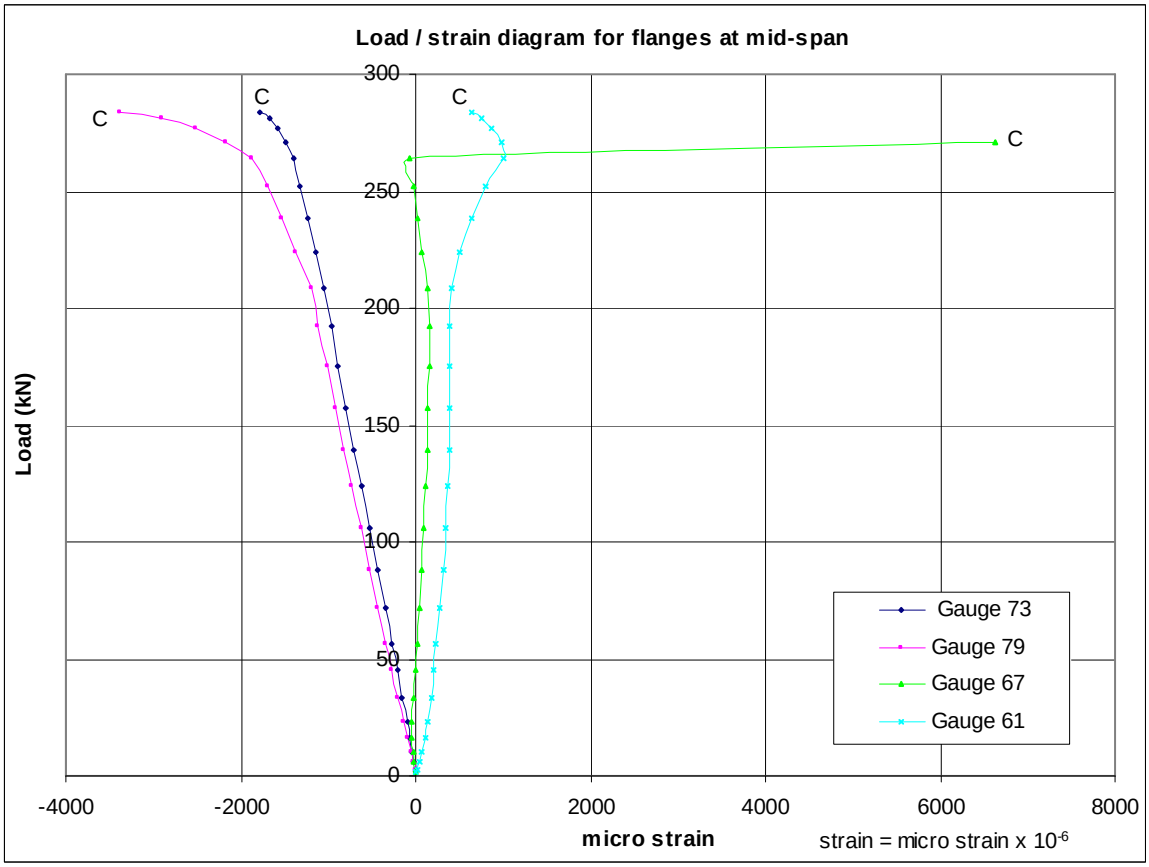

Figure 3.16 Load / strain diagram for flanges at mid-span up to the point of sudden cracking at point C.

The gauges on the top flange experienced compression while the gauges on the bottom flange experience predominantly tension. The graph in Figure 3.16 shows strain gauge readings up to the point of sudden cracking of the beam at point C. At that point the strain gauges on the bottom flange were torn apart. In the graph of Figure 3.16 these gauge readings appear somewhat inconclusive. In particular, gauge 67 appears to fluctuate between tension and compression and ultimately shows relatively significant tension. The reason for such fluctuations was possibly due to the stress concentration just above the notch. For this reason it might be best to disregard the readings in this area and look at the

top flange gauge readings as being more indicative of the true strain variations during loading of the beam. These upper flange gauges continued to give readings after sudden cracking of the lower part of the beam. The strain readings to the point of complete failure are shown in Figure 3.17.

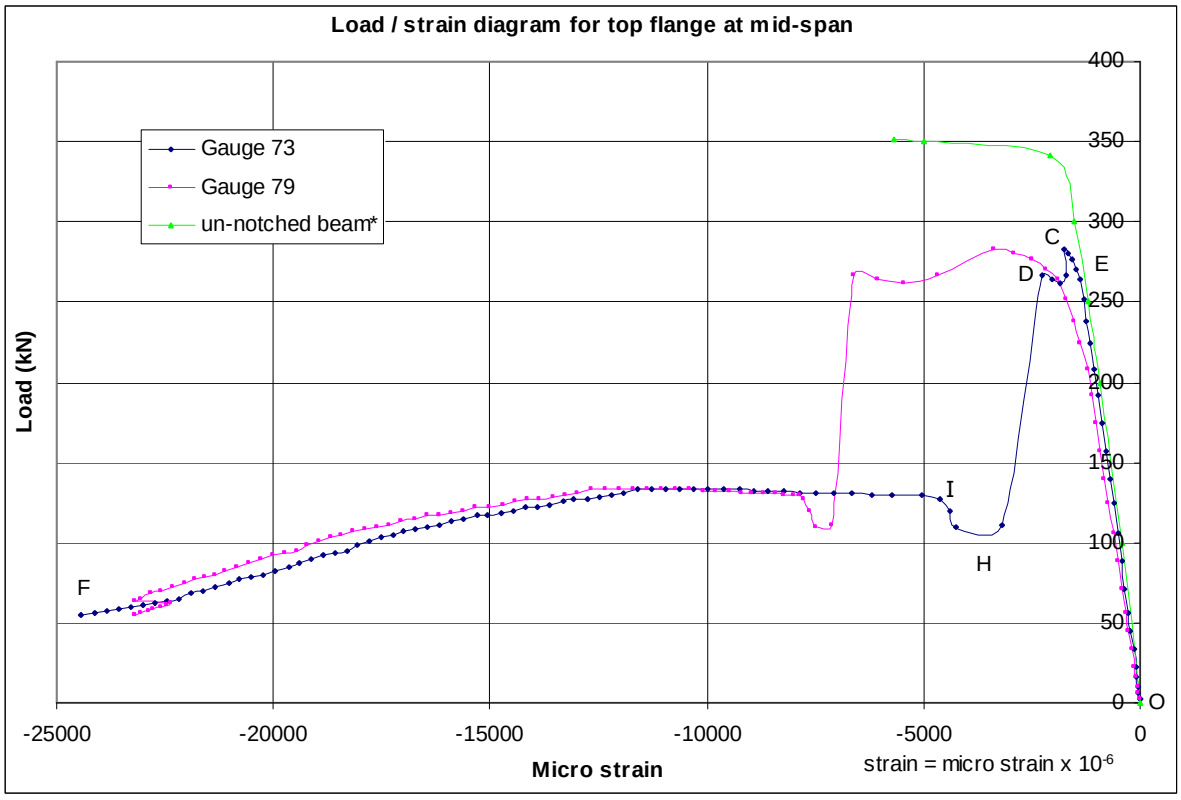

Figure 3.17 Complete load / strain diagram for the top surface of the upper flange at mid-span. Loading occurred by raising the beam at a constant rate of 0.03mm/s = 1.8mm/min. (O'Sullivan 2008 & *Steude 2000)

Both graphs for the notched beam show similar behaviour. One appears to be a horizontally stretched version of the other, indicating that one side of the flange experienced slightly more strain than the other. This is possibly due to a slight lateral movement of the flange. However, any lateral movement was too small to be of any significance. The graphs can be separated into a number of regions of different behaviour. Consider the graph for gauge 73. The first region shows elastic loading up to about 260kN. This is the straight section of the graph from O to E which occurred over a time period of 3.5 minutes. The second region (E to C) where the graph deviates from a straight line involved yielding of the beam material. This period of yielding took place over 40 seconds. When the load reached 283kN at point C, the beam suddenly failed with a visible crack

measuring 60mm in length, which originated from the notch as shown earlier in Figure 3.13. It is not known what arrested the crack but at this point the mid section of the beam effectively became a T-section. Despite the crack, the remainder of the beam section still had some capacity to carry load. The portion of the graph from C to H took place over 50 seconds and appears to contain regions of plasticity and strain hardening. The flatter portion may represent a region of plastic flow whereas the upturn at point D may indicate strain hardening. There is a more significant upturn at point I where the beam appears to have recovered some load carrying capacity. This is probably due to strain hardening of the material. However, while this was happening to the top surface of the beam the crack steadily grew up through the web. The time period for this crack growth which began at point C and ended at point F was 12 minutes. Table 3.1 summarises the different stages of the beam test.

Region of graph in Figure 3.17	Beam behaviour	Duration	Time from start of test (min:sec)
0 to E	Elastic loading. linear load/ displacement behaviour.	3min 30sec	0:00 – 3:30
E to C	Yielding of mid-section of beam. Graph deviates from linear behaviour. Reaches max load of 283kN.	40 sec	3:30 – 4:10
C to D	Sudden crack at load 283kN followed by a small amount of strain hardening.	40 sec	4:10 – 4:50
D to H	Fall in load carrying capacity because of sudden crack extension. Crack becomes clearly visible. 63mm long.	10 sec	4:50 – 5:00
H to I	Some plastic flow and strain hardening leading to small and short-lived gain in load carrying capacity.	20 sec	5:00 – 5:20
I to F	Extensive region of steady crack growth. Loss in section ultimately leading to loss in load carrying capacity. Crack wide open at end of test.	10min 50sec	5:20 – 16:10
	Total time of test:	16 min. 10 sec.	

Table 3.1 Summary of different stages in test of notched beam.

As part of a previous academic project (Steude 2000), the load / strain diagram for the top flange of the un-notched beam was determined for the same loading arrangement. This has been included in Figure 3.17 for comparison with the notched beam. The graphs in Figure 3.17 show that the strain behaviour of both the notched and un-notched beams was very

similar during the regions of elastic loading and yielding. However, the effect of the notch was to reduce the ultimate failure load from 373kN in the case of the un-notched beam to 283kN for the notched beam. In addition, the notched beam failed at a lower value of strain and without any appreciable degree of plastic flow, and there was no warning of imminent collapse in terms of visual deflection, prior to the appearance of the large crack at point C. Complete collapse did not occur when the beam suddenly cracked, but the beam's load carrying capacity was diminished by more than half its original value. The reason complete collapse did not occur was because the loading machine was under displacement control. In other words, the machine raised the beam at a constant rate regardless of whatever cracks or load fluctuations occurred. When the beam cracked there was a reduction in applied load because the beam suddenly deflected. Therefore, the load did not remain at a high level sufficient to finish off the collapse. If, for example, the collapse load had been applied by some heavy object placed on top of the beam, then it would have completely collapsed. Therefore, as a structural member the initial sudden crack can be taken as the terminal failure point of the beam, even though in the bending test it was still partially intact at that point.

Figure 3.18 Notched beam at end of test showing crack through almost entire mid-span section. (Photo by M.O'Sullivan 2008)

3.7 Examination of crack growth and fracture surface of Albert Hall beam.

After the initial sudden cracking of the beam the test was halted and the beam was unloaded so that the cracked beam could be examined safely. Before resuming the test a movement gauge was fixed horizontally across the crack, as shown in Figure 3.20. This movement gauge had only a 10mm working range but it was sufficient to produce the load / displacement graph shown in Figure 3.21.

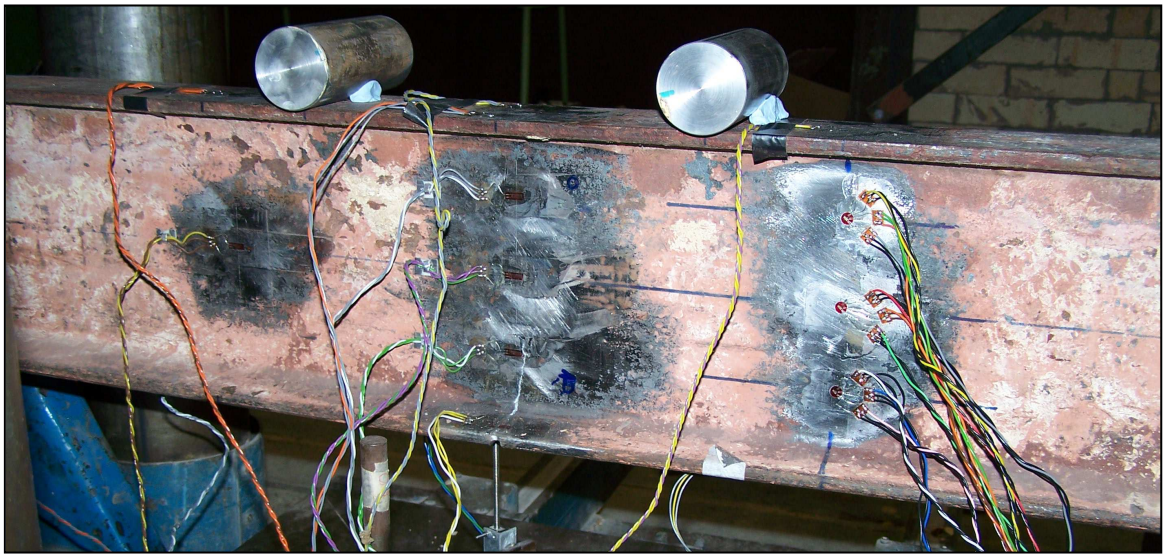

Figure 3.19. Back of beam with crack originating from notch in bottom flange at mid span. (Photo by M.O'Sullivan 2008)

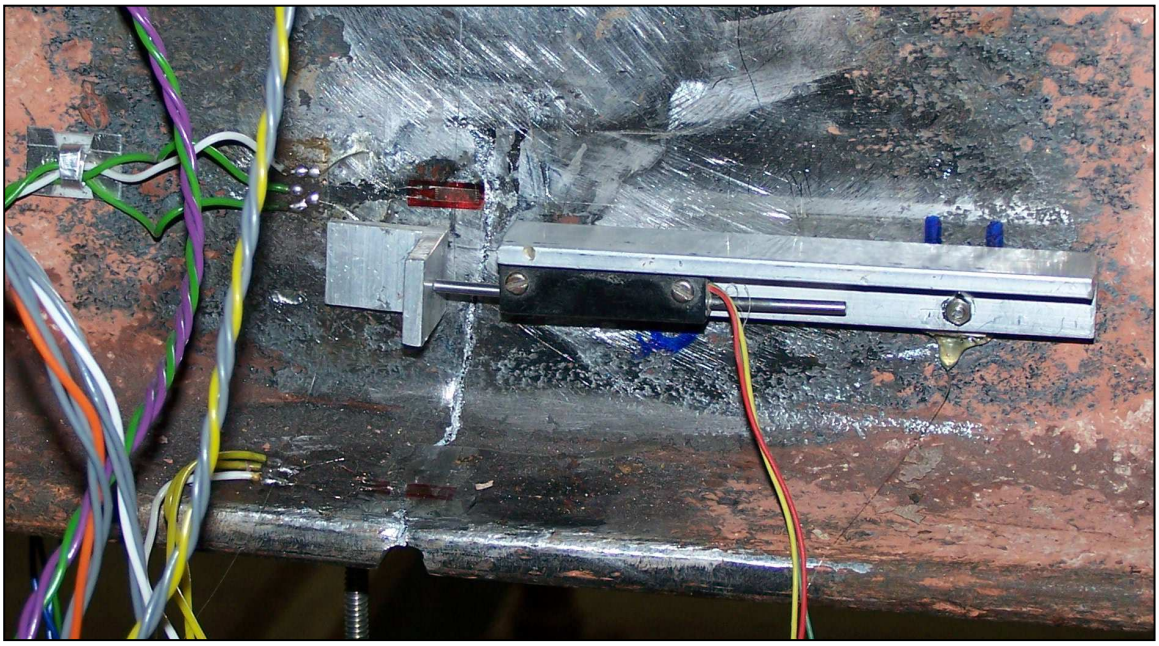

Figure 3.20 Movement gauge fixed across crack to measure crack opening displacement as load is applied. (Photo by M.O'Sullivan 2008)

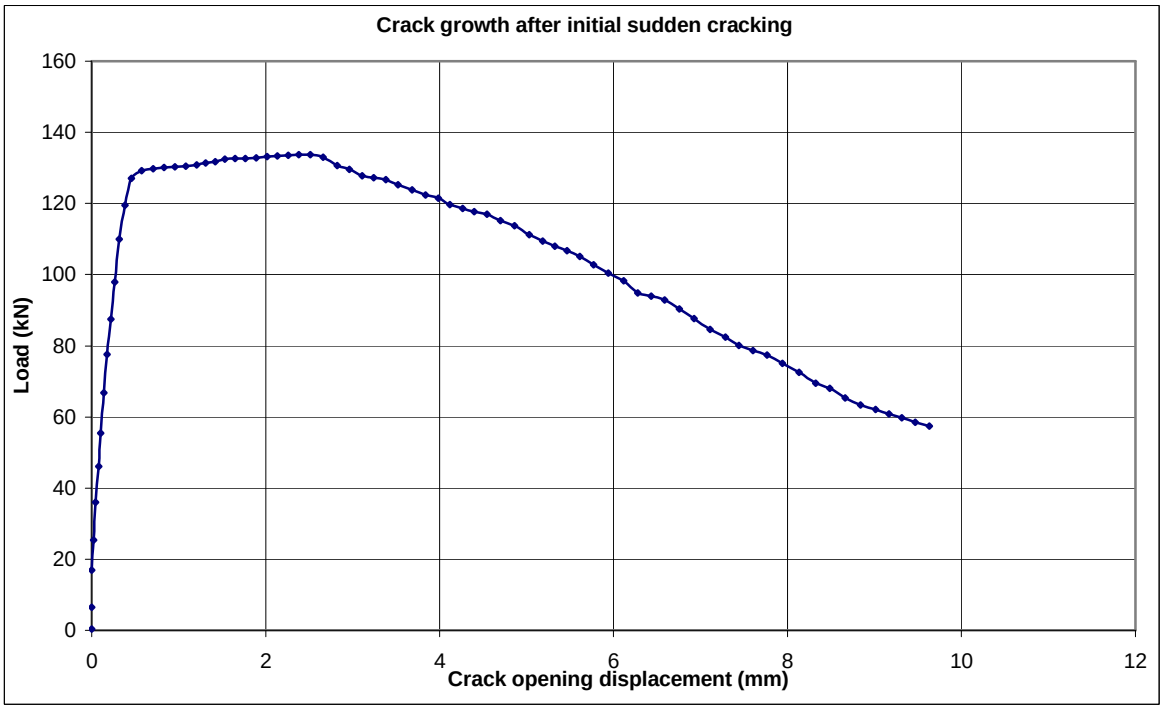

Figure 3.21 Load / crack opening displacement diagram for reloading of beam after initial sudden cracking. This graph was produced by the movement gauge shown in Figure 3.20

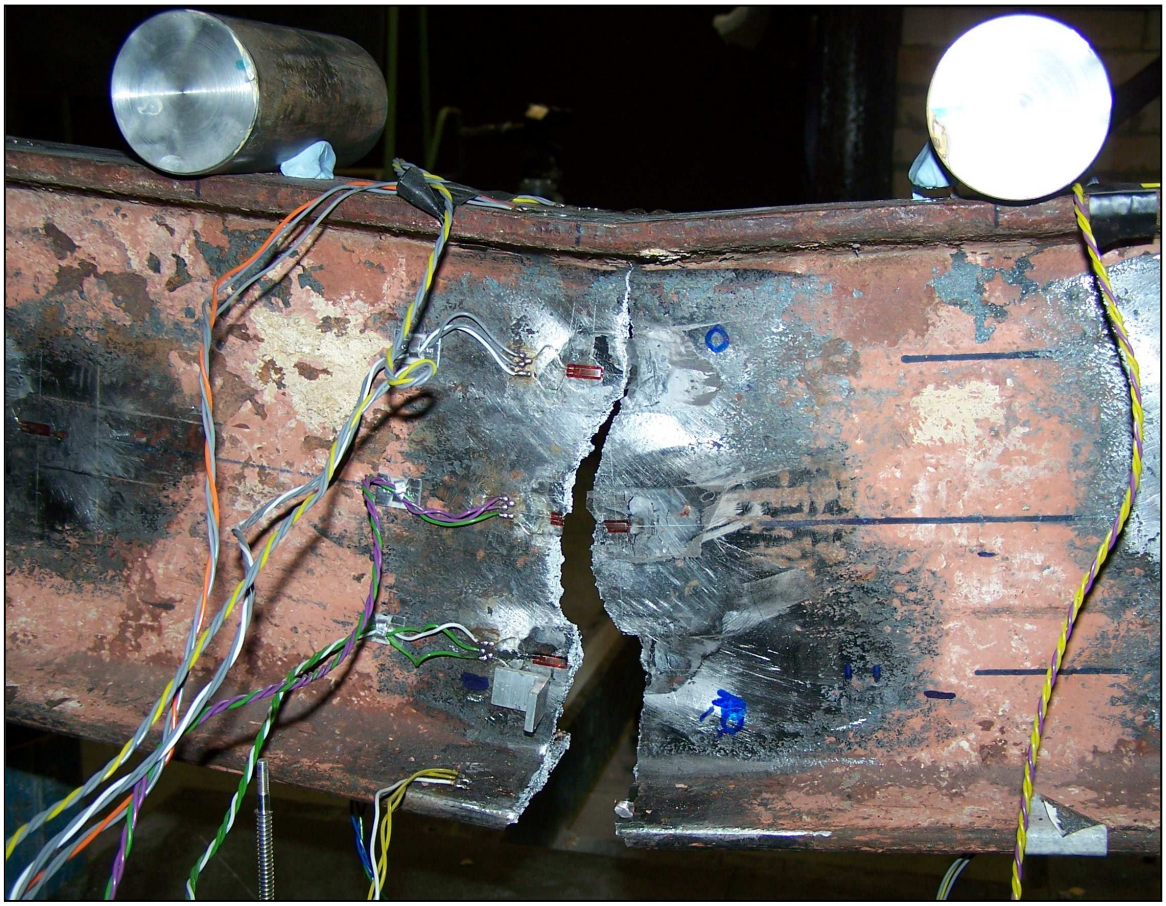

Figure 3.22 Beam at end of test showing extent of crack growth. (Photo by M.O'Sullivan 2008)

The graph in Figure 3.21 shows that as the beam was reloaded after initial cracking the crack did not open very much until the applied load reached about 130kN. This corresponds to point I in Figure 3.17 and indicates the point where the crack growth

resumed. It also indicates the ultimate load carrying capacity of the cracked beam, that is, its capacity just after initial sudden cracking at point C in Figure 3.17.

When the bending test was finished the beam was removed from the testing machine and taken to the saw so that the fractured portion could be cut away and later examined under the microscope

Figure 3.23 Broken beam after removal from testing machine (Photo by M.O'Sullivan 2008)

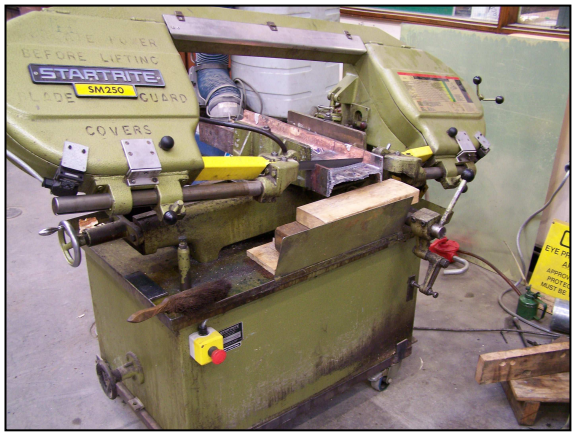

Figure 3.24

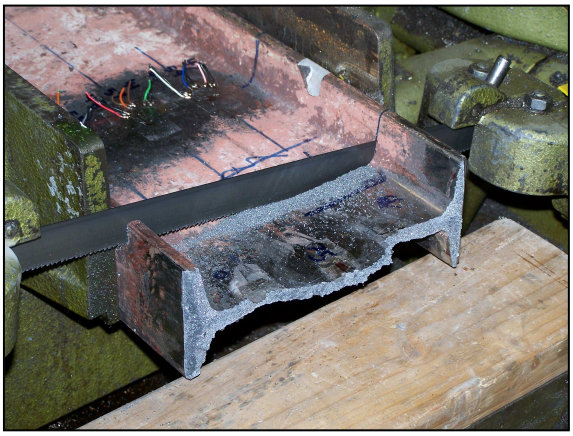

Figure 3.25

Fractured portion of beam being cut off using a band saw. (Photos by M.O'Sullivan 2008)

Figure 3.26

Figure 3.27

Fractured portions of beam (Photos by M.O'Sullivan 2008)

To the naked eye the appearance of the fracture surface varies from predominantly shiny and faceted around the flange areas to dull and fibrous in the central web area.

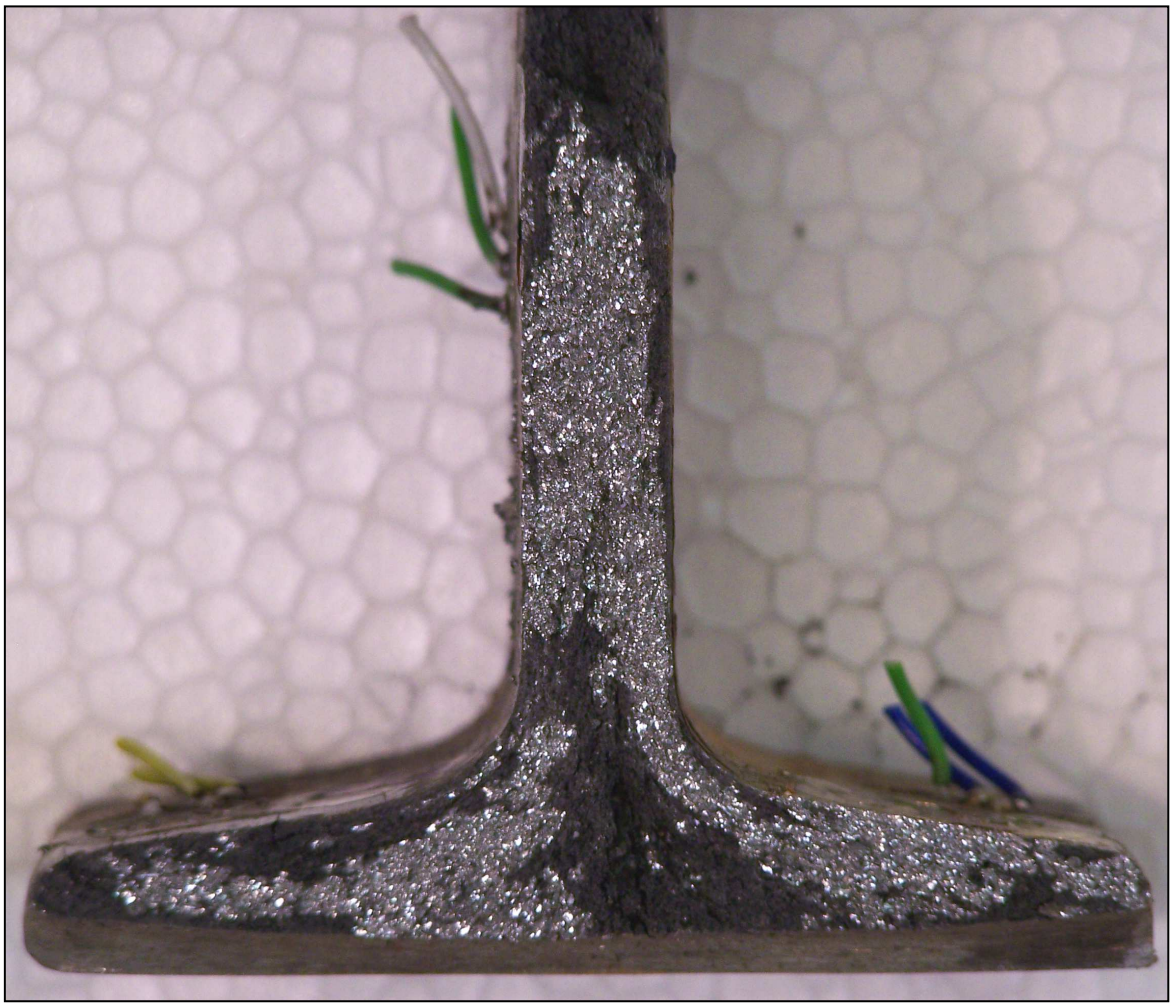

Figure 3.28 Fracture surface of beam at bottom flange area, with predominantly shiny and faceted appearance. The machined groove in the flange can also be seen at the bottom of the picture. (Photo by M.O'Sullivan 2008)

Examination of the fracture surface under an optical microscope did not produce a useful image because of the irregularity of the surface. The best image that could be achieved is shown in Figure 3.28, which was taken with an ordinary digital camera. It is not clear why the fracture surface has regions of two such different appearances. It is possible that the shiny and faceted fracture regions resulted from cleavage of the metal across the metal grains, whereas the dull fibrous appearance resulted from a fracture that followed an inter-granular path through the metal. That is, the dull appearance may have been caused by the metal tearing apart along grain boundaries, instead of across the grains. One possible reason for this may be that the metal comprising the web had less cohesion between the individual grains.

In wrought iron, sulphur is present as iron sulphide (FeS), but it tends to segregate from the ferrite at the grain boundaries. Because iron sulphide has a low melting point, it causes a lack of cohesion between the grains when the iron is heated to a red-hot temperature (Johnson 1939). This is the cause of red-shortness in wrought iron, the condition where the metal cracks or crumbles when being hot worked. It may be possible that the metal from which the beam was made was red-short to some degree. Even though red-shortness only becomes apparent when the metal is red-hot, lack of cohesion during rolling may have caused some lack of cohesion between the grains when the metal was cold. This lack of cohesion may not be apparent on the metal surface but destructive tests such as those described in Section 2.1 could reveal a low quality metal. It is not clear why the web of the beam would suffer from a greater degree of red-shortness that the flanges.

Tensile tests conducted on plate and angle iron from the Edinburgh GPO beams revealed a dull fibrous fracture surface very similar to the dull fracture surface of the Albert hall beam, and in most of those tensile tests the ductility was quite low (< 10% elongation at failure). This would suggest that the Albert hall beam metal was brittle.

Tensile tests conducted during previous research on the Albert Hall beam metal gave a mean ductility of 12.1% elongation at failure from 7 tests of the web metal and 15.5% elongation at failure from 8 tests of the flange metal (Kontos 1996 & Steude 2000). This suggests that the flange metal was more ductile than the web metal.

Regardless of the tensile tests results and of the two different appearances of the fracture surface of the beam, it is certain that the beam failed in a brittle manner. If a modern steel beam had been tested in the same way, it would have demonstrated significantly more plastic deformation before failure.

3.8 Results of bending test of Albert Hall beam – analysis of strain gauge data

The purpose of this section is to present a picture of the stresses and strains at two cross sections along the beam. Consider the cross sections shown in Figure 3.29, labelled Section 1 and Section 2. At Section 1 the beam experienced only bending moment and no shear force. In this region the principal stresses were horizontal. However, at section 2 the beam experienced both bending moment and shear force, so the principal stresses were not horizontal, and could only be determined by measurement of strains in three different directions.

For Section 2 strain gauges were placed on the beam at 5 points, labelled A,B,C,D and E. Single gauges A and E were positioned on the outer surfaces of the flanges. The rest were rosette gauges placed on the web. The rosette at point C was placed at what was expected to be the neutral axis, (i.e. the horizontal centroidal axis of the section). The stresses at each of these points can be pictured on stress elements as shown at (a) and (b) in Figure 3.29.

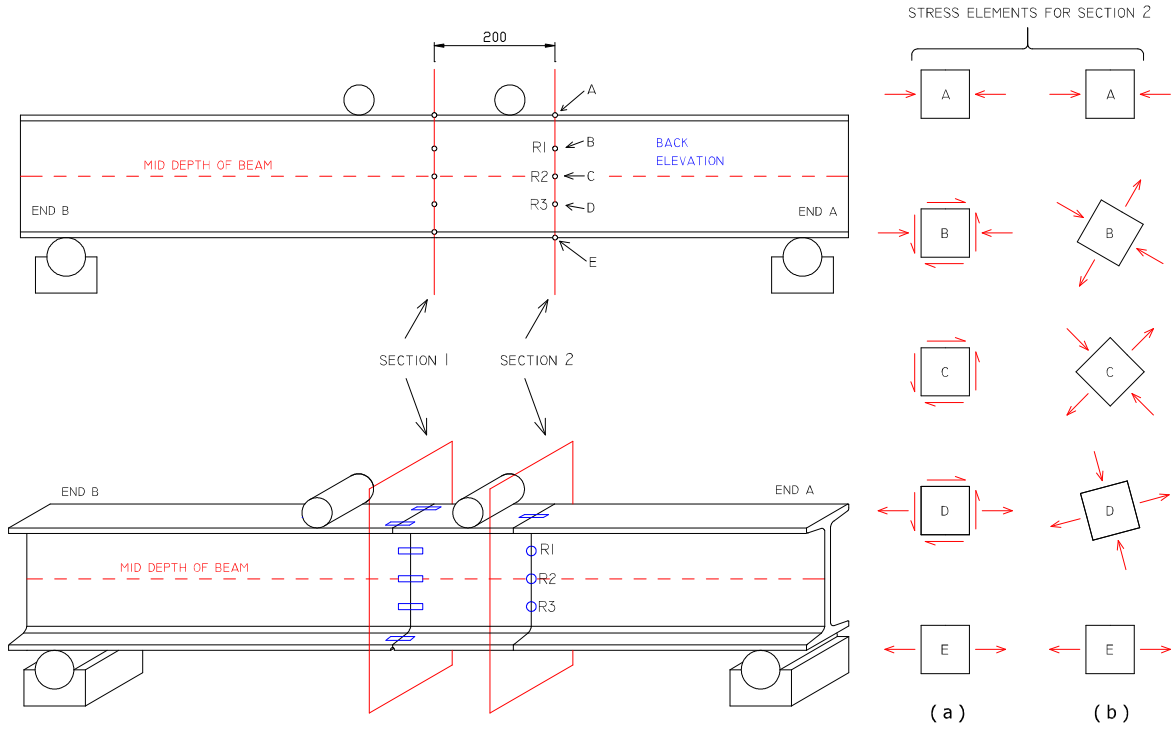

Figure 3.29 Strain gauges locations for examination of stresses and strains acting at two particular cross sections in the beam. (a) Normal and shear stresses acting on stress elements along section 2 at points A,B,C,D and E. (b) Principal stresses at these points. All dimensions are in mm.

The normal strains acting on cross sections 1 and 2 at various times during loading of the beam are shown in Figure 3.30. These strain graphs are linear up to a load of about 260kN. This linear elastic behaviour is in agreement with the load-deflection diagram of Figure 3.17. The strain graphs show that during elastic loading the neutral axis coincides with the horizontal centroidal axis of the beam, as expected for a symmetric section.

The stress distribution at cross section 2 for a load of 90kN on the beam is shown in Figure 3.31. The graphs separately show (D) the normal stresses, (E) the shear stresses, (F) the principal tensile stresses, (G) the principal compressive stresses and (H) the maximum shear stresses, acting on the cross section. The data for these graphs was derived using Mohr's circle of stress and Hooke's law, and was based on strain measurements. A calculation example of how this stress data was obtained is given in section 3.10. The normal strains and the principal tensile and compressive strains for cross section 2 under a total beam load of 90kN are shown at (A), (B) and (C) respectively.

In general the stress graphs (D) to (H) of Figure 3.31 follow expected patterns, however there are a number of unexpected features. It is instructive to compare these graphs with the ideal or expected stress graphs for a rectangular cross section of the same height, which are shown at (I) to (M) of Figure 3.31. The principal stress trajectories for a rectangular beam are shown at (K) in Figure 3.31. In (D) of Figure 3.31 the normal stresses follow a linear behaviour across the cross section, as expected from the strain diagrams. However, the shear stresses acting on the cross section, which are shown in (E) of Figure 3.31, do not appear to have a maximum value at the mid depth of the beam as was expected. The cause of this may be that section 2 is rather close to the load application point which would tend to distort the stress distribution from the ideal prediction. A finite element analysis was used to produce a stress contour view of the beam under a load of 90kN which is shown in Figure 3.32. This stress contour shows a higher stress region near the load application point which extends into the region where the strain was measured during the test.

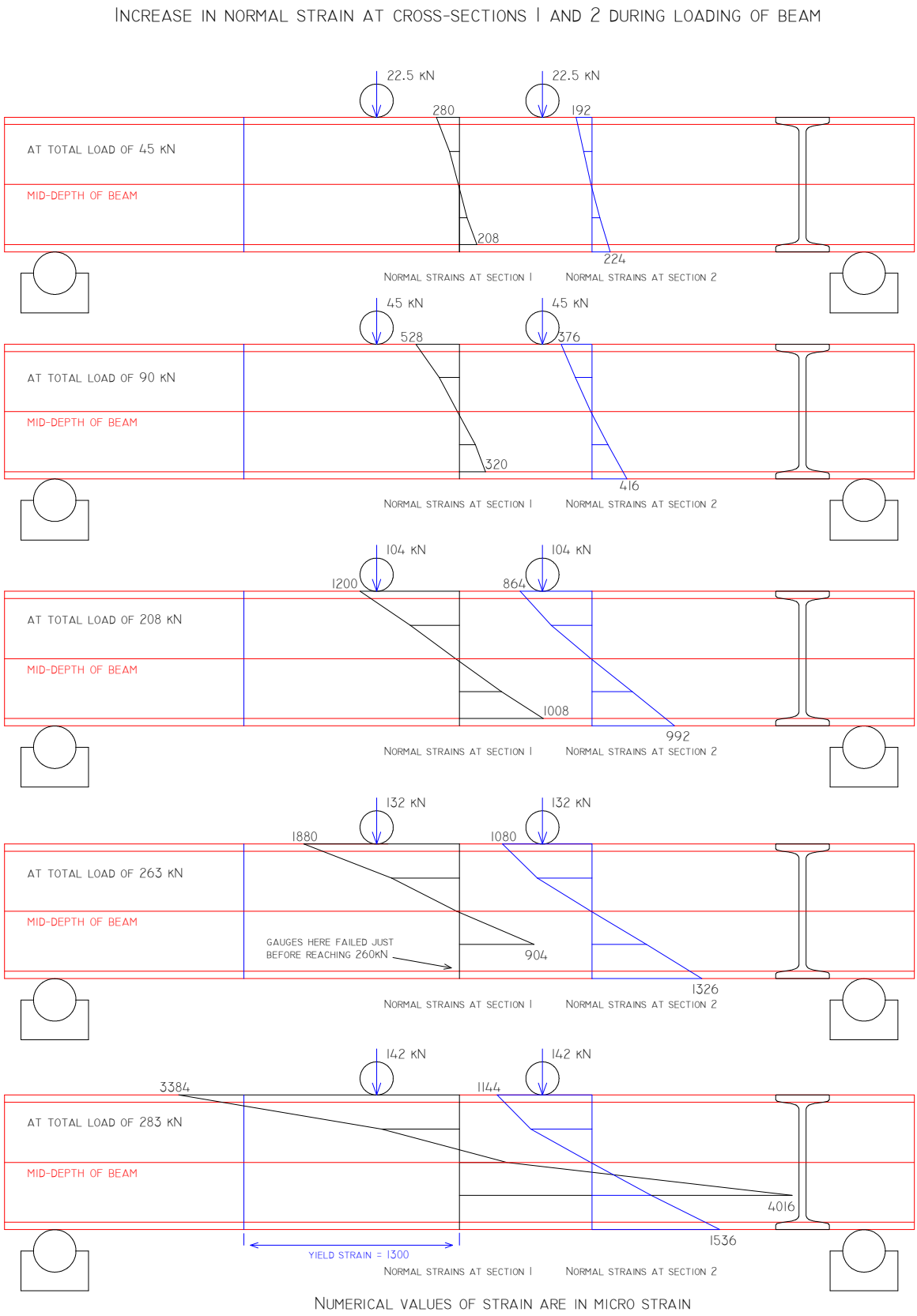

Figure 3.30 Increase in normal strain at cross-sections 1 and 2 during loading of beam.

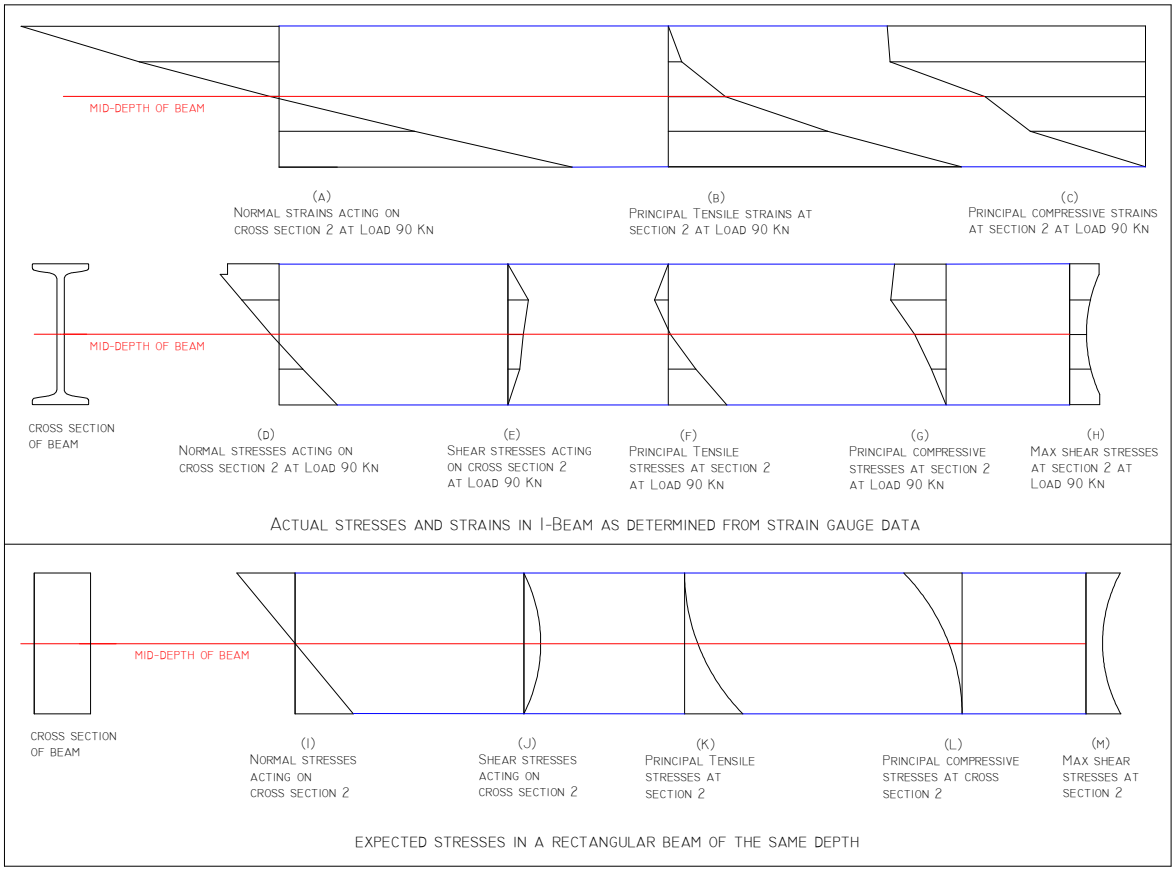

Figure 3.31 Comparison of actual stresses and strains in the I-beam with those to be expected in a rectangular beam of the same depth**.**

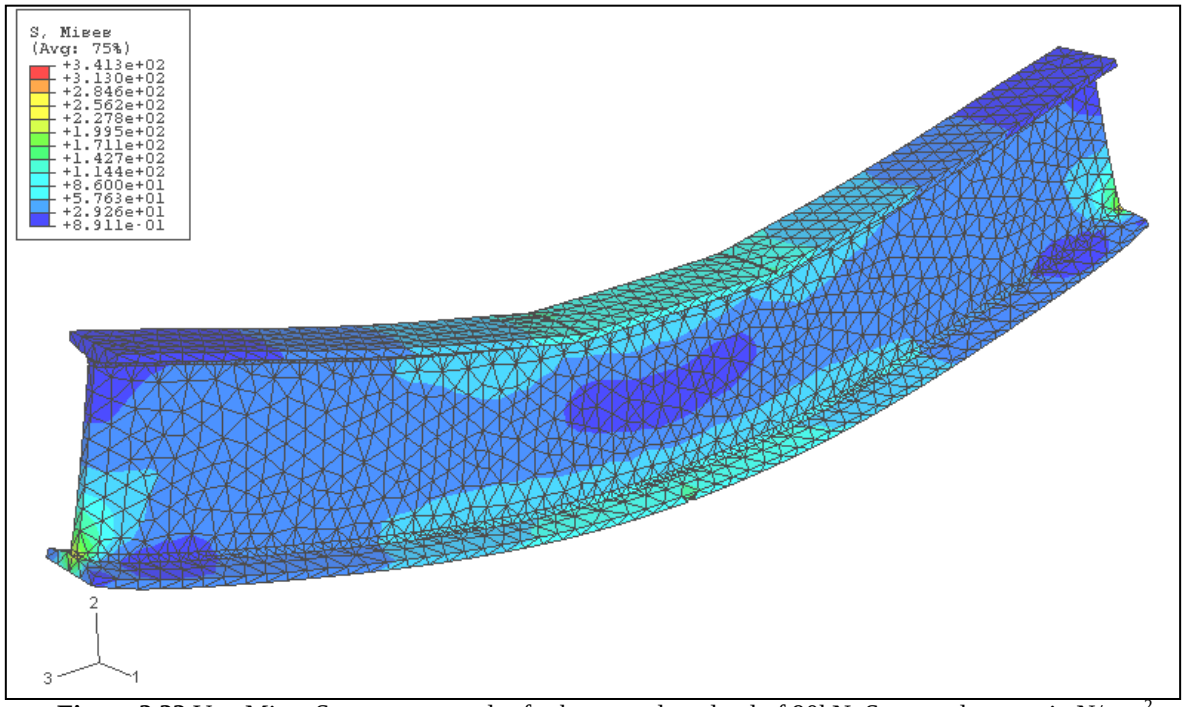

Figure 3.32 Von Mises Stress contour plot for beam under a load of 90kN. Stress values are in N/mm^2.

A finite element analysis ABAQUS model of the beam is shown in Figure 3.32. This was a linear elastic analysis that did not include buckling behaviour or yield.

The principal tensile stresses shown at (F) in Figure 3.31 have a maximum value at the surface of the bottom flange as expected. The principal tensile stresses would be expected to diminish going up the cross section and assume a zero value at the surface of the top flange, as shown at (K) in Figure 3.31.

However, the principal tensile stresses take on a negative value above the mid-depth of the beam. The reason for this is again most likely due to the stress distortion in this region due to its proximity to the load application point. The explanation is clarified by examination of Mohr's circles of stress and strain for that point in the beam, which are shown in Figure 3.33. From Mohr's stress circle, at (b) in Figure 3.33, this point in the beam experienced biaxial compression. However, from Mohr's strain circle at (a) in Figure 3.33 the material experienced a positive strain along the 1 direction. This is due entirely to the Poisson effect caused by the compressive stress along the 2 direction shown at (d) in Figure 3.33. The principal compressive stress along axis 1 of the stress element, shown at (d) was too small to overcome the Poisson effect caused by the other larger principal compressive stress along axis 2. Therefore a positive strain resulted along axis 1.

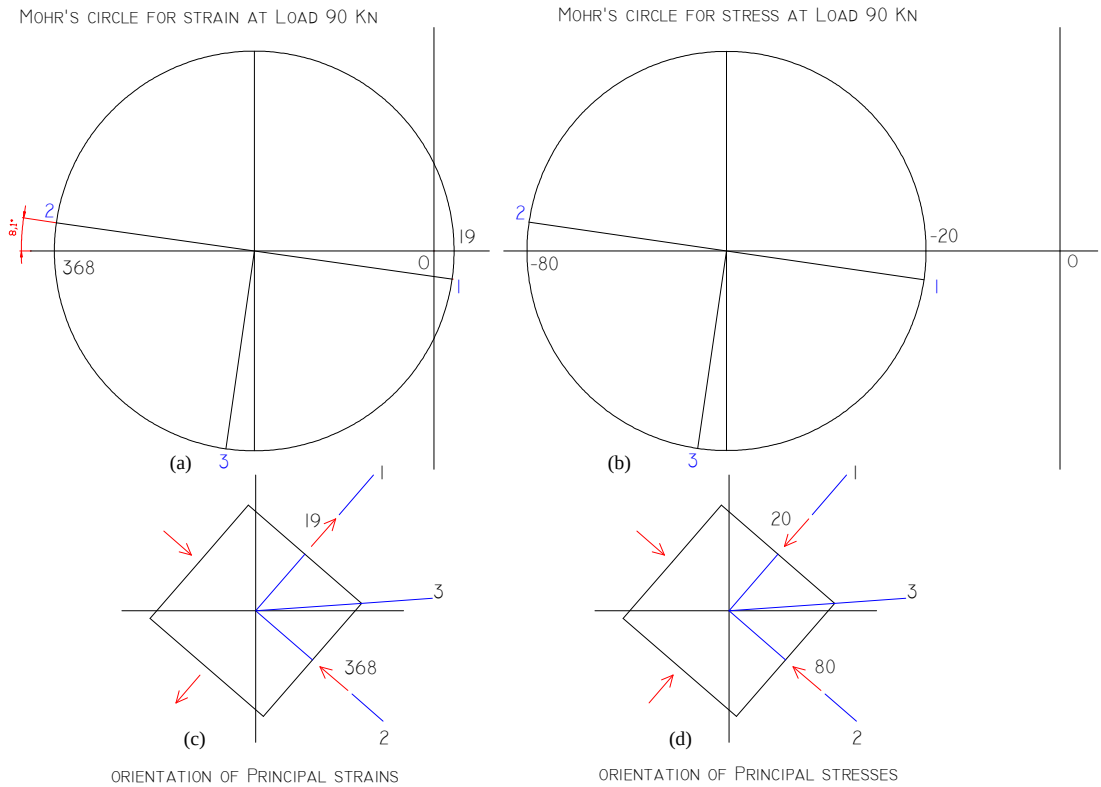

Figure 3.33 Mohr's circle of stress and strain for Point R1 of section 2 under a total beam load of 90kN.

3.9 Calculation example of stress analysis using strain gauge rosette data.

The rosette gauges at points B,C and D are labelled R1, R2, and R3 respectively. R3 is shown in the magnified view of Figure 3.34.

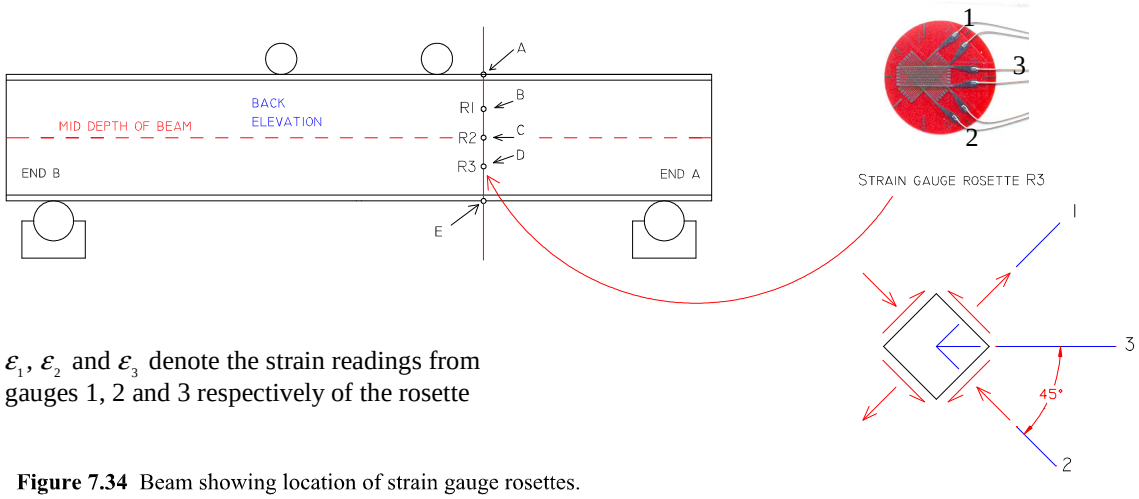

ε_1, ε_2 and ε_3 denote the strain readings from gauges 1, 2 and 3 respectively of the rosette

Figure 7.34 Beam showing location of strain gauge rosettes.

A stress element is shown oriented so that its axes are along the directions of gauges 1 and 2. This element represents the small portion of the beam to which the rosette is attached.

STEP 1: Construct Mohr's circle for strain.

The beam element is in a state of plane stress. At a load of 90kN the strain readings for R3 were:

ε_1 = 144.2 micro strain, ε_2 = -80.4 micro strain, ε_3 = 194.6 micro strain,

Radius of Mohr's circle of strain is given by:

$$R = \sqrt{\left(\frac{\varepsilon_2 - \varepsilon_1}{2}\right)^2 + \left(\frac{\gamma_{21}}{2}\right)^2} = \sqrt{\left(\frac{(-80.4) - (144.2)}{2}\right)^2 + \left(\frac{\gamma_{21}}{2}\right)^2} \qquad \text{Eq.3.1}$$

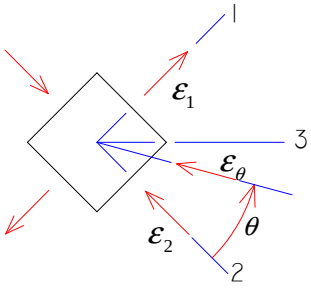

Figure 3.35 Strain element

The strain ε_θ in any direction θ is given by the transformation equation for strain.

$$\varepsilon_\theta = \frac{\varepsilon_2 + \varepsilon_1}{2} + \frac{\varepsilon_2 - \varepsilon_1}{2}\cos 2\theta + \frac{\gamma_{21}}{2}\sin 2\theta \qquad \text{Eq.3.2 (Gere 1999)}$$

For an angle $\theta = 45^o$, $\varepsilon_\theta = \varepsilon_3$

Therefore, $$\varepsilon_3 = \frac{\varepsilon_2 + \varepsilon_1}{2} + \frac{\varepsilon_2 - \varepsilon_1}{2}\cos 90^o + \frac{\gamma_{21}}{2}\sin 90^o \qquad \text{Eq.3.3}$$

Solving for γ_{21} gives $$\gamma_{21} = 2\varepsilon_3 - \varepsilon_2 - \varepsilon_1 \qquad \text{Eq.3.4}$$

$$\Rightarrow \quad \gamma_{21} = 2(194.6) - (-80.4) - (144.2) \quad = \quad 325.4 \text{ micro strain}$$

Substituting this value for γ_{21} into Eq.3.1 gives

$$R = \sqrt{\left(\frac{(-80.4) - (144.2)}{2}\right)^2 + \left(\frac{325.4}{2}\right)^2}$$

$$R = 197.7$$

Mohr's circle of strain is constructed as shown in Figure 3.36.

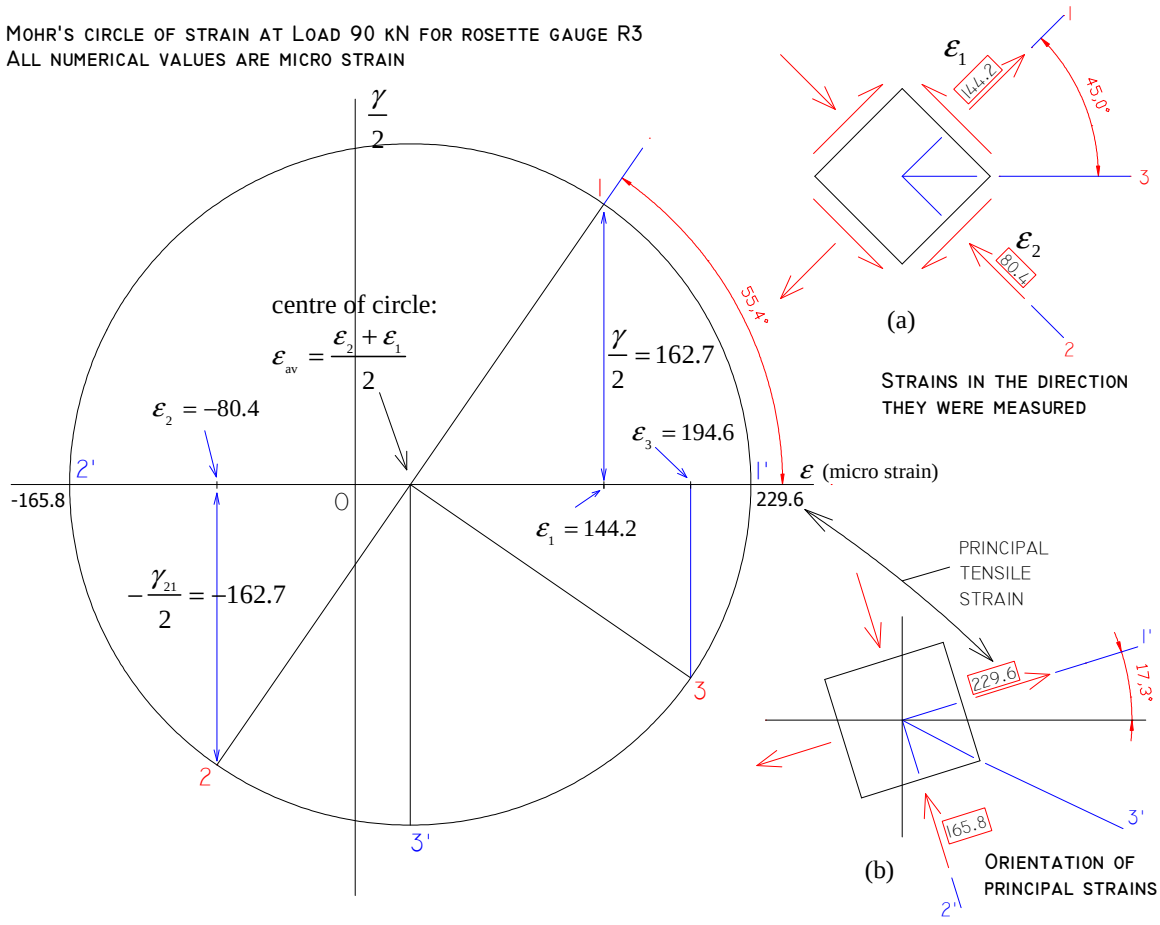

Figure 3.36 Mohr's circle of strain for Rosette R3 at total beam load of 90kN, together with associated strain elements. The strain element at (a) shows the gauge readings in the directions they were measured, while the strain element at (b) shows the magnitude and direction of the principal strains for the same point in the beam.

STEP 2: Use Hooke's law to determine principal stresses

Using Hooke's law the principal stresses associated with the principal strains may be found as follows

$$\sigma_x = \frac{E}{1-\nu^2}\left(\varepsilon_x + \nu\varepsilon_y\right) \quad \sigma_y = \frac{E}{1-\nu^2}\left(\varepsilon_y + \nu\varepsilon_x\right) \qquad \text{Eq.3.5a, b (Hooke's law)}$$

For wrought iron, modulus of elasticity E = $200\text{x}10^3\text{Nmm}^{-2}$ and Poisson's ratio ν = 0.3. Using the values of maximum and minimum strain from Mohr's strain circle (Figure 4.32) the principal stresses are calculated as follows:

$$\sigma_{P1} = \frac{200\times10^3\,\text{Nmm}^{-2}}{1-(0.3)^2}\left(229.59\times10^{-6} + 0.3(-165.79\times10^{-6})\right) \quad = \quad 39.5\text{Nmm}^{-2}$$

$$\sigma_{P2} = \frac{200\times10^3\,\text{Nmm}^{-2}}{1-(0.3)^2}\left(-165.79\times10^{-6} + 0.3(229.59\times10^{-6})\right) \quad = \quad -21.3\ \text{Nmm}^{-2}$$

The maximum shear stresses are found by constructing Mohr's circle for plane stress, as shown in Figure 3.37.

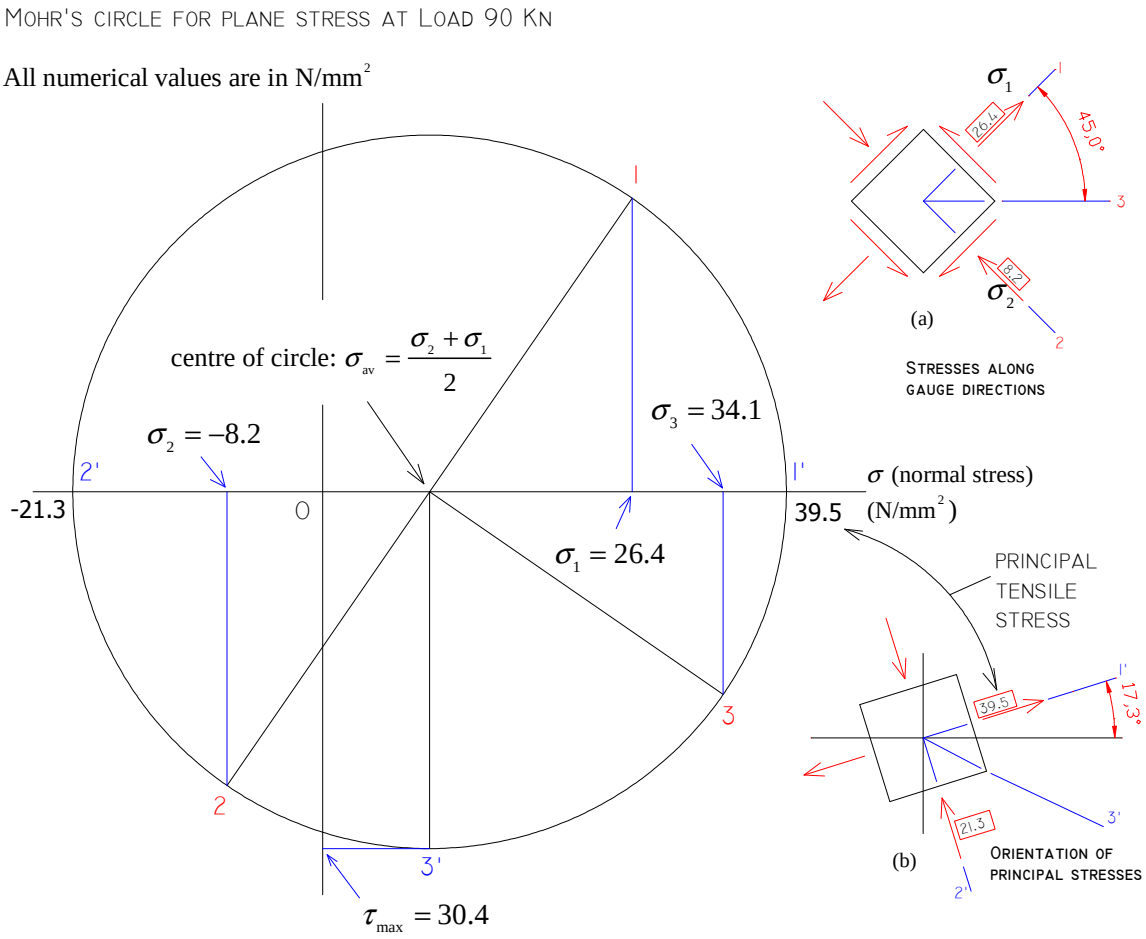

Figure 3.37 Mohr's circle of plane stress for Rosette R3 together with associated stress elements.

3.10 Testing of the Edinburgh GPO beams - Objectives

Two sets of tests were carried out on these beams. In the first, the beam was tested without the timber planks, and in the second set of tests, the beam was tested with the timber planks still bolted to the iron web. The case where the beams had no timber attached will be considered first. A more thorough investigation of the beam in this condition was possible because strain gauges could be applied directly to the metal web of the beam.

To fully investigate the behaviour of the beam, two loadings were carried out. The first (Test 1) involved loading the beam within the elastic range. The second (Test 2) consisted of loading the beam all the way to failure. By keeping the beam within the elastic range for the first loading test no strain hardening of the material occurred. Therefore, the second load test was not tainted by the previous test.

The primary objective was simply to observe how the beam physically responded to heavy loading. Would the beam break in a brittle manner as with the Albert hall beam or would it exhibit plastic deformation like a modern steel beam? Lateral and vertical deflection gauges were placed against and under the beam to monitor movement during testing. These are shown in Figure 3.39. Another objective of the tests was to determine the stresses at various cross sections along the beam. This was achieved by the use of strain gauges, the locations of which are shown in Figure 3.38.

The timber planks of European redwood (red deal) of unknown grade were fixed to the web plate of the beam with wrought iron bolts of 16mm diameter staggered above and below the mid level of the beam as shown in Figure 3.2 and Figure 3.43. The overall horizontal spacing of the bolts was 610mm.

3.11 Arrangement of strain gauges

Because the beam under consideration was built-up from angles and plate, the stress trajectories were likely to be quite different from those for an I-beam rolled from a single piece of metal. In a built-up beam, the stresses between angles and plates are transferred by means of rivets in shear and tension, and by friction between contact surfaces.

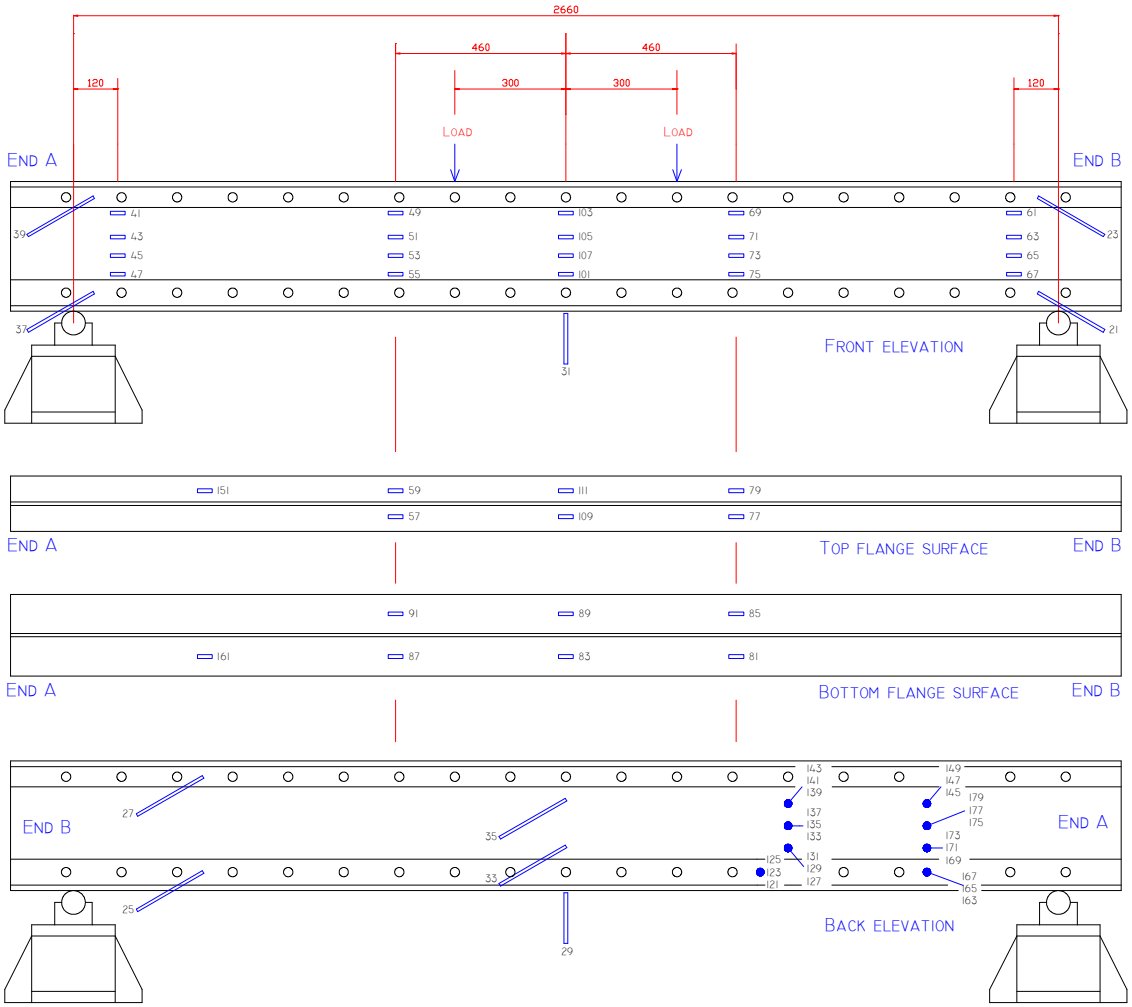

Figure 3.38 Strain gauge locations for testing of Edinburgh GPO beam. All dimensions in mm.

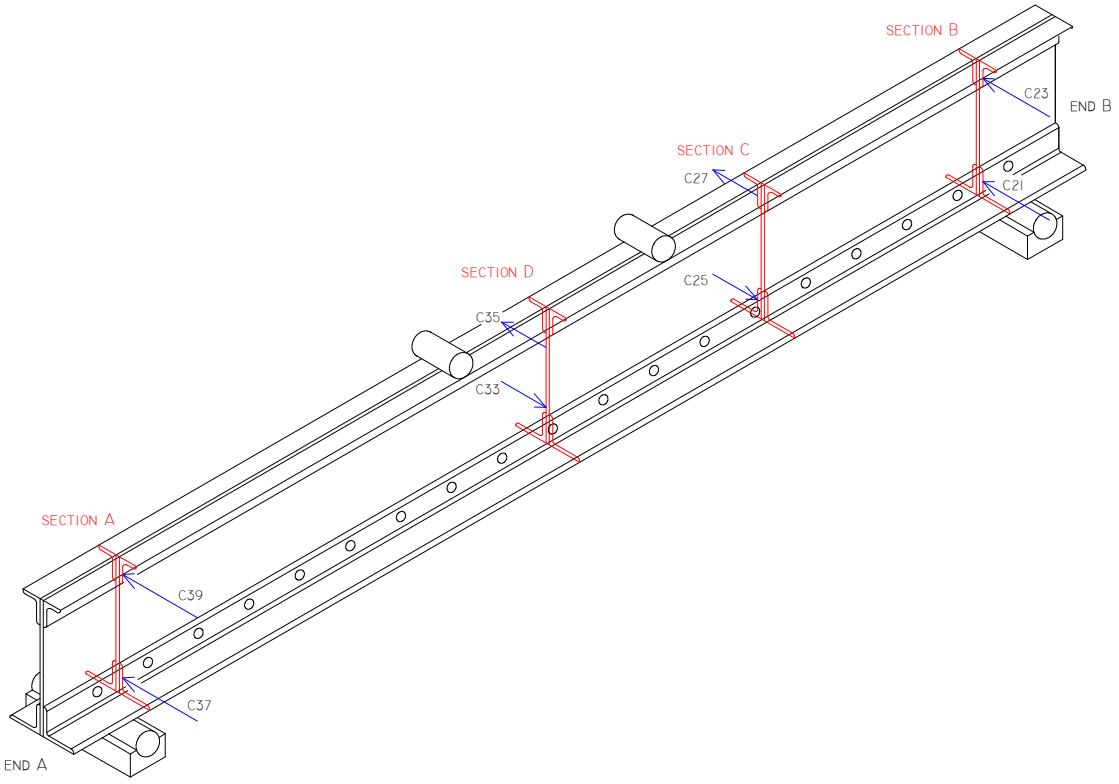

Figure 3.39 Deflection gauge arrangement for testing of Edinburgh GPO beam. Span of beam = 2660mm

The testing arrangement for the Edinburgh GPO beam without timber is shown in Figure 3.40

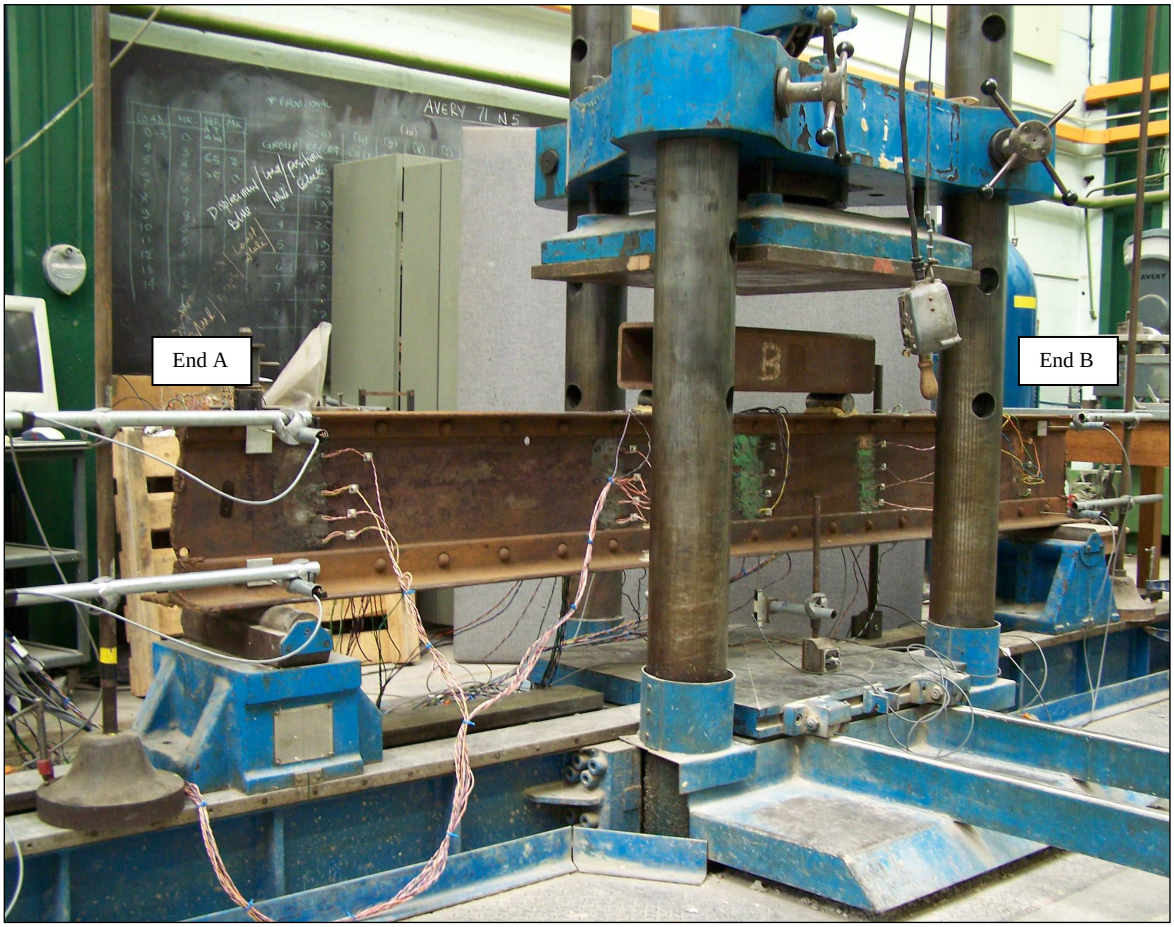

Figure 3.40 Testing arrangement for Edinburgh GPO beam. The front face of the beam shown here will also be referred to as the right-hand side of the beam. (Photo by M.O'Sullivan 2008)

3.12 Results of bending tests of Edinburgh GPO beams – deflection behaviour

The first test of the beam without timber involved loading it up to 135kN, which kept the beam well within the elastic range. The beam with timber attached was also tested within its elastic range. The load / vertical deflection diagrams at mid-span for both beams are shown in Figure 3.41 and indicate that the loading in both cases followed a linear path, which confirmed that the loading remained within the elastic range. The diagrams also indicate that the beams did not fully return to their original positions. This should be ignored, because it is due to settling down of the beam on the supports after the application of some load. The beams were not perfectly flat on the roller supports because the bottom flanges were slightly twisted and uneven. In comparison with the Albert Hall beam it is clear that the Edinburgh beams were not made to the same degree of geometric precision.

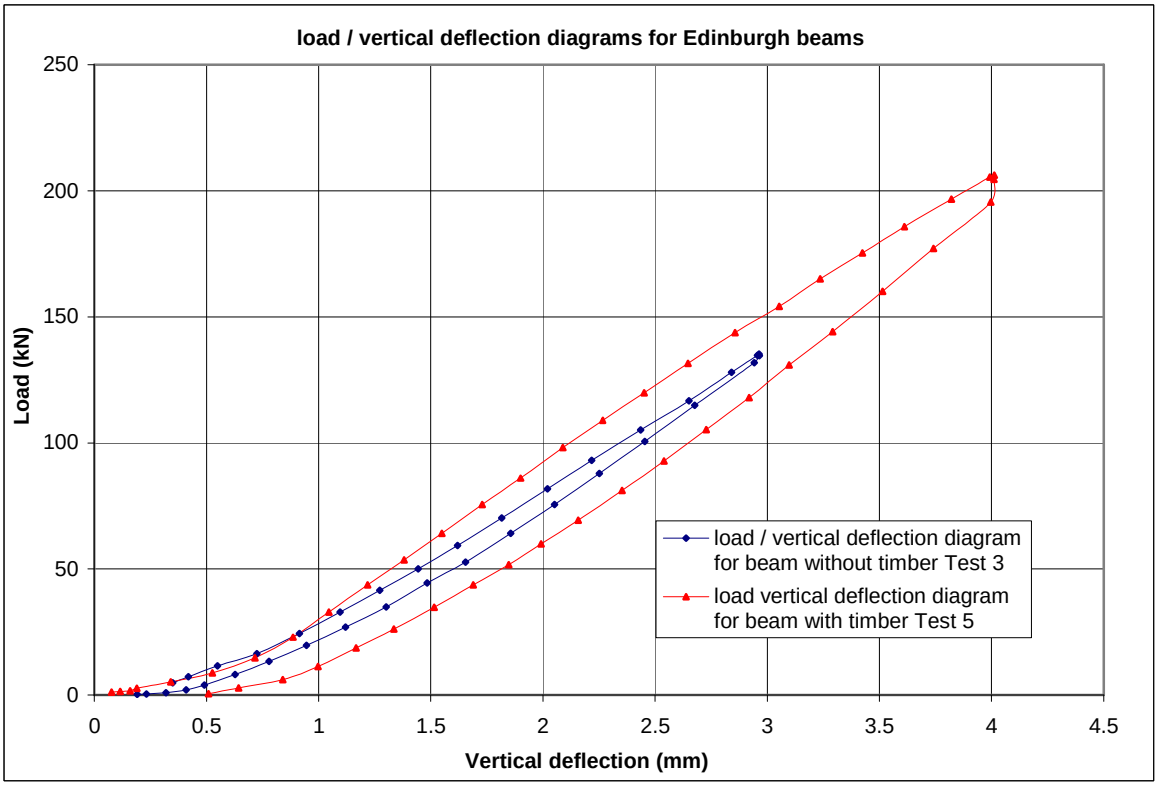

Figure 3.41 Vertical deflection of bottom flange of Edinburgh beams at mid-span, for loading within the elastic range (Test 1)

It is reasonable to expect a greater degree of irregularity in shape in a beam made by riveting together angles and plates, than in a beam rolled in one section.

The graphs in Figure 3.41 indicate that the beam with timber attached was slightly stiffer than that without timber. However, the stiffness of the beam with timber is not so much greater as to indicate that the timber was added to enhance stiffness or strength. It is more likely that the timber was added solely to provide grounds for receiving the timber floor joists spanning between the beams. In addition, the upper flange may have been made narrower than the bottom flange in order to allow the timber joists to be dropped into the chiselled notches. The joists were dovetail notched into the timbers attached to the beams. It is highly likely that the notches were not cut prior to erecting the beams. Instead the notches were chiselled out when the beams were in place in the building. This would allow the timber joists to be accurately laid out. If the iron beams had wide upper flanges they would obstruct placement of the timber joists. (The beam cross section is shown in Figures 3.42 and 3.43).

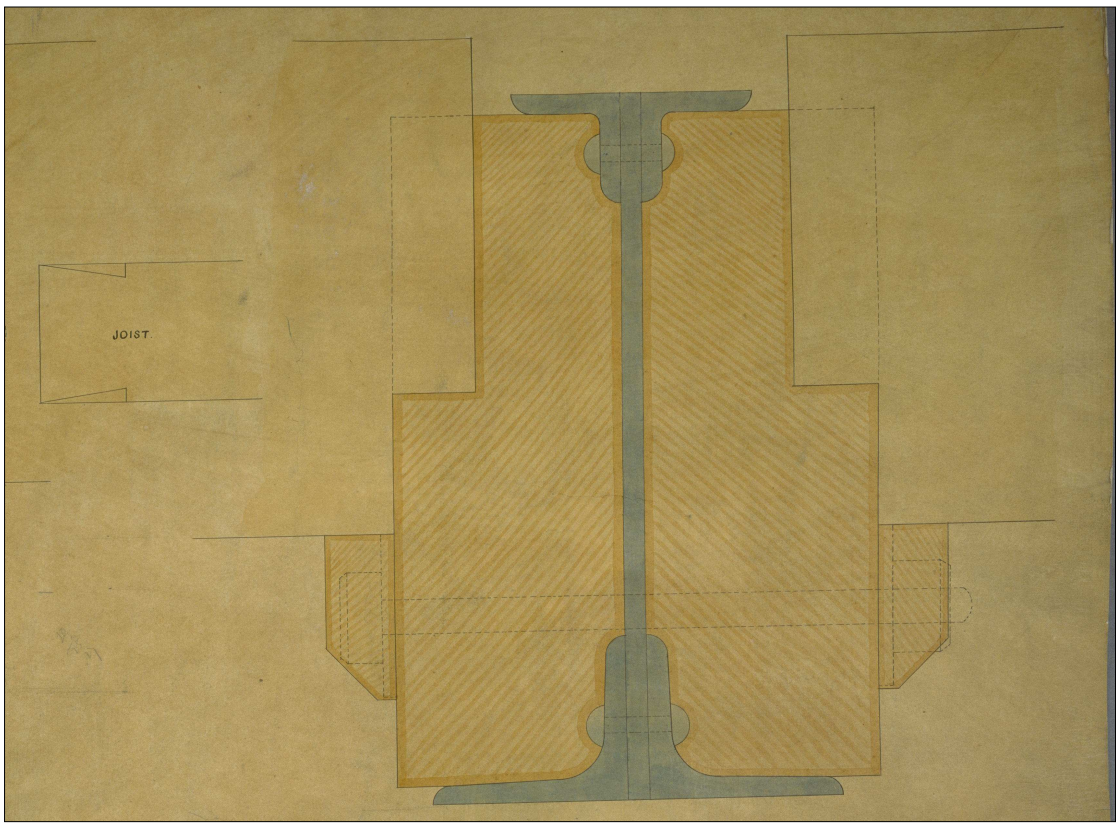

Figure 3.42 Drawing of beam cross section by George Roberts dated Oct 9th 1859. This drawing is housed in the National Archives of Scotland in Edinburgh.

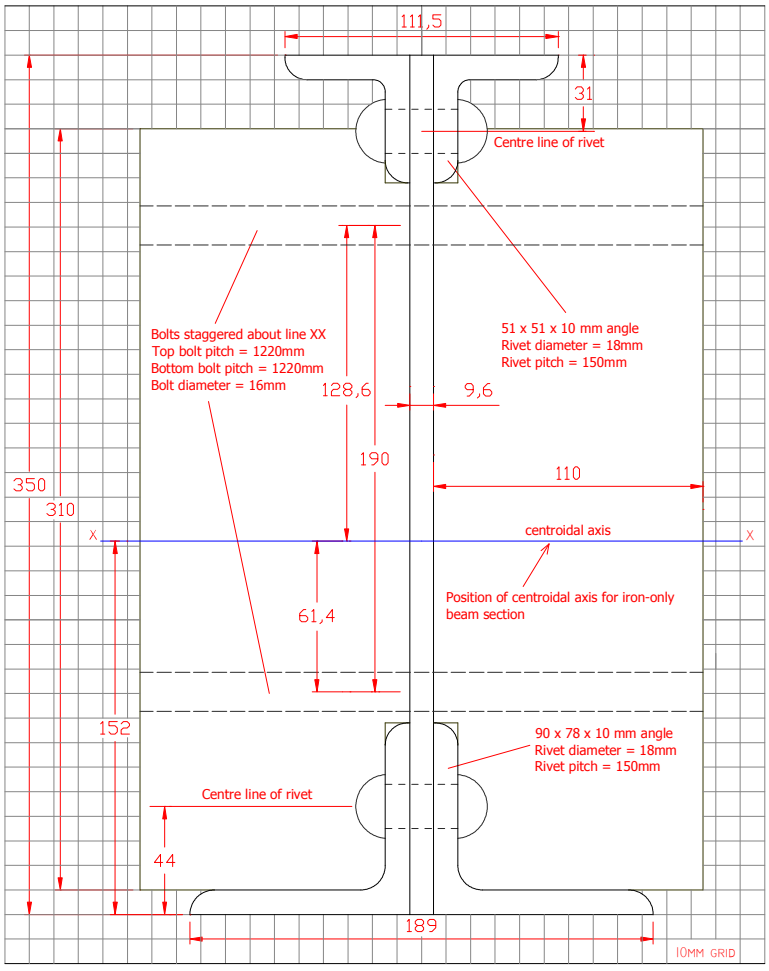

Section properties (iron only):
Area = 8279mm^2
Second moments of area:
I_{xx} = 150862560mm^4
I_{yy} = 6572897mm^4

Figure 3.43 Edinburgh GPO beam cross section (All dimensions in mm).

The bottom flanges of cast iron beams were often made wider than the upper flanges because cast iron is weaker in tension than in compression. It was clear to engineers of the time that wrought iron did not suffer from such a difference in tensile and compressive strength. In 1859, the same year that construction began on the Edinburgh GPO, the Board of Trade in Britain imposed a value of 5 ton/in^2 (77 N/mm^2) as the maximum design stress for wrought iron members in railway bridges. This value was used for the designing of both the top and bottom chords of wrought iron girders (Colburn 1863). This would suggest that engineers of the time considered wrought iron to be equally strong in tension and compression. Therefore, there would have been no need for the Edinburgh GPO beams to have a wider bottom flange other than to avoid hindering placement of the timber floor joists.

During the tests lateral deflections were monitored at the 4 locations shown in Figure 3.39. The test within the elastic range gave the results shown in Figure 3.44.

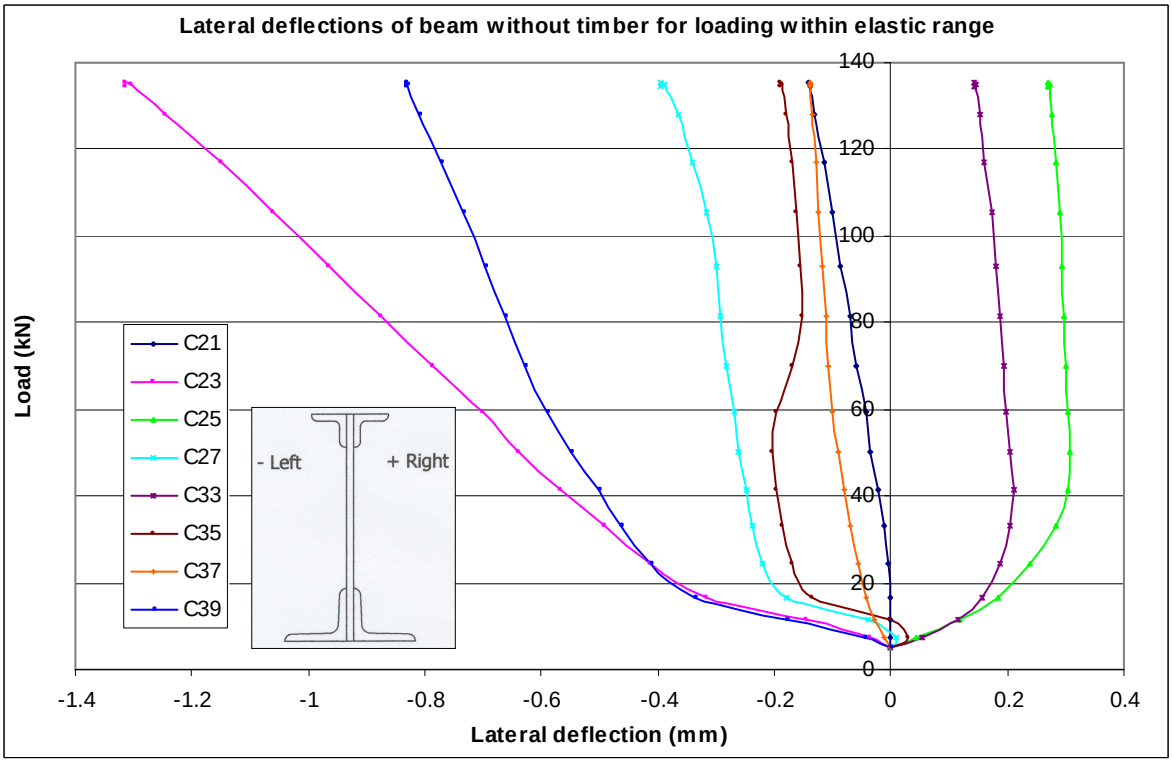

Figure 3.44 Lateral deflections of beam without timber for loading up to 135kN. (Loading within elastic range – Test 1). See Figure 4.39 for deflection gauge locations.

Let the front face of the beam, which is shown in Figure 3.40, also be know as the right-hand side of the beam. In Figure 3.44 deflections with a positive sign indicate movement toward the right and deflections with a negative value indicate movement toward the left. As indicated in Figure 3.45 the beam twisted slightly while under load. However, the magnitude of the lateral deflections during loading of the beam within the elastic range were negligible.

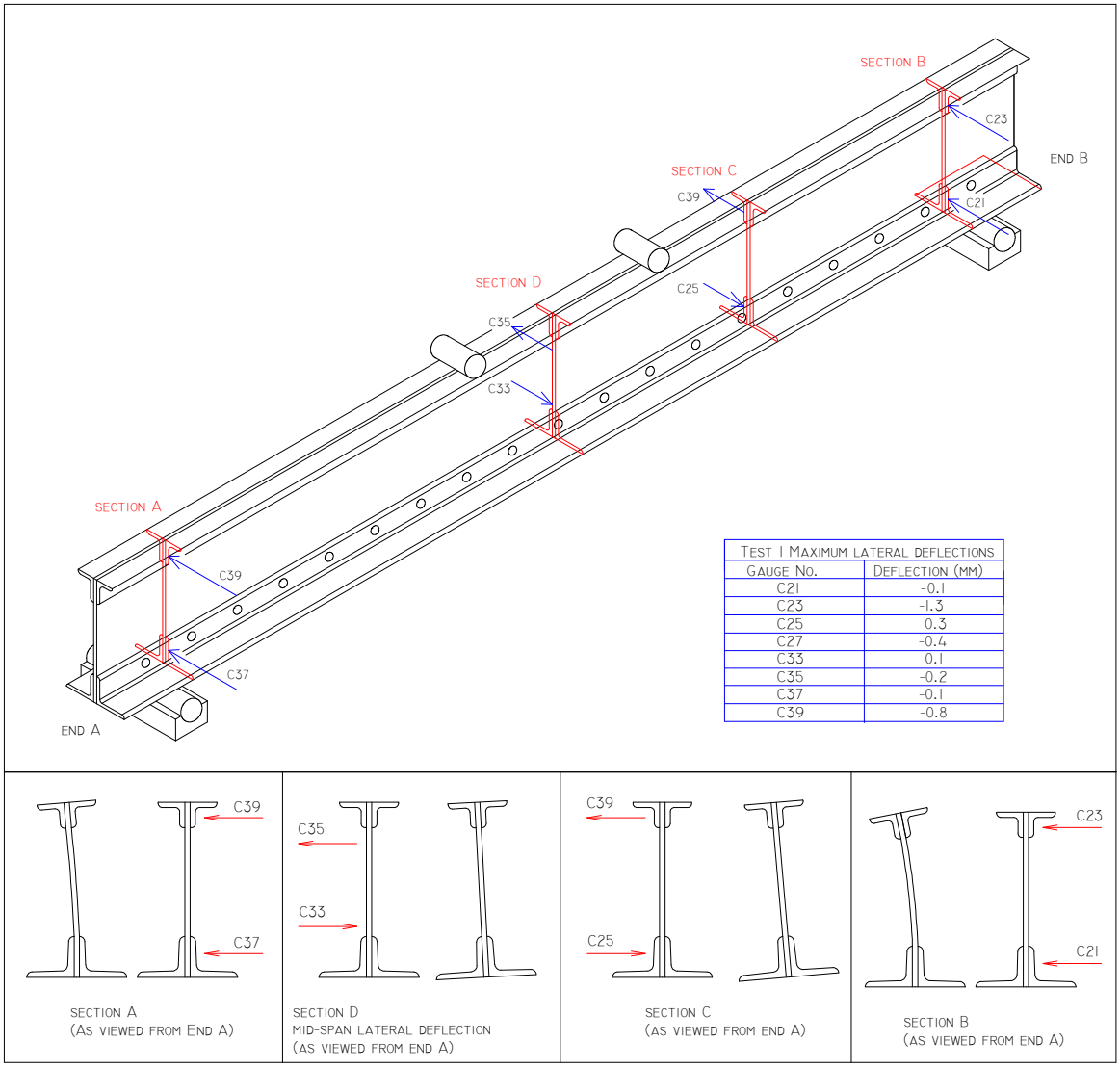

Figure 3.45 Lateral deflections of four cross sections of the beam without timber, for loading up to 135kN. (Test 1 - Loading within elastic range). Deflections of cross sections have been exaggerated for illustration purposes. Negative deflection values indicate movement toward the left-hand side of the beam as viewed from End A.

In the second test, the beam without timber was loaded all the way to failure. The most obvious difference between the built-up Edinburgh beam and the Albert hall beam was that the built-up beam experienced buckling and significant physical distortion during testing to failure. Buckling was the ultimate failure mode of the built-up beam, however the beam yielded within the vertical plane prior to buckling.

The load / vertical deflection diagram for the test to failure of the beam without timber is shown in Figure 3.46. The graph for the test of the beam with timber is also shown for comparison. However, the test of the beam with timber was not carried out to failure because is was planned to use this beam for making tensile test specimens. Loading of the beam with timber was kept within the elastic range so as not to strain harden the material. For the beam without timber there was no clear yield point. The graph shown in Figure 3.46 seems to remain linear up to about 300kN and does not deviate very much until after about 400kN.

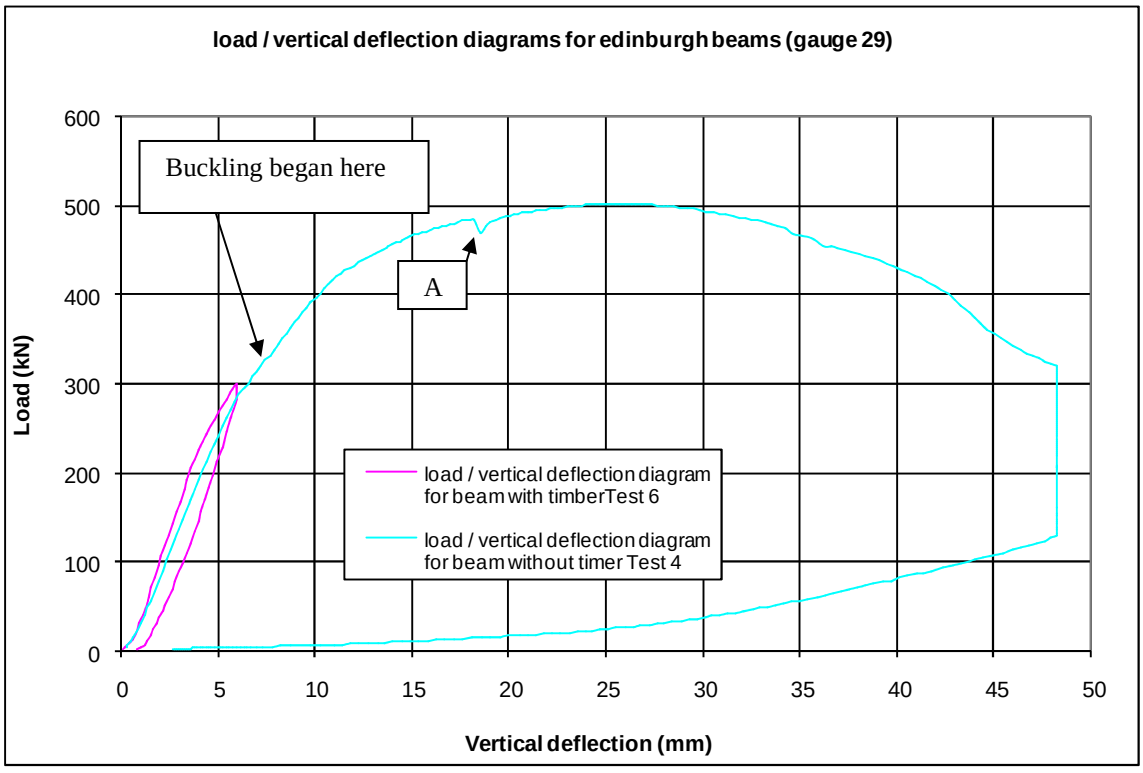

Figure 3.46 Test 2 - Vertical deflection at mid-span of bottom flange of Edinburgh beam without timber, for loading to failure.

There is an irregularity in the vertical deflection graph of Figure 3.39 at point A. This occurred when one of the rivets in the bottom flange snapped in half and a crack occurred at that location in the bottom edge of the web plate. This can be taken as the ultimate failure point of the beam and occurred at a load of 485kN. The angle iron making up the bottom flange did not show any signs of fracture at the location of the crack in the web plate. However, this point in the beam experienced a significant amount of distortion due to buckling and it was this buckling which caused the rivet to snap in tension. The location of the web plate crack and snapped rivet is shown in Figure 3.47. When this region of the beam began to buckle gaps began to open up between the angle iron and the web plate.

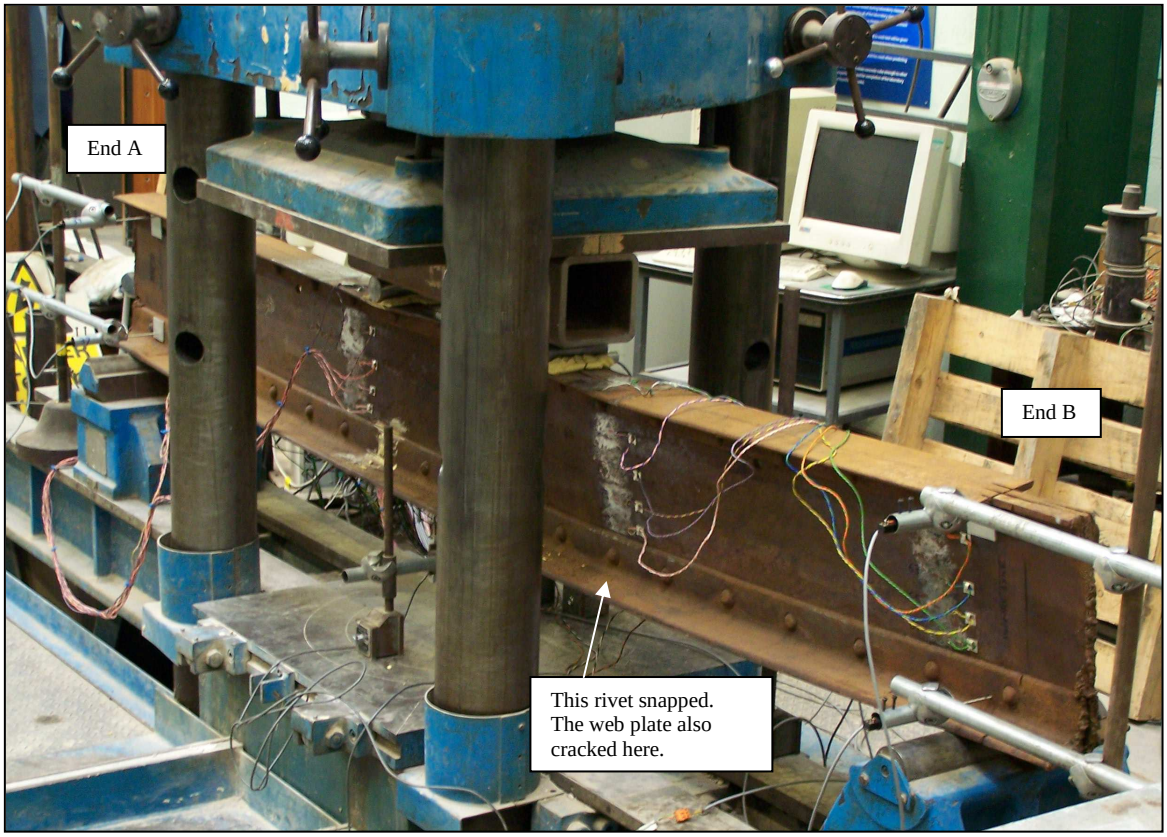

Figure 3.47 Test 2 – Test to failure of beam without timber. The front face of the beam is shown here. End B is in the foreground. (Photo by M.O'Sullivan 2008)

This put the rivet into extreme tension. Following the failure of the rivet and the associated crack in the web plate, the angle irons may have arrested crack propagation in the web plate by holding the bottom of the beam together. That may be why the beam continued to carry an increasing load after point A in Figure 3.46. However, by this time the beam had

buckled significantly, and so, had lost the geometric form needed to carry a vertical load. That is why the load carrying capacity diminished quickly after point A in Figure 3.46.

The ultimate distortion of the beam is shown in Figures 3.49 and 3.50. The upper chord assumed an S-shaped form along its length with significant lateral deflection. In addition, the web bent over as shown in Figure 3.48. Once this happened the applied load tended to press the upper chord sideways so the beam could no longer adequately resist vertical load. This resulted in the downward curve of the load / vertical deflection diagram in Figure 3.46

Figure 3.48 Test to failure of beam without timber. Significant buckling as seen from End B of the beam. (Photo by M.O'Sullivan 2008)

In examining the lateral deflections of the beam during the test to failure, two stages became apparent. The first stage, in which the lateral deflections were very small, consisted of loading the beam within the elastic range. When the load reached about 300kN, there was an abrupt and significant change in both magnitude and direction of the lateral deflections, which corresponded to the onset of buckling. The onset of buckling is indicated in Figure 3.46. The lateral deflection graphs of the beam without timber, for the test to failure, are shown in Figures 3.51 to 3.55. Each Figure contains two graphs of data points and corresponds to one of the four locations along the beam, shown in Figure 3.39.

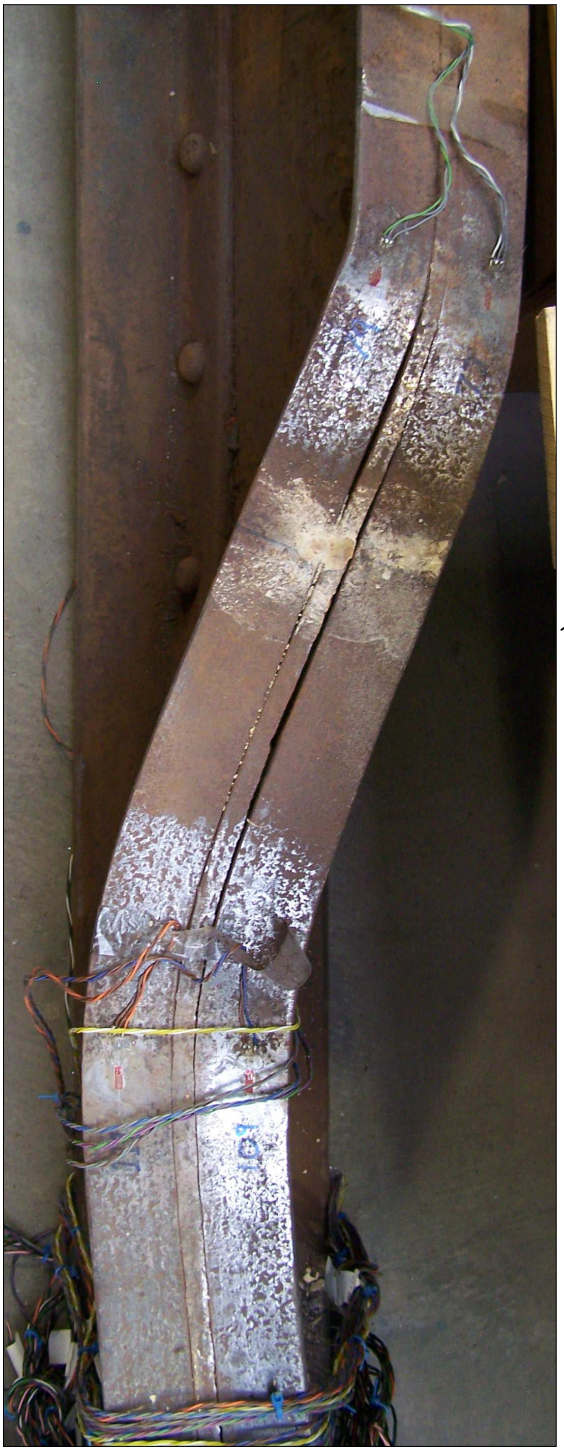

Figure 3.49 Close-up of distorted top flange. Viewed from above. (Photo by M.O'Sullivan 2009)

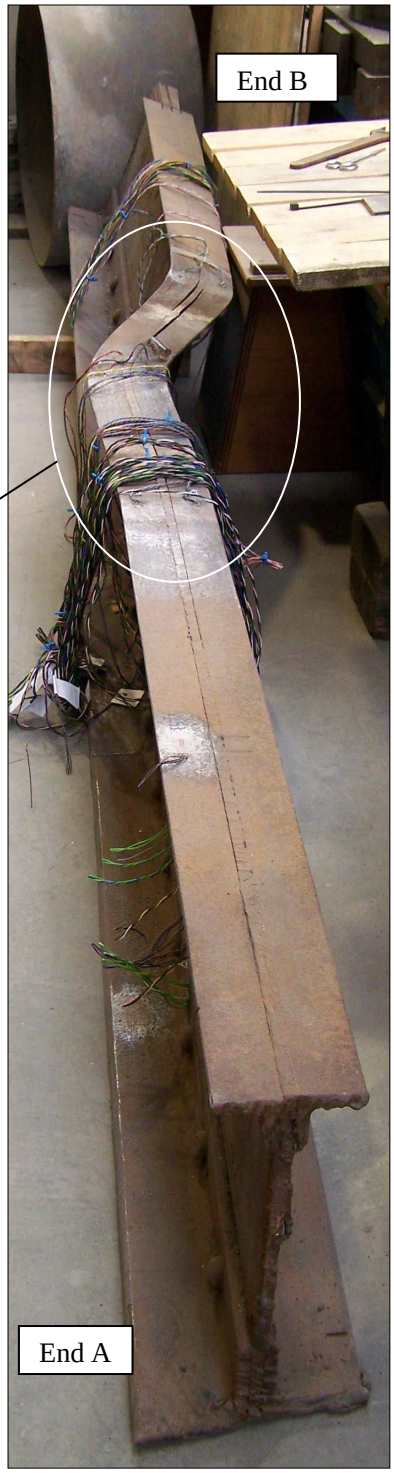

Figure 3.50 Beam after test to failure (Photo by M.O'Sullivan 2009)

The final buckled shape of the beam is shown in Figure 3.49, and 3.50.

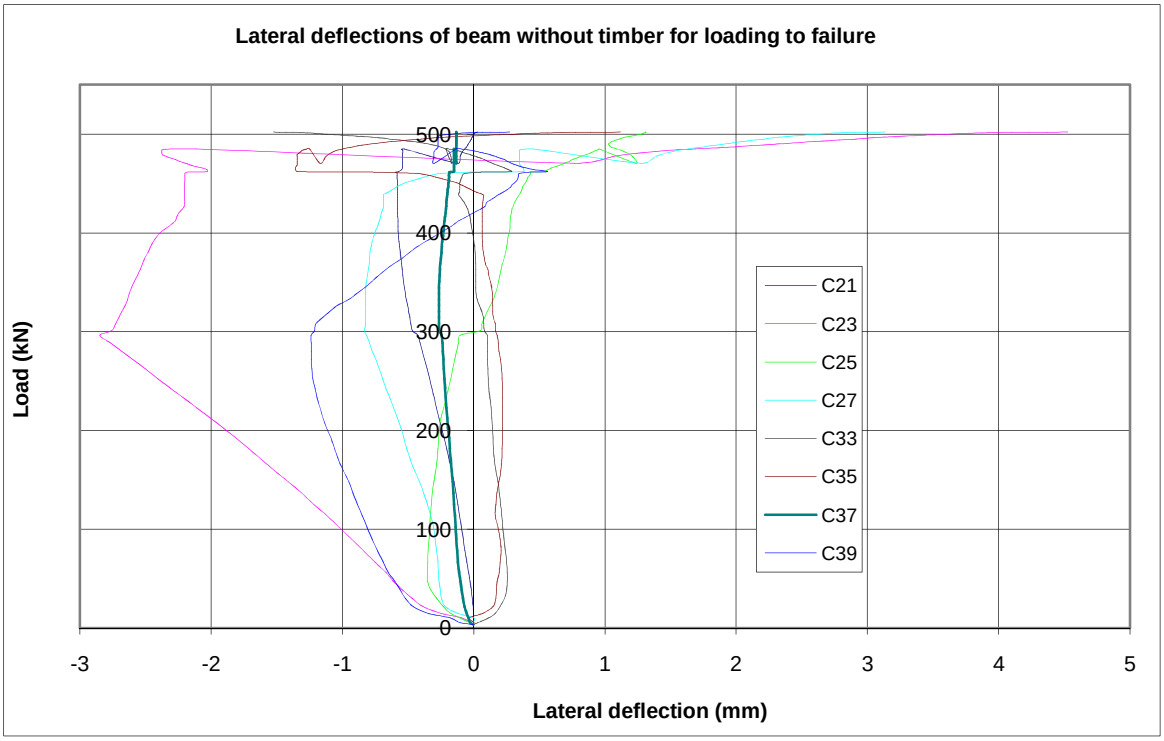

Figure 3.51. Lateral deflections of four cross sections of the beam without timber, for loading to failure. (Test 2). Extreme distortions occurred between 450kN and 500kN. Negative values indicate movement toward the left-hand side of the beam as viewed from End A.

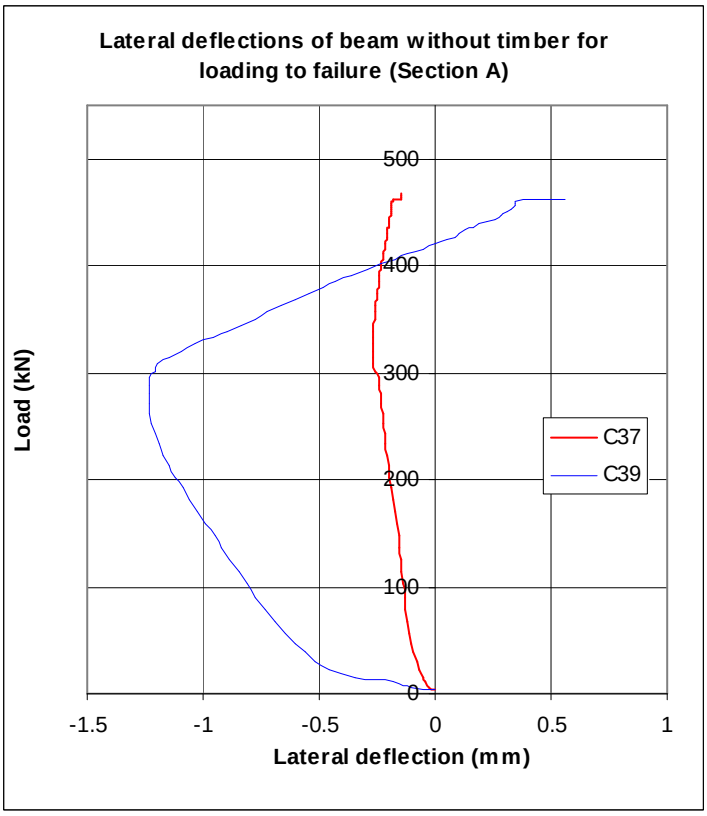

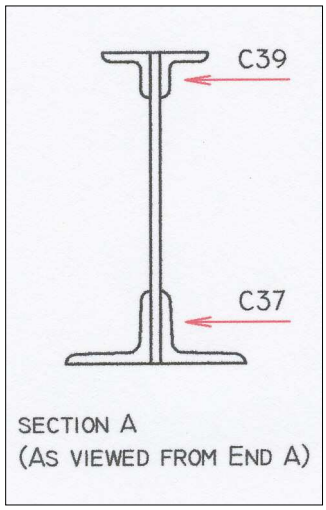

Figure 3.52 End A of beam showing movement gauges (M.O'Sullivan 2009)

Figure 3.53 Lateral deflections of Section A, for loading to failure.

The graph for gauge C37 in Figure 3.53 shows that the deflection of the bottom of the beam at section A was negligible. This was because of the frictional restraint provided by the roller support at that location. Initially the upper part of the section deflected toward the

left but when buckling occurred at around 300kN it moved to the right and ultimately assumed a slightly deflected shape in that direction.

For section B there was negligible movement at the support point. Initially the upper part of the section deflected toward the left but when buckling occurred at around 300kN it moved to the right and ultimately assumed a significantly deflected shape in that direction as shown in Figure 3.54.

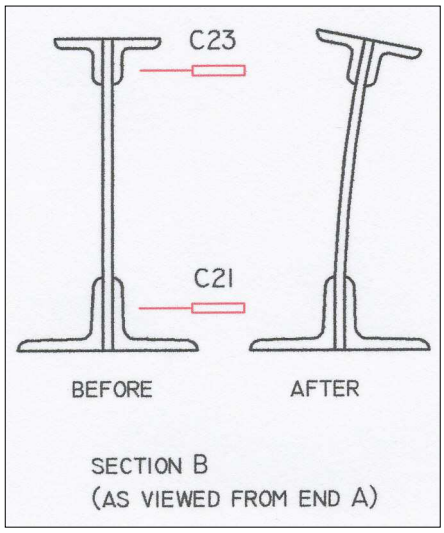

Figure 3.54 Lateral deflections of Section B, for loading to failure.

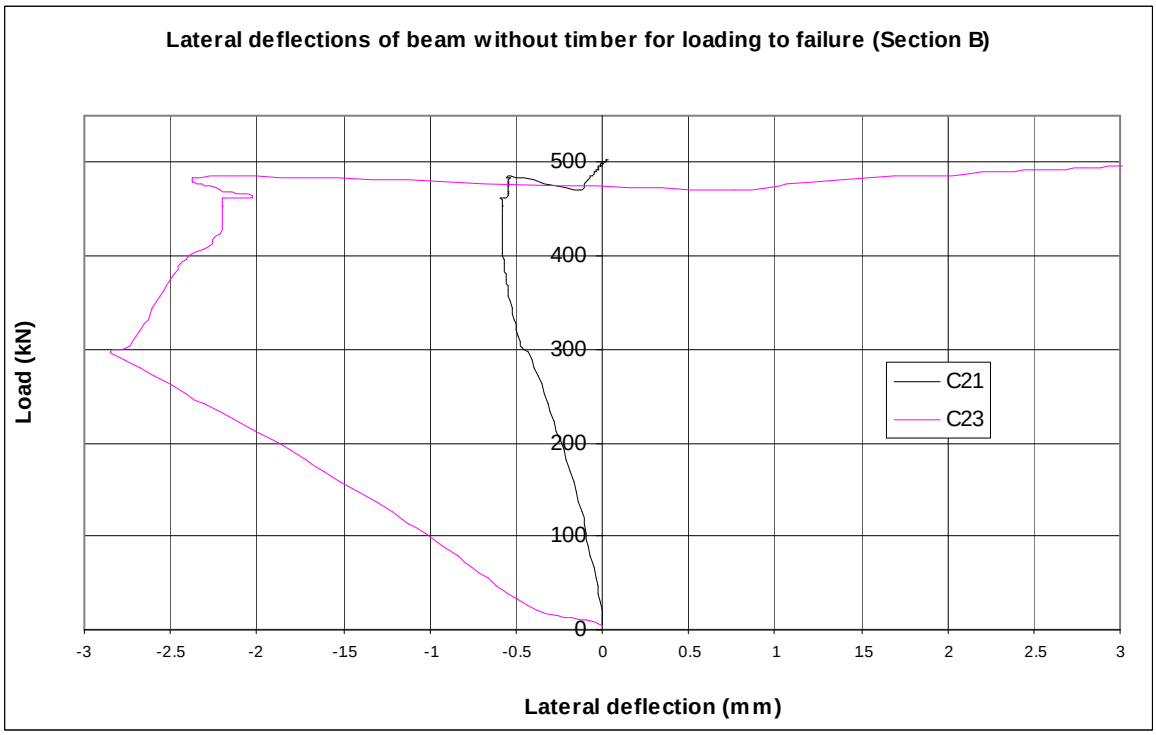

Figure 3.55 Lateral deflections of Section B, for loading to failure.

Section D is located at mid-span and its movement gives a good indication of the degree of lateral restraint provided by the solid steel cylinders used to apply the load to the beam. As shown in Figure 3.57 lateral movement was minimal for the entire elastic range of loading. The frictional restraint prevented buckling for much of the test to failure. But ultimately

buckling occurred as shown in Figure 3.50. The photograph of Figure 3.58 clarifies what happened to this section.

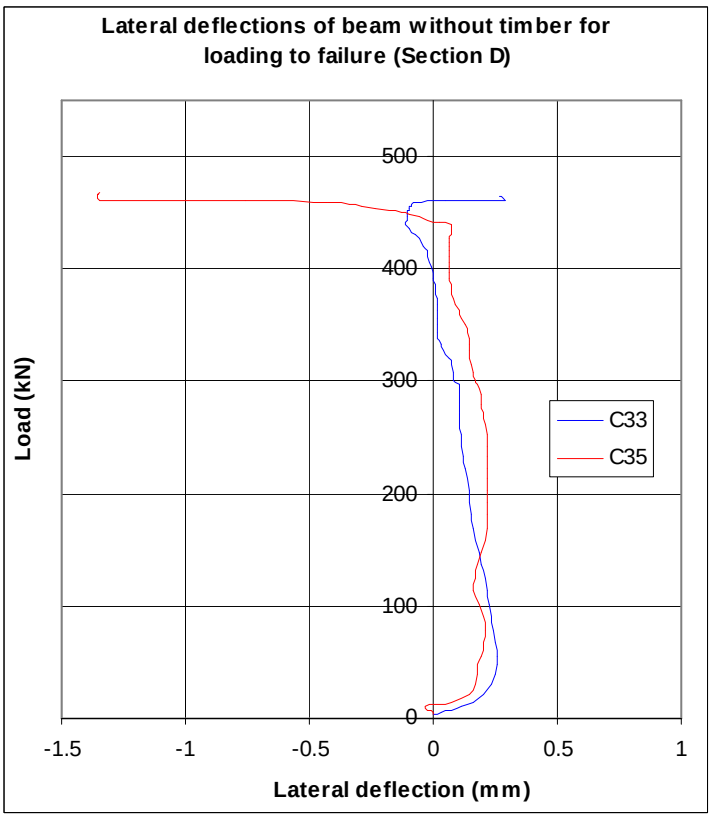

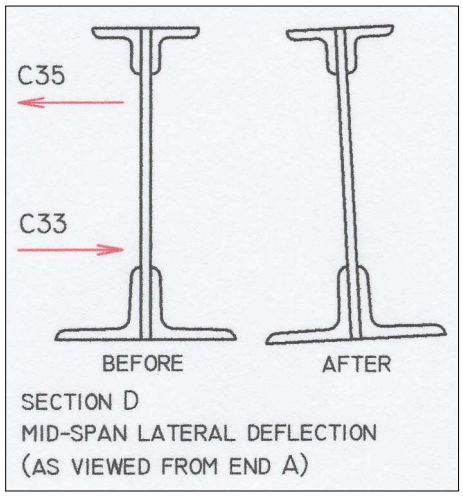

Figure 3.56 Lateral deflection of Section D, at mid-span.

Figure 3.57 Lateral deflection of Section D, at mid-span

Figure 3.58 Lateral deflection of Section D, at mid-span. Jagged edge and corrosion of the end of the beam was caused by cutting torch during demolition and then exposure to the elements after removal from Edinburgh GPO. The Royal Albert Hall beam was cut to length on a bandsaw producing a clean edge.

Section C is located half-way between the support roller at End B and the adjacent applied load point. This cross-section twisted clockwise (as viewed from End A) but also deflected toward the right as a whole. The reason that the results for gauge C25 in Figure 3.59 show

only a small amount of movement is because these two components of movement tended to cancel each other at the probe point of the deflection gauge. The upper part of the section buckled significantly toward the right as shown in Figure 3.50

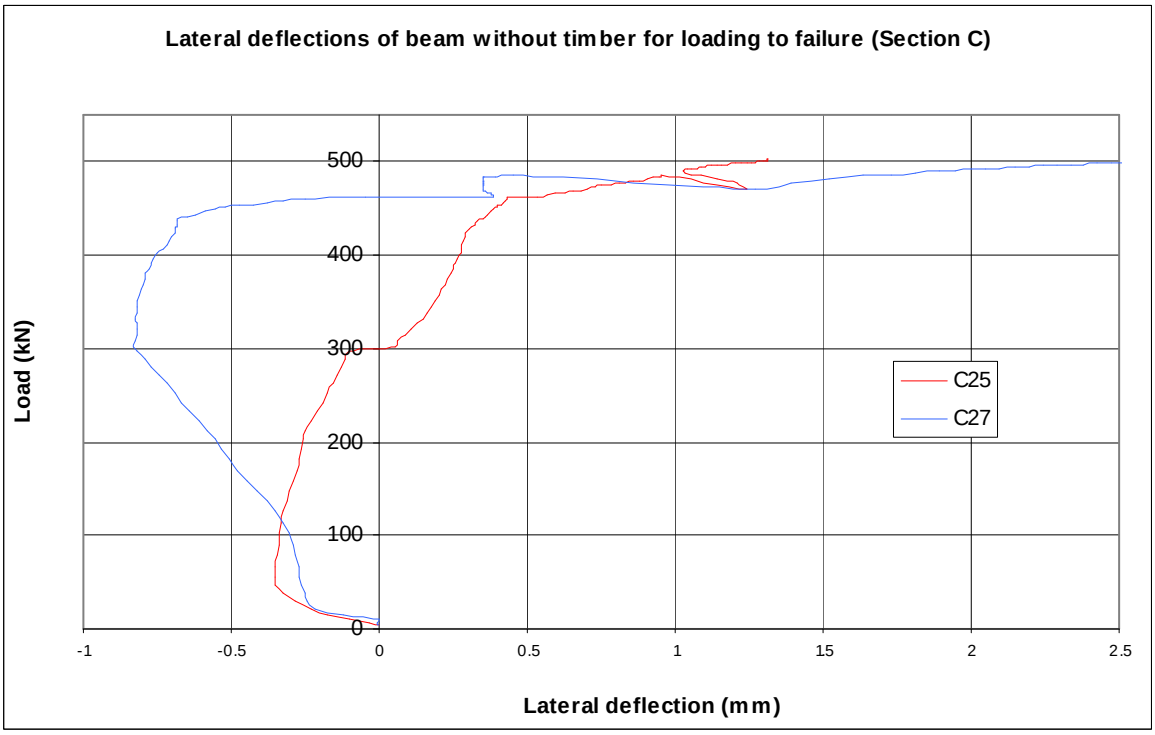

Figure 3.59 Lateral deflections of Section C, for loading to failure.

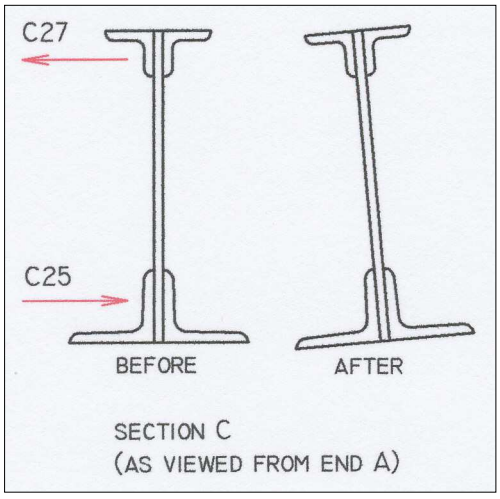

Figure 3.60 Lateral deflection of Section C, for loading to failure.

3.13 Analysis of strain data from Edinburgh GPO beam tests

The load / strain graphs for the top and bottom surfaces of the GPO beam, with and without timber attached, are shown in Figure 3.61. It can be seen from Figure 3.61 that for a given load the top flange strains were greater than the bottom flange strains. This is because the neutral axis is closer to the bottom flange. Comparing the bottom flange strains of the two beams it appears that the beam with timber attached was a little stiffer than that without timber. This is also evident by comparison of the top flange strains.

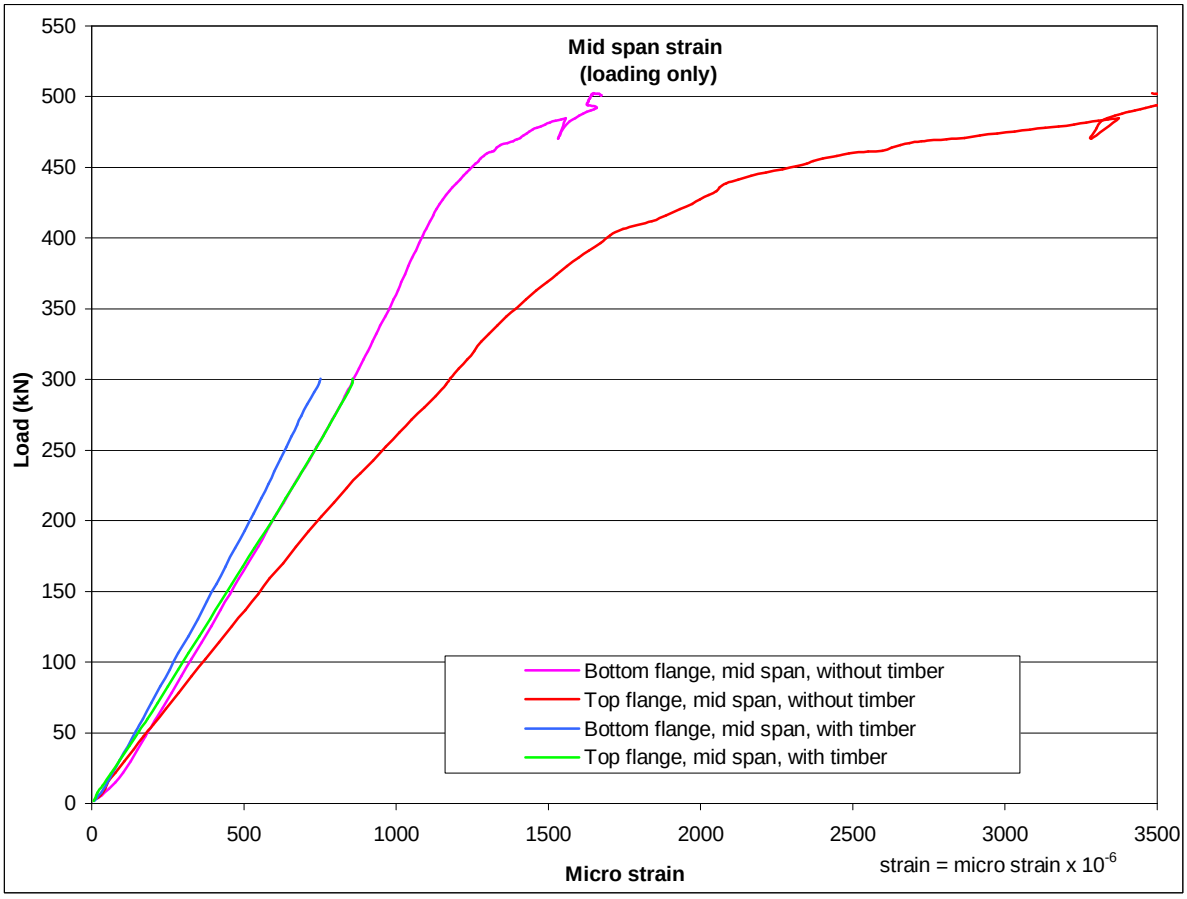

Figure 3.61 Load /strain diagrams for testing of Edinburgh GPO beam, with and without timber.

The graphs in Figure 3.61 also indicate that buckling began at about 400kN. The beam with timber attached was not loaded beyond 300kN to avoid strain hardening the material. The beam without timber was loaded all the way to failure. Only the loading phase of the tests are shown in Figure 3.61.

3.14 Conclusions from beam tests

Elastic loading of the notched Royal Albert Hall beam (see Figure 3.8) indicated that it was stiffer than the un-notched beam. This was unexpected as a notch should reduce the stiffness of the beam. The most likely cause of the difference between the two experimentally generated graphs in Figure 3.8 may be due to the fact that the graph for the un-notched beam was generated by measurement of machine movement, which is controlled by a hydraulic system that is not perfectly stiff. In effect, the graph for the un-notched beam resulted from the combined flexibility of the beam and the hydraulic system, giving the appearance that the un-notched beam was less stiff than the notched beam. The graph for the notched beam is more accurate as it was produced by direct measurement of the deflection of the beam. The expected lower stiffness of the notched beam is evident when compared with the theoretical elastic deflection graph for the un-notched beam.

The aim of inducing a crack originating from the notch proved successful despite the fact that the finite element analysis of the notched beam, conducted prior to testing, showed very little stress elevation around the notch (see Figure 3.32). The reason for inducing cracking at the notch was to enable more control over the manner of failure. The idea was to witness cracking of the beam through the general material of the beam rather than preferential cracking through some internal flaw, such as a large slag inclusion. From the sudden cracking of the beam, under a slowly applied load, it is clear that the beam was quite brittle. The un-notched beam also failed in a sudden and brittle manner. Throughout the bending test of the beam lateral deflections were insignificant and loading to failure occurred within the vertical plane. This is not surprising given the brittleness of the beam. A ductile beam would exhibit considerable lateral and vertical deflection before failure and would ultimately buckle laterally as occurred with the Edinburgh GPO beam.

The graphs in Figure 3.17 show that the strain behaviour of both the notched and un-notched Royal Albert Hall beams was similar during the regions of elastic loading and

yielding. However, the test results indicate that the effect of the notch was to reduce the ultimate failure load from 373kN in the case of the un-notched beam to 283kN for the notched beam. In addition, the notched beam failed at a lower value of strain and without any appreciable degree of plastic flow, and there was no warning of imminent collapse in terms of visual deflection, prior to the appearance of a large crack. All of these observations lead to the conclusion that these wrought iron beams from the Royal Albert Hall were brittle, and therefore unsafe for continued use.

The Edinburgh GPO beam exhibited considerable deformation during testing indicating that it possessed considerable ductility, typical of good wrought iron. The graphs in Figure 3.41 indicate that the beam with timber attached was slightly stiffer than that without timber. However, the stiffness of the beam with timber was not so much greater as to indicate that the timber was added to enhance stiffness or strength. Lateral torsional buckling was the ultimate failure mode of this built-up beam. Using BS5950, the buckling resistance moment of the beam was calculated to be 49.7kNm which would mean that the load at which lateral torsional buckling would be expected to occur would be 97kN. However, buckling occurred at a higher value, as indicated in Figure 3.46, this may have been due to partial localised horizontal restraint of the compression flange provided by the friction between the two load application points and the top flange. Had full lateral restraint been provided along the entire length of the beam then lateral torsional buckling would have been avoided.

Chapter 4 Mechanical tests on wrought iron samples

4.1 Tensile testing of wrought iron samples

For this research project 20 tensile tests were conducted. Two types of specimen shape were used. Seven round test pieces were turned from bolt iron. The remaining 13 test pieces were machined from flat iron to form pieces of rectangular cross section. The shapes and sizes of the test pieces are shown in Figure 4.1 and Table 4.1. Both test specimen shapes comply with British Standard EN 10002-1:2001

Wrought iron from three types of structural component were tested. These were, plate iron, angle iron, and bolt iron, all from the Edinburgh GPO beam. (see Chapter 3). The rivets from the beam were too short to make desirable tensile test pieces. In order to measure modulus of elasticity and obtain an accurate stress strain relationship, a gauge length of 50mm was necessary, so that an extensometer could be applied. This was not possible as the rivets were only 50mm long. However, the rivets were tested in shear. The rivet tests are discussed in section 4.7.

Of the 13 flat test pieces 8 were selected for testing using a rosette of three strain gauges fixed to the middle of the piece as shown in Figure 4.2. The purpose of this was to enable measurement of Poisson's ratio.

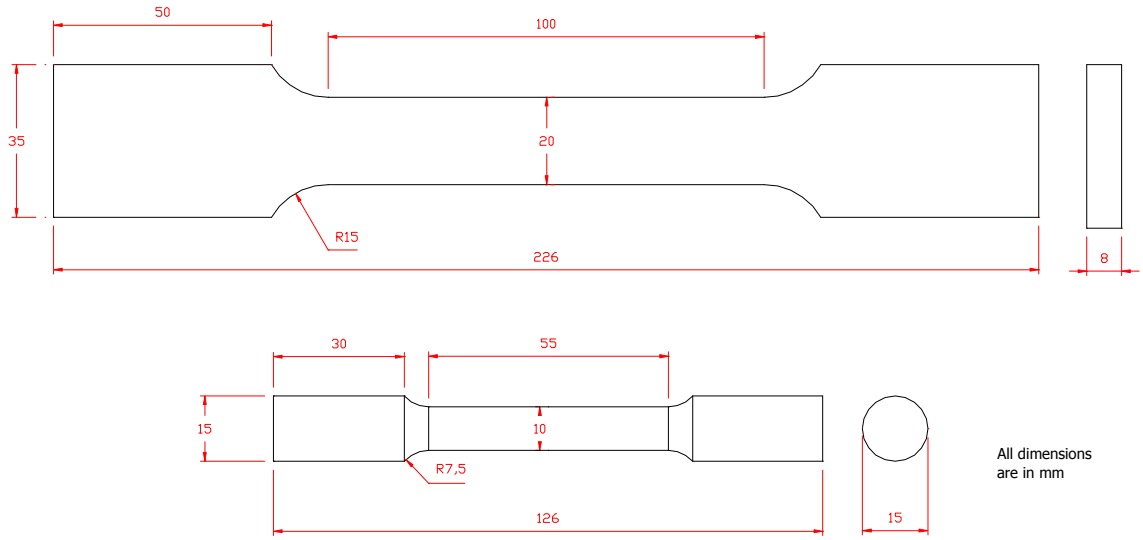

Figure 4.1 Shape of tensile test pieces

Specimen name	Shape of cross section	Source of test piece	Width	Thickness	Diameter	Area of cross section	Gauge length*	Parallel length
			(mm)	(mm)	(mm)	(mm^2)	(mm)	(mm)
A1	Rectangular	Angle	19.90	8.33	---	165.8	50	100
A2	Rectangular	Angle	19.90	8.33	---	165.8	50	100
A3 *	Rectangular	Angle	19.98	8.33	---	166.4	6	100
A4 *	Rectangular	Angle	19.91	8.31	---	165.5	6	100
A5 *	Rectangular	Angle	19.97	8.29	---	165.6	6	100
A6 *	Rectangular	Angle	19.92	8.35	---	166.3	6	100
P1	Rectangular	Plate	19.95	8.33	---	166.2	50	100
P2	Rectangular	Plate	19.89	8.31	---	165.3	50	100
P3	Rectangular	Plate	19.80	8.28	---	163.9	50	100
P4 *	Rectangular	Plate	19.76	8.30	---	164.0	6	100
P5 *	Rectangular	Plate	19.87	8.27	---	164.3	6	100
P6 *	Rectangular	Plate	20.05	8.33	---	167.0	6	100
P7 *	Rectangular	Plate	19.94	8.36	---	166.7	6	100
B1	Round	Bolt	---	---	9.72	74.20	50	55
B2	Round	Bolt	---	---	9.81	75.58	50	55
B3	Round	Bolt	---	---	9.67	73.44	50	55
B4	Round	Bolt	---	---	9.96	77.91	50	55
B5	Round	Bolt	---	---	9.87	75.51	50	55
B6	Round	Bolt	---	---	9.94	77.60	50	55
B7	Round	Bolt	---	---	10.00	78.54	50	55

Table 4.1 Summary of physical dimensions of tensile test specimens. Specimens with the symbol * had a rosette of strain gauges attached for which the gauge length was 6mm, while the other specimens had a extensometer attached with a gauge length of 50mm. All test pieces came from the Edinburgh GPO beam.

In all the tests, load was applied by stretching the specimens in an INSTRON 4507 testing machine at a steady rate of 1mm/min. In the case of one of the rectangular specimens with strain gauge attached, the test proceeded as shown in Figures 4.2 to 4.4.

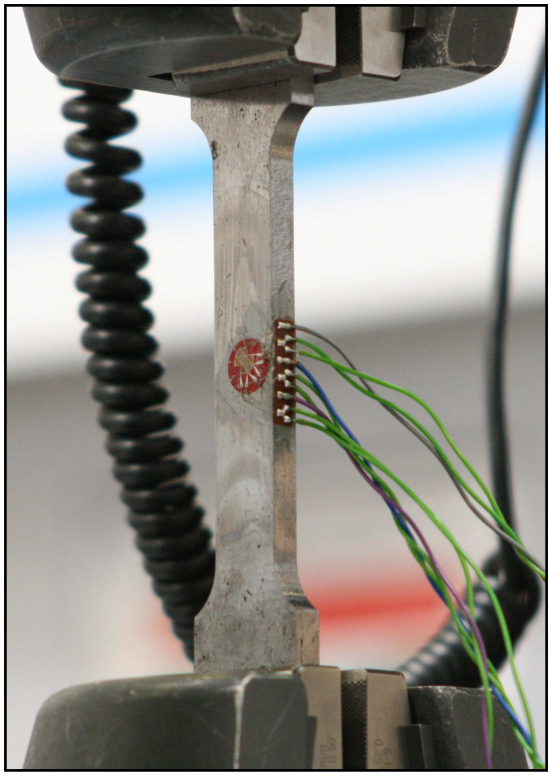

Figure 4.2 Arrangement of rosette strain gauge on rectangular specimen T2 at start of test.
(Photo by M.O'Sullivan 2009)

After 3mins 30s the bar entered the plastic range and after a total time of 4mins 56s it stretched too much for the glue to hold the connections in place.

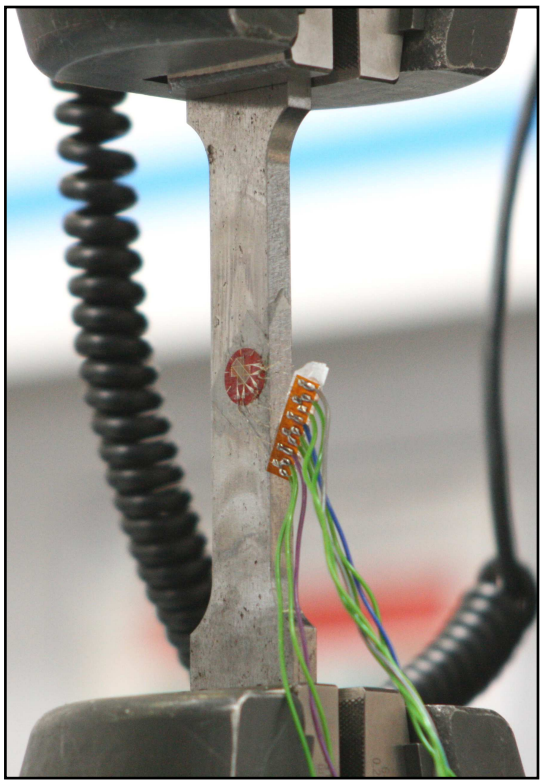

Figure 4.3 Test bar T2 near end of test (photo by M.O'Sullivan 2009)

The entire elastic range of the test was recorded before loss of the strain gauge.

The greatest elongation occurred after the material entered the plastic range of loading. Even though the gauge failed before the bar broke the testing machine measured the ultimate failure load. The arrangement for the round tensile test pieces is shown in Figure 4.6. The results of all tests are summarised in Table 4.2.

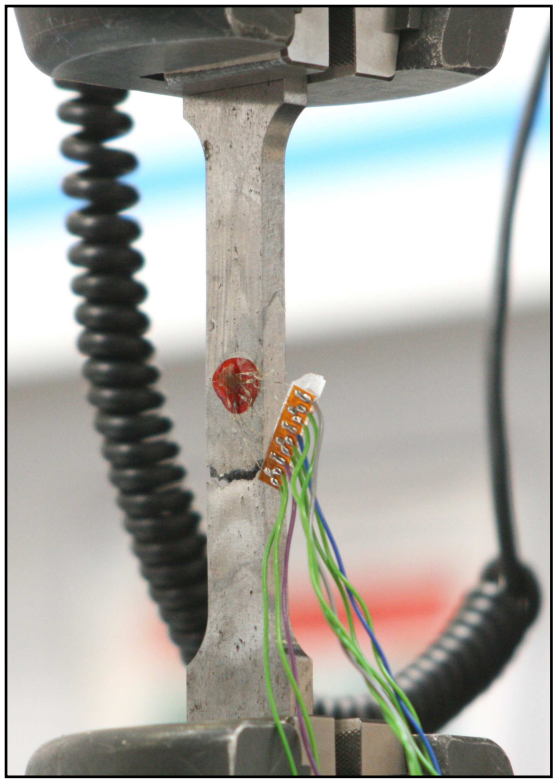

Figure 4.4 Ultimate failure occurred 5mins 58sec after the start of the test. (photo by M.O'Sullivan 2009)

Photographs of tensile testing of round test pieces made from wrought iron bolts.

Figure 4.5 Test arrangement for round specimen

Figure 4.6 Close-up of test piece showing extensometer attached

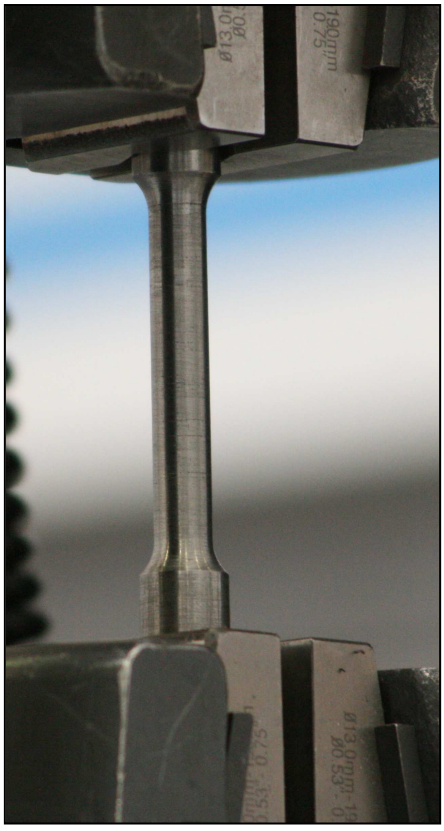

Figure 4.7 Test piece after removal of extensometer.

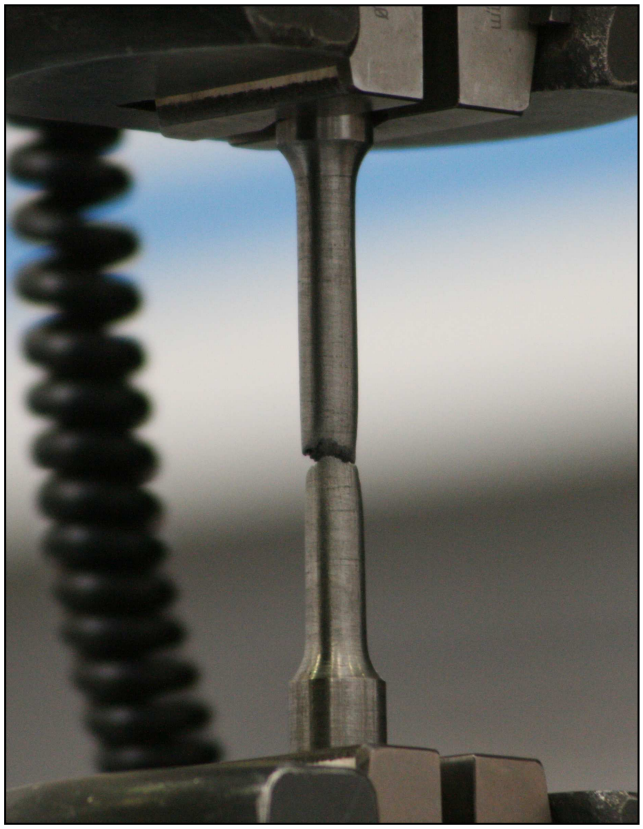

Figure 4.8 Test piece after fracture showing necking at fracture site.

(All photographs by M.O'Sullivan 2009)

4.2 Results of tensile tests

Name	Shape of cross section	Source of test piece	Yield strength	Ultimate strength	Modulus of elasticity	Poisson's ratio	Shear modulus	Reduction of area at fracture	Ultimate strain
			(N/mm^2)	(N/mm^2)	(N/mm^2)		(N/mm^2)	%	%
A1	Rectangular	Angle	249	296	145403	---	---	---	---
A2	Rectangular	Angle	250	346	185345	---	---	18.5	12.0
A3 *	Rectangular	Angle	198	341	166870	0.21	68693.6	20.2	---
A4 *	Rectangular	Angle	223	342	201073	0.27	78957.1	20.7	---
A5 *	Rectangular	Angle	247	358	177321	0.27	69982.6	21.5	---
A6 *	Rectangular	Angle	256	356	181406	0.25	72770.7	25.5	---
Mean			**237**	**340**	**176236**	**0.25**	**72551**	**21.3**	---
Standard deviation			22	23	18794	---	4474	2.6	---
Characteristic value			**189**	**291**	**135264**	---	**60785**	**15.2**	---
P1	Rectangular	Plate	247	316	143955	---	---	11.9	7.4
P2	Rectangular	Plate	251	300	169783	---	---	8.2	5.4
P3	Rectangular	Plate	254	308	130033	---	---	8.4	5.3
P4 *	Rectangular	Plate	264	334	194641	0.22	79480.6	9.3	---
P5 *	Rectangular	Plate	261	325	184523	0.24	74253.8	8.4	---
P6 *	Rectangular	Plate	255	324	174686	0.25	70038.7	9.9	---
P7 *	Rectangular	Plate	249	316	176817	0.25	70593.7	9.1	---
Mean			254	318	167777	**0.24**	**73592**	**9.3**	**6.0**
Standard deviation			6	11	22832	---	4349	1.3	1.2
Characteristic value			**241**	**293**	**118917**	---	**62155**	**6.6**	**2.0**
B1	Round	Bolt	267	368	212669	---	---	28.2	23.7
B2	Round	Bolt	263	398	198860	---	---	27.9	21.8
B3	Round	Bolt	286	375	193802	---	---	31.6	23.0
B4	Round	Bolt	288	390	188967	---	---	42.7	25.0
B5	Round	Bolt	271	414	189433	---	---	34.3	29.0
B6	Round	Bolt	272	389	184167	---	---	36.4	26.5
B7	Round	Bolt	285	398	183968	---	---	39.3	26.9
Mean			**276**	**390**	**193124**	---	---	**34.3**	**25.1**
Standard deviation			10	15	10086	---	---	5.6	2.5
Characteristic value			**254**	**357**	**171540**	---	---	**22.4**	**19.8**

Table 4.2 Summary of tensile test results. Specimens with the symbol * had a rosette of strain gauges attached which enabled measurement of Poisson's ratio. All test pieces came from the Edinburgh GPO beam. Test specimen A1 failed in the jaws of the testing machine hence the absence of a ductility result.

For calculation of characteristic values of material properties Eq.4.1 is used. The characteristic value is the value below which 5% of the results are expected to lie.

$$x_{char} = \bar{x} - k\sigma \quad \text{Eq.4.1 (Bussell 1997)}$$

where $\bar{x} =$ mean value

$\sigma =$ standard deviation from mean

$k =$ factor depending on number of samples tested (see Table 4.3)

No. of samples	3	4	5	6	8	10	20	∞
k	3.37	2.63	2.33	2.18	2.00	1.92	1.76	1.64

Table 4.3 Relationship between 'K' factor and number of samples. (Bussell 1997)

The stress-strain graphs for some of the tensile tests listed in Table 4.2 are shown in Figure 4.9. These graphs are obviously very congested, therefore a smaller number of graphs have been selected for closer examination. and are shown in Figure 4.11. However, Figure 4.9 has been presented to show the differences in ultimate strain and ultimate strength between the round test pieces and the rectangular ones. It can be seen in Figure 4.9 that the round test pieces, which are bolt iron (with symbol B in Figure 4.9) experienced much higher ultimate strain and had somewhat higher ultimate strength than the rectangular test pieces (with symbol A for angle iron and P for plate iron). In effect, this means that the bolt iron was much tougher than the plate or angle iron. Toughness is the energy absorbed up to the point of fracture, which in equal to the area under the stress strain curve. The reason for this difference may be that bolt iron underwent greater refinement in the puddling and rolling process. Greater refinement reduces the slag content and makes the remaining slag inclusions smaller and more even dispersed. However, in the case of two of the round test pieces, large slag inclusions were present and were of a size sufficient to cause the test pieces to split. This is discussed further in section 4.3.

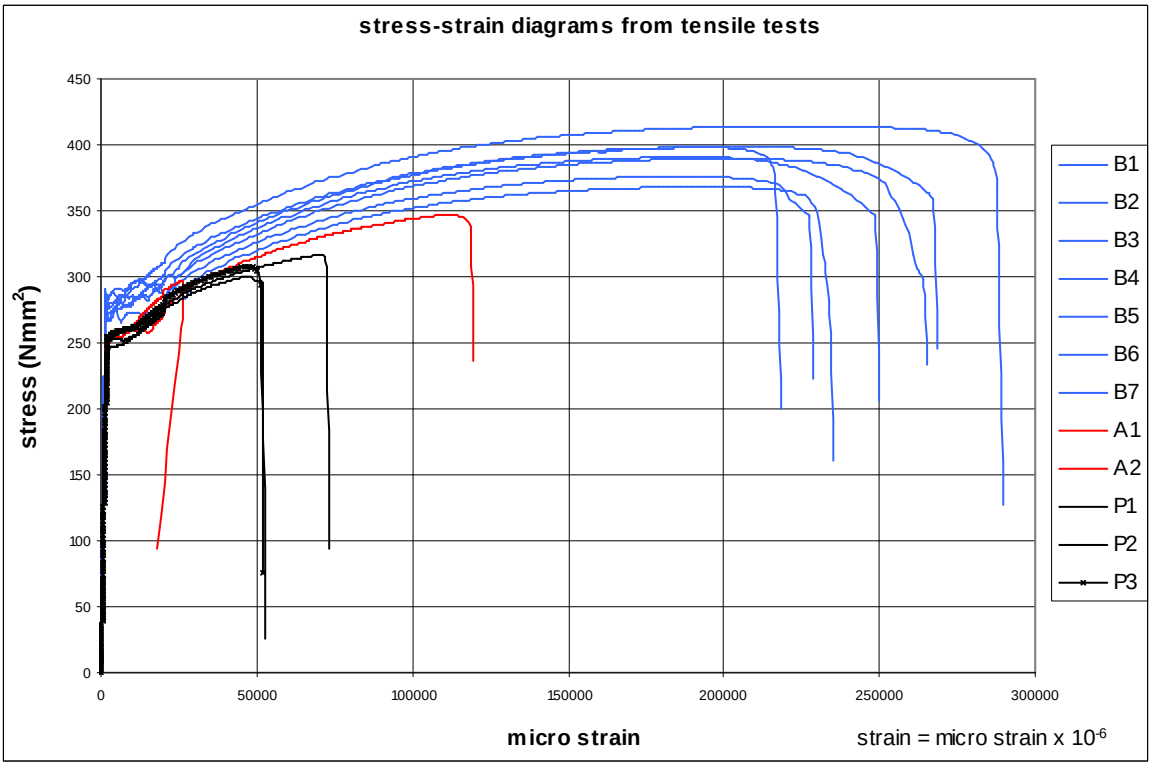

Figure 4.9 Stress strain graphs for tensile tests described in Table 4.2

During plastic deformation the sides of the flat test pieces drew inward in the middle more than at the corners as shown in Figure 4.10.

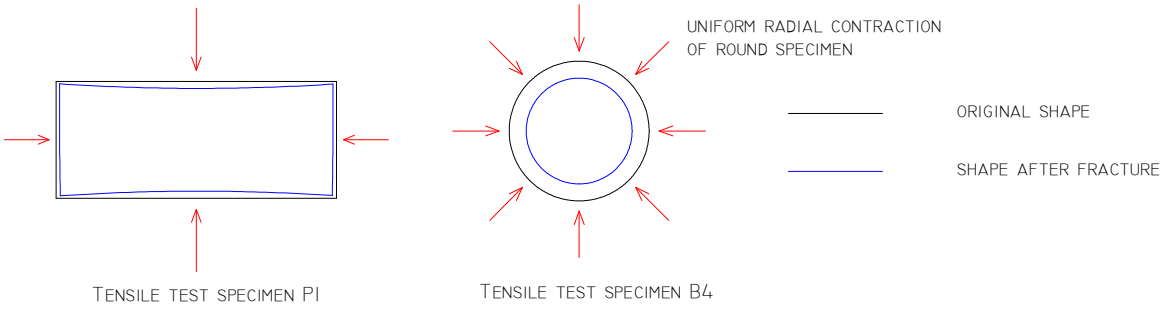

Figure 4.10 Deformation of cross section of test pieces at fracture site.

Of the test results listed in Table 4.2 not all of the stress-strain graphs have been presented because eight of the test pieces had rosette strain gauges attached, which fell off before fracture, thereby preventing a stress-strain plot to the point of failure. However, the ultimate strengths were measured and are given in Table 4.2.

The most important part of the stress-strain diagram is the portion up to yielding of the metal. Therefore, a close-up of the elastic portion of the stress-strain graphs of Figure 4.9 is shown in Figure 4.11 for one sample of each component type. Generally the elastic regions of the graphs follow a similar slope which means little variation in the value of elastic modulus. However, there is an obvious difference in the values of yield strength between the round specimens and the rectangular ones. The round test pieces follow a relatively similar trend with a yield stress above 250N/mm^2, whereas graph P6 in Figure 4.11, for the rectangular test piece clearly deviates from a linear trajectory at about 170N/mm^2. At this point the rectangular test piece began to yield. However, it completely yielded just above 250 N/mm^2. All of the graphs for the rectangular test pieces deviated from linearity before the round test pieces did so. This indicates that bolt iron is stronger than angle or plate iron, but the shape of the test specimen may also have contributed to this result.

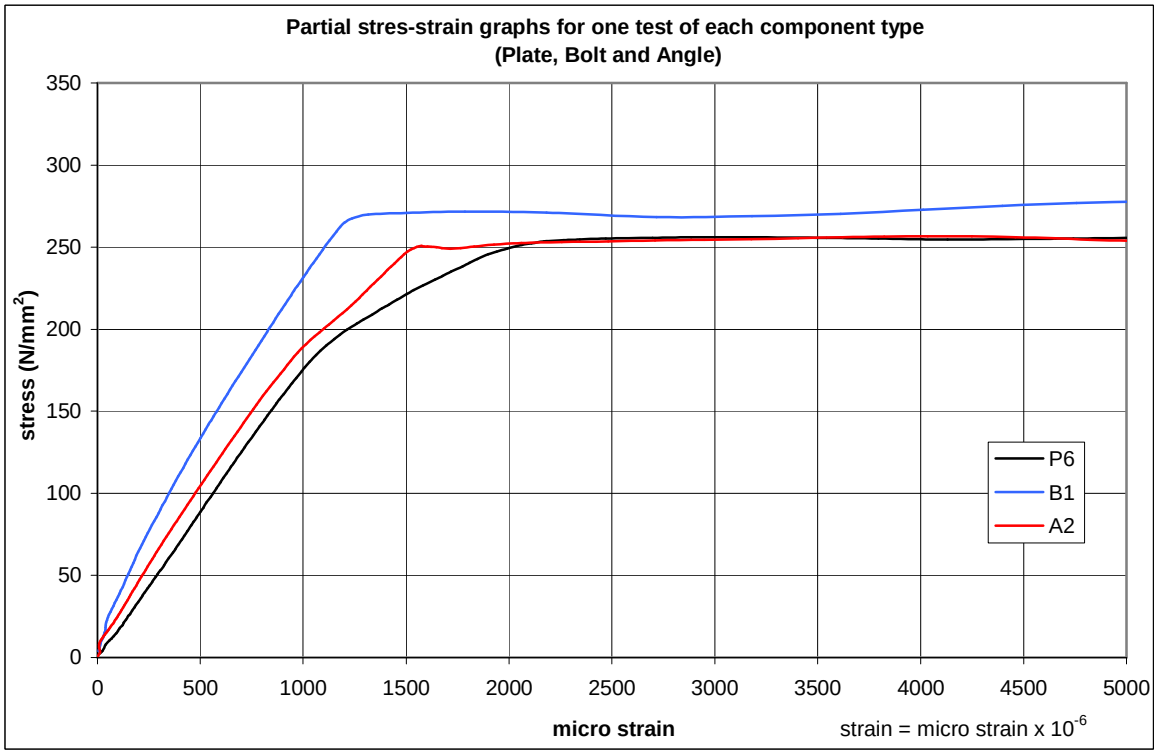

Figure 4.11 Partial stress-strain graphs for one test of each component type.

4.3 Ductility of tensile specimens

Both the rectangular and round test pieces experienced obvious necking at the fracture site. Both the ultimate elongation and the reduction in cross sectional area, expressed as percentages were used as measures of ductility and are included in Table 4.2. The degree of necking of one of the round test pieces is shown in Figure 4.12. This particular test piece had a long slag inclusion, which in the photograph, is shown edge-on and appears as a black streak along almost the entire length of the piece.

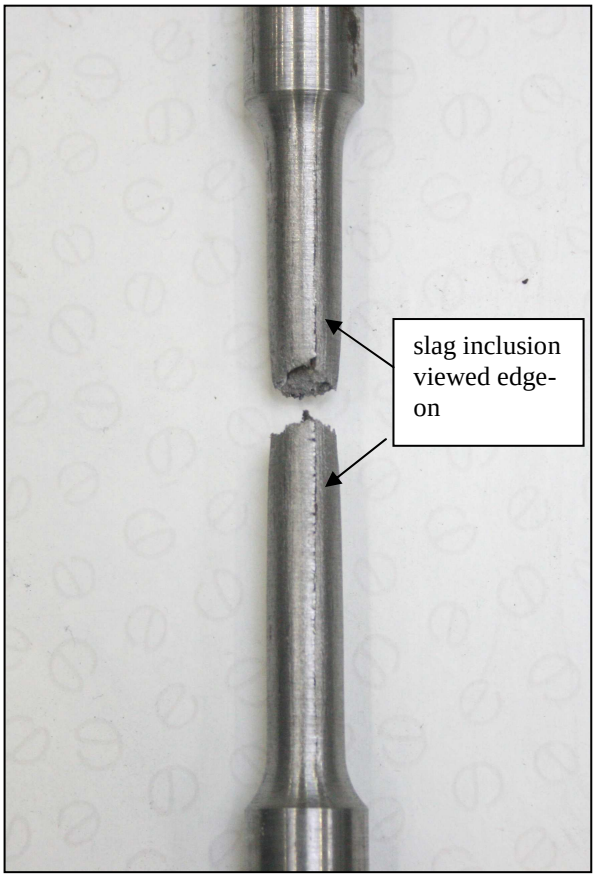

Figure 4.12 Tensile test piece with long slag inclusion. (Photo by M. O'Sullivan 2009)

In another round test piece, shown in Figure 4.13, two splits formed in the longitudinal direction along two long flat slag inclusions. The shape of these inclusions is a consequence of the rolling action during manufacture. The compression from the rolls causes the liquid slag to spread out flat, forming a broad separation of the metal. Wide inclusions, such as these, provide planes on which the metal can easily slip under high tension, hence the formation of the splits.

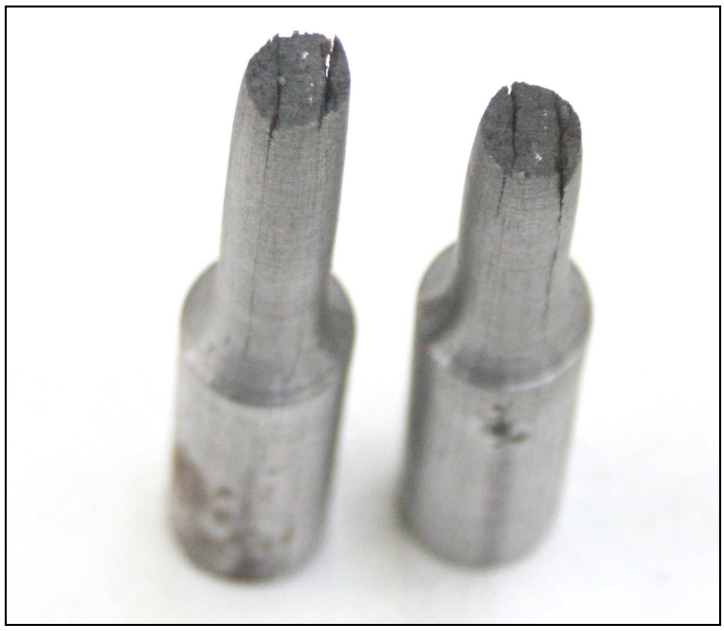

Figure 4.13 Test piece with longitudinal splits. (Photo by M.O'Sullivan 2009)

Usually small components such as bolts and rivets were highly refined to avoid such large slag inclusions. The round test pieces were turned from 5/8in (15.8mm) diameter bolts. The maximum diameter was left on the bolts when machining the test pieces in order to minimise the detrimental influence of slag inclusions.

This particular example demonstrates why the longitudinal direction of structural components normally followed the direction of rolling. Had the inclusion been across the bolt rather than along it, fracture would have occurred much more easily. In the case of the web plate of the beam the directionality of the slag inclusions showed that the longitudinal direction of the beam was along the rolling direction.

The tensile test pieces exhibited narrowing at the fracture cross section as shown earlier in Figure 4.10. This can also be seen in Figure 4.14. However, there was also a marked difference in the surface texture of the test pieces after testing. This can be seen in Figure 4.14 where the surface of the metal has become rough. This was caused by radial contraction, which the round test pieces experienced as they were stretched. In addition, it caused the surface of the metal to undergo circumferential contraction, which gave the metal surface a rough texture.

Figure 4.14 Stretching the test piece caused radial contraction across the section, and circumferential contraction of the metal surface, which gave it a rough texture. (M.O'Sullivan 2009)

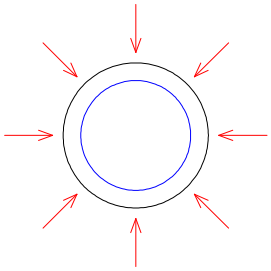

Figure 4.15 Radial and circumferential contraction of round tensile test piece.
(M.O'Sullivan 2009)

There appears to be a distinct difference in the ductility results of the three metal components tested. The ultimate strain of the 8 test pieces with rosette strain gauges attached, was not measured, because the gauges detached before fracture. Therefore, the most complete set of ductility results is the reduction of area at fracture. From these results, the components listed in order of increasing ductility are: Plate, Angle, and Bolt, with mean ductility values of 9.3%, 21.3%, and 34.3% respectively. The bolt iron is clearly the most ductile component, which is to be expected of a small component, as such items would normally have been made from a higher grade of metal. That is, small metal components would need to be made form a metal that had small and evenly distributed slag

inclusions. Refinement of the slag inclusions was achieved by subjecting the metal to more cycles of puddling, piling and rolling.

The results also show that angle iron is more ductile than plate iron. It may be, that components which required a greater degree of forming and shaping, needed greater care during manufacture. Bad metal was generally spotted during the forming process. Red-short iron was easily identified as it would crumble during hot rolling. Plate iron did not need any special shaping during rolling and so slightly inferior metal may not have been detected. Examination of the metal under a microscope shows that the angle iron is generally clearer than the plate iron, in that, the angle iron has much less slag, as shown in Figure 4.16.

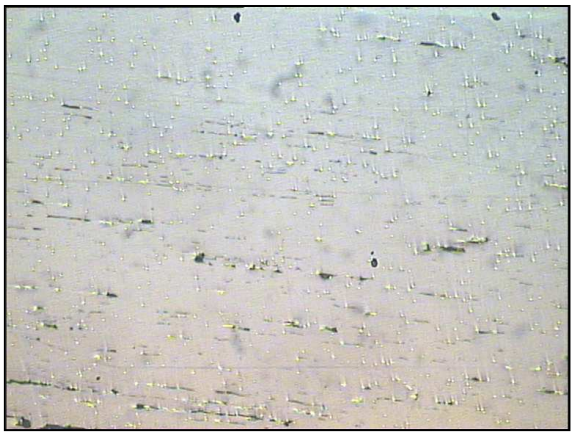

Figure 4.16 Angle iron under x5 magnification (Photo by M.O'Sullivan 2009)

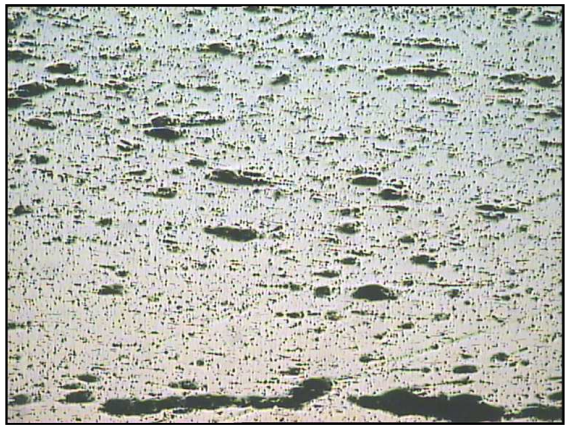

Figure 4.17 Plate iron under x5 magnification (Photo by M.O'Sullivan 2009)

It is difficult to know whether or not some of the black dots in Figure 4.17 are due to pitting or small slag inclusions, but wherever the black dots appear elongated, it is certainly a slag inclusion. Both photographs show the metal in the left-to-right rolling direction. The surface shown was a fresh-cut longitudinal section through the thickness of the component, so any pitting cannot be due to rust but rather to polishing imperfection.

4.4 Use of strain gauges to determine mechanical properties

The rosette gauges applied to 8 of the flat tensile test pieces enabled determination of modulus of elasticity, Poison's ratio, shear modulus of elasticity, and measurement of the maximum shear stresses in the test pieces. This section is concerned with demonstrating how these mechanical properties were determined for one of the test pieces. Consider test piece P5 shown in Figure 4.18.

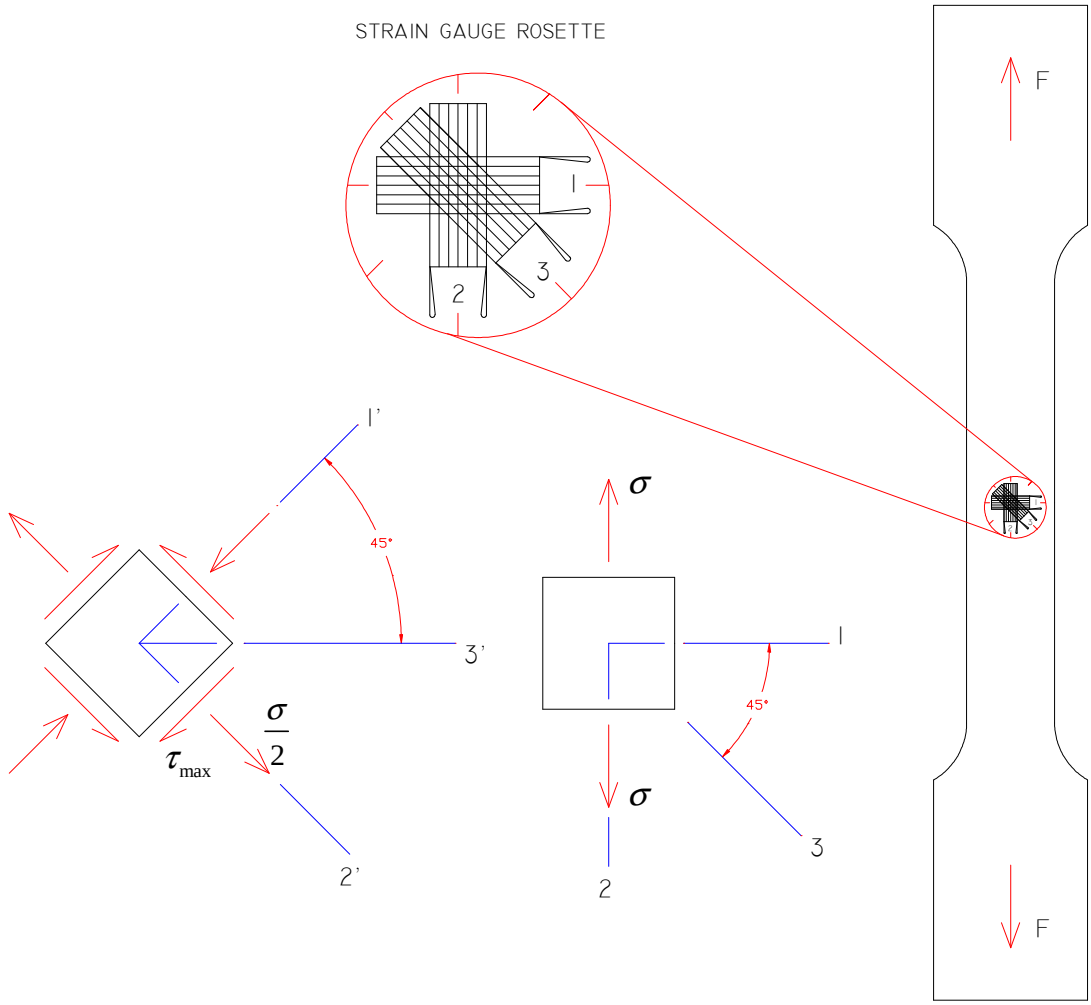

Figure 4.18 Test piece P5 with rosette strain gauge and associated stress elements. (M.O'Sullivan 2009)

Also shown in Figure 4.18 is a close-up of the rosette strain gauge and two stress elements for the point on the test piece, where the gauge was applied. In uniaxial tension the maximum shear stresses occur on planes oriented at 45^{o} to the direction of applied load.

4.5 Determination of Poisson's ratio and shear modulus of elasticity

The rosette gauge measures strain in three directions. Poisson's ratio is the magnitude of the ratio of the strain readings from gauges 1 and 2, chosen at any load within the elastic range. The load-strain diagrams for all three gauges are shown in Figure 4.20. At load 30kN the test piece is within the linearly elastic range of the metal. At this point the strain readings for gauges 1 and 2 were -241 micro-strain and 992 micro-strain, giving a Poison's ratio value of 241/992 = 0.24. Since the modulus of elasticity (E) has already been determined from the slope of the linear portion of the stress-strain graph (E = 184523 N/mm^2), the shear modulus of elasticity (G) can be calculated using Eq.4.2. The complete set of results for E, G and ν are given in Table 4.2.

$$G = \frac{E}{2(1+\nu)} = \frac{184523\ N/mm^2}{2(1+0.24)} = 74404\ N/mm^2 \qquad \text{Eq.4.2}$$

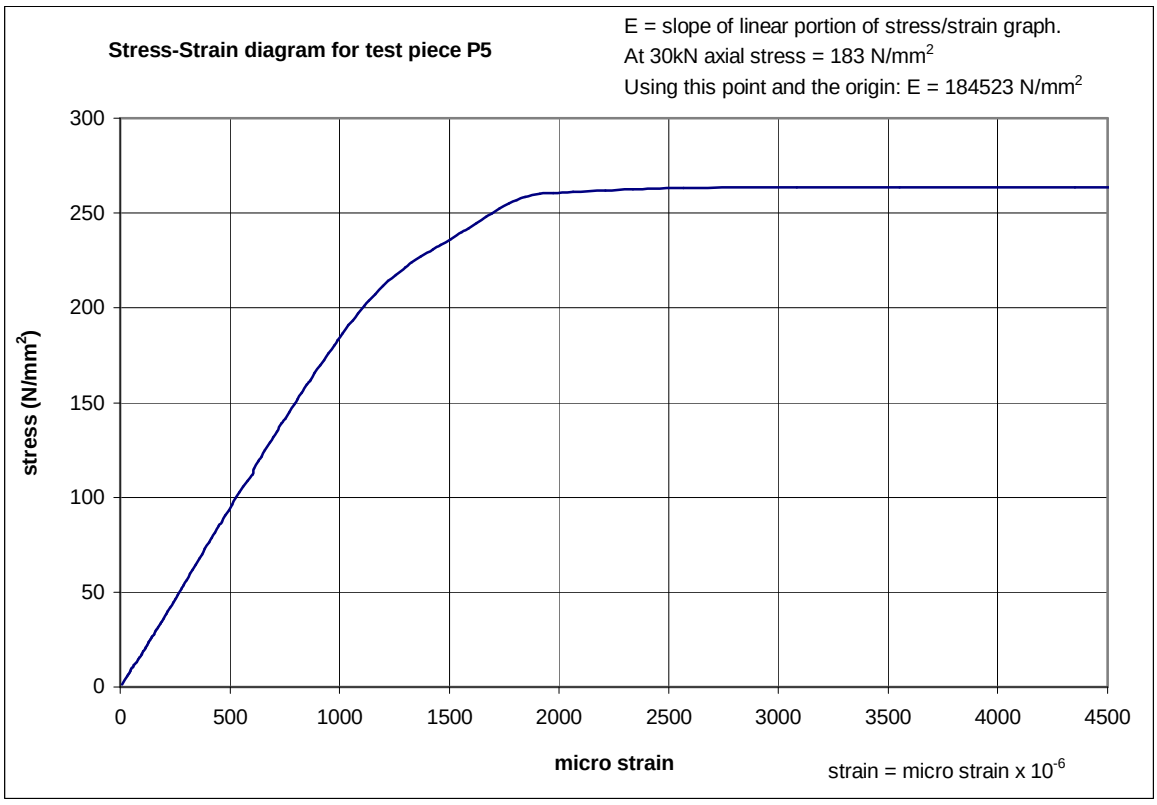

Figure 4.19 Stress/ strain diagram for test piece P5

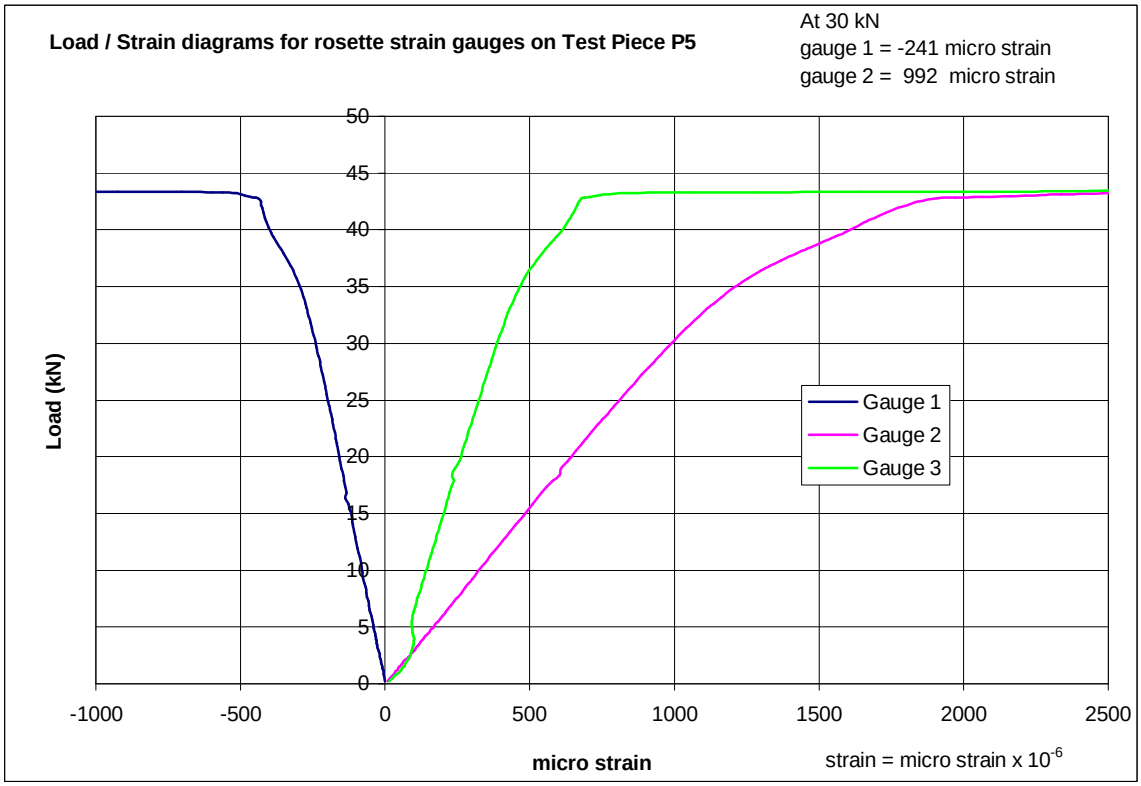

Figure 4.20 Load / strain diagrams for the rosette gauge on test piece P5

4.6 Determination of maximum shear stresses in tensile test piece

Step 1: Construct Mohr's circle of strain

The test piece is in uniaxial tension, which is a special case of plane stress, (i.e. uniaxial stress). As shown in Section 4.2, the metal experienced strain in all three perpendicular directions. However, the presence of a strain ε_z does not affect the geometric relationships used in the derivations of the strain transformation equations for the x-y plane. Therefore, the equations are valid even when a strain ε_z exists.

The rosette gauge could measure strains in one plane only. The difference between the strains in the two principal directions (i.e. directions 1 and 2) on the face of the test piece are illustrated in Figure 4.20. The greatest strain due to the pulling force was along the longitudinal axis of the test piece (i.e. direction 2) while the transverse strain, along direction 1, was due to the Poisson effect. In the discussion that follows ε_1 , ε_2 and ε_3 denote the strain readings from gauges 1, 2 and 3 respectively, of the rosette.

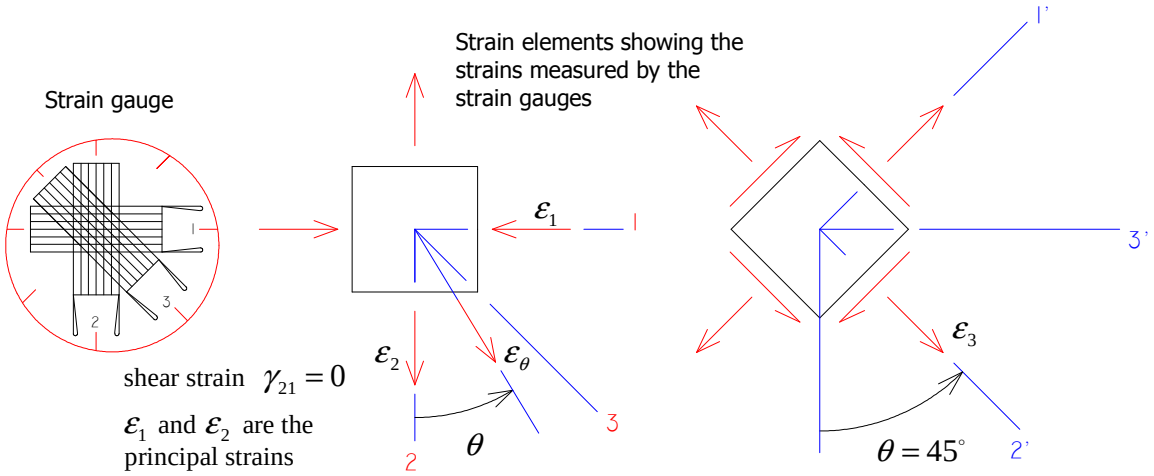

Figure 4.21 Strain elements showing the strains measured by the strain gauges

Under a tensile load of 30kN the strain readings were:

ε_1 = -240.6 micro-strain, ε_2 = 991.8 micro-strain, ε_3 = 375.6 micro-strain,

Radius of Mohr's circle is given by:

$$R = \sqrt{\left(\frac{\varepsilon_2 - \varepsilon_1}{2}\right)^2 + \left(\frac{\gamma_{21}}{2}\right)^2} = \sqrt{\left(\frac{991.8 - (-240.6)}{2}\right)^2 + \left(\frac{\gamma_{21}}{2}\right)^2} \qquad \text{Eq.4.3}$$

The strain ε_θ in any arbitrary direction θ is given by the transformation equation:

$$\varepsilon_\theta = \frac{\varepsilon_2 + \varepsilon_1}{2} + \frac{\varepsilon_2 - \varepsilon_1}{2}\cos 2\theta + \frac{\gamma_{21}}{2}\sin 2\theta \qquad \text{Eq.4.4 (Gere 1999)}$$

For an angle $\theta = 45^o$, $\varepsilon_\theta = \varepsilon_3$

Therefore, $\varepsilon_3 = \frac{\varepsilon_2 + \varepsilon_1}{2} + \frac{\varepsilon_2 - \varepsilon_1}{2}\cos 90^o + \frac{\gamma_{21}}{2}\sin 90^o$ from Eq.4.4

Solving for γ_{21} gives $\gamma_{21} = 2\varepsilon_3 - \varepsilon_2 - \varepsilon_1$ Eq.4.5

$\Rightarrow$ shear strain $\gamma_{21} = 2(375.6) - 991.8 - (-240.6) = 0$

Putting this value for γ_{21} into Eq.3.4 gives the radius of Mohr's circle: R = 616.2 micro-strain.

centre of circle: $\varepsilon_{av} = \frac{\varepsilon_2 + \varepsilon_1}{2} = \frac{991.8 + (-240.6)}{2} = 375.6$ Eq.4.6

Mohr's circle of strain is shown in Figure 4.22 together with two strain elements showing the strains measured by the rosette strain gauge.

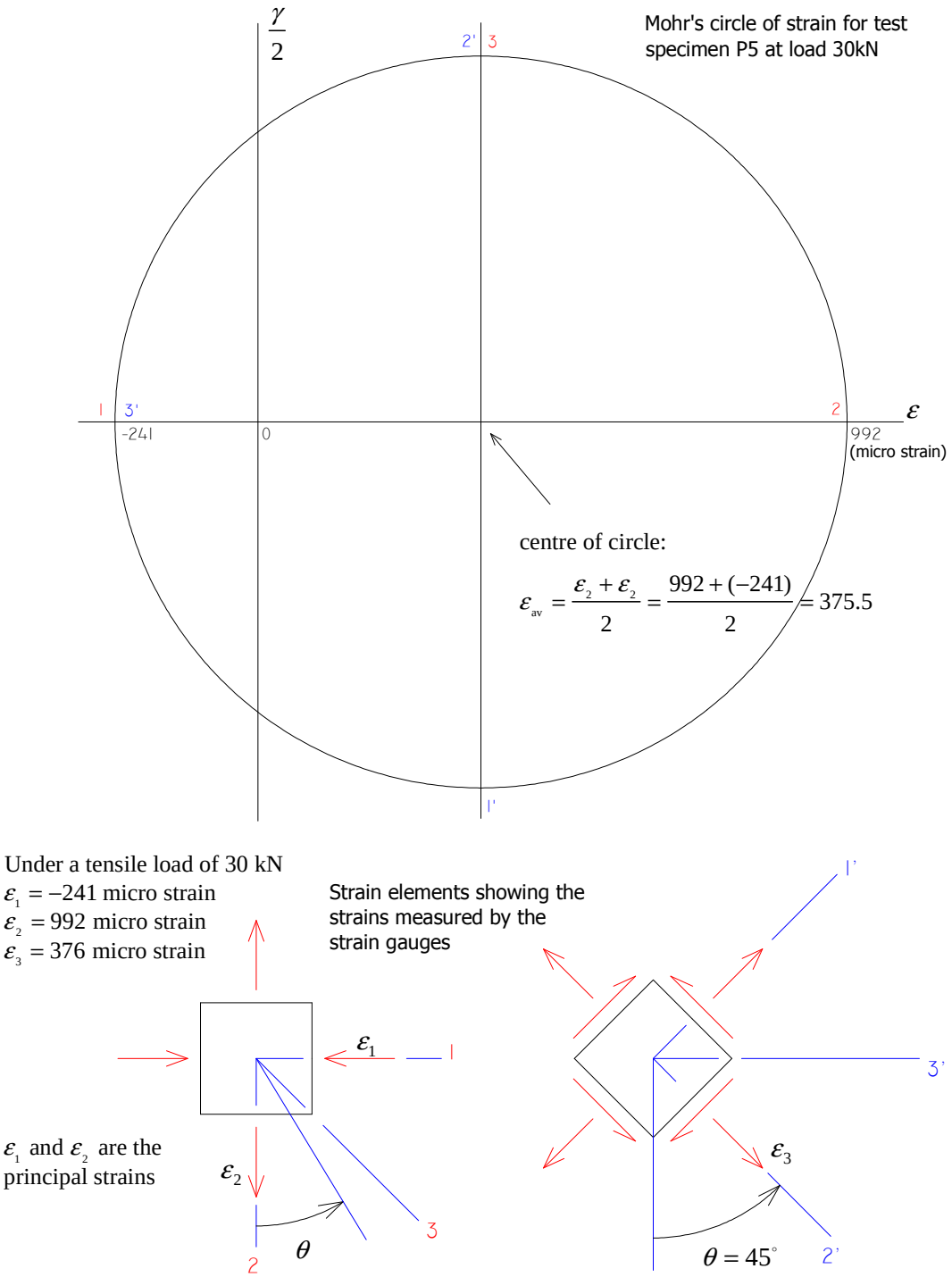

Figure 4.22 Mohr's circle of strain for test specimen P5 at load 30kN, together with associated strain elements. Gauges 1 and 2 of the rosette directly measure the principal strains ε_1 and ε_2 respectively.

STEP 2: Use Hooke's law to determine principal stresses

Using Hooke's law the principal stresses associated with the principal strains may be found as follows

$$\sigma_2 = \frac{E}{1-\nu^2}(\varepsilon_2 + \nu\varepsilon_1) \qquad \sigma_1 = \frac{E}{1-\nu^2}(\varepsilon_1 + \nu\varepsilon_2) \qquad \text{Eq.4.7a,b (Hooke's law)}$$

For test piece P5, modulus of elasticity E = 184523 Nmm^{-2} and Poisson's ratio ν = 0.24. Using the maximum and minimum values of strain from Mohr's circle, the principal stresses are:

$$\sigma_{P2} = \frac{E}{1-\nu^2}(\varepsilon_2 + \nu\varepsilon_1) = \frac{184523\ \text{Nmm}^{-2}}{1-(0.24)^2}\left(991.8\times10^{-6} + 0.24(-240.6\times10^{-6})\right)$$

$$= 183\ \text{Nmm}^{-2}$$

$$\sigma_{P1} = \frac{E}{1-\nu^2}(\varepsilon_1 + \nu\varepsilon_2) = \frac{184523\ \text{Nmm}^{-2}}{1-(0.24)^2}\left(-240.6\times10^{-6} + 0.24(991.8\times10^{-6})\right)$$

$$= -0.5\text{Nmm}^{-2}$$

This value for σ_{p1} should be taken as zero. The maximum shear stresses are most easily found by constructing Mohr's circle for plane stress, which is shown in Figure 4.23.

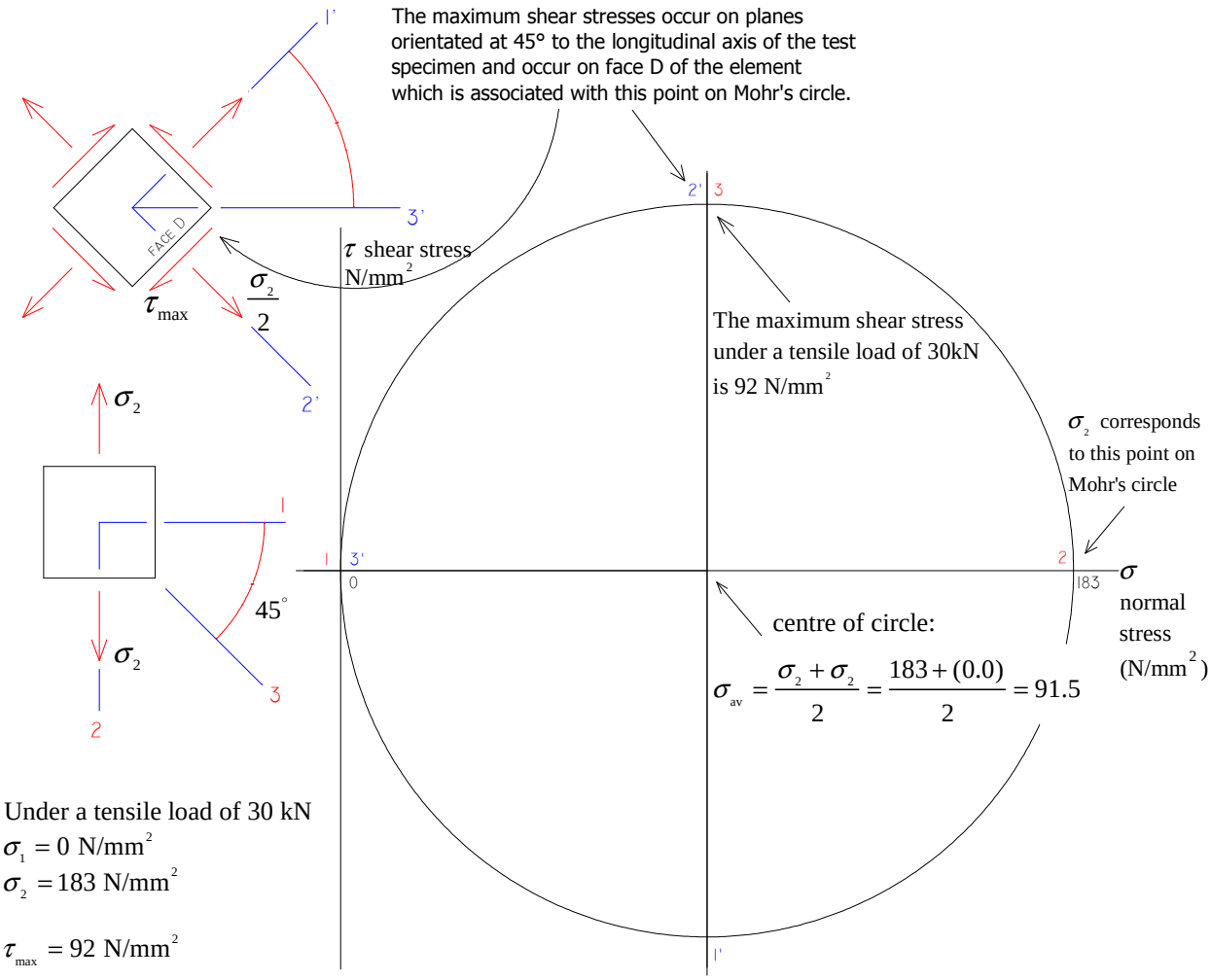

Figure 4.23 Mohr's circle of stress for test specimen P5 at load 30kN, together with associated stress elements. All units are in N/mm^2.

4.7 Testing of rivets in shear

Three rivets from the Edinburgh beam were tested in double shear using the arrangement shown in Figure 4.24. By applying a compressive load to the test piece the rivet experienced a shearing force at two cross sections. The beam was assembled using 3/4 inch (18mm) diameter rivets throughout.

Figure 4.24

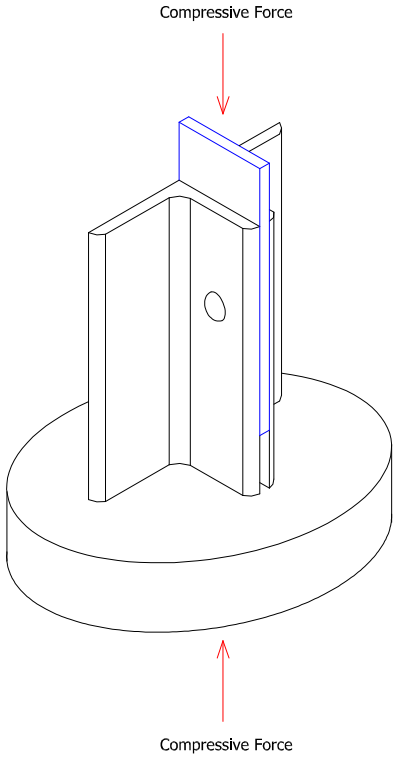

Figure 4.25

Testing of a riveted joint in shear by application of a compressive load to the test piece (M. O'Sullivan 2010)

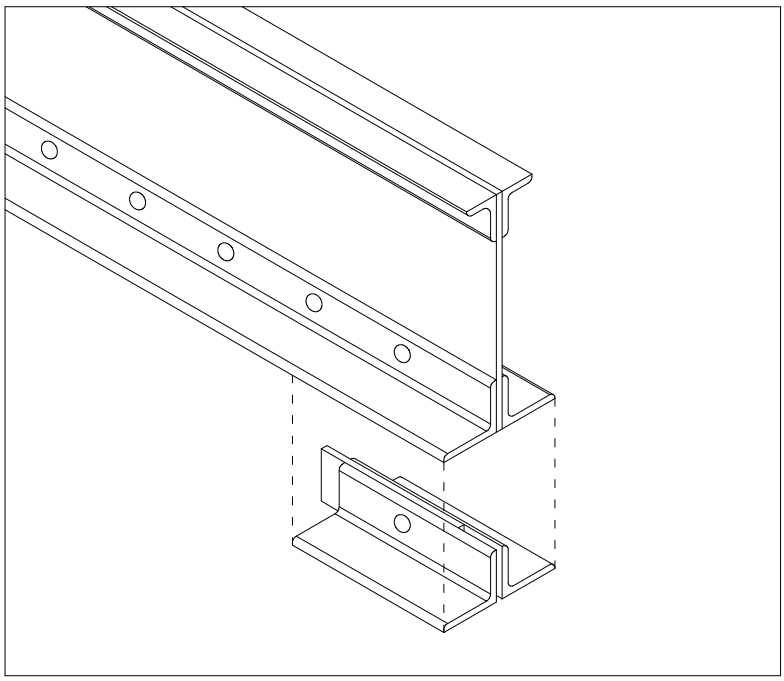

Figure 4.26 Extraction of rivet test piece from beam

Figures 4.27 and 4.28 show the progress of the test as the compressive load increased.

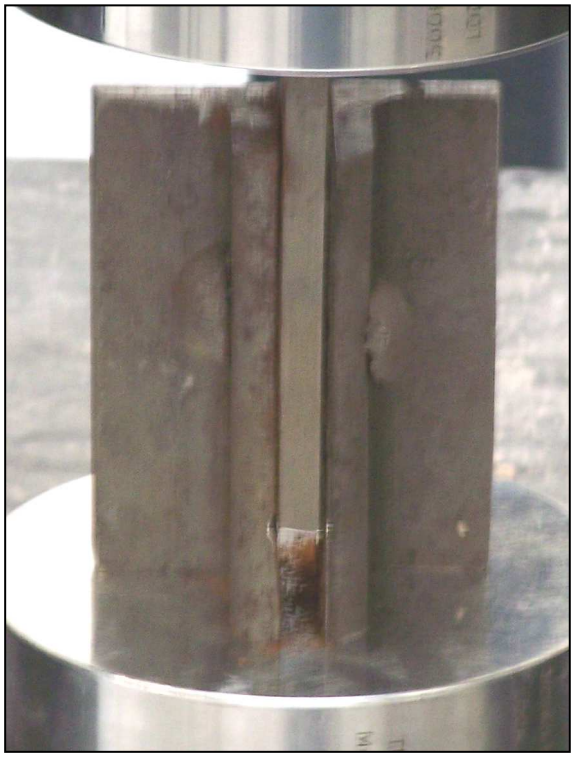

Figure 4.27 Onset of yielding of the rivet

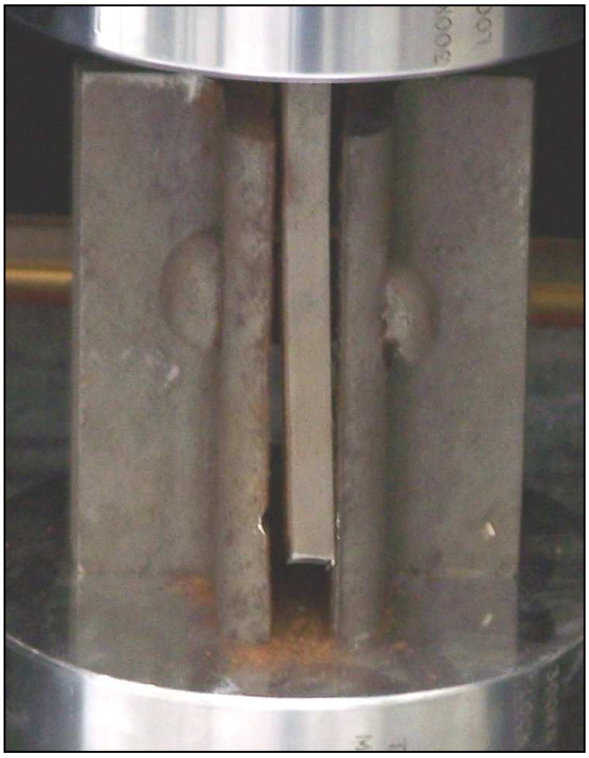

Figure 4.28 As the load increased to the point of failure there was significant deformation of the rivet.

From Figure 4.28 it can be seen that as the load increased there was a tendency for the central plate to buckle forcing apart the angle irons. Thus, the rivet experienced some degree of tension in addition to shear. However, this effect would have been much less in the early part of the test when the central plate remained straight. The stress / displacement diagrams for the three tests are shown in Figure 4.29. Unlike the tensile test diagrams, there were no clear yield points in any of the rivet tests. The initial portion of the graph where there appears to be no significant increase in stress should be ignored because it is due to the load settling down on the test piece. The test piece shifted in response to the load due to slightly non-parallel machined surfaces. Once this initial settling-in occurred there was a steady increase of stress with increasing load, with a reasonably linear relationship, up to a load of about 117kN for rivet 1, 74kN for rivet 2, and 87kN for rivet 3. Therefore, the yield stresses in shear in each case were 230N/mm^2, 145N/mm^2, 171N/mm^2 respectively. But it should be kept in mind that the rivet holes were not perfectly aligned with each other and this may have affected the results.

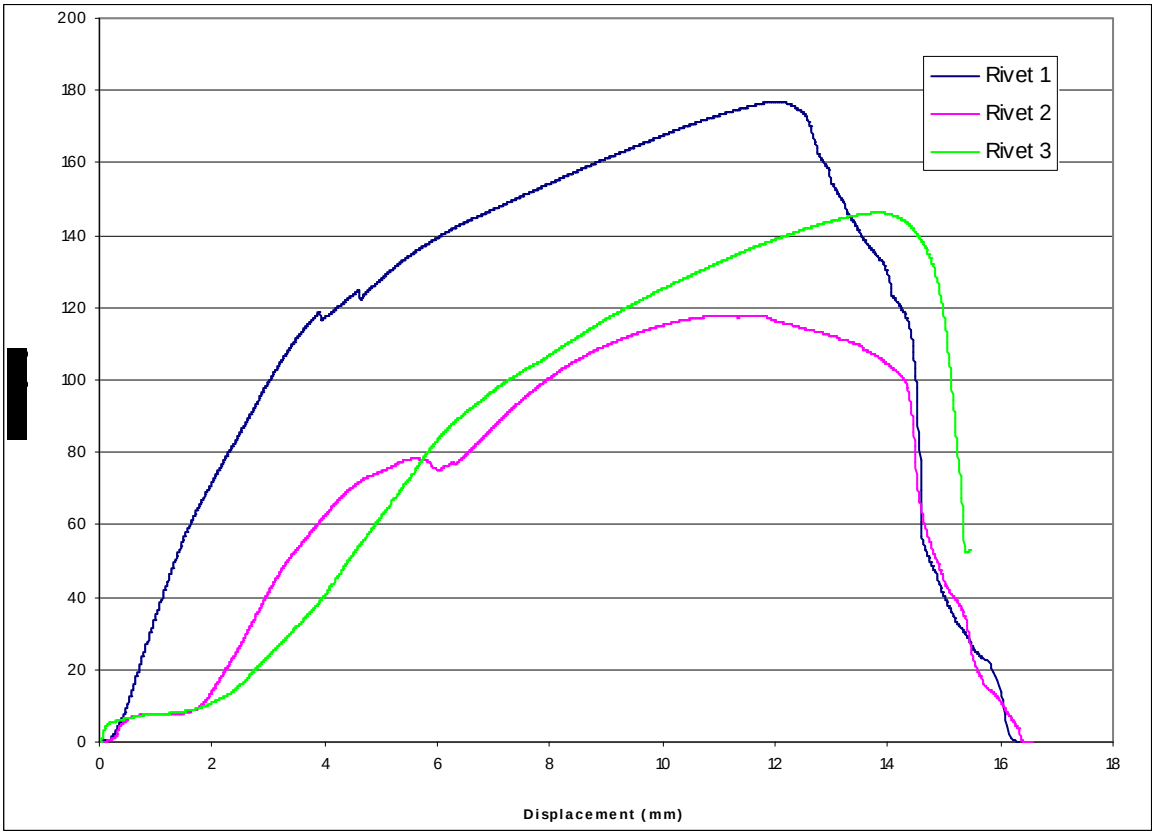

Figure 4.29 Load / displacement graphs for shear tests (M. O'Sullivan 2010)

Lack of exact alignment of rivet holes was not uncommon in 19th century ironwork. The reason for occasional misalignment in the beam under consideration is unknown, as some holes are perfectly aligned while others are less so. The holes in these angles were punched rather than drilled. The evidence for this is seen in the somewhat tapered and rough holes in both the angle and plate. Punching causes greater removal of the metal on the ejection side of the hole than on the impact side. This is illustrated in Figure 4.30.

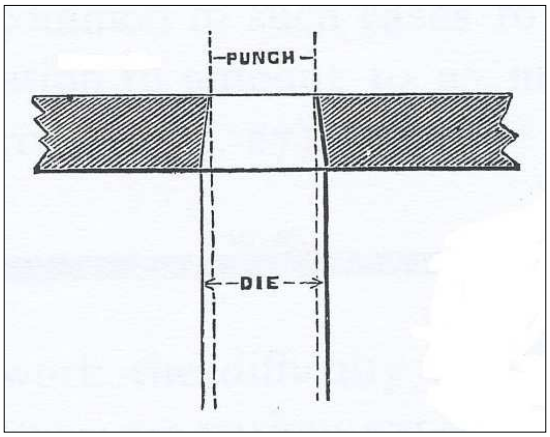

Figure 4.30 Punching causes a tapered hole. (Hutchinson 1879).

Punching should not have contributed to the misalignment of the holes. The most likely cause is lack of care while positioning the angle on the punching machine.

Rivet 1 was the only rivet tested whose holes were properly aligned, in both angles and plate. That is, the rivet was straight and perpendicular to the web of the beam. Rivet 1 gave the highest strength value, which may suggest that distorted rivets form weaker connections. A strong riveted connection is achieved when the rivet is inserted into the holes while it is white hot and immediately hammered to form a domed head. A modern example of steel riveting is shown in Figure 4.31. As the rivet cools it contracts which causes the plates to pull together tightly. Thus, a good riveted connection should establish considerable friction between the plates and the rivet itself should be under some degree of tension.

Figure 4.31 Steel riveting operation in the refurbishment of Hercilio Luz Bridge, Brazil (Lamb 2008).

The deformability of white-hot iron enables rivets to form a joint even with misaligned rivet holes, as shown in Figure 4.32, in the case of the Edinburgh beam.

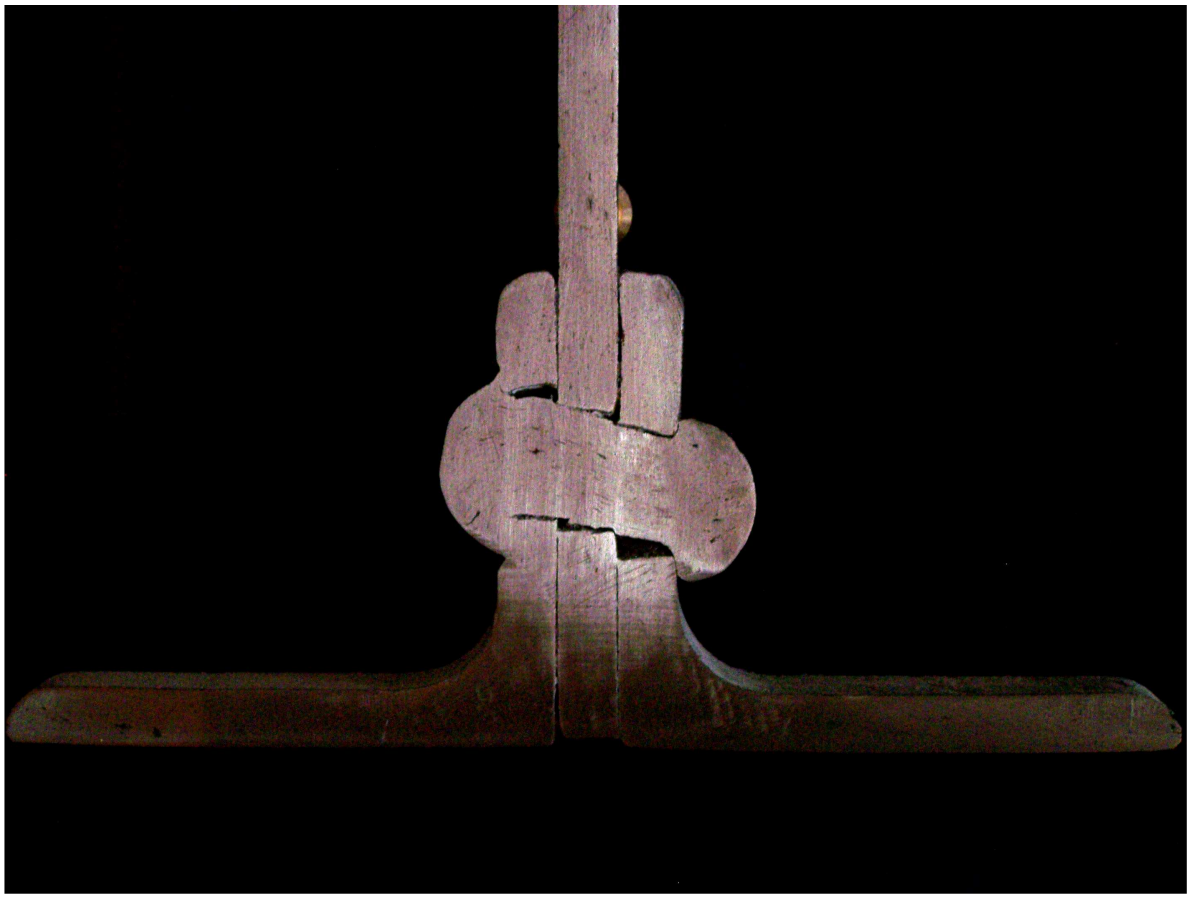

Figure 4.32 Beam cross-section through riveted joint showing misaligned rivet holes (O'Sullivan 2009)

The tapered form of the rivet holes in the plate and angles is clearly visible in the riveted joint cross section shown in Figure 4.33. The manner in which the hot deformable rivet iron was forced to occupy the rivet holes is also visible, so too is the slag pattern. Rivet iron was usually of a more refined grade than angle iron.

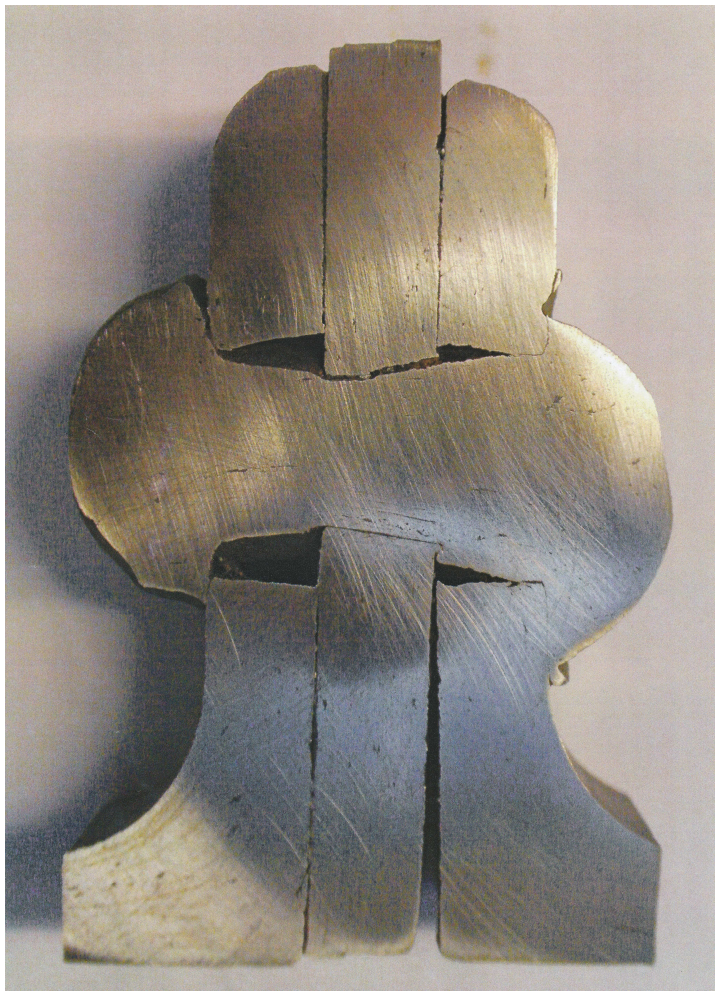

Figure 4.33 Riveted joint cross section showing tapered rivet holes. (O'Sullivan 2009)

4.8 Use of rivet strength data to estimate beam strength

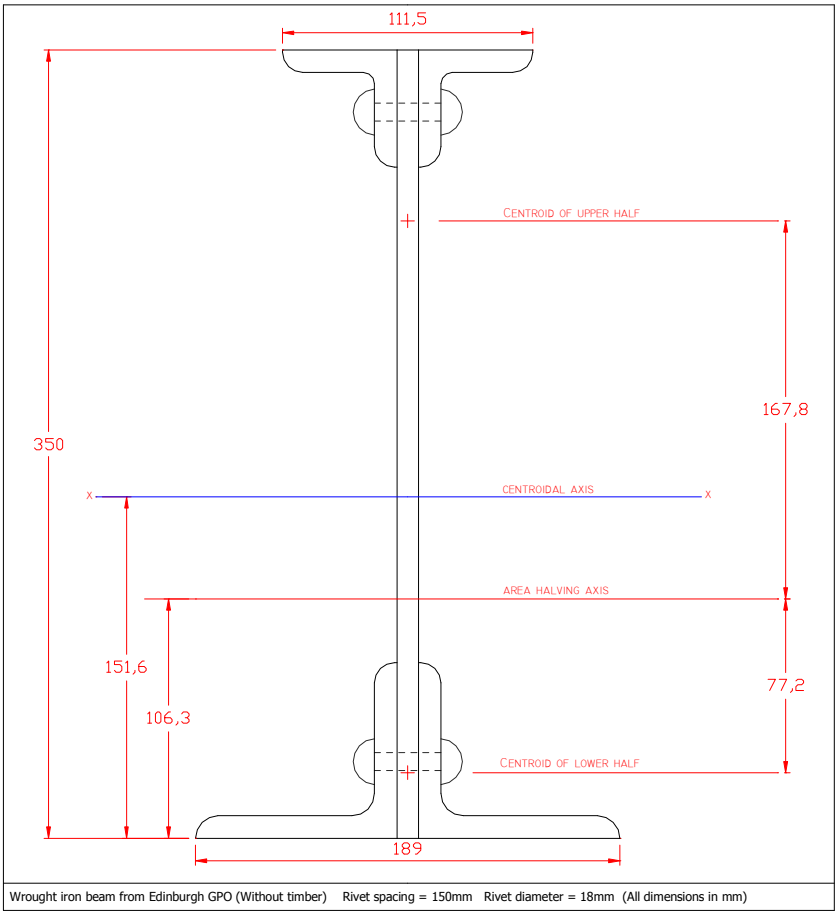

Figure 4.34 Cross sectional dimensions of Edinburgh GPO beam (O'Sullivan 2009)

Total Depth d	Max Width b	Web thickness t	Area of section A	Density of iron ρ	Mass Per metre	Second moment of area I_x	Second moment of area I_y	Plastic modulus Z_x
mm	mm	mm	mm^2	kg/m^3	kg/m	mm^4	mm^4	mm^3
350	189	9.6	8279	7761	64.25	150862560	6572897	1013940

Table 4.4 Section properties of wrought iron beam from Edinburgh GPO (without timber).

If it were not for the rivets, the angles at the top (or bottom) would move horizontally relative to the web. The force necessary to prevent this motion is the total horizontal shear force carried by the rivets.

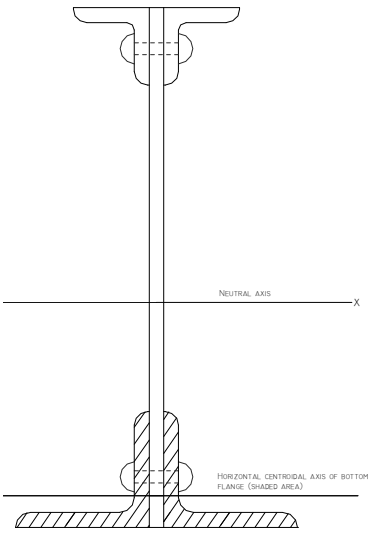

Let F = Shear force carried by rivet in single shear.

Take maximum strength of rivets in shear as $\tau = 230N/mm^2$

Diameter of rivets = d = 18mm

Spacing of rivets = s = 150mm

Figure 4.35 Bottom flange angles restrained from moving by rivets.

Horizontal shear force transmitted
by rivets between lower flange and web = $\frac{VQ}{I}$
per unit length of beam

V = shear force acting on cross section.

Q = first moment of area of lower flange about neutral axis (shaded area) = 406 x 10^3mm^3

I = second moment of area of beam cross section about neutral axis = 150.9 x 10^6 mm^4.

A = cross sectional area of bottom flange = 3119mm^2 (shaded area).

Horizontal shear force transmitted
by rivets between lower flange and web = 2F
over a length s of the beam.

Horizontal shear force transmitted
by rivets between lower flange = 2F/s
and web per unit length of beam.

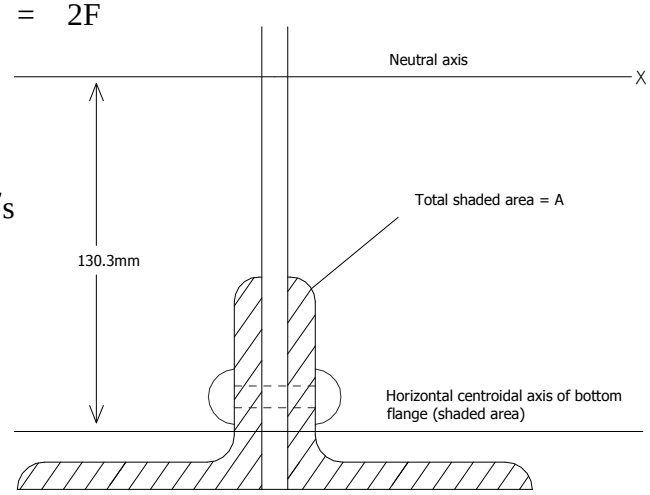

$$\Rightarrow \quad \frac{VQ}{I} = \frac{2F}{s}$$

$$\Rightarrow \quad V = \frac{2FI}{Qs} \qquad \text{Eq.4.8}$$

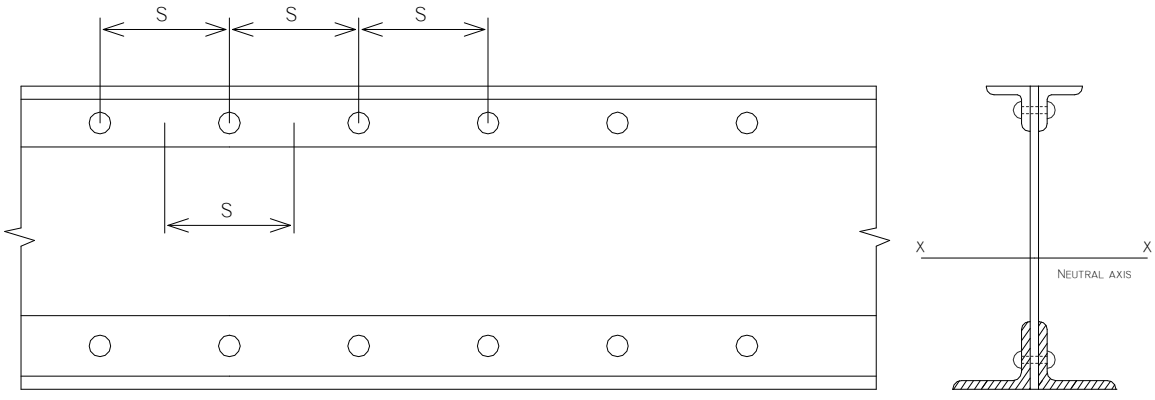

Figure 4.36 Spacing of rivets along beam.

In a simply supported beam of span L carrying a uniformly distributed load w (N/mm) the maximum shear force occurs at the supports and is given by V = wL/2

Therefore, for a simply supported beam:

$$\frac{wL}{2} = \frac{2FI}{Qs}$$

$$\Rightarrow \quad w = \frac{4FI}{QsL} \qquad \text{Eq.4.9}$$

The maximum shear force that the rivets can carry is $F_{max} = \tau\,(\pi\, d^2/4)$

$$F_{max} = (230\text{N/mm}^2)\frac{\pi(18mm)^2}{4} = 58528\text{N}$$

Therefore, $$w_{max} = \frac{4F_{max}I}{QsL}$$

$$\Rightarrow \quad w_{max} = \frac{4(58528\text{N})(150 \text{ x } 10^6\text{mm}^4)}{(406 \text{ x } 10^3\text{mm}^3)(150\text{mm})L} = \frac{576630}{L} \quad \text{(N/mm with L in mm)}$$

Eq.4.9 can be used to determine the uniformly distributed load that will cause the beam to fail by shearing of the rivets.

For example if L = 6000mm then $w_{max} = \frac{576630}{6000} = 96\text{N/mm} = 96\text{kN/m}$

Because this is such a large value of load it is unlikely that the beam would fail by shearing of the rivets. The test to destruction of the beam confirmed this, as nearly all of the rivets remained intact. Those that failed did so only because the beam distorted extensively due to buckling.

4.9 Impact fracture Testing

The purpose of conducting impact fracture tests was to determine whether or not wrought iron experiences a ductile-to-brittle transition with decreasing temperature and, if so, the range of temperatures over which it occurs. In total 55 specimens were made for Charpy impact testing, which included 19 specimens from the web of the GPO beam, 18 specimens from the angle iron of the GPO beam and 18 specimens from the flange of the Albert hall beam. All specimens were made with the grain along the long dimension of the test piece, as shown in Figure 4.37.

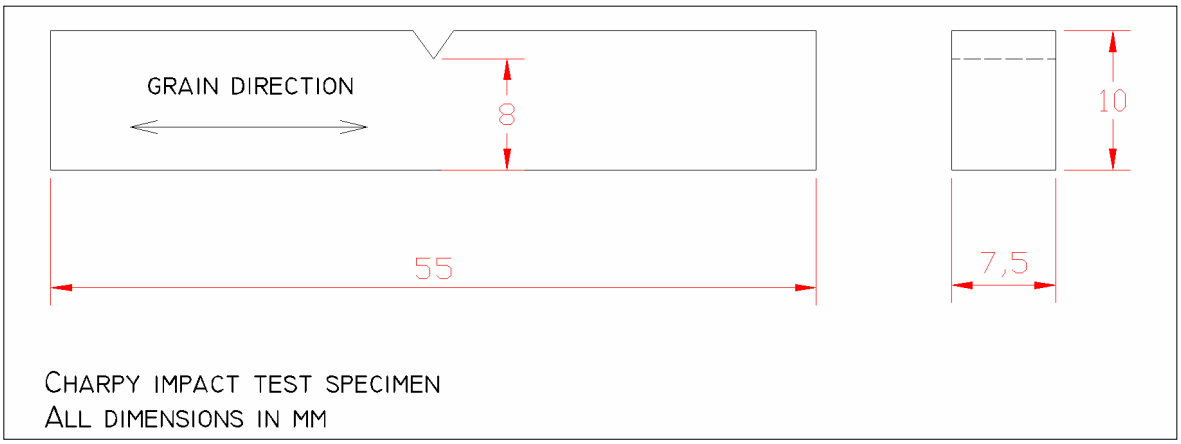

Figure 4.37 Charpy test specimen

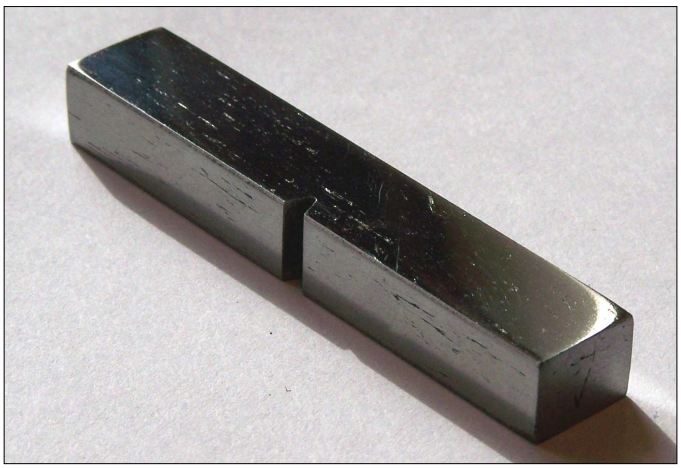

Figure 4.38 Charpy test specimen (M.O'Sullivan)

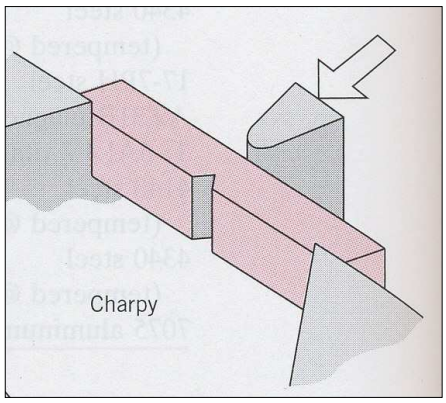

Figure 4.39 Charpy test specimen (Callister 2000)

The tests were conducted over the temperature range -20 ^{o}C to 90^{o}C. The cold temperatures were achieved using the cold vapour rising from liquid nitrogen.

The results of the Charpy tests are given in Figure 4.40. For all three component types there was a general decrease in toughness with decreasing temperature. In other words, the

metal became more brittle at lower temperatures. However at ordinary environmental temperatures such as between 20 and 30 ^{o}C there was no apparent difference in toughness compared with a temperature of -20^{o}C. This suggests that wrought iron can be expected to break in a brittle manner at ordinary temperatures. The transition to ductile fracture does not appear until above 40^{o}C and in the case of the Albert Hall beam metal and the plate metal from the web of the GPO beam, there does not appear to be any transition to ductile fracture. In general, these results agree with Morgan's test results conducted on wrought iron from the S.S. Great Britain, which showed that wrought iron is susceptible to brittle fracture by sudden impact at ordinary temperatures (Morgan 1996). Morgan's results are shown in Figure 4.41.

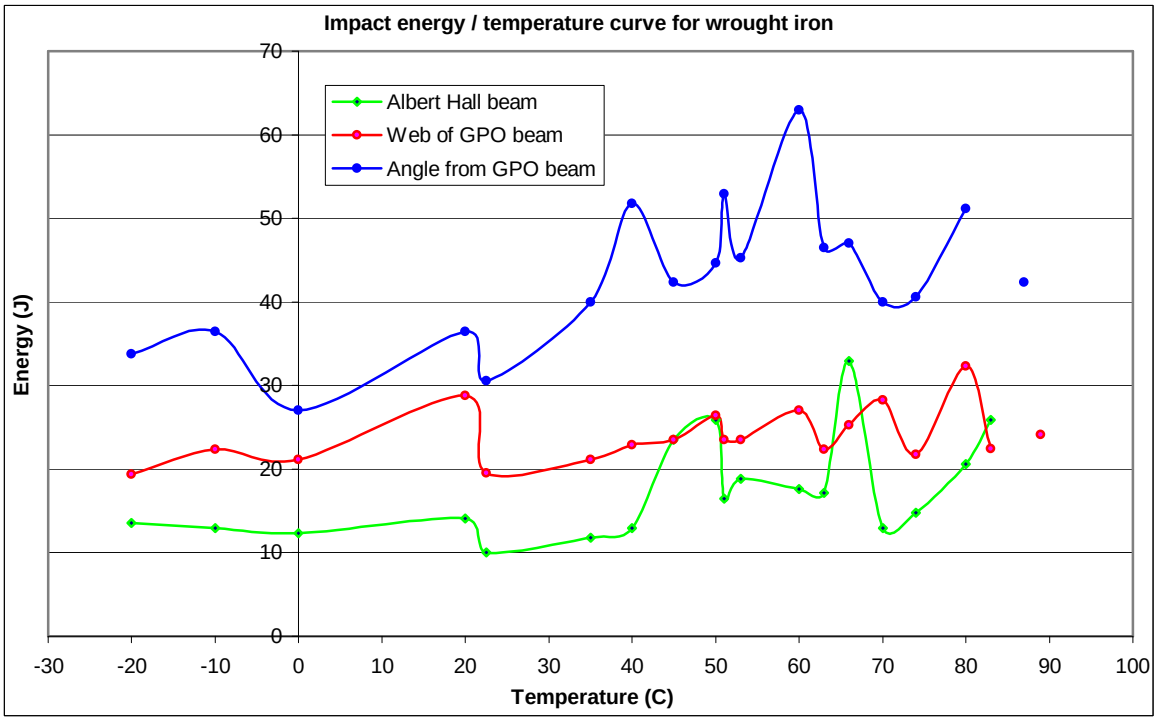

Figure 4.40 Impact energy / temperature curves for wrought iron obtained from Charpy impact tests

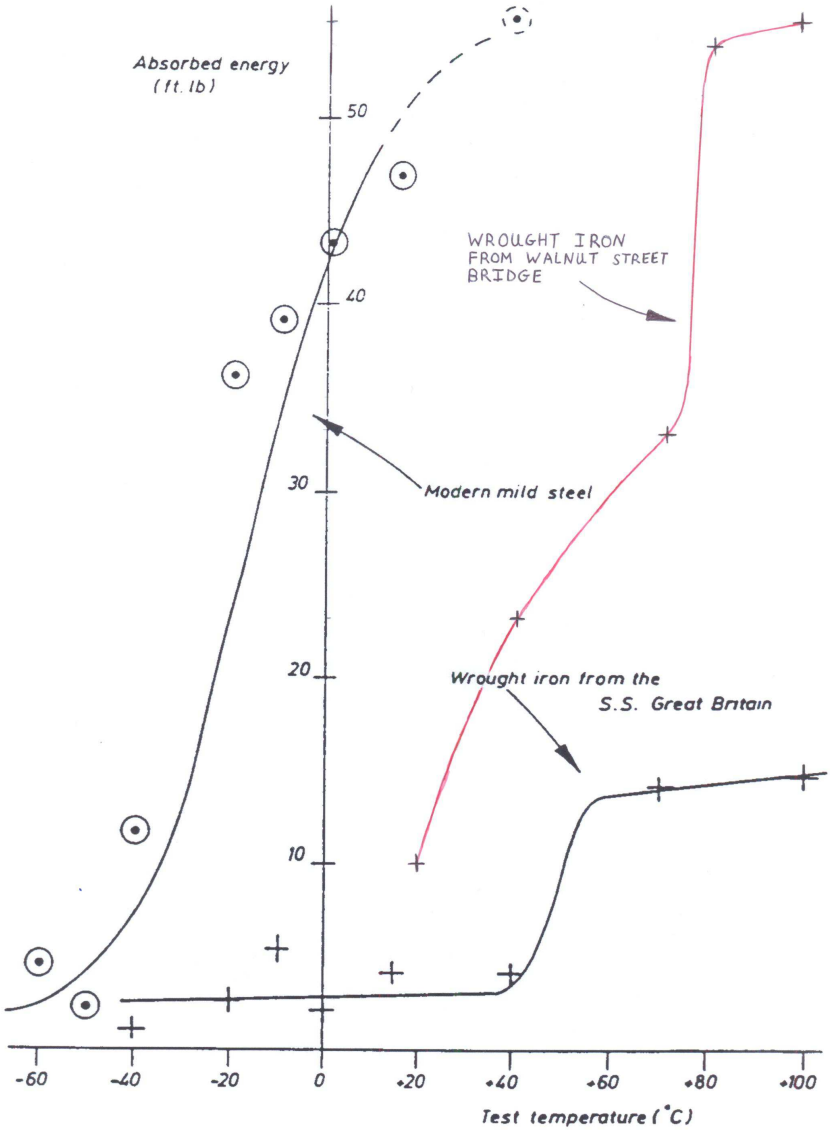

Figure 4.41 Impact Energy – Temperature curve for the wrought-iron of the S.S. Great Britain (Morgan 1996) with similar impact data from Walnut Street Bridge (Green 1999).

Chapter 5 Development of an assessment method for structural wrought iron

5.1 An initial assessment of the quality of wrought iron using tensile test data

The tests performed on the Albert Hall beam material (see Chapter 3) showed that a high strength value does not necessarily indicate a good quality wrought iron. High strength wrought iron may have low ductility and thus may be quite brittle. In this section a method has been proposed for assessing the quality of wrought iron, which takes into account both strength and ductility. A new parameter called the 'quality score' (Q_s) for wrought iron has been defined, in terms of a combination of strength and ductility. Each tensile test result has been assigned a quality score, which can be compared with a lower bound quality score, in much the same way that one would compare the tensile strength from a single tensile test with the characteristic tensile strength. The purpose of developing a quality score is to try to bring together strength and ductility into a single quantity that will enable engineers to rank the quality of a metal against a scale of quality values from a database of test results. Toughness, being the area underneath a stress-strain graph is a quantity that incorporates strength and ductility, and would seem to be the best measure of quality. However, most historical sources simply list the yield and ultimate strengths and elongation at failure (i.e. ductility) and not the full stress strain relationships, and thus provide insufficient data to determine a toughness value. In order to make use of the large number of historical tensile test results, in the creation of a measure of quality, the measured strength and ductility may be combined in an arbitrary way into a single numerical quantity that may act as an alternative measure of quality to that of toughness.

5.2 (a) Defining a quality score for wrought iron

The quality score will be defined by means of an example. Consider a tensile test on a sample of plate iron where the results are as follows.

Yield strength $\sigma_y = 253$ N/mm^2

Ultimate strength $\sigma_{ult} = 381$ N/mm^2

Elongation at failure ε_{ult} = 25% (This is the measure of ductility. It is the failure strain expressed as a percentage)

The quality score is defined in terms of these quantities. The question which must be considered first is, how significant to the quality of the metal are each of these factors. It can be argued that ductility is just as important to the quality of a metal as strength. Therefore, 50% of the quality score will be based on ductility and 50% on strength. However, strength has two values, so it must be decided how significant these two values are to the quality of the metal. Engineers design structural components using yield strength as a reference point. Even in the days when only ultimate strength could be measured engineers used such large factors of safety that they ensured the stress within the metal remained within the elastic range under working loads. Furthermore, "the variability of the elongation to failure of wrought iron means that plastic analysis would be inappropriate and all design should be based on elastic behaviour." (Moy 2009). Therefore, ultimate strength will be omitted as a contributing factor to the quality score. Attributing 50% to yield strength and 50% to ductility would seem reasonable. Thus the quality significance of the contributing factors are summarised as follows:

Yield strength $\sigma_y \rightarrow$ 50 % significance on quality score

Ultimate strength $\sigma_{ult} \rightarrow$ 0 % significance on quality score

Failure strain $\varepsilon_{ult} \rightarrow$ 50% significance on quality score

A database of tensile test data has been collected as part of this research project. Using this database it is necessary to establish a practical range over which each of the two contributing tensile test data factors vary. For plate iron the database contains 561 test results and shows that the maximum values of strength and ductility are as summarised in Table 5.1

	Maximum measured value	Max value on practical scale
Yield strength σ_y	365	365
Ultimate strength σ_{ult} (omitted)	475	475
Failure strain ε_{ult}	38	38

Table 5.1 Maximum practical values on scales of strength and ductility

The maximum measured values from the database may be used as the highest values on the practical scale. Calculating the measure of quality is like calculating the score a student gets in an exam of two questions where the weights for each question are each 50%, and the working range of marks for each question are 365 and 38 respectively.

The quality score for the example case may be computed as follows:

$$\text{quality score} = \frac{\sigma_y}{\sigma_{y\,max}}(50\%) + \frac{\varepsilon_{ult}}{\varepsilon_{ult\,max}}(50\%) \qquad \text{Eq.5.1}$$

$$\text{quality score} = \frac{253}{365}(50\%) + \frac{25}{38}(50\%)$$

$$\text{quality score} = 34.7\% + 32.9\% = 67.6\%$$

The value of this quality score on its own is not useful, it is its value relative to the quality scores of all the other test results in the database that indicates the quality of the metal. By applying the above computation to all 561 test results in the database a scatter diagram can be produced as shown in Figure 5.1. The horizontal axis represents the number designation of each individual test and the vertical axis is the quality score based on Eq.5.1.

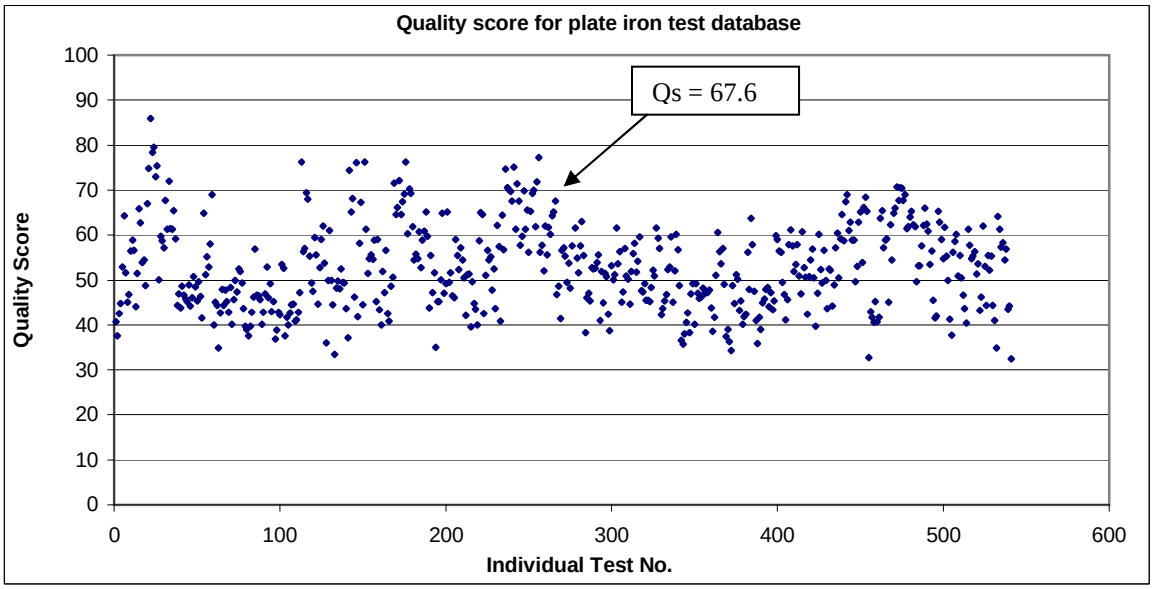

Figure 5.1 Scatter diagram of quality scores obtained from Eq.5.1

The diagram in Figure 5.1 illustrates the variation in quality of all the metals tested in the database. At this point it may be better to disregard the notion of the quality score as a percentage. That is, 67.6% can now be taken as 67.6.

This quality score, gives this particular metal a high ranking compared with the other quality scores, which is reasonable, as the metal had very good ductility (ε_{ult} = 25.0 %), and good yield strength (σ_y = 253 N/mm^2). In order to make the notion of quality scores useful they should be related to the average quality score of all 561 test results, which is 53.0. It is the variation in the quality score from the average value that represents the true quality of the metal, this is shown in Figure 5.2.

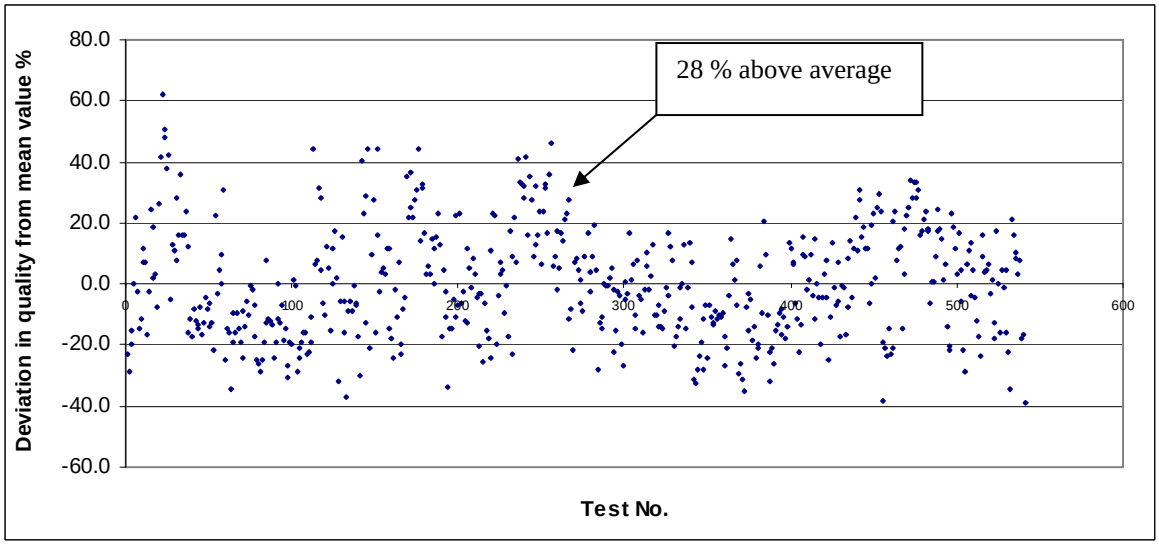

Figure 5.2 Deviation of quality scores from mean value

For example, one can see whether a particular sample is above or below average quality, and the extent to which it varies from the average. For the test sample under consideration with a quality score of 67.6, the metal's quality is 28% above average. Considering another sample, in which the yield strength was 236N/mm^2, the ultimate strength was 363N/mm^2 and the elongation at failure was 11.4%, the quality score is 47, which is 11% below average. Despite the fact that it's quality is below average it is certainly not a bad quality wrought iron. Therefore, a lower bound should be established such that everything below that value can be considered as bad iron and everything above it as acceptable. A bad iron would have low strength and/or low ductility.

This lower bound value will be referred to as the minimum acceptable quality of wrought iron Q_{min} and its determination is entirely arbitrary. For example, consider the set of sample results shown in Table 5.2, where the samples are listed in descending order of quality.

Deviation in quality from mean %	Yield strength N/mm^2	Ultimate strength N/mm^2	Elongation at failure %	Reason for quality value
-10	236	349	11.3	Acceptable quality
-15	250	318	8.1	Acceptable strength, low ductility
-16	209	328	11.8	Low strength, acceptable ductility
-20	251	336	6.2	Acceptable strength, low ductility
-25	227	290	6.7	Acceptable strength, low ductility
-25	195	359	10	Low strength, acceptable ductility
-29	217	279	6	Acceptable strength, low ductility
-30	216	247	5.5	Acceptable strength, low ductility
-36	207	232	3.9	Low strength, low ductility

Table 5.2 Reason for below average quality scores of wrought iron samples.

It appears that in the majority of cases where the quality falls below the average it does so because of a low ductility value. This is illustrated in Figure 5.6. Morgan suggested an elongation at failure of less than 10% as indicative of poor ductility (Morgan 1999). It is proposed that a quality deviation of more than 20% below the mean may be used as a lower bound value of quality on this quality scale. On this basis 84% of the samples in the database are of an acceptable quality.

One obvious problem with the scheme proposed above is that the initial allocation of the percentage significance (i.e. yield strength $\sigma_y \rightarrow$ 50% significance on quality score) is completely arbitrary. But the proposal here is to use the standard information obtained from a tensile test to rank the quality of a single piece of iron within a database of test results.

Using Kirkaldy's data, Morgan showed that in a single tensile test, where the ductility was more than 10%, the measured ultimate strength would most likely lie within 10% of the mean ultimate strength value. This is illustrated in Figure 5.3. Thus, a ductility value of 10% indicates a lower bound of quality.

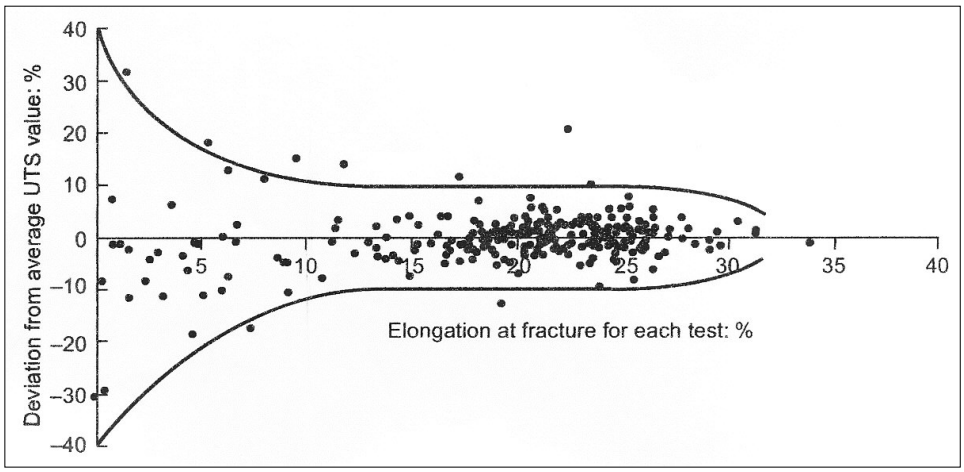

Figure 5.3 Kirkaldy's tensile test results replotted to examine the scatter of values. (Morgan 1999)

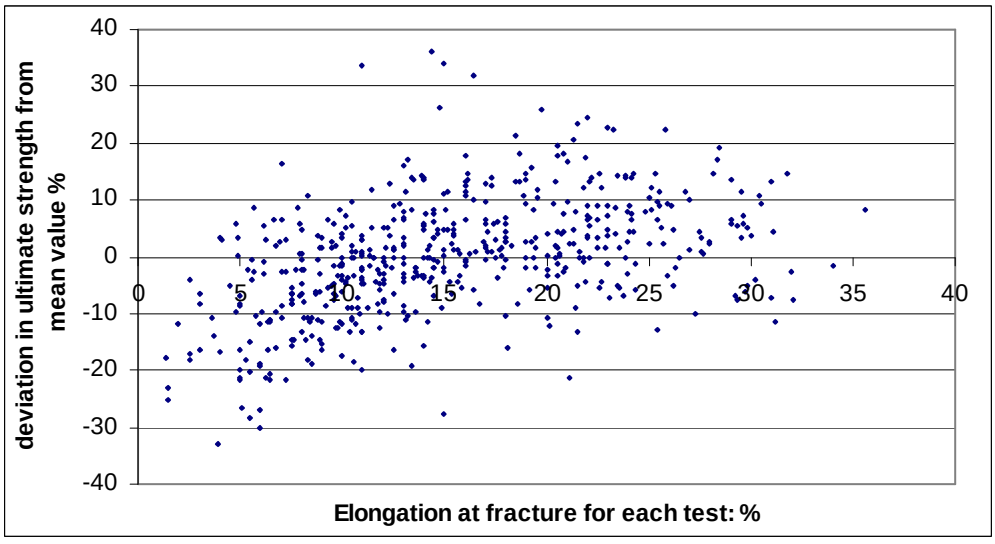

Figure 5.4 Tensile test results for plate iron replotted to examine the scatter of values. (Source: Cass Hayward database and various test results collected as part of present research project)

Using the database of tensile test results from Cass Hayward Consulting Engineers and test results collected as part of this research project, a plot of results similar to Morgan's can be produced as shown in Figure 5.4. This plot would seem to cast some doubt on Morgan's conclusion, as it shows considerable scatter. Of the 561 test results plotted in Figure 2.20, 72% (i.e. 393 samples) had a ductility greater than 10%. Of these 393 test samples, 279 had an ultimate strength value within 10% of the mean. That is, 71% of the 393 test samples had an ultimate strength within 10% of the mean. Overall, 52% of the 540 test results had both a ductility greater than 10% and an ultimate strength within 10% of the mean. If one considers 10% as a lower bound for acceptable ductility and a deviation of more than 10% below the mean ultimate strength as a lower bound for acceptable ultimate strength then the number of acceptable samples is 351 which is 65% of the total number of samples. Thus on this basis only 65% of the material is of acceptable quality.

5.2 (b) Statistical assessment of proposed quality score scheme

The problem of trying to combine ductility and yield strength into a single quantity that will serve as a measure of the quality of the metal is that one particular attribute, such as good ductility might co-exist with very poor yield strength, resulting in an acceptable measure of quality. This is illustrated in Figure 5.5 where some samples at the lower right of the scatter diagram have an above average quality of about 20%, but these same samples have yield strengths which are among the lowest in the database. This would indicate that the quality scheme proposed here is not really indicative of good quality metal and that if one is to decide upon the quality of a metal one must look at both ductility and yield strength as two independent parameters, and set a lower bound for each, such that everything above these bounds is acceptable. A lower bound of 10% for elongation at failure has already been proposed for ductility. A lower bound yield strength has yet to be proposed, but it may be better to simply use the characteristic yield strength from the database as a reference point against which to judge quality.

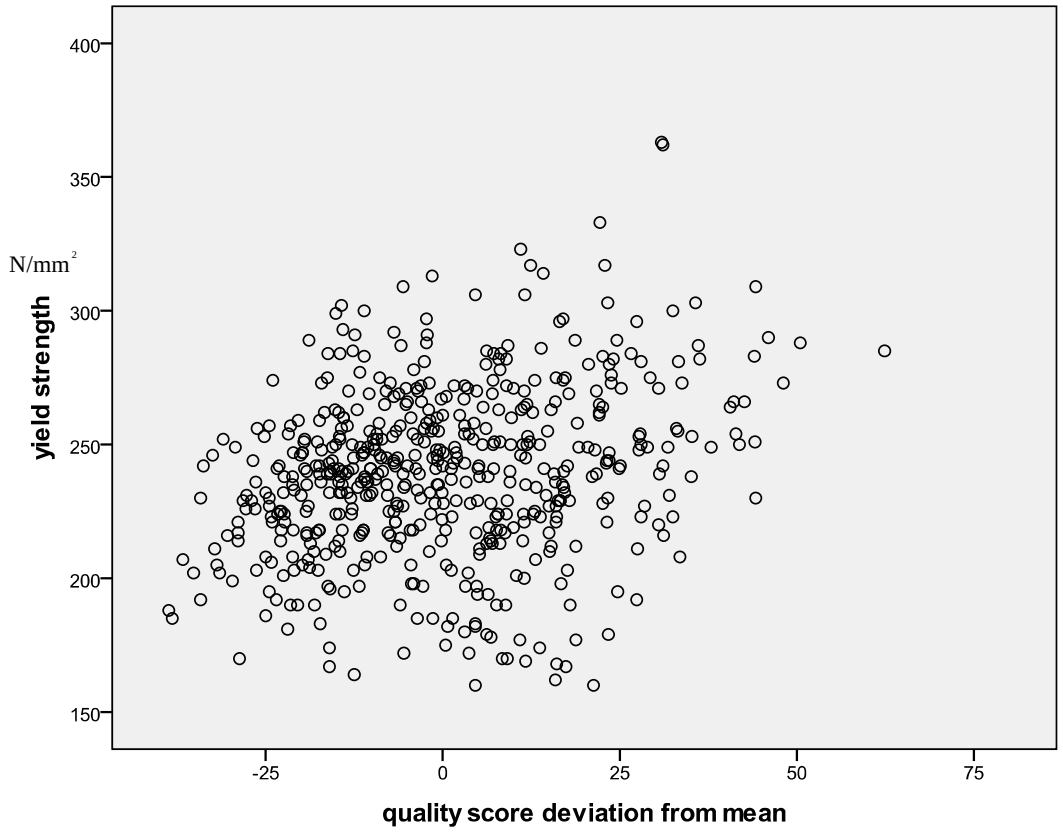

Figure 5.5 Yield strength for plate iron plotted against quality score deviation from mean values.

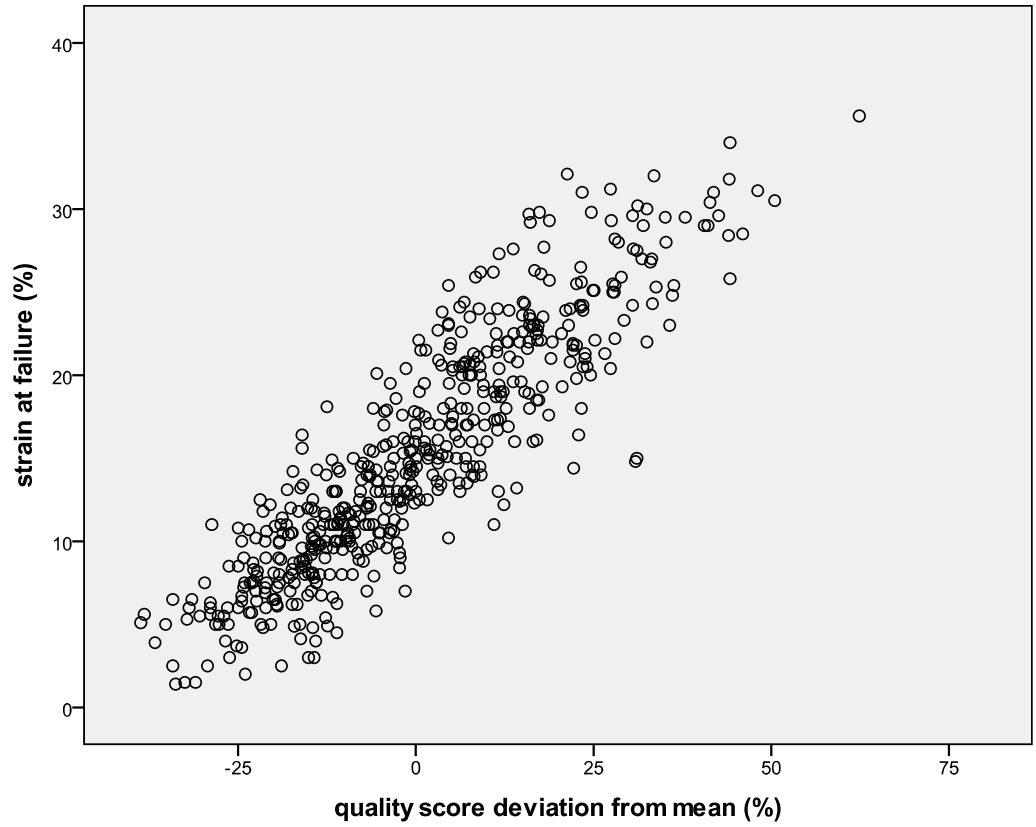

Figure 5.6 Ductility of plate iron plotted against quality score deviation from mean values.

5.3 Refinement of tensile test data for use in an alternative assessment method

One of the conclusions on this research project is that different structural component types possess different characteristic material properties. It is proposed to incorporate this observation into the formation of an alternative assessment method for wrought iron structures. The large volume of tensile test data collected as part of this research project has been separated according to component type, and the result is summarised in Tables 5.3 to 5.8

The following components types are considered.

1 Plate iron (along grain)

2 Plate iron (across grain)

3 Square and round bars

4 Angles and tees

5 Bolts and rivets

6 Rolled beams

Plate iron. Tested parallel to grain.				
	Yield strength	Ultimate strength	Elongation at failure	Modulus of elasticity
	N/mm^2	N/mm^2	%	kN/mm^2
Number of tests	561	561	548	12
Range	154 - 363	232 - 470	1 - 36	130 - 206
Mean	240	345	15	180
Standard deviation	32	35	7	23
Characteristic value	187	287	3	142
Number of tests with elongation at failure > 10% = 397				

Table 5.3 Summary of tensile test data for plate iron tested along the grain direction.

Plate iron. Tested perpendicular to grain.			
	Yield strength	Ultimate strength	Elongation at failure
	N/mm^2	N/mm^2	%
Number of tests	117	117	115
Range	154 - 298	183 - 389	0.1 - 29.2
Mean	208	296	8
Standard deviation	36	39	7
Characteristic value	163	225	0.8
Number of tests with elongation at failure > 10% = 41			

Table 5.4 Summary of tensile test data for plate iron tested across the grain direction.

Rectangular and Round bars Tested parallel to grain.				
	Yield strength	Ultimate strength	Elongation at failure	Modulus of elasticity
	N/mm^2	N/mm^2	%	kN/mm^2
Number of tests	330	335	328	171
Range	150 - 328	278 - 533	4 - 37	149 - 253
Mean	205	352	22	196
Standard deviation	33	27	7.2	13
Characteristic value	151	308	10	175
Number of tests with elongation at failure > 10% = 303				

Table 5.5 Summary of tensile test data for rectangular and round bars tested along the grain direction.

Angles and Tees Tested parallel to grain.				
	Yield strength	Ultimate strength	Elongation at failure	Modulus of elasticity
	N/mm^2	N/mm^2	%	kN/mm^2
Number of tests	100	100	95	6
Range	193 - 351	296- 448	4 - 37	145 - 201
Mean	244	368	22	197
Standard deviation	27	30	7.0	19
Characteristic value	200	319	10	145
Number of tests with elongation at failure > 10% = 90				

Table 5.6 Summary of tensile test data for angles and tees tested along the grain direction.

Bolts and Rivets Tested parallel to grain.				
	Yield strength	Ultimate strength	Elongation at failure	Modulus of elasticity
	N/mm^2	N/mm^2	%	kN/mm^2
Number of tests	45	45	45	9
Range	205 - 332	318 - 414	18 - 41	184 - 213
Mean	257	365	30	194
Standard deviation	30	24	6	9
Characteristic value	207	325	20	176
Number of tests with elongation at failure > 10% = 45				

Table 5.7 Summary of tensile test data for bolts and rivets tested along the grain direction.

Rolled Beams Tested parallel to grain.				
	Yield strength	Ultimate strength	Elongation at failure	Modulus of elasticity
	N/mm^2	N/mm^2	%	kN/mm^2
Number of tests	24	24	18	23
Range	221 - 355	326 - 478	5 - 27	159 - 243
Mean	299	423	14	199
Standard deviation	38	45	6	19
Characteristic value	232	343	4	165
Number of tests with elongation at failure > 10% = 14				

Table 5.8 Summary of tensile test data for rolled beam iron tested along the grain direction.

5.4 Defining design strength in terms of quality and significance of components

The principal objective in developing a new method for assessment of wrought iron structures is to avoid unnecessary removal of structural components and therefore preserve as much of the original structure as possible. Although the UK Highway Standard BD21/01 acknowledges the wide variability in the material properties of wrought iron it provides only a single value of characteristic yield strength for wrought iron, i.e. 220N/mm^2, and a single material safety factor of 1.2. The analysis of tensile test data carried out in this research project has revealed that different wrought iron component types have different characteristic strength and ductility values, and this can provide a means of refining the current assessment method. Furthermore it is proposed that instead of applying a uniform safety factor to all members of a wrought iron structure larger factors of safety are assigned to more significant members while lower factors of safety are assigned to members of lower significance. The term significance in this context refers to the importance of the component in resisting collapse.

As part of this method a numerical value of significance is assigned to all members of the structure in order to clearly identify the degree to which a component contributes to the stability of the structure. Their contribution to structural stability is based on the stress they experience under assessment loading. Members which carry higher stress are considered as contributing more to the stability of the structure and thus are classified as more significant or more important.

The basis of the proposed method is the creation of a new definition of component resistance for use in the assessment of wrought iron structures. In this context the term 'component resistance' means 'assessment yield strength' or 'design yield strength'.

Under the current method the resistance of wrought iron members is given by

$$R^* = F_c . \frac{f_k}{\gamma_m} \quad = \quad \text{condition factor} . \frac{\text{characteristic yield strength}}{\text{material safety factor}} \qquad \text{Eq.5.1}$$

$$\Rightarrow \qquad R^* = F_c . \frac{220\text{N/mm}^2}{1.2} \quad = \quad F_c (183\text{N/mm}^2)$$

Under the new method it is proposed that the resistance of wrought iron be given by

$$\text{Design yield strength} \; = F_c . \frac{(\text{characteristic yield strength})\,\beta}{1.2\,\alpha} \qquad \text{Eq.5.2}$$

where α is the significance factor of the component

and β is the quality factor of the component.

The function of the significance factor is to adjust the safety factor according to the importance of the component within the structure.

The function of the quality factor is to adjust the characteristic strength according to the ductility of the metal.

5.5 Defining a quality factor for wrought iron components

In Section 5.3 it was shown that different wrought iron component types have different characteristic strength and ductility values. It is proposed that the quality factor β of a component, is defined as the probability that the component has an elongation at failure of more than 10%:

$$\beta = \text{ probability that a sample has an elongation at failure} > 10\% \qquad \text{Eq.5.3}$$

The data analysis presented in Section 5.3 for different component types is partially summarised in Table 5.9. The quality factor β is given for each component type.

Elongation at failure of various component types						
Component type	Plate iron (along grain)	Plate iron (perpendicular to grain)	Square and Round bars	Angles and Tees	Bolts and Rivets	Rolled beams
Number of tests	548	115	328	95	45	18
Range (%)	1 - 36	0.1 - 29	4 - 37	4 - 37	19 - 41	5 - 27
Mean (%)	15	8	22	22	30	14
Standard deviation (%)	7	7	7.2	7.0	6	6
No. of tests with elongation at failure > 10%	397	41	303	90	45	14
Probability that a sample component has elongation at failure > 10% (i.e. β factor)	0.761	0.36	0.953	0.956	0.999	0.749

Table 5.9 Summary of data related to elongation at failure of various component types

It was shown in Section 2.3(c) that the tensile test data follows a normal distribution. Therefore, the area under the standardized normal curve or normal probability curve may be used to calculate the probability that a sample component has an elongation at failure greater than 10%. For example, using the data for plate iron tested along the grain, the normal standard variate (i.e. z-value) is given by

$$z = \frac{x - \bar{x}}{\sigma} = \frac{x - 15}{7}$$

where $\bar{x}$ is the mean value and σ is the standard deviation from the mean.

An elongation at failure of 10% has a z-value of $\frac{10 - 15}{7} = -0.71$ standard deviation. (See Figure 5.7)

The probability that a sample of plate iron has a elongation at failure of more than 10% is equal to the shaded area under the normal probability curve shown in Figure 5.2, and is equal to 0.7611. Given that there are 548 results for plate iron tested along the grain, this means that 548 x 0.7611 = 417 of these are likely to have a elongation at failure greater than 10%. The actual number of tests with elongation at failure greater than 10% is known, to be 397. This small discrepancy is expected as probabilities based on the normal distribution are approximations. According to the definition the quality factor β in this case is equal to 0.76.

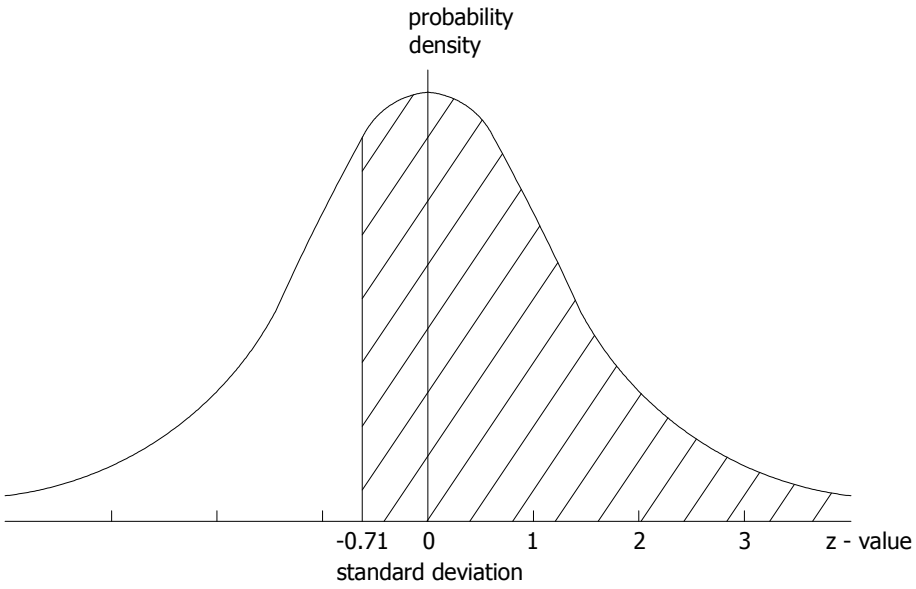

Figure 5.7 Normal probability curve

If it is found that the test results do not follow a normal distribution, as is the case with plate iron tested perpendicular to the grain, then the quality factor β may be defined as the ratio

$$\beta = \frac{\text{Number of tests with elongation at failure > 10\%}}{\text{Total number of tests}} \qquad \text{Eq.5.4}$$

5.6 (a) Defining a significance factor for wrought iron components

One objective in creating the proposed method was that it should agree with the existing method for the most significant members, so that the new method is just as safe as the existing one. However, the proposed method is less conservative toward members of lower significance. An examination of the database of tensile test results reveals that the characteristic yield strength value of 220N/mm^2 under the current method is too high a value. In particular bar iron was found to have a characteristic yield strength of just 151N/mm^2 and plate iron a characteristic yield strength of 187N/mm^2. Thus, the present method overestimates the strength of wrought iron. Therefore, under the proposed method the characteristic strength value of 220N/mm^2 will be discarded, but the material safety factor will be retained as shown in Eq.5.2. The purpose of the α factor is to adjust the safety factor, and the next step in the development of the proposed method is to establish the numerical range of the α factor.

In just the same way as each component type has a specific quality factor β, so too will each component type have a unique range of possible significance factors. The actual significance of the component depends entirely on its importance within the structure and is based on the stress it carries, but the significance factor depends on what type of component it is. In order to establish a working range for the significance factor of a particular component type consider plate iron as an example.

Under the proposed method the design yield strength is given by:

$$\text{new design yield strength} = F_c.\frac{f_k\ \beta}{1.2\ \alpha} \qquad \text{(from Eq.5.2)}$$

$$= F_c.\frac{f_k\ (0.761)}{(1.2)\ \alpha} \qquad \text{(for plate iron tested along the grain)}$$

where f_k is the characteristic yield strength. For this example consider that F_c = 1.0.

It is intended that the design yield strength under the new method should equal the design yield strength under the existing method for the most significant components. Therefore, for the most significant component α should be 0.761.

$$\text{new design yield strength} = \frac{f_k\ 0.761}{(1.2)\ 0.761} = \frac{f_k}{1.2} = \text{old design yield strength}$$

For a component of no significance the design yield strength may equal the characteristic yield strength. Therefore,

$$\text{new design yield strength} = \frac{f_k\ 0.761}{(1.2)\ 0.634} = \frac{f_k}{1.2}(1.2) = f_k = \text{characteristic yield strength}$$

Therefore the range of significance factor values for plate iron is:

$$(0.634 \leq \alpha \leq 0.761) \qquad \text{Eq.5.5 (for plate iron along the grain)}$$

The range of significance factors for each component type are given in Table 5.10.

	Characteristic yield strength	α factor range	β factor
Plate iron (along grain)	187	0.634 - 0.761	0.761
Plate iron (perpendicular to grain)	163	0.3 - 0.36	0.36
Rectangular and Round bars (including eyebars)	151	0.794 - 0.953	0.953
Angles and Tees	200	0.797 - 0.956	0.956
Bolts and Rivets	207	0.833 - 0.999	0.999
Rolled beams	232	0.624 - 0.749	0.749

Table 5.10 Parameters used in design strength adjustment.

Having defined the range of values that the significance factor can have for a particular component type the method is ready for implementation. The first quantity required for the calculation of the design yield strength of a component under the proposed method is the

significance of the component within the structure. This is a value expressed as a percentage. For example, one might calculate that a particular component is 70% significant. The basis of establishing such a figure is the stress in the component.

Members with the highest stress values are assigned the highest significance values because these members contribute most to the stability of the structure. That is, they do more work in supporting the load. The loading on the structure used for determination of component stresses employs the standard load safety factors, i.e. 1.5 for live load and 1.05 for dead load. (BD21/01). It is clear that a safety factor applied to the external loading will affect all components. The only way of tailoring the safety factor for individual members, based on their significance, is by adjusting the material safety factor rather than the load safety factor. Furthermore, placing the significance factor in the denominator of Eq.5.2 ensures that members with the highest significance have the lowest design yield strength. This ensures that safe assessment is maintained. Members of low significance will have a greater design yield strength, which is acceptable as these members have a high safety margin to begin with.

Therefore, the first step in the proposed method is the calculation of the initial safety margin of all components in the structure under standard factored assessment loading. The initial safety margin of a component is based on the limit state that failure is expected if the stress in a member reaches the characteristic yield strength value for wrought iron, i.e. 187N/mm^2 for plate iron or 151 N/mm^2 for bar iron. Therefore,

Initial stress safety margin = characteristic yield strength - stress in component Eq.5.6

The significance of the structural members is then calculated. The proposed assessment method has two different forms depending on whether the structure being assessed is

statically determinate or indeterminate. The procedure for determinate structures is simpler and will be discussed first by considering a truss.

5.6 (b) Calculating the significance factor for a component in a determinate structure

The details of the proposed method for a plate iron component are as follows.

Calculate the stress in all components under factored loading. Then calculate the significance of all components according to Eq.5.7.

$$\text{Component significance} = \frac{\text{stress in component}}{\text{characteristic yield strength}} \times \frac{\text{Area lost as a result of collapse}}{\text{Total area of structure}}$$

Eq.5.7

It is difficult to place a fixed value of significance on a structural member. For example, consider the case of a zero force member in a truss under a particular loading arrangement. Loss of the member under that particular loading arrangement is theoretically of no consequence as it carries no load, and so it could be argued that the member has zero significance under that loading arrangement. However, the member may carry load under an alternative loading arrangement, and thus, obviously has some significance. The expression for significance given by Eq.5.7 may lead to the conclusion of zero significance for a particular loading arrangement. In that case a different loading arrangement should be applied. In practical terms there is a limited number of ways in which load can be applied to a structure, so it would not be an exhaustive process to determine the range of stress values that a component is likely to carry. The largest stress value in this range should be the one on which significance is calculated.

However, significance should also depend upon the degree of destruction that would result upon loss of the component, and this can be based on the area of collapse if the component is lost. It is proposed that the measure of significance of a component should be directly proportional to the fraction of the characteristic yield stress it carries and to the fraction of the total area lost upon loss of the member, as expressed by Eq.5.7.

One consequence of basing the significance of a component on the stress it carries is that under higher loads the component will register as being more significant. This provides a way of placing greater significance on components within structures exposed to higher than average forces, such as on an exposed costal site or in an industrial building.

For Liverpool Lime Street Station roof (see Chapter 8) it is assumed that progressive collapse does not occur with the loss of an individual truss. If a critical component is lost, such as a bottom chord tie, then the truss will collapse taking with it the purlins resting on it. The area of roof lost would be $1112m^2$. The total area covered by the roof is $11206m^2$. Therefore, the fraction of the building area lost, if one truss collapses, would be $1112m^2$ / $11206m^2 = 0.099$. In this case the significance of the truss members is given by Eq.5.8.

$$\text{Total Component significance} = \frac{\text{stress in component}}{\text{characteristic yield strength}} \times 0.099 \qquad \text{Eq.5.8}$$

In the next step of the proposed method the significance value, expressed as a percentage, provides a way of calculating the significance factor α.

The range of significance percentage values can be found from Eq.5.8. If a component has a stress value approaching the characteristic yield strength, meaning that it is on the verge of limit state violation, then its safety margin would be zero and the significance of the component would be at maximum, which indicates that the component is essential for stability, (and that it requires reinforcing). If the stress in a component approaches zero, then the safety margin would be equal to the characteristic yield strength. In that case the component is effectively doing nothing to resist collapse and is redundant, with significance equal to zero. However the loading arrangement should be changed to see if

the component has a non-zero stress, which means it may have some significance. Thus the theoretical range of component significance values is

$$0 \leq \text{Total component significance} \leq 0.099$$

Although the collapse of a single truss is less severe than the collapse of the entire structure it is obvious that the collapse of a single truss is very serious and one may regard the collapse of even one truss as totally unacceptable. In that case the only measure of significance that matters is the local significance value given by Eq.5.9.

$$\text{Local Component significance} = \frac{\text{stress in component}}{\text{characteristic yield strength}} \qquad \text{Eq.5.9}$$

For this interpretation of significance the practical range of significance values is

$$0 \leq \text{Local component significance} \leq 1.0 \qquad \text{Eq.5.10}$$

Using the range of local significance values given by Eq.5.10 it is possible to relate the significance of a component to the significance factor α for the adjustment of the design yield strength. The range of significance factor values for plate iron is:

$(0.634 \leq \alpha \leq 0.761)$ Eq.5.5 (repeated)

and $0 \leq \text{sig} \leq 1.0$ Eq.5.10 (repeated)

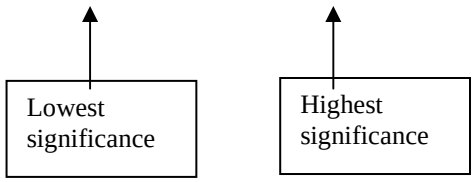

For example, consider that the significance value (sig) of the component has been determined to be 0.75. Then its significance is 75%.

Using this percentage value of significance, a proportional α value may be calculated as follows.

The size of the α value range is given by

highest α – lowest α = $0.761 - 0.634 = 0.127$

75% of $0.127 = 0.09525$

$\Rightarrow$ α value corresponding to 75% significance $= 0.634 + 0.09525 = 0.72925$

In general, the α factor is given by:

α = lowest α factor in range + (significance) $\times$ (size of α factor range) Eq.5.11

Therefore under the proposed method the design yield strength for this component can be adjusted as follows

$$\text{new design yield strength} = F_c.\frac{f_k\ \beta}{1.2\ \alpha} = F_c.\frac{187\text{N/mm}^2\ (0.761)}{(1.2)\ 0.729} = F_c.\ (163\ \text{N/mm}^2)$$

If no account of the significance or ductility of the component is applied then the design strength of this component would be

$$\text{design yield strength} = F_c.\frac{f_k}{1.2} = F_c.\ \frac{187\text{N/mm}^2}{1.2} = F_c.\ (156\ \text{N/mm}^2)$$

The new design yield strength is not very much greater than the original design yield strength because the component was quite significant. It was already stated that for members of high significance the proposed method would not differ very much from the existing assessment method. However, for members of lower significance the increase in design yield strength is greater. For example, if the stress in a component was just 15N/mm^2, the initial safety margin would be 172N/mm^2, and the significance of the component would be 8.0%, which is obviously very small. The resulting adjustment in the design strength is an increase from a standard value of 156N/mm^2 to 184N/mm^2. Therefore, this particular component, which is of very little significance, would be allowed to experience a greater stress level than would be allowed under the present assessment method. Such an elevated stress may result from a loss in section due to corrosion. Thus,

under the proposed method, this member, may continue in service, whereas under the present assessment method it may be deemed necessary to replace it at an earlier date.

In summary, the proposed method provides a greater, yet safe, design yield strength than the existing assessment method for individual components. Using the characteristic yield strength of wrought iron, and the stress in the components under factored assessment loading the significance of the components within the structure is calculated. Knowing the significance of the components allows a proportional reduction in the material safety factor, resulting in a greater design strength. The practical consequence of this adjustment is that a component of less than critical significance is not subjected to an overly conservative safety assessment and may be allowed to continue in service for a longer period of time.

The application of the proposed method to statically indeterminate structures is explained by means of a number of case study examples in Chapters 6 to 8 but the general considerations when dealing with indeterminate structures are outlined in Section 5.7.

5.7 Application of the proposed assessment method to indeterminate structures

The basis of the proposed method is that the significance of a component is the contribution of the component to resisting the ultimate limit state of collapse of the structure. In a statically determinate structure all components are necessary for stability, and so, all make some contribution to resisting collapse. It is therefore appropriate to base the significance of the components of such structures on the fraction of the failure stress that they carry, and this is what Eq.5.9 does.

$$\text{Local Component significance} = \frac{\text{stress in component}}{\text{characteristic yield strength}} \qquad \text{Eq.5.9 (repeated)}$$

However, in structures where loss of a component, due to over-stress of the component, does not result in collapse, the definition of component significance as expressed by Eq.5.9 would register the component as 100% significant, which is not the case, as other components come into action to resist collapse. The lost component was only partially significant. Therefore, Eq.5.9 does not apply to statically indeterminate structures.

For example, the roof truss of Liverpool Lime Street Station (see Chapter 8) is probably as close to statically determinate as one is likely to encounter, but it is not statically determinate because the upper chord is a continuous arch. If a component within the truss is lost, but collapse does not occur, redistribution of internal forces would take place, which would involve an increase in the stresses in the remaining members. Thus loss of an active component would likely reduce the safety margin of the structure as a whole. Therefore, the lost component had some partial significance in that its presence gave the structure a greater safety margin (and greater robustness), but its significance in doing so is not properly quantified by Eq.5.9.

For an indeterminate structure, it would be more realistic to base the significance of a particular component (i.e. component X) not upon its own stress value, but upon the reduction in the safety margin of the structure as a whole, if component X is lost. Loss of a component would have to be investigated by scenario simulation in order to determine the extent of the reduction of the safety margin of the structure associated with the loss of that component. The greater the reduction in the safety margin of the structure, associated with the loss of a particular component, the greater is the significance of the lost component.

To obtain the significance of component X one must decide if the component is critical or not. For example, the bottom chord of the roof truss of Liverpool Lime Street Station is critical, even though it is a statically indeterminate structure, because it is certain that

collapse would occur if a segment of the bottom chord were lost. However the web members of the truss are not critical, because one may be lost without causing collapse of the truss.

If a component is critical, but it is made up from parts, such as the eyebar composed bottom chord segments of Liverpool Lime Street Station roof truss, then the objective of the assessment is to determine how significant are the individual eyebars in the chord segment. Are the individual eyebars critical or can one or two be lost without loss of the chord segment ?

This question is answered by simulating the loss of one or two eyebars and calculating the reduction in the initial safety margin of the chord segment. The significance of the removed members may then be defined as:

$$\%\ \text{Significance of component X} = \frac{\left(\begin{array}{c}\text{Reduction in initial safety margin of structure} \\ \text{after removal of component X}\end{array}\right)}{\text{Initial safety margin of intact structure}} \times 100$$

Eq.5.12

In this case the significance of the eyebars is determined by removing them from the critical member, namely the bottom chord segment. It was the measurement of stress in the remaining member that allowed determination of the significance of the removed members.

However if it is desired to know the significance of a non-critical member, such as a web member in the truss, then it is necessary to identify the most highly stressed critical member remaining that is most influenced by the removal of the web member. And the significance of the removed member is based on the reduction in the initial safety margin of the remaining critical member. In this concept, the safety margin of the structure is taken as equal to the safety margin of the most highly stressed critical member.

Because the objective of the proposed method is to obtain a new design yield strength based on significance, the design yield strength of a wrought iron component is a variable

quantity. In the application of the proposed method to indeterminate structures, the stress safety margin of a component is used to determine the significance of a component. But since the design yield strength is not yet known, it cannot be used to determine significance. Instead, it is proposed to use the characteristic yield strength to determine the stress safety margin of the component for the purpose of calculating significance, because the characteristic yield strength is a constant irrespective of significance. Therefore, for the purpose of calculating significance the safety margin of a component is defined as the 'initial stress safety margin' according to Eq.5.6.

Initial stress safety margin = characteristic yield strength - stress in component

Eq.5.6 (repeated)

Having determined the significance of component X as a percentage according to Eq.5.12 the procedure for the adjustment of the design yield strength is the same as that for statically determinate structures, described in Section 5.6.

In an indeterminate structure a component is considered critical if loss of that component results in the design stress safety margin of another component, which is critical, approaching zero. The design stress safety margin is defined as:

Design safety margin of component = adjusted design yield strength - stress in component

Eq.5.13

Eq.5.13 is used to decide upon the onset of criticality when simulating the loss of parts from a multi-component member, after the application of the proposed adjustment to the design yield strength.

An overall outline of the proposed assessment method is given in Figure 5.8.

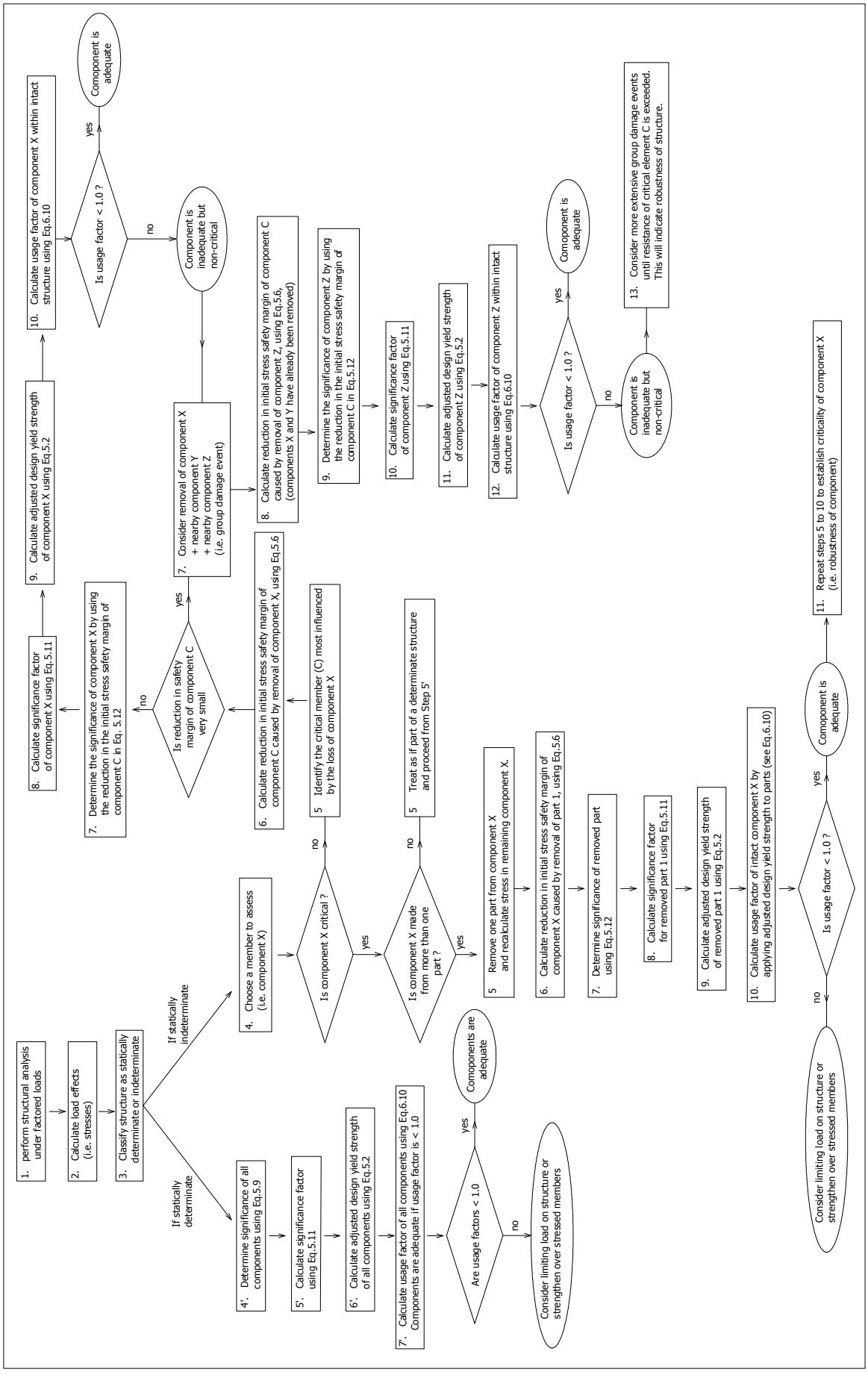

Figure 5.8 Overall outline of the proposed assessment method

Chapter 6 Assessment of Irwell Street Bridge, Manchester

6.1. History of Irwell Street Bridge

Irwell Street Bridge carries Irwell Street in Salford across the River Irwell to join New Quay Street in Manchester; because of this it is also known as New Quay Street Bridge. It was built in 1877 and consists of two wrought-iron bowstring braced girders which span between dressed masonry abutments. The bridge is slightly on the skew in relation to the abutments, the north abutment is out of perpendicular with the centre-line of the bridge by 10^{o} and the south abutment by 13^{o}. (Manchester City Council 1994). The result of this skewed form is that the upstream girder spans 117ft. 6in (35.81m) while the downstream girder spans 120ft. 4in. (36.68m). (Manchester Corporation 1907). The main girders are spaced 52ft 6in (15.85m) apart, between centres. They are 15ft deep at the midpoint, with the top chords of circular form. (Manchester Corporation 1907).

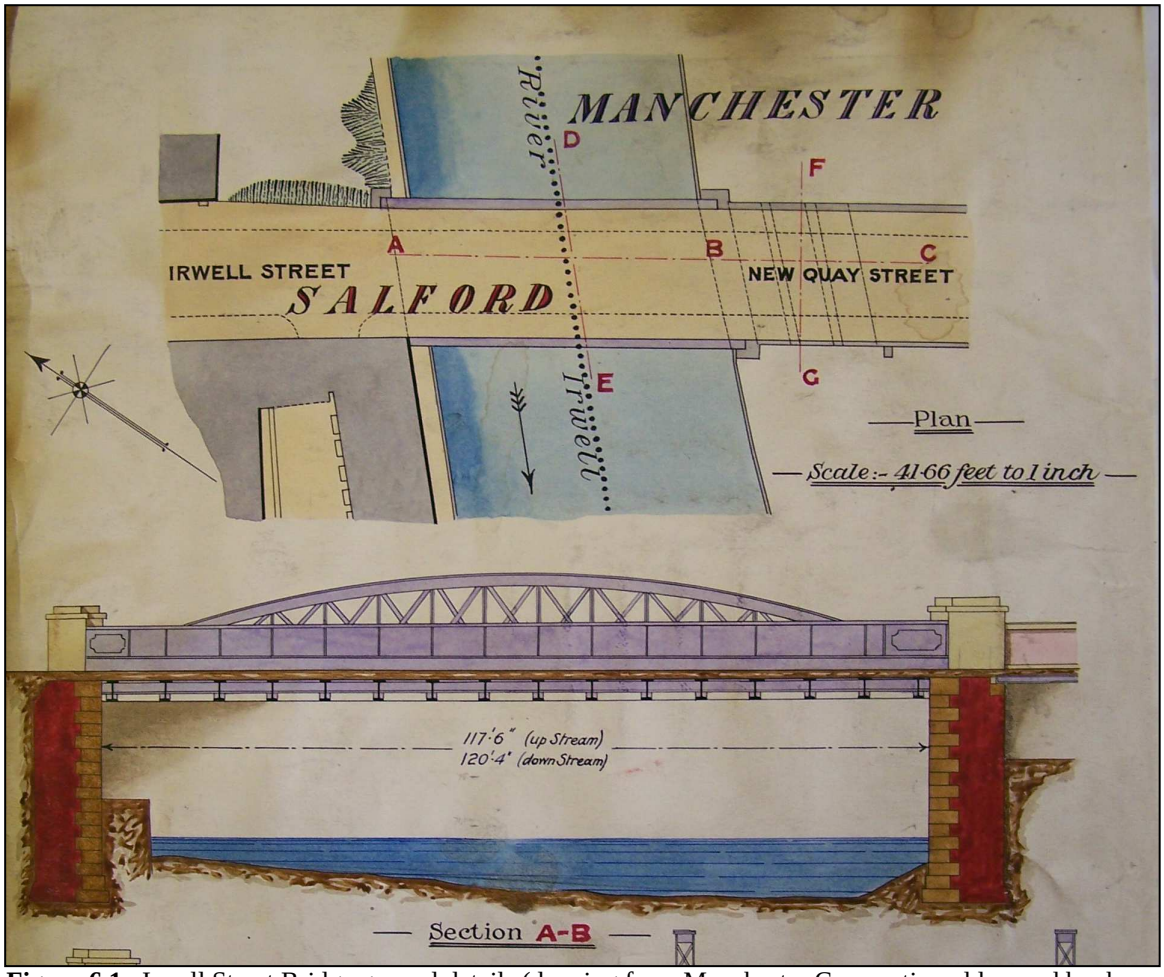

Figure 6.1 Irwell Street Bridge general details (drawing from Manchester Corporation old record book, dated 1907) (Manchester Corporation 1907).

The bridge was designed by civil engineer James Gascoigne Lynde of Manchester Corporation. Lynde was appointed City Surveyor by Manchester Corporation in 1857, a position he held until his resignation in 1879. (AMSES 1883). Prior to this period Lynde had worked for many years as a civil engineer in London as a member of the firm of Lynde and Sympson, George Street, Westminster. (AMSES 1883). Irwell Street Bridge was one of the last structures Lynde worked on as City Surveyor. Following his resignation from the City Corporation Lynde worked with his son James Henry Lynde as a civil engineer in Manchester. (AMSES 1883). James Gascoigne Lynde died in 1883 having completed his fiftieth year as a member of the Institution of Civil Engineers. (AMSES 1883). Lynde was also a member of the Institution of Mechanical Engineers and a Fellow of the Geological Society of London. (AMSES 1883). He was also the second president of the Association of Municipal and Sanitary Engineers and Surveyors. (AMSES 1883).

Figure 6.2 Irwell Street Bridge opened in February 1877. (The Engineer 1877)

The contractor for the ironwork of Irwell Street Bridge was the Stockton Forge Company, Stockton-on-Tees and contractors for the masonry abutments were Messrs Ellis and Hinchliffe of Manchester. (The Engineer 1877). The ironwork cost £14,849 and the

masonry work cost £7,468. The total cost of construction was £22,946 of which Salford Corporation contributed £10,035. (The Engineer 1877). After the bridge was completed £6,000 was paid to Manchester and Salford Corporations jointly by the Lancashire & Yorkshire Railway Company towards the construction of the bridge. (Manchester Corporation 1907).

Working drawings of the bridge were produced by Mr. Lynde's assistant Mr. G.B. Jerram but these no longer exist. All technical and historical information about the bridge has been obtained directly from Manchester City Council's records and from an article about the bridge which appeared in the journal 'The Engineer' dated August 6th 1877. Since its erection the bridge has undergone two strengthening projects, one in 1926 and another more significant project in 1996. The latter project was primarily concerned with the bridge deck. Despite its age and the significant road traffic which it carries the bridge is presently in very good condition. Apart from the deck suspension bolts which will be described later the main bridge span retains all of its original ironwork. The longevity of the bridge is probably due, in part, to the accessibility of all components of the bridge for painting. All of the structural connections are clearly visible, and so can easily be monitored for signs of deterioration.

For the purposes of this research project a set of drawings were produced which are based on a combination of drawings from "The Engineer" article and Manchester City Council's own sketch records, and direct field measurements by the author. These drawings are in Figures 6.28 and 6.29 at the end of this chapter. The historic dimensional information matches the as-built state of the bridge. The original service load for the bridge was for a highway. The bridge was built to support a roadway and not a railway.

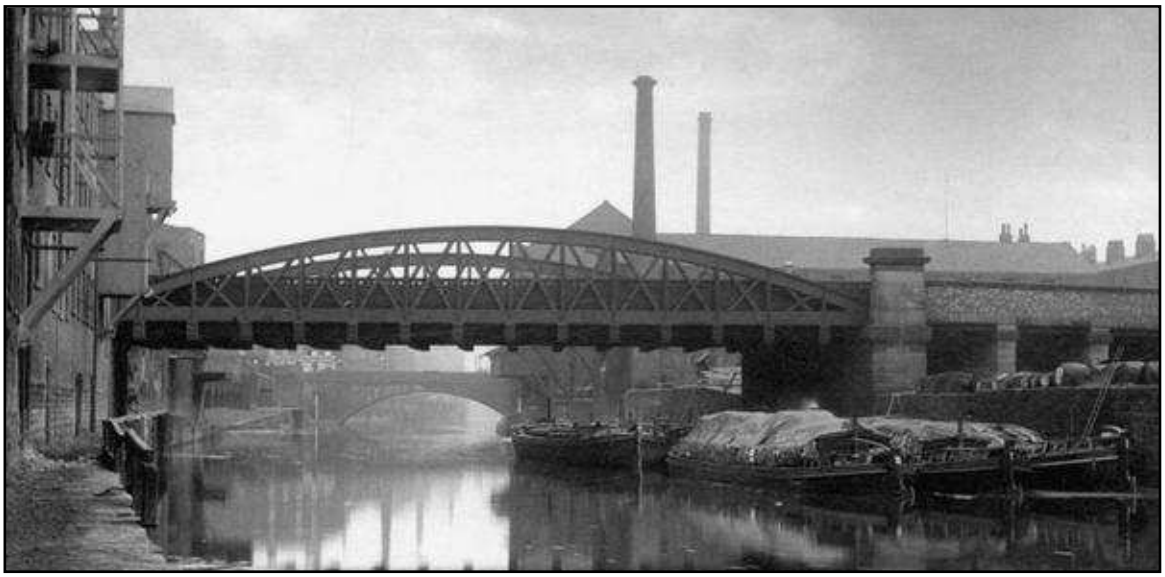

Figure 6.3 Irwell Street Bridge Manchester, looking upstream, photographed by J. Black in 1892 (Photograph courtesy of the Manchester Public Library 2007)

Figure 6.4 Irwell Street Bridge, looking upstream. (Photograph by M O'Sullivan 2008)

6.2 General description of bridge - Main girders

The bridge is entirely composed of riveted plate and angle construction. The top and bottom chords of the main girders are trough shaped, the top being composed of seven plates 9/16in. (14.3mm) thick and the bottom of six plates of the same thickness, 3ft.6in. (1067mm) wide, attached by four angle irons, 4in. by 4in. by 5/8in.,(i.e. 100mm x 100mm x 16mm) to two rows of web plates consisting of two plates 2ft. deep by 5/8in. thick. The rivets are all 7/8in. diameter.(The Engineer 1877).

The curved webs of the top chords were made by first cutting the plates to shape. Then the positions of the rivets were marked on one plate and the two plates making up the web were bolted together at a few locations only, just to hold them temporarily. They were then passed under a radial drilling machine to drill out all of the rivet holes. (The Engineer 1877). Manageable lengths of the upper chord webs were riveted in the contractor's yard and then transported to the site where assembly of the entire girder was completed. (The Engineer 1877).

Figure 6.5 Side view of top chord of main girder. **Figure 6.6** View of top chord.
No sign of inter-plate rusting. Some edge rusting is visible in Figure 2.6 (Photographs by M.O'Sullivan 2008)

The flange plates and angle iron were drilled in position on site by means of portable drilling machines having fourteen spindles. (The Engineer 1877). Because the flanges are composed of up to 7 layers of plate drilling rather than punching was the only option. There are a number of practical reasons for this. Firstly, it would have been impossible to punch through 7 layers of 9/16in. (14.3mm) thick iron (a total thickness of 4in.(100mm)). Punching or drilling each plate separately would also not work, because when a plate is punched or drilled it is flat, but when the plate is then bent to fit the intended curve of the upper chord, alignment of rivet holes would be impossible to achieve. In inferior work misalignment of rivet holes often occurred. In order to achieve a riveted connection in such a case, it was necessary to use a 'drift' or 'rhymer' (or reamer), which was a blunt punch made of soft steel. (Hutchinson 1879). The rhymer forced a rough passage by deforming any obstructions in its way. The consequence was that the plates were forced apart slightly

due to thickening at the edges of the rivet holes. The gaps between the plates could allow the ingress of water and subsequent rusting. See Figures 6.5 and 6.6.

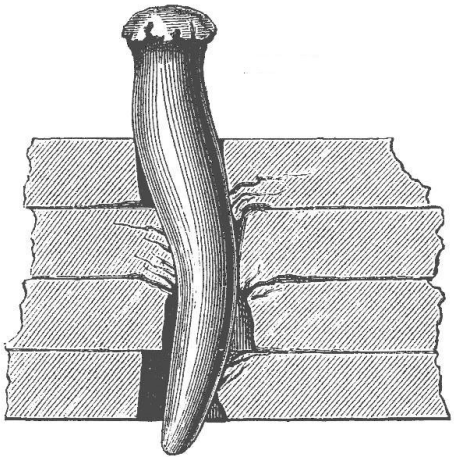

Figure 6.7
Opening a rivet hole in misaligned plates using a rhymer.

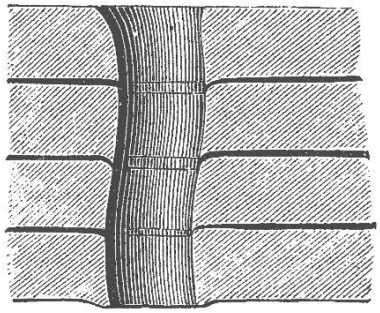

Figure 6.8
Rivet hole after use of rhymer.
Thickening of plate edges around hole causes gaps between the plates (Hutchinson 1879)

In the layers of plates making up the chord flanges shown in Figures 2.5 and 2.6 there is minimal sign of rusting between the plates. It would appear that onsite drilling and mechanical riveting have resulted in a sufficiently tight joint to prevent water penetration. Of course maintenance of a good layer of paint is essential to prevent rusting. Manchester Corporation stipulated that the bridge should be repainted every 4 years. Records show that this was the case certainly up until the 1920's after that records of painting were not kept. (Manchester Corporation 1907)

Figure 6.9 Side view of top chord of main girder.

Figure 6.10 View of main girder.
Extensive riveting was employed to fix the 7 layers of plate iron of the top chord flange. (Photos by M.O'Sullivan 2008)

The vertical struts within the main girder are each composed of a flat plate between two T-irons. The struts are braced together across the width of the girder using 2in.x 2in. (50mm x 50mm) angle iron as shown in Figure 6.12. Figure 6.11 shows the connection of the vertical strut to the inside of the upper chord web.

Figure 6.11 Connection of vertical strut and diagonal ties to inside of upper chord web. (Photo by M.O'Sullivan 2008)

Figure 6.12 Braced vertical struts of main girder (Photo by M.O'Sullivan 2008)

The diagonal members of the main girder consist of a flat bar and are also cross braced to prevent buckling. The longer diagonals toward the middle of the girder are wider and thicker than those nearer the abutments. For example, the bars in the middle bay are 8in x 1in. (203mm x 25.4mm), whereas those in the end bays are 6in x 0.5in. (152mm x 12.7mm).

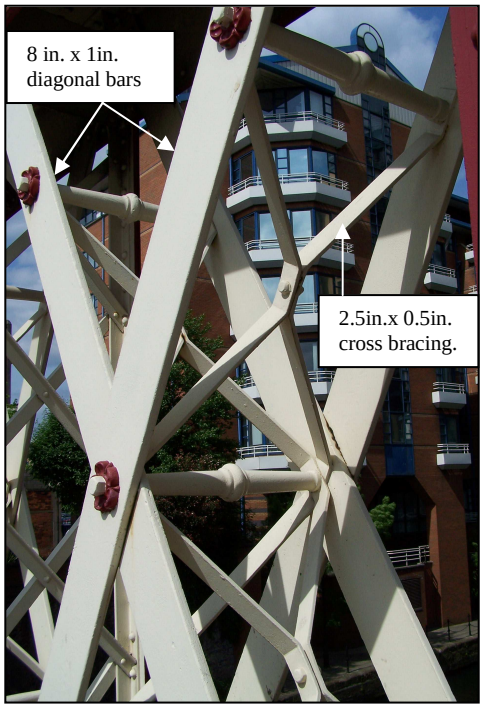

Figure 6.13 Cross braced diagonal members of main girder. (Photo by M.O'Sullivan 2008)

6.3 Abutments

The Abutments are composed of brick faced with cut and dressed stone (i.e. ashlar) and stand 6.5m above water level. (Manchester City Council 1994) The north abutment is 18.9m long, and the south abutment is 19.8m long. The thickness of the abutments as determined from core holes is 3.13m, of which 760mm is the stone face and the rest is solid brick masonry. (Manchester City Council 1994) The abutments are founded on spread footings at a depth approximately 2.5m below ordinary water level, according to the old bridge records. (Manchester Corporation 1907) Judging by rock outcrops visible on the banks and available site investigation details around the region, the founding material may be weathered sandstone. (Manchester City Council 1994)

Figure 6.14 South abutment of Irwell Street Bridge as seen from the towpath on the opposite side of the river.(Photo by M. O'Sullivan 2008)

Allowance was made for thermal expansion and contraction of the bridge at the supports. The main girders rest on cast iron bed plates with gun-metal strips separating the underside of the girders and the cast iron bed plates. The gun-metal strips and the underside of the girders were planed to allow the girders to slide when expanding and contracting. The benefit of this capability was seen during construction of the bridge when in a period of hot

weather the girders expanded and contracted in length by 5/8in. (15.8mm). (The Engineer 1877). However, at some subsequent date, all of the four bearings of the main girders were encased in concrete, thereby limiting free movement in the longitudinal direction. (Manchester City Council 1994) In a modern assessment carried out by Manchester City Council, to which this author had access, it was estimated that a temperature variation of ± 15 ^{o}C would result in horizontal movement of the main girder by ± 6.7mm. (Manchester City Council 1994) Encasing the bearings in concrete prevents free movement of the bridge relative to the masonry abutments. Yet despite this, the abutments are in good condition with no cracks or open joints in the masonry. However, cracks immediately behind the abutments were observed. It has been suggested that as the bridge lengthens in hot weather the abutments are pushed back against the earth fill. (Manchester City Council 1994) When the bridge contracts the abutments return to there original position showing no openings in the masonry but leaving behind cracks between the back of the abutments and the earth fill. (Manchester City Council 1994)

6.4 Cross girders

The cross girders are 55ft. 6in.(16.9m) long, 3ft. 5in.(1.04m) deep in the middle and 2ft. 8in.(0.813m) deep at each end. (The Engineer 1877). They were completely prefabricated in the contractor's yard and like the main girders all the rivet holes were drilled rather than punched. (The Engineer 1877). Original design calculations show that the cross girders are capable of bearing a safe load of 50tons in the centre. (Manchester Corporation 1907) The cross girders are spaced 8ft. 4in.(2.54m) apart. (The Engineer 1877). The most important connection in the bridge is that between the cross girder and the main girder (shown in Figures 6.15 and 6.16). The cross girders are effectively hung from the lower chord of the main girders by means of 24 bolts of 1in.(25.4mm) diameter at each end. Each of these bolts was made in one piece without welding and tested prior to erection with a dead weight of 4 tons (which implies a stress of 79Nmm^{-2}). (The Engineer 1877).

Figure 6.15
View of cross girder connection from above
(Photo by M O'Sullivan 2008)

Figure 6.16
View of cross girder connection from below
(Photo by M O'Sullivan 2008)

6.5 Small longitudinal girders

Small girders at a spacing of 3ft (914mm)apart, span 8ft 4in. between the cross girders and complete the framing for the road deck. They are composed of a 3/8 in. (9.5mm) thick by 2ft (610mm) deep web plate with flanges formed by a pair of 3in x 3in.x 0.5in.(76mm x 76mm x 12.7mm) angles. (The Engineer 1877).

6.6 Bridge Deck

The deck is composed of curved buckle plates which span the 3ft (914mm) distance between the small girders and are the same length as the small girders. The undersides of the curved buckle plates are visible in Figure 6.17.

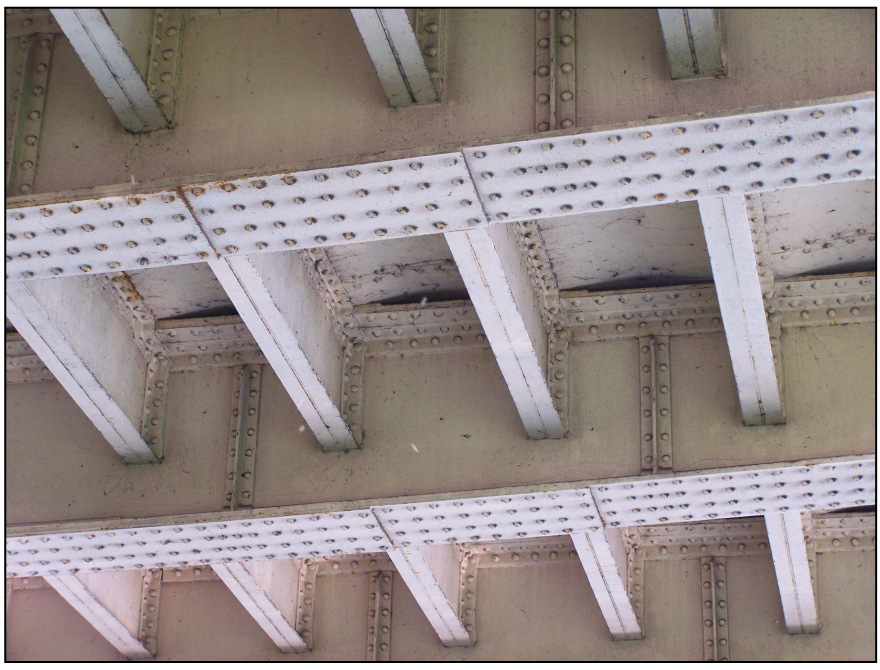

Figure 6.17 Underside of road deck showing curved buckle plates. (Photo by M. O'Sullivan 2008)

The plates are 5/8in.(15.8mm) thick and are riveted to the supporting girders and to each other on all four sides. (The Engineer 1877). Collectively the deck plates give the bridge rigidity in the horizontal plane as well as providing a surface for the roadway material.

6.7 Construction material and bridge design

The bridge was made from 'Cleveland' wrought-iron and was designed so that the heaviest expected load would induce a stress in any member no greater than 4.5 ton/in^2 (70 N/mm^2) in either tension or compression. (The Engineer 1877). The iron was subjected to tensile tests prior to its use. "No iron was used that had a permanent set after 13 ton/in^2 (200 N/mm^2) of tension was applied, or that broke with less than 24 ton/in^2 (370 N/mm^2). (The Engineer 1877). The girders were built to be "more than the usual strength" due to the heavy coal traffic the bridge had to carry and to allow for a certain amount of corrosion, which was expected due to the "exceptional atmospheric impurities which rise from the river". (The Engineer 1877).

6.8 Strengthening of the bridge in 1926

At some date a number of the diagonal members at the narrow ends of the main girders buckled. The locations of these members are shown shaded in Figure 6.18. In 1926 the buckled members were braced and a number of the associated diagonal ties were strengthened. The strengthening consisted of welding additional flat bar lengths to the original flat bar member in order to create a channel section. This is shown in Figure 6.19. Furthermore, the members which buckled were also cross braced by welding 2in. x 2in. x 0.5in. (50mm x 50mm x 12.7mm) angles to them as shown in Figure 6.21. Cross bracing provided sufficient triangulation between the two ties to enable them to act as a rigid ensemble. It would appear that the buckled members were not removed but were braced in their buckled state. In Figure 6.19 the buckled form of the flat bar member is quite visible, this particular member deflected one inch out of plane. The connection of the strengthened

tie member to the web of the upper flange is shown in Figure 5.23. The weld line is clearly visible. From the date of the work it is most likely that the introduced elements were steel and not wrought iron.

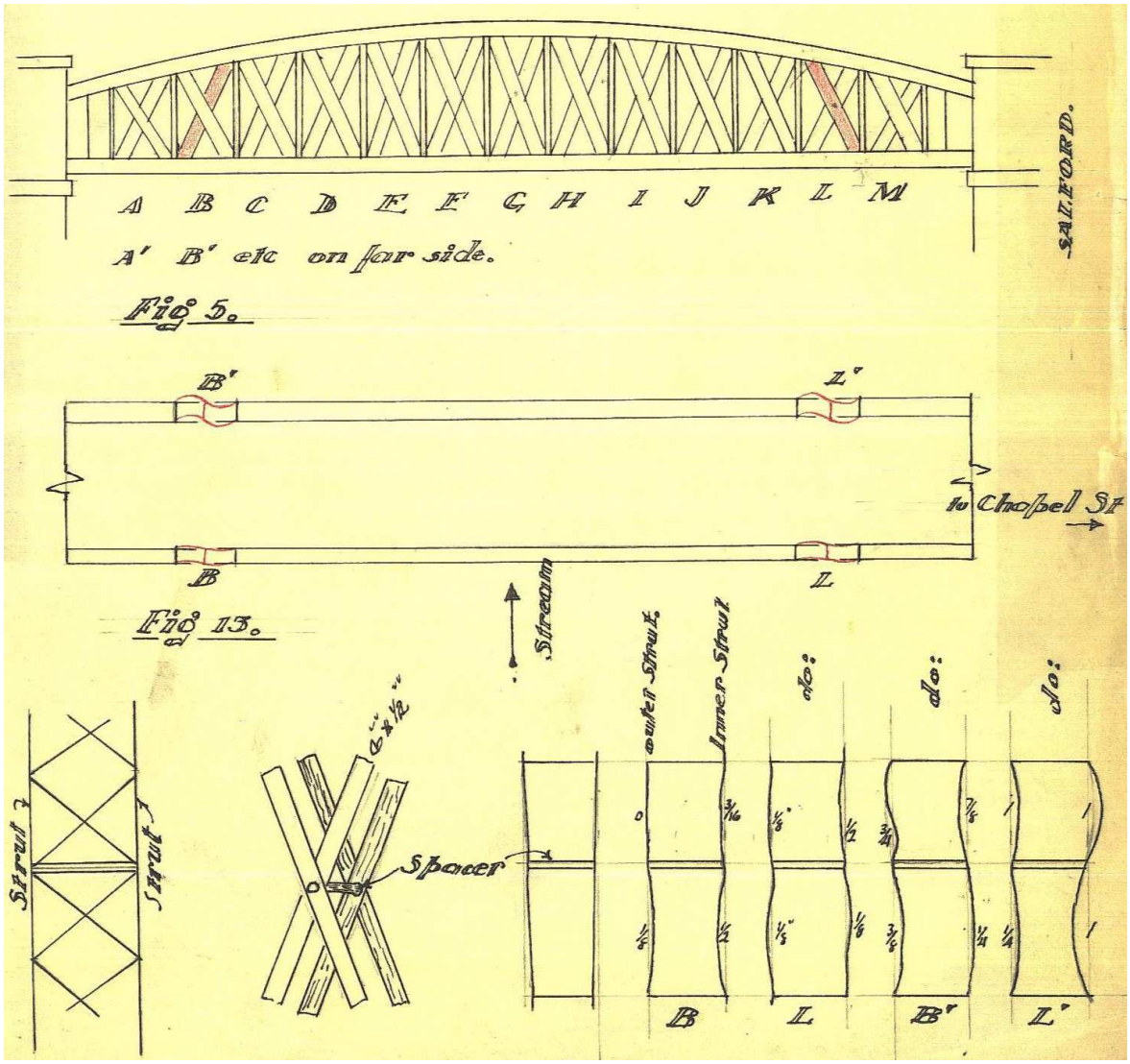

Figure 6.18 Excerpt from report on buckled members of Irwell street bridge. (source: Manchester Corporation records dated March 10th 1926, found in old record book, reference Manchester Corporation 1907)

The assessment of Irwell Street Bridge performed by this author for the present research project was compared with the assessment carried out in 1994 by Manchester City Council and the results showed close agreement between the two assessments.

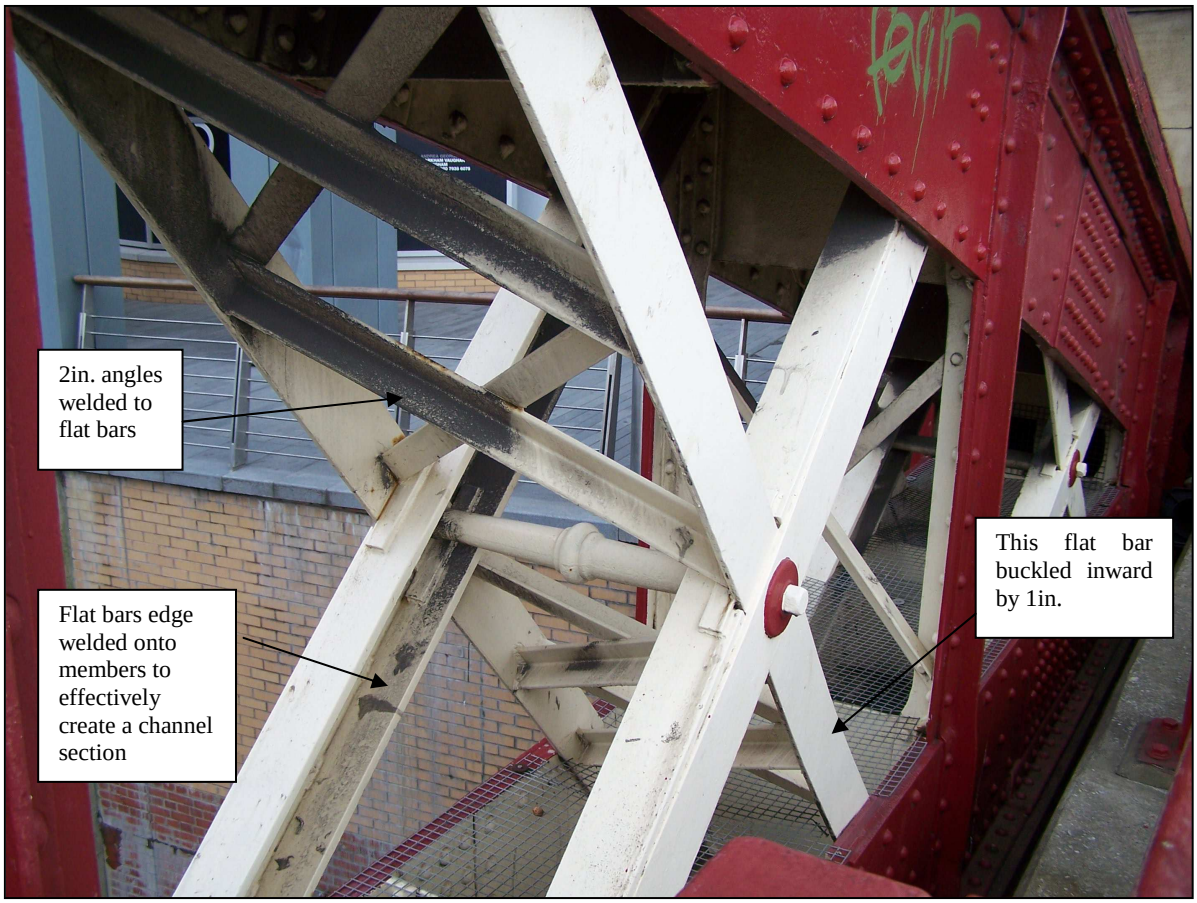

Figure 6.19 Strengthened members of the bow-string girder. (Photo by M. O'Sullivan 2008)

Figure 6.20
Typical tie-bar to upper chord connection.
(Photo by M.O'Sullivan 2008)

Figure 6.21
Tie-bar strengthened by creating a channel section.
(Photo by M.O'Sullivan 2008)

6.9 Irwell Street Bridge - Structural Assessment

The method of assessment proposed in this report is a modification of the current assessment method. To demonstrate the relationship between the two methods when applied to a bridge girder the current assessment method will be carried out first and then the modified method will be employed for comparison.

6.9 (a) Basis of current assessment method

The assessment was carried out in accordance with BD 21/01 The Assessment of Highway Bridges and Structures.

Assessment loads

The assessment loads Q_A^*, are determined from the nominal loads, Q_K, according to the equation:

$$Q_A^* = \gamma_{fl} \cdot Q_K \qquad \text{Eq.6.1 (BD 21/01 cl.3.7)}$$

where γ_{fl} is a partial load factor for each type of loading.

For dead loading of wrought iron structures γ_{fl} = 1.05
For superimposed dead loading (e.g. surfacing material) γ_{fl} = 1.75
For live loading γ_{fl} = 1.5 (BD 21/01 Table 3.1)

Assessment load Effects

The assessment load effects, S_A^*, (such as axial stress) are obtained from the assessment loads by the relation:

$$S_A^* = \gamma_{f3} \text{ (effects of } Q_A^*) \qquad \text{Eq.6.2 (BD 21/01 cl.3.7)}$$
$$= \gamma_{f3} \text{ (effects of } \gamma_{fl} \cdot Q_K)$$

where γ_{f3} is a factor which takes account of the inaccurate assessment of the effects of loading such as unforeseen stress distribution in the structure, inherent inaccuracies in the calculation model, and variations in the dimensional accuracy from measured values.

The value of γ_{f3} shall be taken as 1.1. (BD 21/01 cl.3.10).

Assessment of Resistance

The assessment resistance, R_A^*, (i.e. yield strength of the component) shall be determined from the calculated resistance, R^*, multiplied by the overall condition factor, F_c, as follows:

$$R_A^* = F_c \ . \ R^* \qquad \text{Eq.6.3} \quad \text{(BD 21/01 cl.3.11)}$$

Calculated Resistance

The calculated resistance, R^* determined from material strengths and measured section properties shall be calculated from the following expression:

$$R^* = \frac{1}{\gamma_m} \ function \ \left(f_k \right) \qquad \text{Eq.6.4} \quad \text{(BD 21/01 cl.3.14)}$$

where γ_m is the partial factor for material strength and f_k is the characteristic yield strength.

For wrought iron γ_m = 1.2. (BD 21/01 Table 3.2)

Condition Factor

"If the measurement of sound thickness is not possible, or if there are other uncertainties in the determination of resistance, a condition factor F_{cm} shall be estimated to account for any deficiencies that are noted in the inspection, but cannot be allowed for in the determination of calculated resistance R^*. The value of F_{cm} shall represent, on the basis of engineering judgment, an estimate of any deficiency in the integrity of the structure." (BD 21/01 cl.3.18).

Verification of Structural adequacy

Structures shall be deemed to be capable of carrying the assessment load when the following relationship is satisfied:

$$R_A^* \geq S_A^* \qquad \text{Eq.6.5} \quad \text{(BD 21/01 cl.3.20)}$$

i.e.

$$F_c \ . \ function \ \frac{f_k}{\gamma_m} \ \geq \ \gamma_{f3} \ \left(effects \ of \ \gamma_{fl} \ . \ Q_K \right) \qquad \text{Eq.6.6} \quad \text{(BD 21/01 cl.3.20)}$$

For steel and wrought iron structures the relationship may be rearranged as follows:

$$\frac{F_c}{\gamma_{f3}\gamma_m} . \ function\left(f_k \right) \ \geq \ \left(effects \ of \ \gamma_{fl} \ . \ Q_K \right) \qquad \text{Eq.6.7} \quad \text{(BD 21/01 cl.3.20)}$$

6.9 (b) Method of Analysis

Only ultimate limit state calculations were carried out in accordance with BD 21/01 Chapter 3. For the purposes of this example only the Main Girder was assessed.

Given the substantial gusset and stiffening plates at the joining of the top and bottom chords the analysis was conducted by treating the joined top and bottom chord as a plane frame, that is braced internally throughout its length by vertical and diagonal members.

Given the substantial riveting of the connections of the web members to the top and bottom chords they were modelled as rigidly jointed. Preliminary analysis has shown that this is the most realistic assumption particularly with regard to the support area.

The assessment of the girder was performed on the assumption that one end is fixed and the other end is free to move longitudinally. The analysis carried out was a linear elastic analysis, without yield, using Oasys GSA. Bar elements simulated pin ended components and beam elements simulated rigidly jointed components. Thermal stresses were not included in the analysis and buckling checks were performed on compression members using strut curve data for steel from BS5950.

6.9 (c) Material properties: Wrought iron

Characteristic yield strength = 220N/mm^2. (BD 21/01 cl.4.9)

Modulus of elasticity = 200,000 N/mm^2.

γ_m = 1.2. (BD 21/01 Table 3.2)

The characteristic yield strength value of 220N/mm^2 for wrought iron stated by BD 21/01 is given as a general guide for material of satisfactory quality, but the standard also states that when defects are present testing is required. If tests are carried out the characteristic yield strength is given by

$$f_k = \bar{x} - 1.645\sigma\left(1 + \frac{1}{\sqrt{n}}\right)$$ Eq.6.8 (BD 21/01 C1)

where σ is the kown standard devialtion, to be taken as 26N/mm^2,

$\bar{x}$ is the mean of the test results,

and n is the number of test results.

The formula given in Eq.6.8 is based on the assumption that the standard deviation of results is the same for the samples taken from the particular structure as that determined from the larger number of results on which the value of 220 N/mm^2 is based. This method is suitable for small numbers of results, though the allowance for uncertainty given by Eq.6.8 necessarily increases as the number of results is reduced.

An alternative, but similar method of calculating the characteristic yield strength from a set of test results is given by Eq.6.9

$$f_k = \overline{x} - k\sigma \qquad \text{Eq.6.9 (Bussell 1997)}$$

where $\overline{x}$ is the mean of the test results,

and σ is the standard deviation, given by

$$\sigma = \sqrt{\left(\frac{\sum\left(x-\overline{x}\right)^2}{n}\right)}$$

where n is the number of test results. For k factor see Table 6.1.

No. of samples	3	4	5	6	8	10	20	∞
k	3.37	2.63	2.33	2.18	2.00	1.92	1.76	1.64

Table 6.1 Relationship between 'K' factor and number of samples. (Bussell 1997)

It is stated in BD21/01 that "the yield stress of wrought iron determined from samples varies over a wide range, typically from 180 to 340 N/mm^2, and this range is not necessarily much narrower when samples are taken from the same structure. It is therefore unlikely that a few test results will provide any more reliable information about the yield stress of the material in the structure as a whole than the value of 220 N/mm^2, which is based on a large number of tests." (BD 21/01)

6.9 (d) Loading

Dead and Superimposed Dead Loads:

Unit masses: Wrought iron 7700 kg/m^3

Concrete (plain) 2300 kg/m^3

Stone 2600 kg/m^3

Wearing surface 2400 kg/m^3

Because the entire road deck effectively hangs from the underside of the main girders all loading is applied to the main girders as point loads at the girder nodes (i.e. the locations of the cross girders).

Carriageway: Width between kerbs = 9.238m

Thickness of wearing surface (assumed) = 100mm

Thickness of stone setts = 100mm

Thickness of concrete filling = 100mm

Consider a 1m length of the carriageway (i.e. longitudinal direction).

Weight of 1 m length = volume of material x unit mass x 9.81 N/kg

= (0.1m)(1.0m)(9.239m) x (2300 kg/m^3) x 9.81 N/kg (Concrete)

+ (0.1m)(1.0m)(9.239m) x (2600 kg/m^3) x 9.81 N/kg (Stone)

+ (0.1m)(1.0m)(9.239m) x (2400 kg/m^3) x 9.81 N/kg (Wearing surface)

= 66.2 kN

Total weight of carriageway = (66.2 kN/m) x (length of carriageway)

= (66.2 kN/m) x (37.622m) = 2491 kN

Weight of carriageway transmitted to each main girder = (2491kN) / 2 = 1246 kN

This load is transmitted to the main girder by means of 14 cross girders.

Therefore, nodal loads from carriageway dead load = 1246kN / 14 = 89 kN

Design nodal load = unfactored nodal load x γ_{fL} = (89 kN)(1.75) = **155.7kN**

Footways: Width of each footway = 2.66m

Total thickness of footway (concrete and paving slabs) = 340mm

Consider a 1m length of one footway (i.e. longitudinal direction)

weight of 1 m length = volume of material x unit mass x 9.81 N/kg

= (0.340m)(1.0m)(2.66m) x (2300 kg/m^3) x 9.81 N/kg (Concrete)

= 20.4 kN

Total weight of one footway = (20.4 kN/m) x (length of footway)

= (20.4 kN/m) x (37.622m) = 767 kN

This load is transmitted to the main girder by means of 14 cross girders.

Therefore, nodal loads from weight of footway = 767kN / 14 = 54.8 kN

Design nodal load = unfactored nodal load x γ_{fL} = (54.8 kN)(1.75) = **95.9kN**

Short Longitudinal Girders

Cross sectional area = 0.012852m^2

length = 2.463m

Weight of one short girder = (0.012852m^2)(2.463m)(7700 kg/m^3)(9.81N/kg) = 2.39kN

Each cross girder supports one end of 34 short girders.

Total weight of short girders transmitted to each cross girder = [(2.39kN)(34)] / 2 = 40.6kN

Total weight of short girders transmitted to main girder node via cross girder = (40.6kN)/ 2 = 20.3kN.

Design nodal load = unfactored nodal load x γ_{fL} = (20.3kN)(1.05) = **21.3kN**

Cross Girder:

Cross sectional area = 0.074589m^2

length = 16.916m

Weight of one cross girder = (0.074589m^2)(16.916m)(7700 kg/m^3)(9.81N/kg) = 95.3kN

Weight of cross girder transmitted to main girder node = (95.3kN) / 2 = 47.7kN.

Design nodal load = unfactored nodal load x γ_{fL} = (47.7 kN)(1.05) = **50.1 kN**

Live loads (carriageway):

The structure was assessed for Type HA loading and knife edge load (KEL) equivalent to a 40 tonne assessment live loading in accordance with Chapter 5 of BD 21/01.

Footway loading of 5 kN/m^2 was considered in combination with carriageway loading.

Width of carriageway (measured between kerbs) = 9.238m (actual)

deck span (centre to centre of bearings) = 37.622m (actual)

Loaded length = 38m (rounded)

Number of notional lanes = 3 (BD 21/01 Table 5.1)

Notional lane width = 9.238m / 3 = 3.079m

Type HA loading (UDL) = 29.4kN/m (per notional lane) (BD 21/01 Table 5.2)

Knife edge load (KEL) = 120kN (per notional lane) (BD 21/01 cl. 5.18)

The KEL shall be applied at one point only in the loaded length of each loaded lane (BD 21/01 cl. 5.19).

The HA UDL and KEL are to be dividing by the following adjustment factor (AF)

For $20 < L < 40$

$$AF = 1 + \left(\frac{a_L}{2.5 - 1}\right)\left(2 - \frac{L}{20}\right)$$

where a_L = 3.65m and L is the loaded length (m). (BD 21/01 cl.5.23)

$\Rightarrow$ AF = 1.24

Adjusted HA UDL = (29.4kN/m) / 1.24 = 23.7 kN/m

Adjusted KEL = (120kN) / 1.24 = 96.8 kN.

Design HA UDL = (23.7 kN/m) x γ_{fL} = (23.7 kN/m) (1.5) = **35.6 kN/m**

Design KEL = (96.8 kN) x γ_{fL} = (96.8 kN) (1.5) = **145.2 kN** (BD 21/01 Table 3.1)

The most severe loading position of the KEL is at mid span.

Total KEL (3 notional lanes) = 3 x (145.2 kN) = 435.6kN

KEL load transmitted to each of the two nearest cross girders = 435.6kN / 2 = 217.8kN

KEL load transmitted to each main girder from one cross girder = 217.8kN / 2 = **109 kN**

(See Figure 7.22 for illustration of loaded main girder)

Total HA load on entire deck = No. of notional lanes x (35.6 kN/m) x (length of deck)

= 3 x (35.6 kN/m) x (37.622m) = 4018 kN

Total HA load per main girder = 4018 kN / 2 = 2009kN

This load is transmitted to the main girder by means of 14 cross girders.

Therefore, design nodal loads from HA loading = 2009kN / 14 **= 143.5kN**

(See Figure 6.22 for illustration of loaded main girder)

Live loads (footway): Width of each footway = 2.66m

Total unfactored load on one footway = (37.622m)(2.66m)(5 kN/m^2) = 500kN

This load is transmitted to the main girder by means of 14 cross girders.

Therefore, nodal loads from unfactored live load on footway = 500kN / 14 = 35.7kN

Design nodal load = unfactored nodal load x γ_{fL} = (35.7kN)(1.5) = **53.6kN**

Load type	Magnitude (kN)	Location of load on Main Girder
Carriageway (Superimposed Dead)	155.7	Every bottom chord node
Footway (Superimposed Dead)	95.9	Every bottom chord node
Short girders (Dead)	21.3	Every bottom chord node
Cross girder (Dead)	50.1	Every bottom chord node
Carriageway (Live: Type HA)	143.5	Every bottom chord node
Carriageway (Live: Type KEL)	109	Two central nodes only
Footway (Live)	53.6	Every bottom chord node

Table 6.2 Summary of loads applied to main girder in analysis

The self weight of the main girder is taken into account in the computer analysis model.

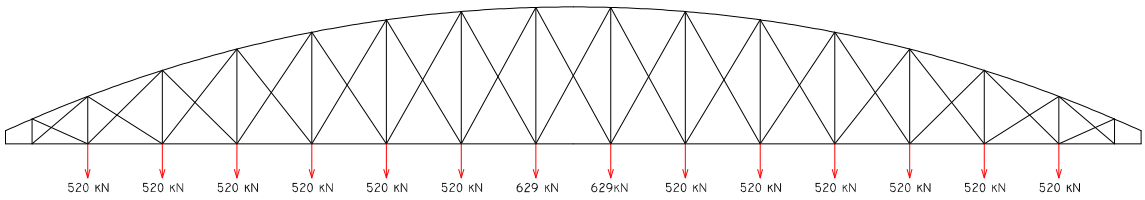

Figure 6.22 Loads used in analysis of Irwell Street Bridge.

6.9 (e) Condition Factor (F_c): (Main Girder)

Top chord

The components are in good condition and no loss of section was observed. A condition factor of 1.0 in the middle and 0.9 at the support region (to allow for any corrosion effects in the areas where access for efficient repainting is not possible) were applied.

Bottom chord

No loss of section is evident, but some corrosion is possible on the interface between the deck and the bottom chord. It is also possible for corrosion to occur inside the U-shaped member due to inefficient drainage. An overall factor of 0.9 was applied.

Diagonal Ties and Vertical Hangers

These components were is good condition so a condition factor of 1.0 was applied.

6.9 (f) Results of Structural Analysis - Unstrengthened bridge

The results of the analysis for a 40 tonne assessment live loading are given in Table 6.3. The bridge was strengthened in 1926. The analysis results given in Table 6.3 are for the bridge prior to this strengthening. The unstrengthened bridge was analysed in order to demonstrate the reason for strengthening.

The strength of a component (R_A^*) is related to the load effects (S_A^*) by a factor U defined as the "Usage Factor", which represents the ratio S_A^*/ R_A^*. Values of U greater than 1.0 indicate a non-compliance with current assessment standards.

$$U = \frac{S_A^*}{R_A^*} = \frac{\gamma_{f3}\left(effects\ of\ \gamma_{fl}\ .\ Q_K\right)}{F_c\ .\ function\ \frac{f_k}{\gamma_m}} \qquad \text{Eq.6.10 (from Eq.5 and Eq.6)}$$

$$= \frac{1.1\left(effects\ of\ \gamma_{fl}\ .\ Q_K\right)}{F_c\ .\ \frac{220\text{N/mm}^2}{1.2}}$$

Component Type	Component Number	Condition Factor (F_c)	R_A N/mm^2	S_A (Axial + Bending stress) (N/mm^2)	U	Comment
Top Chord	61	1.0	183	-170	0.93	
	66	1.0	183	-82.6	0.45	
	67	1.0	183	-83.1	0.45	
	68	1.0	183	-83.7	0.46	
	73	1.0	183	-155	0.85	
	83	1.0	183	-151	0.82	
	84	1.0	183	-138	0.75	
Bottom Chord	86	0.9	165	98.2	0.60	
	87	0.9	165	73.1	0.44	
	92	0.9	165	72.0	0.44	
	93	0.9	165	72.1	0.44	
	94	0.9	165	71.9	0.44	
	99	0.9	165	71.5	0.43	
	100	0.9	165	92.0	0.56	
Vertical ties	10	1.0	183	30.2	0.16	
	13	1.0	183	29.2	0.16	
	14	1.0	183	29.6	0.16	
	17	1.0	183	31.0	0.17	
	77	1.0	183	99.1	0.54	
	38	1.0	183	183	1.00	
	39	1.0	183	180	0.98	
	48	1.0	183	173	0.94	
	49	1.0	183	179	0.98	
	78	1.0	183	94.3	0.51	
Diagonal Ties	4	1.0	183	34.0	0.19	
	23	1.0	183	38.4	0.21	
	27	1.0	183	364	**1.99**	Later strengthened
	40	1.0	183	321	**1.75**	Later strengthened
	43	1.0	183	24.1	0.13	
	44	1.0	183	25.2	0.14	
	45	1.0	183	301	**1.64**	Later strengthened
	47	1.0	183	342	**1.87**	Later strengthened
Diagonal Struts	3	1.0	183	-200	**1.09**	buckled
	5	1.0	183	12.6	0.07	
	22	1.0	183	10.7	0.06	
	24	1.0	183	-217	**1.18**	buckled
	28	1.0	183	-268	**1.46**	
	46	1.0	183	-251	**1.37**	

Table 6.3 Results of structural analysis of unstrengthened Irwell Street Bridge

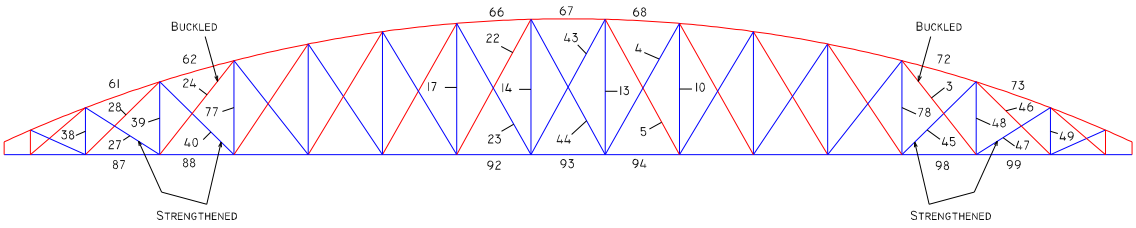

Figure 6.23 Irwell Street Bridge component numbers used in analysis. Blue indicates tension and red indicates compression.

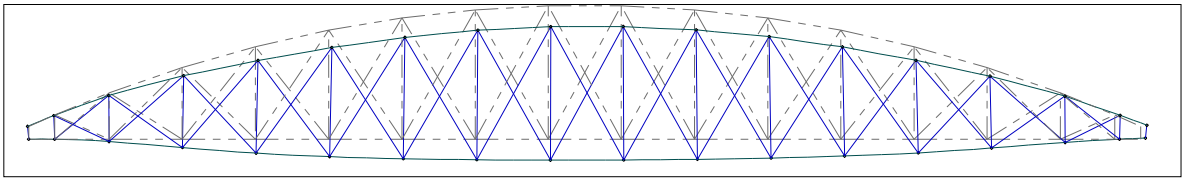

Figure 6.24 Exaggerated deflected form of bridge.

6.9 (g) Results of Structural Analysis - strengthened bridge

The results of the analysis for a 40 tonne assessment live loading on the bridge after the 1926 strengthening are given in Table 6.4.

Component Type	Component Number	Condition Factor (F_c)	R_A N/mm^2	S_A (Axial + Bending stress) (N/mm^2)	U	Comment
Top Chord	61	1.0	183	14	0.08	
	66	1.0	183	-37	0.20	
	67	1.0	183	-39	0.21	
	68	1.0	183	-38	0.21	
	73	1.0	183	-1	0.00	
	83	1.0	183	124	0.68	
	84	1.0	183	69	0.38	
Bottom Chord	86	0.9	165	100	0.61	
	87	0.9	165	40	0.24	
	92	0.9	165	70	0.42	
	93	0.9	165	71	0.43	
	94	0.9	165	71	0.43	
	99	0.9	165	48	0.29	
	100	0.9	165	81	0.49	
Vertical ties	10	1.0	183	30	0.16	
	13	1.0	183	28	0.16	
	14	1.0	183	30	0.16	
	17	1.0	183	32	0.17	
	77	1.0	183	39	0.21	
	38	1.0	183	56	0.31	
	39	1.0	183	30	0.16	
	48	1.0	183	32	0.18	
	49	1.0	183	63	0.34	
	78	1.0	183	39	0.21	
Diagonal Ties	4	1.0	183	31	0.17	
	23	1.0	183	42	0.23	
	27	1.0	183	184	**1.00**	After strengthening
	40	1.0	183	210	**1.15**	After strengthening
	43	1.0	183	21	0.11	
	44	1.0	183	28	0.16	
	45	1.0	183	207	**1.13**	After strengthening
	47	1.0	183	182	0.99	After strengthening
Diagonal Struts	3	1.0	183	-113	0.62	Previously buckled
	5	1.0	183	14	0.08	
	22	1.0	183	8	0.04	
	24	1.0	183	-154	0.84	Previously buckled
	28	1.0	183	-178	0.97	
	46	1.0	183	-163	0.89	

Table 6.4 Results of structural analysis of Irwell Street Bridge after 1926 strengthening work was carried out.

Comparison of the analysis results for the bridge before and after strengthening show that prior to strengthening the members which buckled did so because they were over stressed, as were the diagonal ties that were later strengthened. However, two of the strengthened diagonal ties are still over stressed under modern assessment load. Yet this has no practical effect on the strength of the bridge as a whole. Even with two of the diagonal ties

registering as over stressed the principal members of the bridge, namely the top and bottom chords are still quite below limit state violation. The most important member of the main girder is the bottom chord, as the entire road deck hangs from it. The maximum stress in the bottom chord is only 74N/mm^2. Given the safety margin of the principal members and the amount of cross bracing in the web of the girder, the minor limit state violation of two diagonal ties may be allowed without further action being required

This analysis was conducted in accordance with the standard BD 21/01 The Assessment of Highway Bridges and Structures, which uses 220N/mm^2 as the characteristic yield strength of wrought iron. However, one of the conclusions of this research project is that 220N/mm^2 is too high a value for the characteristic yield strength of wrought iron. The bridge is made of plate iron, bar iron and angle iron, which according to this research project has characteristic yield strength values of 187N/mm^2, 151N/mm^2 and 200N/mm^2 respectively. Therefore, if one were to use these values of characteristic strength in the assessment, one would find that by direct comparison of the usage factor of any one particular component the bridge has a lower safety margin, as shown by the values in Table 6.5. In addition, a number of diagonal ties exhibit limit state violation, but the principal members, such as the top and bottom chords, do not, nor do the vertical ties. Therefore, one may conclude that although the bridge has members which register as over stressed under modern assessment loading, these members are not critical to the continued function of the bridge in carrying the required load. The over stressed regions are the diagonal web members near the supports but the top and bottom chords at any point over the entire bridge are not over stressed. Given that the top and bottom chord act together as a rigid frame rather than a truss, the over stressing of some of the diagonal members may be acceptable as it appears to have little effect on the overall safety margin of the structure. In this case the overall safety margin of the structure is based on the stresses in the top and bottom chords alone.

Component Type	Component Number	Condition Factor (F_c)	R_A N/mm^2	S_A (Axial + Bending stress) (N/mm^2)	U	Comment
Top Chord	61	1.0	156	14	0.09	
	62	1.0	156	-13	0.08	
	66	1.0	156	-37	0.24	
	67	1.0	156	-39	0.25	
	68	1.0	156	-38	0.25	
	73	1.0	156	-1	0.01	
	83	1.0	156	124	0.80	
	84	1.0	156	69	0.45	
Bottom Chord	86	0.9	140	100	0.71	
	87	0.9	140	40	0.28	
	88	0.9	140	54	0.38	
	92	0.9	140	70	0.50	
	93	0.9	140	71	0.51	
	94	0.9	140	71	0.51	
	99	0.9	140	48	0.35	
	100	0.9	140	81	0.58	
Vertical ties	10	1.0	167	30	0.18	
	13	1.0	167	28	0.17	
	14	1.0	167	30	0.18	
	17	1.0	167	32	0.19	
	77	1.0	167	39	0.23	
	38	1.0	167	56	0.34	
	39	1.0	167	30	0.18	
	48	1.0	167	32	0.19	
	49	1.0	167	63	0.38	
	78	1.0	167	39	0.23	
Diagonal Ties	4	1.0	126	31	0.24	
	23	1.0	126	42	0.33	
	27	1.0	126	184	**1.46**	Strengthened 1926
	40	1.0	126	210	**1.67**	Strengthened 1926
	43	1.0	126	21	0.17	
	44	1.0	126	28	0.23	
	45	1.0	126	207	**1.64**	Strengthened 1926
	47	1.0	126	182	**1.44**	Strengthened 1926
Diagonal Struts	3	1.0	126	-113	0.90	Braced 1926
	5	1.0	126	14	0.11	
	22	1.0	126	8	0.06	
	24	1.0	126	-154	**1.22**	Braced 1926
	28	1.0	126	-178	**1.42**	
	46	1.0	126	-163	**1.29**	

Table 6.5 Results of analysis of strengthened Irwell Street Bridge using lower characteristic yield strength values. (i.e. 187N/mm^2 for plate iron, 151N/mm^2 for bar iron, and 200N/mm^2 for tee iron).

6.10 (a) Application of the proposed assessment method to Irwell Street Bridge

The proposed method fits into the current assessment method in that it only provides a different way of calculating the component resistance. The difference being that the proposed method takes into account a closer examination of the quality of the material and the significance of the component within the structure. Under the current method the component resistance (i.e. design yield strength) is given by:

$$R_A^* = F_c \,.\, R^* \;=\; F_c \,.\, \frac{f_k}{1.2} \;=\; F_c \,.\, \frac{220\text{N/mm}^2}{1.2}$$ from Eq.6.3 and Eq.6.4

Under the proposed method the component resistance is given by:

$$R_A^* = F_c \,.\, R^* \;=\; F_c \,.\, \frac{f_k\,\beta}{1.2\,\alpha}$$

where f_k is the characteristic yield strength depending on component type,

α is the significance factor of the component,

and β is the quality factor of the component type, based on ductility.

The values of α and β are determined from a database of test results on wrought iron and not on any tests of samples from the structure being assessed. The reason for this is to avoid misleading assumptions about strength or weakness based on examination of just a few samples. Even the current assessment standard BD21/01 concedes that a few test results will not provide any more reliable information about the yield stress of the material in the structure than the value determined from a large number of tests.

The values of α and β to be used in the assessment of Irwell Street Bridge are given in Table 6.6

	Characteristic yield strength	α factor range	β factor
Plate iron (along grain)	187	0.634 - 0.761	0.761
Rectangular and Round bars	151	0.794 - 0.953	0.953
Angles and Tees	200	0.797 - 0.956	0.956

Table 6.6 Parameters used in design strength adjustment. From Table 5.4.

Assessment of the web members of the main girder, using the proposed method, provides a good example of the method, because some of these members were found to be over stressed under the current method, yet did not result is failure of the structure or further strengthening action being taken. These members are non-critical and the steps in the proposed assessment procedure which apply to these members are outlined in Figure 6.25

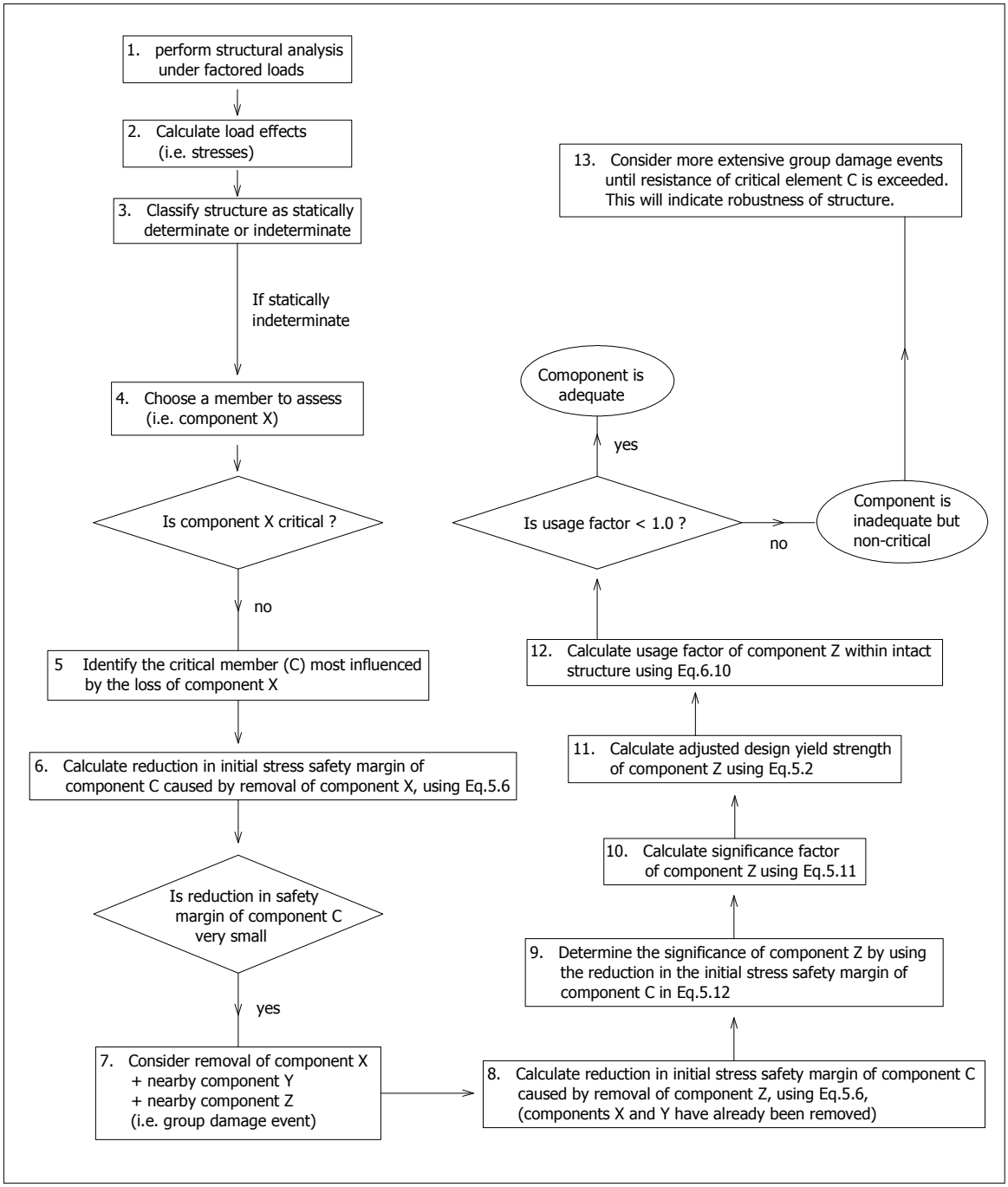

Figure 6.25 Outline of steps in proposed method for the assessment of the girder web members.

The present example of Irwell Street Bridge is an indeterminate structure consisting of a rigid frame in the form of a truss. The analysis of the unstrengthened bridge has shown that the structure can withstand some damage and remain completely functional. The evidence for this is the stress safety margin of the principal members, namely the top and bottom chords, and the obvious functionality of the bridge even when some of its members were calculated to be in limit state violation. The most critical elements of the bridge are the

bottom chords. In Step 5 each web component listed in Table 6.5 was removed from the structure one at a time to see what reduction in stress safety margin occurred in the top and bottom chords. The member in the top or bottom chord which was most affected by the loss of the test component was used as a reference point on which to base significance. In other words the ratio of the greatest reduction in the initial stress safety margin of the top or bottom chord, to the safety margin of the same locality within the intact structure was taken as the measure of significance. (see Eq.5.6) As each member was removed its effect on the chord members was recorded, and this provided a scale of significance for the members that were removed. However, it was observed that the loss of an individual web member on its own had very little effect on the stresses in the chord members. The reason for this is that the structure was modelled as a rigid frame, so that the loss of just one relatively slender web element would have little effect on the overall structure.

Although the removal of a single member provides a logical way of determining the significance of a particular member within the intact structure, it does not provide a very useful measure of significance for non critical elements, when the effect on the safety margin of the structure of losing the element is very small. Furthermore, it does not take into account the possible simultaneous loss of a group of members, such as might occur in an explosion, or if a truck crashed into the side of the bridge.

Under the proposed method significance is a variable quantity that depends on the state of the structure. The members of a damaged structure are more significant than in an intact structure, because there are fewer of them present to share the load. In Chapter 8 it is shown with reference to Liverpool Lime Street Station, that under the proposed method, when one member is lost, the significance of the remaining members increases. It is possible to calculate the significance of members individually in a progressive collapse mechanism, where one member fails after another. Therefore, it is proposed that in a group

damage event, i.e. where a number of members are lost simultaneously, the significance of each should be calculated as if lost sequentially.

Steps 8 and 9 of the procedure involve the calculation of significance of a component when the component is involved in a group damage scenario.

The result of both interpretations of significance is that a member will have a certain individual significance if it is part of the intact structure, but it will have a greater value of significance if it is imagined to be lost as part of a group damage scenario.

6.10 (b) Step 6: Component significance based on loss of one element only.

Member no.23 will be used as an example of how to calculate component significance within the intact structure. The significance of a component is given by:

$$\text{significance of removed member} = \frac{\text{greatest reduction in local safety margin of structure}}{\text{local safety margin of intact structure}}$$

(from Eq.5.12)

In this case the greatest effect on the chord members, when member no.23 is removed, is an increase in the bending moment in the bottom chord, directly below the removed member. The total stress in this part of the bottom chord increases from 70N/mm^2 to 77N/mm^2 when member no.23 is removed. Therefore,

Initial safety margin before removal of no.23 = 187 N/mm^2 - 70 N/mm^2 = 117 N/mm^2

Initial safety margin after removal of no.23 = 187 N/mm^2 - 77 N/mm^2 = 110 N/mm^2

Applying Eq.5.6, the reduction in the initial stress safety margin, due to the removal of member no.23 = 117 N/mm^2 - 110 N/mm^2 = 7 N/mm^2.

Therefore the significance of member no.23 is given by:

$$\text{significance of member no.23} = \frac{7\text{N/mm}^2}{117\text{N/mm}^2} = 0.06 = 6.0\% \qquad \text{(from Eq.5.12)}$$

By following this procedure the individual significance values for the members of the structure are calculated as shown in Table 6.7.

Component removed	S_A of bottom chord (N/mm^2)	Local initial safety margin of bottom chord (N/mm^2)	Reduction in initial safety margin (N/mm^2)	Significance of removed component %
Intact structure	70	117	---	---
43	71	116	1	0.9
14	72	115	2	1.7
22	68	119	0	0
23	77	110	7	6.0
17	70	117	0	0

Table 6.7 Significance of members within intact structure

In Table 6.7 it can be seen that member no.17 registers as having zero significance. This does not mean that it has no function. Within the intact structure member no.17 carries a tensile stress of 22 N/mm^2, and so, is a functioning member of the structure. But when it is removed the forces within the web members alter slightly to compensate for the loss, with the consequence that the stress in the bottom chord does not alter. Thus in terms of the bottom chord, member no.17 is insignificant, but it is only insignificant because it has other members around it to compensate for its loss. This example demonstrates that removal of a single non-critical member can lead to a misleading interpretation of significance, and in that case more than one member should be removed to determine the functioning significance of a component, as is done in Step 7

6.10 (c) Step 7: Component significance based on loss of a group of elements.

In calculation of significance based on the single event loss of a group of components, the group of components removed should be adjacent to one another because this will correspond to the most adverse damage event, but it is also the most realistic damage scenario because a truck crash will most likely destroy a group of components in close proximity to each other. As an example, consider the central group of web members. The group damage event consists of the loss of the members in the following sequence: member nos. 43, 44, 14, 22, 23, and is illustrated in Figure 6.26 The local reference point for calculation of safety margin is the bottom chord where it is joined to the vertical tie member no.14.

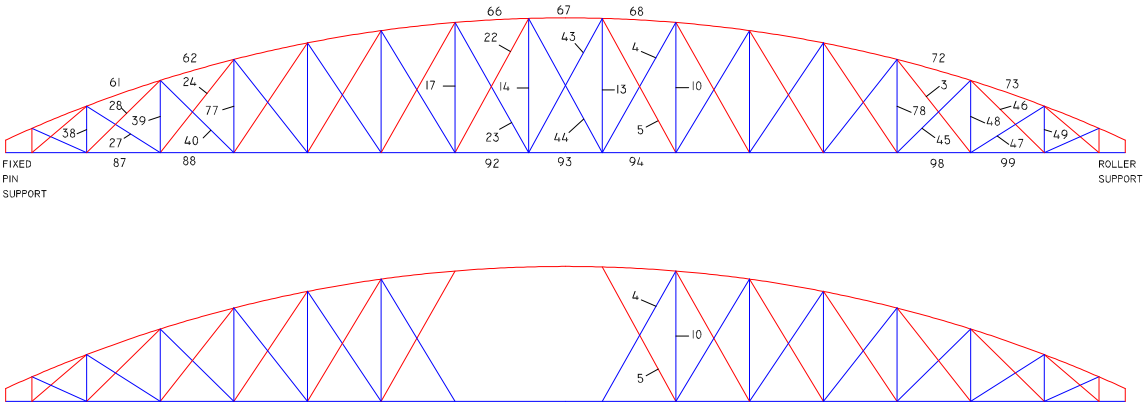

Figure 6.26 Group damage scenario used to determine significance of lost members. Member No. given.

Components removed	S_A of bottom chord (N/mm^2)	Local initial safety margin of bottom chord (N/mm^2)	Reduction in initial safety margin of chord (N/mm^2)	Significance of removed component %
Intact structure	70	117	---	---
43 + 44	71	116	1	0.9
43 + 44 +**14** + **13**	73	114	2	1.7
43 + 44 +14 + 13 + **22**	75	112	2	1.7
43 + 44 +14 + 13 + 22 **+ 23**	93	94	18	15.4
43 + 44 +14 + 13 + 22 + 23 + **17**	97	90	4	3.4

Table 6.8 Significance of members involved in the single event damage scenario depicted in Figure 6.26

As an example of how the values in Table 6.8 were obtained consider the removal of member no 23 from the damaged structure. In this case it is imagined that members 43, 44, 14, 13 and 22 have already been lost, and then member no.23 is removed.

Because of the way significance has been defined a component with a significance less than 100% may be essential for stability. The decision about the criticality of a component is not based on its percentage value of significance, but should be based on the design safety margin of the structure after the loss of the component. If loss of a component results in the design safety margin of the structure reducing to zero then the removed component is a critical component. The design safety margin is based on the design yield strength, which is the strength of a component after the adjustment for significance and quality have been made.

The significance of member no.23 is based on the reduction in the initial safety margin of a nearby critical component. In this case the bottom chord of the girder was chosen as the critical member most influenced by loss of member no.23.

With the girder in its damaged state, after the removal of members 43, 44, 14, 13, and 22 the bottom chord has a local total stress of 75 N/mm^2 resulting in a local design safety margin of 65N/mm^2. After the removal of member no.23 the stress in the bottom chord increases to 93N/mm^2, thereby reducing the safety margin of the bottom chord to 47N/mm^2. The reduction in the safety margin resulting from the removal of member no.23 is 65N/mm^2 - 47 N/mm^2 = 18 N/mm^2. Therefore, the significance of member no.23 is given by:

$$\text{significance of component X} = \frac{\left(\begin{array}{l}\text{Reduction in initial safety margin of structure} \\ \text{after removal of component X}\end{array}\right)}{\text{Initial safety margin of intact structure}}$$

Eq.5.12 (repeated)

$$\text{significance of member no.23} = \frac{18 \text{ N/mm}^2}{117 \text{ N/mm}^2} = 0.154 = 15.4\%$$

It is clear from the values in Table 6.8 that the most significant member in the group, involved in the damage event, is member no 23, because its loss resulted in the greatest incremental reduction in the safety margin of the bottom chord. In Step 6 the significance of member no.23 was determined by simulating removal of just that member alone, and in that case the significance was calculated to be 6.0%. Clearly, when components are lost as a group their significance is greater. The lower value of 6.0% significance would lead to a higher design yield strength for the component. Using the larger value of significance would lead to a lower design yield strength and is therefore a safer approach to assessment.

This example shows that the safest approach to assessment under the proposed method involves simulating the worst case damage scenario and it is not necessary to simulate the

loss of individual components unless those component are obviously critical components. The chords of a truss are obviously critical components. Therefore, the loss of a single part from a chord member would be regarded as a significant damage event and should be simulated in order to determine the significance of the removed part. This is illustrated for the bottom chord of the roof trusses of Liverpool Lime Street Station in Chapter 8.

6.10 (d) Steps 10 and 11: Calculation of design yield strength of components

Member no.23 will be used as an example of how the component resistance is adjusted. This member is a diagonal web member consisting of a flat bar.

Firstly, the significance factor α used in adjusting the component resistance is determined as follows:

The size of the α value range is given by

highest α – lowest α = $0.953 - 0.794 = 0.159$ (from Table 6.6)

$15.4\% \text{ of } 0.159 = 0.0245$

$\Rightarrow$ α value corresponding to 15.4% significance $= 0.794 + 0.0245 = 0.818$

Therefore, the resistance for this component can be adjusted using Eq.5.2 as follows:

$$\text{new design yield strength} = \frac{F_c(151\ \text{N/mm}^2)\beta}{1.2\alpha} = \frac{1.0(151\text{N/mm}^2)(0.953)}{1.2(0.808)} = 147\ \text{N/mm}^2$$

Without this adjustment the component resistance would be: $\frac{151\text{N/mm}^2}{1.2} = 126\ \text{N/mm}^2$

Therefore, under the proposed method a non critical component has a higher design yield strength than under the current assessment method

The design safety margin of the component (i.e. member no. 23) is given by:

Design safety margin of member = adjusted design strength - stress in component

$= 147\text{N/mm}^2 - 42\text{N/mm}^2$

$= 105\ \text{N/mm}^2$

Without this adjustment in the design yield strength, the design safety margin of the component within the intact structure would be 126N/mm^2 - 42N/mm^2 = 84N/mm^2. Therefore, the proposed method provides a greater safety margin than the existing assessment method, in cases where members are non critical.

6.10 (e) Step 6 applied to the web members near the girder supports

The analysis results of Section 6.9(g) showed that the most stressed members in the structure are the diagonal web members near the supports, and that under the current assessment method some of these members exhibit limit state violation. The proposed assessment method, provides an adjusted component design yield strength, and in the case of non critical members provides a more accommodating limit state. In this section the significance of the diagonal web members in the region near the supports is determined by considering a group damage event consisting of the loss of members 24, 40, 27, and 28. The most acute consequence of this event, with regard to the bottom chord, is an increase in the bending moment in members 87 and 88 (which in reality are the same member). This member is used as a reference point on which to base the significance of the lost members.

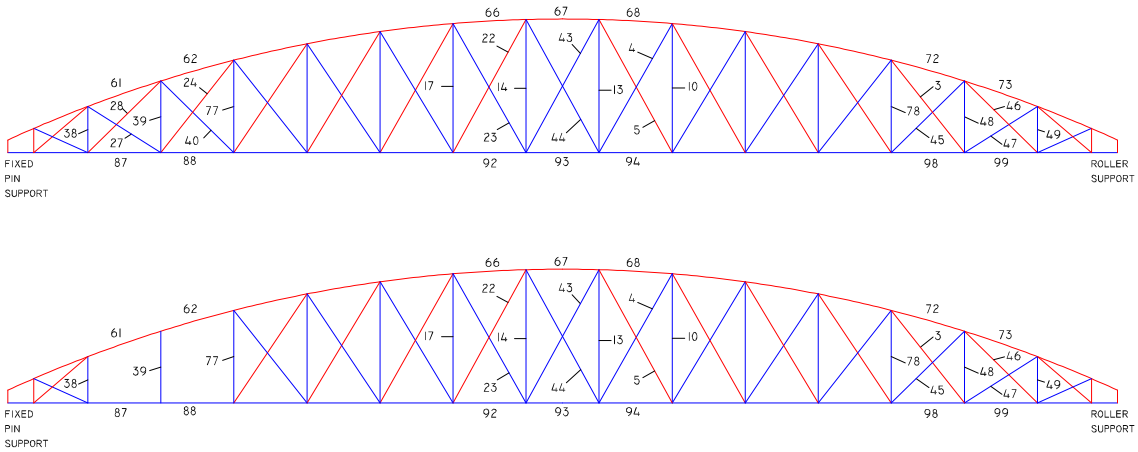

Figure 6.27 Group damage scenario used to determine significance of lost members. Member numbers are given.

The procedure for determination of component significance is the same as demonstrated in Section 6.11 (c). The results are summarised in Table 6.9.

Components removed	S_A of bottom chord (N/mm^2)	Local initial safety margin of bottom chord (N/mm^2)	Reduction in initial safety margin of chord (N/mm^2)	Significance of removed component %
Intact structure	54	133	---	---
24	61	126	7	5.3
24 + **40**	83	104	22	16.5
24 +40 +**28**	95	92	12	9.0
23 +40 +28 + **27**	215	0	92	69.2

Table 6.9 Significance of members within damaged structure

The analysis results summarised in Table 6.9 show that removal of all four diagonal members near the supports will result in an initial safety margin of zero in the bottom chord. This is limit state violation. Removal of the first three members, namely 24, 40 and 28 did not result in limit state violation. Therefore the structure can withstand the loss of these members but member no.27 is left as a critical member if this occurs. The final step in the proposed method is to calculate the adjusted design yield strengths of the components and their adjusted usage factors

6.10 (f) Steps 9 to 12: Calculation of adjusted component resistance and usage factor

The component design yield strengths, with and without the use of the α and β factors, are given in Table 6.10. In both methods reported in Table 6.10 the lower characteristic yield strength values, determined during this research project, (i.e. 151N/mm^2 for bar iron and 200 N/mm^2 for angle iron) were used. The 'Full Method' design yield strength uses the lower characteristic yield strength values in addition to the use of the α and β factors. Clearly the inclusion of the influence of component significance and ductility serves to increase the design yield strength and thus results in a lower usage factor for all components. None of the components considered were critical components on their own, so the proposed method has a noticeable effect in registering the components as safer than previously recorded.

Member	Significance of member %	α	Full Method design yield strength (N/mm^2)	Design yield strength without α or β (N/mm^2)	Full Method design safety margin of component (N/mm^2)	Full Method usage factor U	Usage factor without α or β U
43 bar	0.9	0.795	151	126	130	0.14	0.17
44 bar	0.9	0.795	151	126	123	0.19	0.23
13 angle	1.7	0.800	199	167	171	0.14	0.17
14 angle	1.7	0.800	199	167	169	0.15	0.18
22 bar	1.7	0.797	151	126	143	0.05	0.06
23 bar	15.4	0.818	147	126	105	0.29	0.33
17 angle	3.4	0.802	199	167	167	0.16	0.19
24 bar	5.3	0.802	149	126	buckled	**1.03**	**1.22**
40 bar	16.5	0.820	146	126	0	**1.44**	**1.67**
28 bar	9	0.808	148	126	buckled	**1.20**	**1.42**
27 bar	69.2	0.904	133	126	0	**1.39**	**1.46**

Table 6.10 Component design yield strengths with and without adjustment factors applied.

However, four of the components still register as violating the ultimate limit state. These components are the ones that were imagined to have been lost in Section 6.10 (e), in which it was determined that if all four of these members are lost the structure would be unsafe under the 40 tonne assessment loading. The reason why, these members register as over stressed under the proposed method, while under the current method they are not, is because the current method uses $220N/mm^2$ as the characteristic yield strength for wrought iron, whereas the proposed method uses yield strength values of $151N/mm^2$ and $200\ N/mm^2$ for bar iron and angle iron respectively.

If the proposed method retained the use of a general value of $220N/mm^2$ as the characteristic yield strength of wrought iron, while applying the α and β factors, the results in Table 6.13, under column heading 'Partial Method', would be achieved.

Following the same procedure as in sections 6.10 (c) and (e) the significance of components would be calculated as shown in Tables 6.11 and 6.12.

Components removed	S_A of bottom chord (N/mm^2)	Local initial safety margin of bottom chord (N/mm^2)	Reduction in initial safety margin of chord (N/mm^2)	Significance of removed component %
Intact structure	70	117	---	---
43 + 44	71	116	1	0.9
43 + 44 +**14** + **13**	73	114	2	1.7
43 + 44 +14 + 13 + **22**	75	112	2	1.7
43 + 44 +14 + 13 + 22 **+ 23**	93	94	18	15.4
43 + 44 +14 + 13 + 22 **+** 23 + **17**	97	90	4	3.4

Table 6.11 Significance of members involved in the group damage event depicted in Figure 6.26

Components removed	S_A of bottom chord (N/mm^2)	Local initial safety margin of bottom chord (N/mm^2)	Reduction in initial safety margin (N/mm^2)	Significance of removed component %
Intact structure	54	133	---	---
24	61	126	7	5.3
24 + **40**	83	104	22	16.5
24 +40 +**28**	95	92	12	9.0
23 +40 +28 + **27**	215	0	92	69.2

Table 6.12 Significance of members involved in the group damage event depicted in Figure 6.27

Member	Significance of member % And (α factor)	Partial method design yield strength (N/mm^2)	Full method design yield strength (N/mm^2)	Partial method usage factor U	Full method usage factor U	Current method usage factor U
43 bar	0.5 (0.795)	220	130	0.10	0.14	0.11
44 bar	0.5 (0.795)	220	130	0.13	0.19	0.16
13 angle	1.0 (0.799)	219	199	0.13	0.14	0.16
14 angle	1.0 (0.799)	219	199	0.14	0.15	0.16
22 bar	1.0 (0.796)	220	130	0.04	0.05	0.04
23 bar	9.6 (0.809)	216	127	0.20	0.29	0.23
17 angle	2.1 (0.800)	219	199	0.15	0.16	0.17
24 bar	3.7 (0.800)	218	129	0.71	**1.03**	0.84
40 bar	12 (0.813)	215	126	0.99	**1.44**	**1.15**
28 bar	6.4 (0.804)	217	128	0.82	**1.20**	0.97
27 bar	49 (0.872)	201	122	0.95	**1.39**	**1.00**

Table 6.13 Significance of members within damaged structure

In Table 6.13, 'Full Method' refers to the use of lower characteristic yield strength values of 151N/mm^2 and 200 N/mm^2, for bar iron and angle iron respectively, and includes the use of the α and β factors. 'Partial Method' refers to the use of 220 N/mm^2 as the characteristic yield strength for wrought iron and includes the use of the α and β factors. 'Current Method' refers to the use of 220 N/mm^2 as the characteristic yield strength for wrought iron and does not include the use of the α and β factors. The current method is that employed by BD21/01.

From Table 6.13 it can be seen that the partial application of the proposed method leads to the least conservative assessment method and registers the structure as completely safe under assessment loading. Yet its application ignores one of the main findings of this research project, which is that the characteristic yield strength of wrought iron is less than 220N/mm^2. Under the full application of the method the structures may be deemed unsafe because an excessive number of non critical components are over stressed, such that, collectively they lead to the overstressing of a critical member, namely the bottom chord. This conclusion was reached by simulating the loss of the four over stressed members. But in the intact truss the over stressed members will still function in carrying load. Some may buckle and some may deform plastically under assessment loading, but the tension members will still perform full load carry function. Thus the safety of the structure due to over stressing of some web members may not be as undermined as depicted in Figure 6.27.

Under the current method of assessment the over stressed members (i.e. no. 40 and 27) are allowed to remain in place without further strengthening. This is because these members are not considered significant and only two of them are overstressed. It would appear that sensible engineering judgment is applied after the usage factor results are obtained. The proposed method strives to incorporate sensible engineering judgement into the workings of the assessment by use of a measure of significance and quality. In doing so the usage factor results for the 'partial method' show that no members of Irwell Street Bridge are overstressed under modern assessment loading.

However, it is recommended not to ignore the conclusion from the data collected during this research about the lower characteristic yield strength of wrought iron. The limit state violation in the bottom chord, resulting from the hypothetical loss of the four over stressed diagonal members 24, 40, 28 and 27, consists of a tensile stress of 215N/mm^2 at the top edge of the trough shaped bottom chord in member no.87. It is possible that the plate iron of which the bottom chord is made is stronger than the characteristic value of 187N/mm^2,

and this explains the stability of the bridge. If not this, then it is possible that the bottom chord can accommodate some plastic deformation of its outer edge, with the bulk of the section remaining elastic. This may allow redistribution of stresses within the rigid frame such that the structure remains functional and safe. But it is most likely that limit state violation is avoided simply because the structure did not lose the diagonal members in question. They may be over stressed, but they are still functioning to their fullest capacity. In that case, analysis of the intact structure reveals that even though some of the diagonal members may be overstressed the greatest stress in the bottom chord at the location of member no. 87 is just $40N/mm^2$ (see Table 6.4) and thus the structure is quite safe.

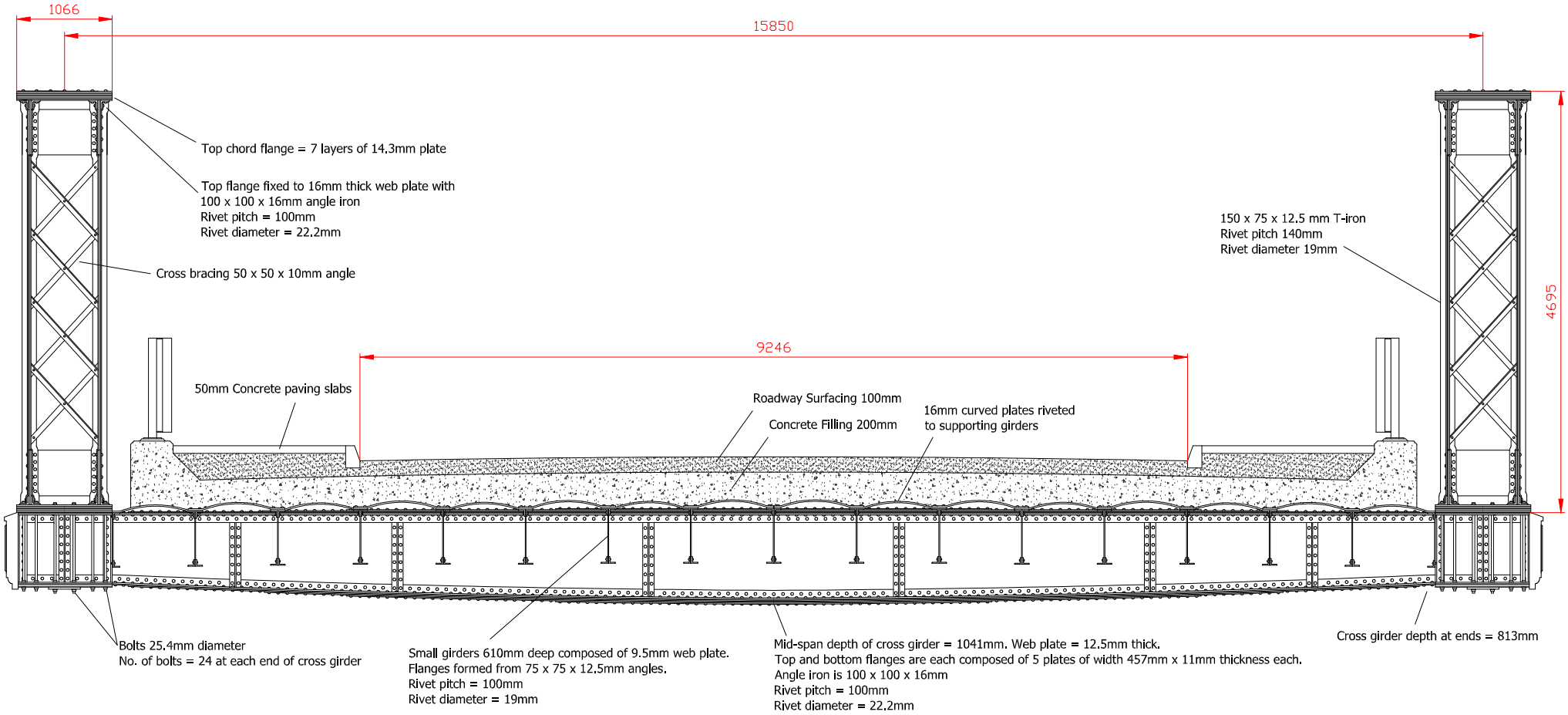

Figure 6.28 Cross section of Irwell Street Bridge. All dimensions in mm. (Drawing by M.O'Sullivan 2008)

Irwell Street Bridge, Manchester

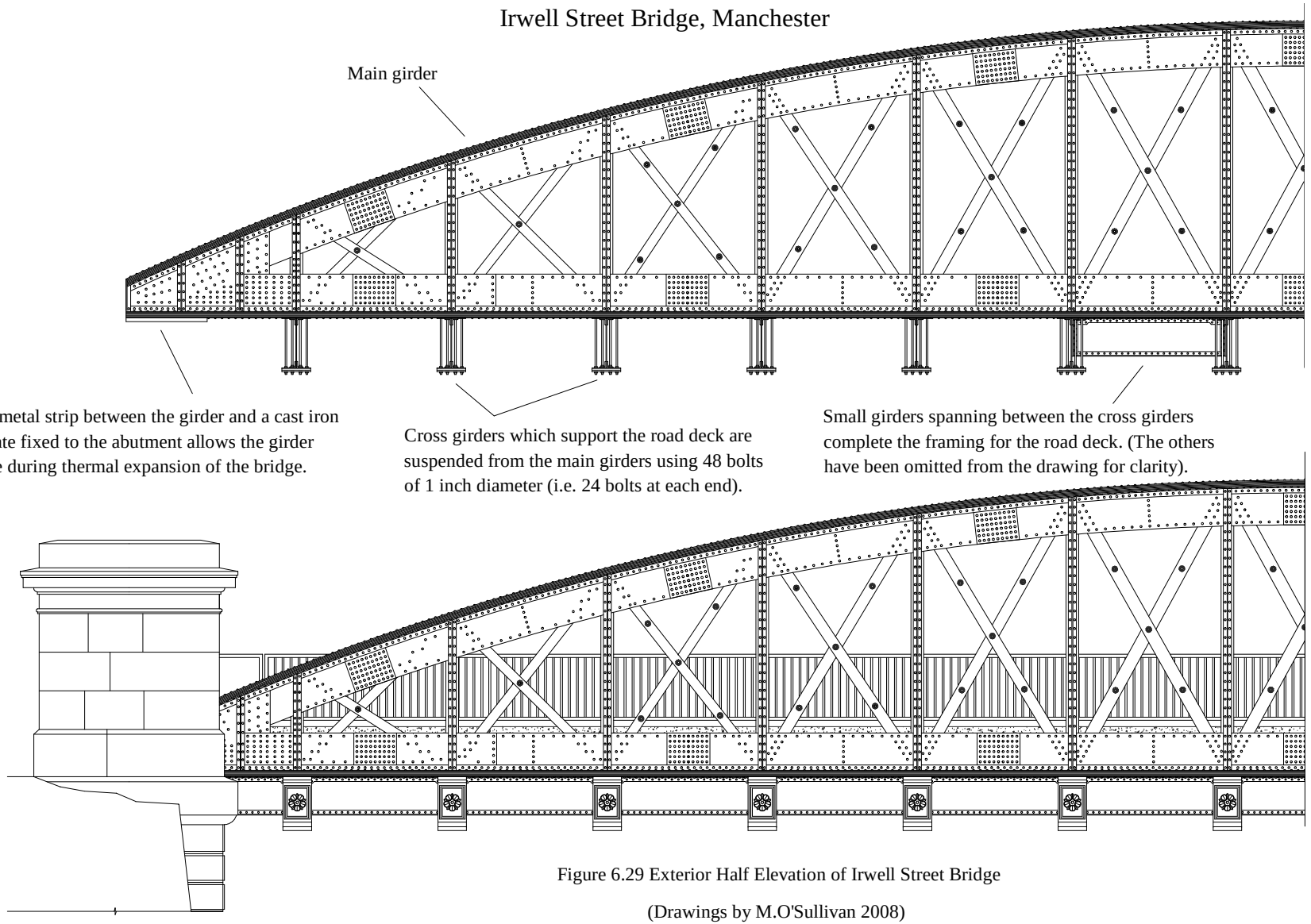

Figure 6.29 Exterior Half Elevation of Irwell Street Bridge

(Drawings by M.O'Sullivan 2008)

Chapter 7 Structural assessment of Clifton Suspension Bridge

7.1 Purpose and scope of assessment

In this Chapter the assessment method outlined in Chapter 5 is presented as an example of how the method may be applied to a suspension bridge. Clifton Suspension Bridge was chosen because it is a good example of a wrought iron eye-bar chain bridge that is still in use. For this example the assessment focuses on the most critical members, which are:

1 Chain eyebars,

2 Hanger rods

3 Deck stiffening girders.

The assessment method proposed in this report is concerned with adjusting the design strength of wrought iron components so that the quality of the metal and the significance of the components are taken into account. The first step in the proposed method is the structural analysis of the bridge. For initial analysis of the bridge, it was decided to use David Steinman's application of the flexibility method, as it provides a convenient way of calculating the stresses resulting from an understanding of the most adverse loading arrangement. Steinman's analysis employs derived algebraic formulas into which the user can substitute the bridge parameters of the particular structure being assessed. The parameter's of Clifton Suspension Bridge are listed in Section 7.4 and are illustrated in Figure 7.7. The basis of Steinman analysis is outlined in Section 7.5.

7.2 Historic background of Clifton Suspension Bridge

With the development of Bristol in the 18th century the desire grew among many of its financially successful citizens to live outside the city, in the nearby areas of Clifton and Leigh Wood. The Clifton and Leigh Wood areas which are situated on opposite sides of the spectacularly deep Avon Gorge required connection by some form of bridge. In 1753, wine merchant William Vick left £1000 in his will to the Society of Merchant Venturers for the purpose of being left to accumulate, by the addition of compound interest, to a some sufficient to fund the construction of a stone bridge. (Mitchell-Baker 1988). He had estimated that £10,000 should be enough, but, by 1829, the account had reached just £8,000, by which time it was clear that this account alone would never be enough to fund the construction of a bridge. (Mitchell-Baker 1988).

In 1830 an Act of Parliament granted permission for a toll bridge to be constructed of iron instead of stone. One of Isambard Kingdom Brunel's designs for a suspension bridge was chosen and work began in 1831. (Mitchell-Baker 1988). The work advanced very slowly, but the pace quickened with the arrival of the Great Western Railway. (Mitchell-Baker 1988). However, by 1843 with the bridge towers almost complete the construction funds had been completely depleted, and so, all work ceased. (Mitchell-Baker 1988). The iron work that had already been purchased was sold in 1851 to pay the contractors and was used to construct the Royal Albert Bridge. (Mitchell-Baker 1988). The construction of the Clifton Suspension Bridge was officially abandoned in May 1853.

When Brunel died in 1858 a number of leading engineers at the Institution of Civil Engineers proposed that the Clifton Suspension Bridge should be completed in honour of Brunel. Also, at that time, the Charing Cross Railway was under construction with John Hawkshaw as lead engineer. As part of that project it was decided to replace the Hungerford Suspension Bridge, which had been designed by Brunel, with a girder bridge. (Barlow 1867). Thus the opportunity arose for the acquisition of ready made eye-bar chain links at a relatively low cost. A company was formed for the completion of the Clifton

Suspension Bridge for which William Barlow and John Hawkshaw were appointed as joint principal engineers, and a Act of Parliament was obtained in 1861 for the resumption of work. (Barlow 1867). The contractors, Cochrane Grove of Dudley (who were also the contractors for the new Hungerford, or Charing Cross Bridge, previously mentioned) began work in November 1862, and the bridge was completed and opened to traffic in 1864. (Barlow 1867).

Figure 7.1 Clifton Suspension Bridge (photo obtained from http://devonvisitor.blogspot.com accessed 2012)

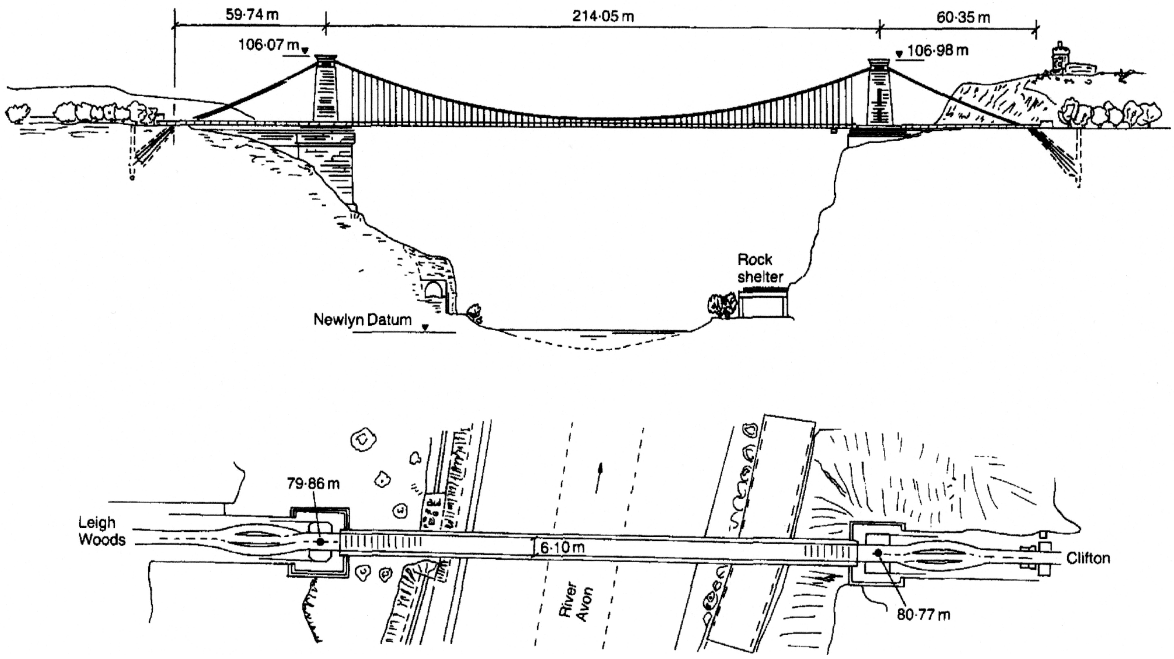

Figure 7.2 Plan and elevation of Clifton Suspension Bridge (Mitchell-Baker 1988)

7.3 Description of bridge

Eyebar chains and hanger rods

Brunel's design for the Clifton Suspension Bridge had to be altered to make it compatible with the Hungerford eye-bars. In his original design only two rows of chains, one above the other, were to support each side of the bridge. In the new design there were to be three rows of chains, one above the other, as shown in Figure 7.3. New eye-bars had to be made to supplement those from the Hungerford Bridge. (Barlow 1867).

Figure 7.3 Clifton Suspension Bridge (photo source: commons.wikimedia.org accessed 2012)

The hangers supporting the deck are connected to the chains via the linking pins of the eye-bars. The joints in each chain are staggered relative to those in the chains above or below, such that one hanger is supported by each chain link connection, and the hangers are all spaced 8ft apart. At each chain link connection 10 eyebars in one chain segment are interleaved with 11 eyebars in the other chain segment, except at the towers where there are 12 eyebars in the chain. All eyebars are 7 inches wide and 1 inch thick. The eyebars

near mid-span are 24ft long but the other eyebars increase in length toward the towers. (Barlow 1867). The eyebar chain links and the hanger rods were made by hammer welding (i.e. forge welding) eyes to the ends of their shafts. (Cullimore 1988).

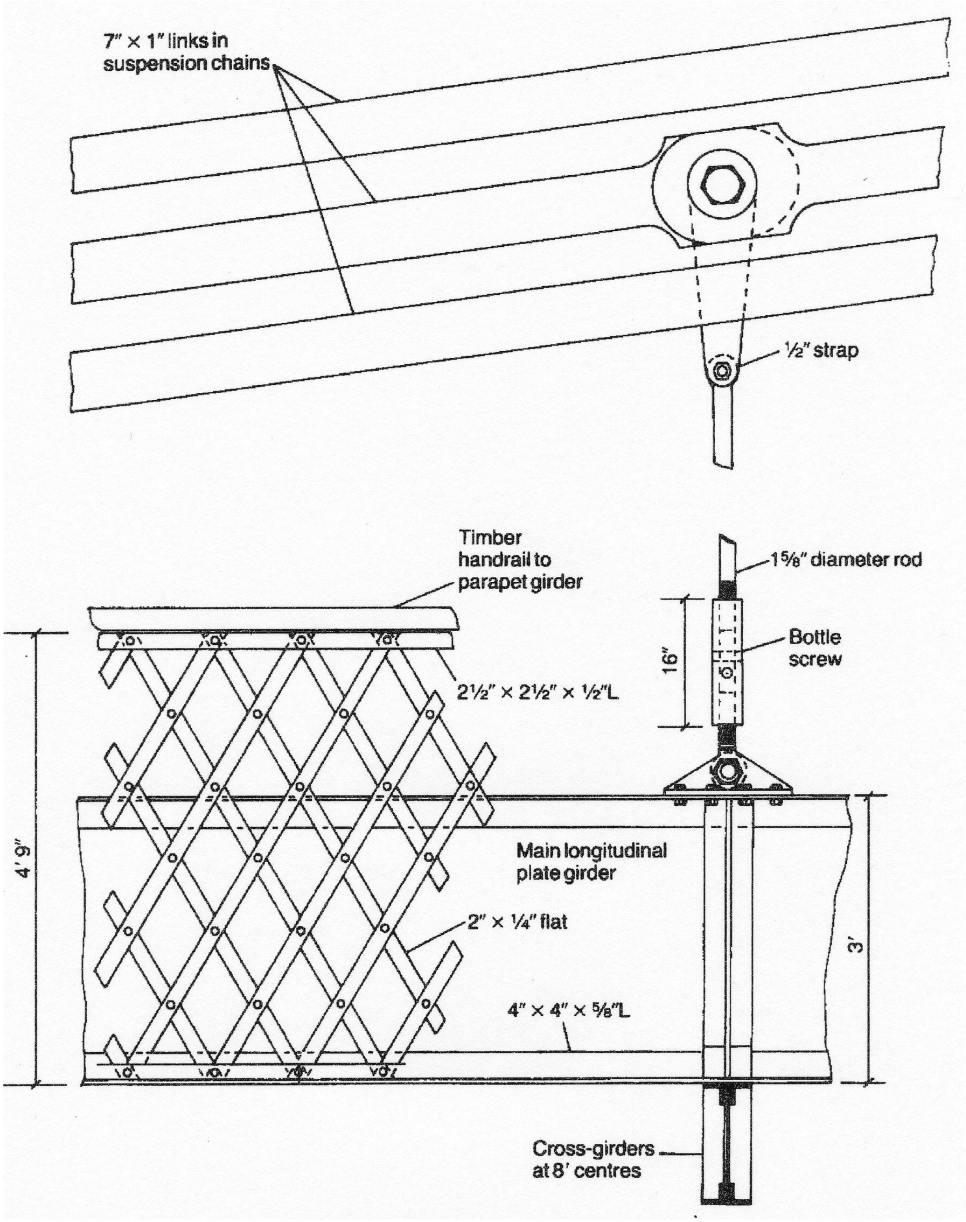

Figure 7.4 side elevation of chains, hanger rod, stiffening girder and parapet girder (Mitchell-Baker1988)

The hanger rods also have a turnbuckle (labelled "bottle screw" in Figure 7.4) near their lower end to allow adjustment in length. The details of the hanger rod connection to the longitudinal girder are shown in Figure 7.5. In 1923 three hanger rods were removed for testing. One complete rod was tested to destruction at Kirkaldy's Testing Works at Southwark Street, London, where it was determined that the weld between the head and

shaft had an efficiency of 86%. (Mitchell-Baker 1988). Machined specimens from the other rods gave an ultimate tensile strength of 22.3 ton/in^2 (344 N/mm^2) with an elongation at failure of 13%. (Mitchell-Baker 1988). More recent tests on samples from these rods gave an ultimate tensile strength of 343 N/mm^2 and elongation at failure of 11% for material from the weld, and a ultimate tensile strength of 366 N/mm^2 and elongation at failure of 30.5% for material from the non-welded region of the rod. (Cullimore 1988). According to Barlow the maximum working stress of the hanger rods would be 4.25 ton/in^2 (66 N/mm^2). (Barlow 1867). The hanger rods bear the mark of the Round Oak Ironworks. (Cullimore 1988).

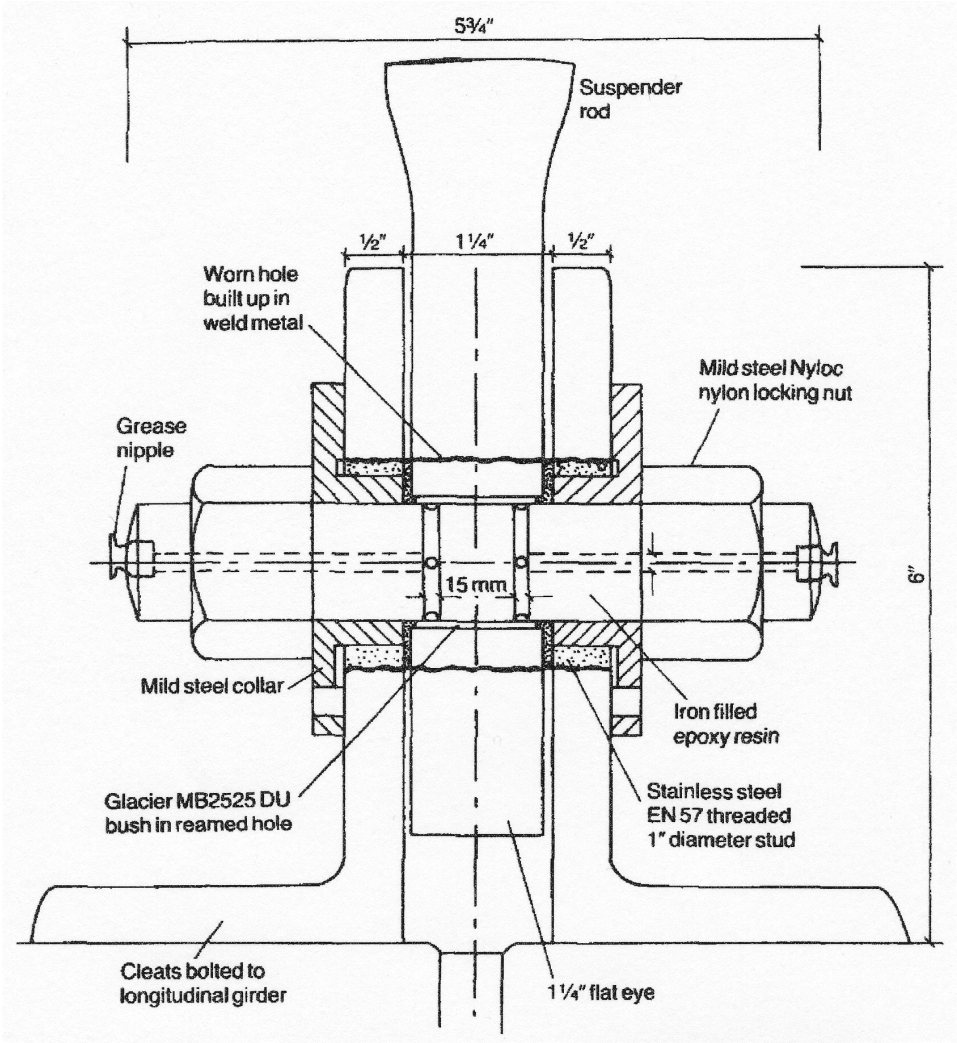

Figure 7.5 Bolt assembly at connection of hanger rod to longitudinal girder. This connection has undergone modern modification involving nylon and mild steel components, which were not part of the original structure. (Mitchell-Baker 1988)

In 1838 Brunel had designed the chains of the proposed bridge to carry a maximum working stress of 5 ton/in^2 (77 N/mm^2). (Porter 1974). All of the eyebars in the Hungerford

Bridge had been tested to a stress of 10 ton/in^2 (155 N/mm^2) prior to use in that bridge and all of the new eyebars needed for the Clifton Suspension Bridge were also proof tested to this stress level. (Barlow 1867). Barlow estimated that the maximum working stress in the chains would be 4.76 ton/in^2 (74 N/mm^2). (Barlow 1867). The diameter of the eye-bar linking pins is 4.625in (117mm).

Figure 7.6 Land side chains of Clifton Suspension Bridge (photo source: bristol.cityseekr.com accessed 2012)

7.4 Bridge dimensions

The main dimensions of the bridge are given in Figure 7.7 and are described as follows:

Distance centre-to-centre of towers: l' = 214.05m

Span of stiffening girder: l =195m

Height of each tower above level of stiffening girder = 25m

Angle of depression of chord AB joining tops of towers: $\alpha = 0.24^o$

Angle of depression of main span stiffening girder: $\alpha = 0.24^o$

Angle of depression of straight land side chains: $\alpha_1 = 22.6^o$

Horizontal distance from tower centre to land saddle: l_1 = 60m

Length of chain from land saddle to anchorage = 25.8m

Effective horizontal distance from tower to anchorage: l_2 = 93.34m.

Transverse distance centre to centre of chains = 20ft (6.1m)

Width of bridge including roadway and footpath = 31ft (9.5m)

Second moment of area of stiffening girder: I = 3362 x 10^6 mm^4 (= 3362 x 10^{-6} m^4).

Chain sag measured over length of stiffening girder (i.e. mid-span sag of main span chain measured from chord AB): f = 17.76m

Total chain sag: f_t = 21.405m, which makes the total sag to total span ratio:

f_t / l' = 21.405/214.05 = 1/10 = 0.1.

Total cross sectional area of triple chain arrangement: A = 135636mm^2 (= 0.135636 m^2)
This is the combined cross sectional area of 30 eyebars, each of cross sectional dimensions 7in x 1in.

For the purpose of the structural analysis the above quantities and designations will be used. An exaggerated labelled structural diagram of the bridge is shown in Figure 7.7, which illustrates the meaning of each term.

Although the towers are the same height above their respective abutments they are not level with each other. (Barlow 1867). The tower on the Clifton side of the bridge is 3 feet higher than that on the Leigh Wood side and the entire bridge has an average inclination of 1 in 233, hence the inclusion of the angle $\alpha = 0.24^o$ described above. (Barlow 1867).

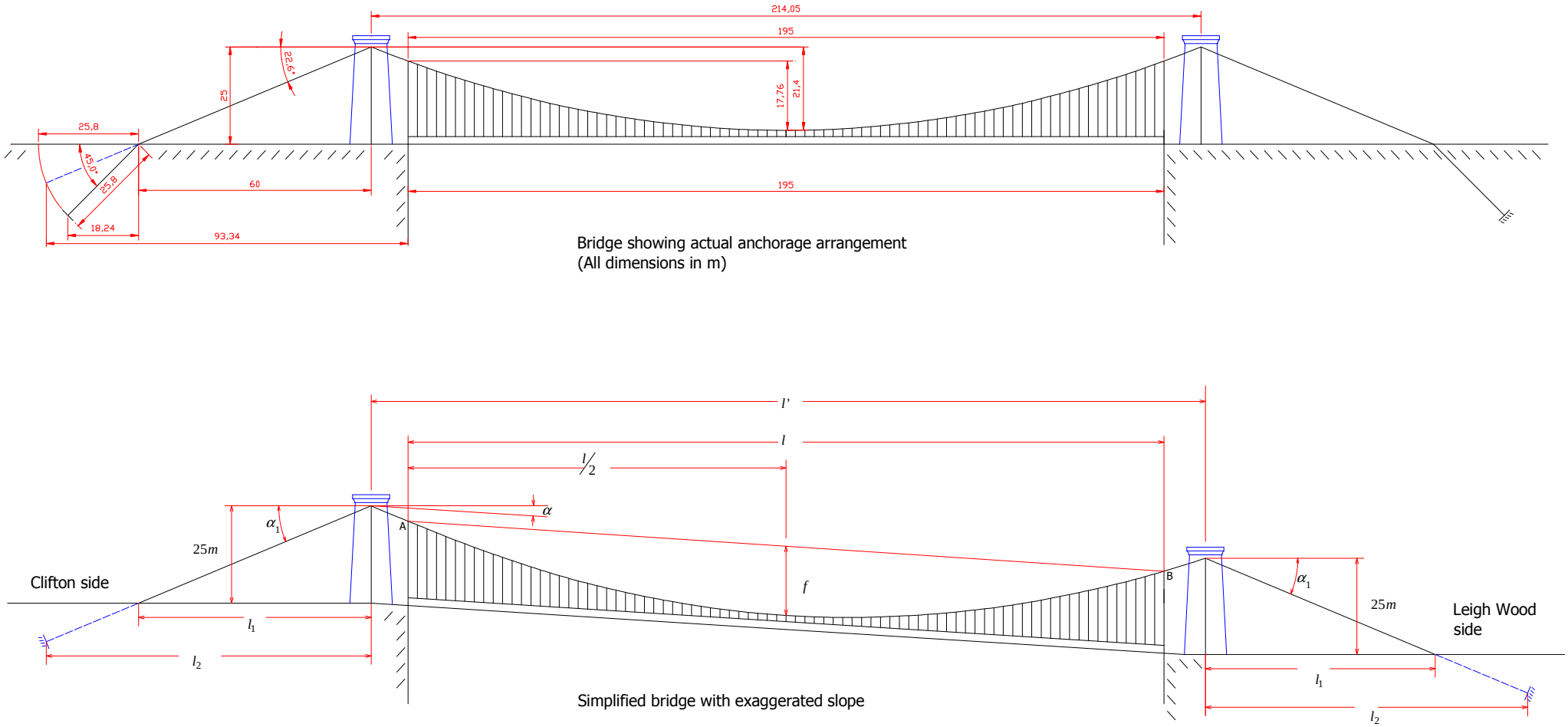

Figure 7.7 Simplified diagrams of Clifton Suspension Bridge

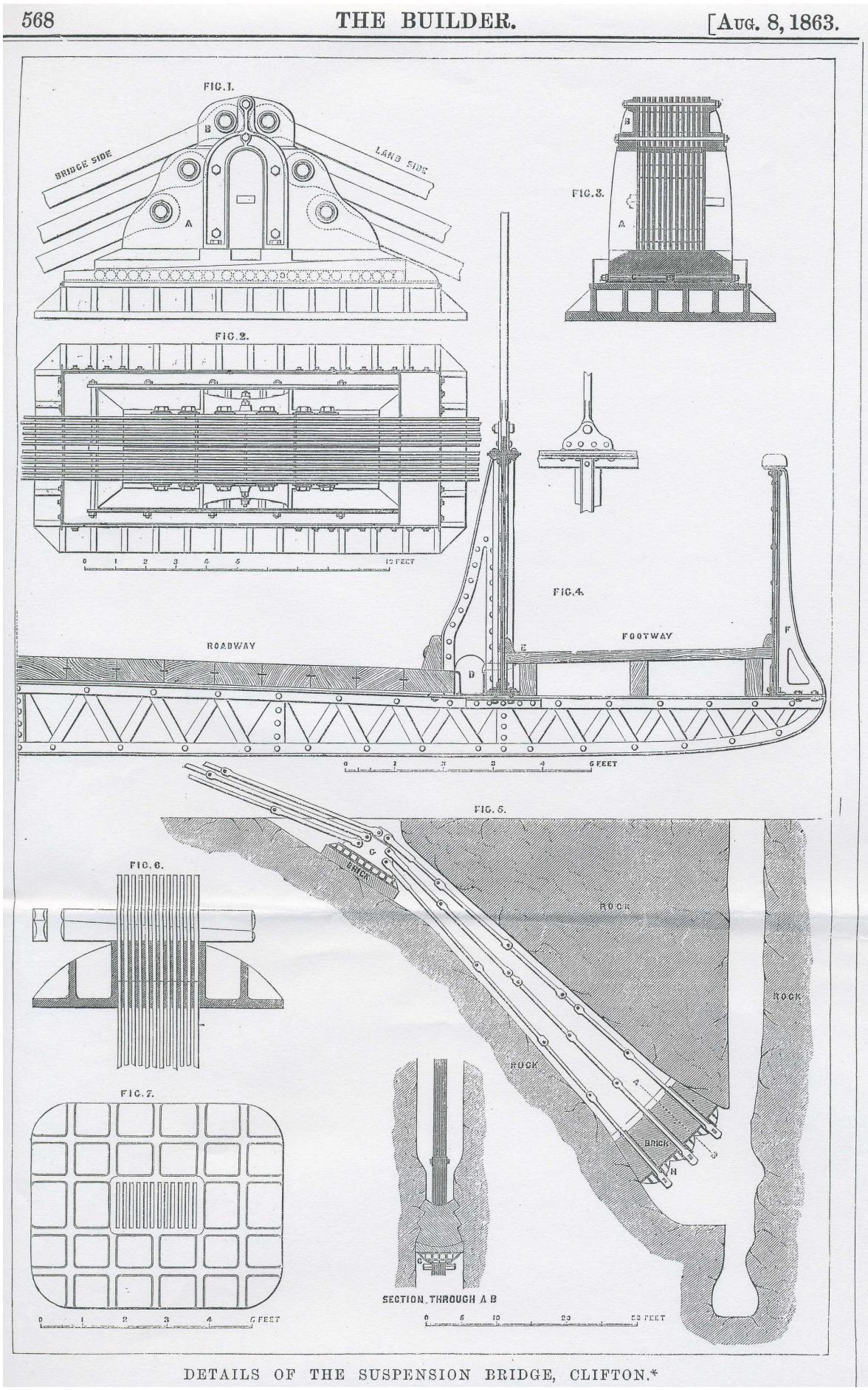

DETAILS OF THE SUSPENSION BRIDGE, CLIFTON.*

Figure 7.8 Details of Clifton Suspension Bridge (The Builder 1863)

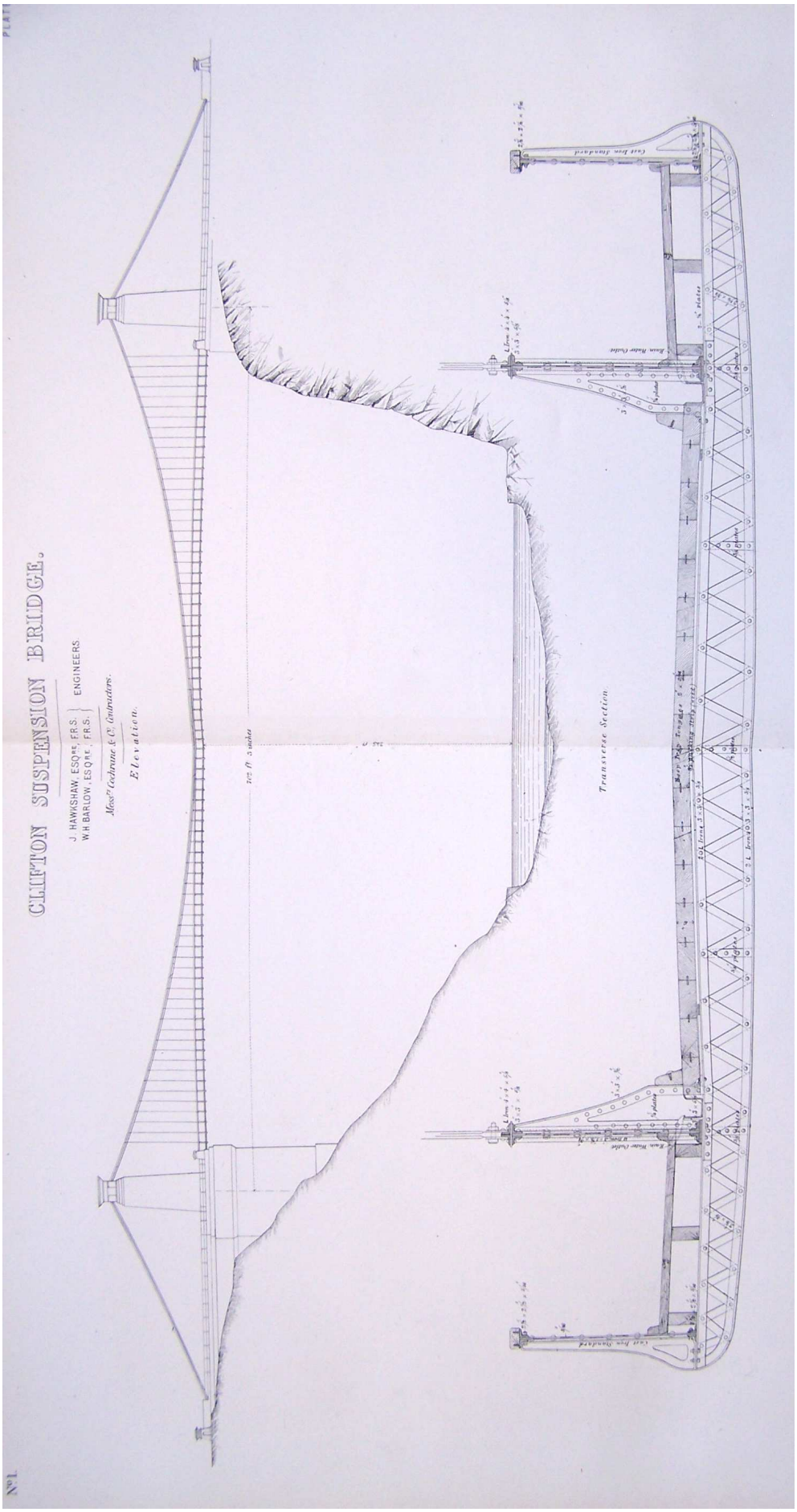

Figure 7.9 Clifton Suspension Bridge (Humber 1870)

7.5 Outline of structural analysis of Clifton Suspension Bridge

In this section the background to Steinman's analysis of this structural form is summarised and the particular formulas required for the calculation of component stresses identified. This method of analysis is algebraic and in order to make it mathematically workable by hand some simplifications have been made. Firstly, the flexural stiffness of the bridge is due in part to a 3ft deep longitudinal girder, but also due to a 4ft. 9in. deep lattice parapet girder. In the analysis any stiffening effect from the lattice girder was ignored. Thus mention of the stiffening girder refers only to the 3ft deep longitudinal girder.

Secondly, the analysis is conducted as if the three chains were in fact one chain, and this single chain is assumed to have complete flexibility as if it was a cable. Therefore, in the analysis, reference is made to the cable rather than the actual triple chain arrangement. The stress in one of the real chains is taken as one third the calculated cable stress.

The objective of this analysis is to determine the tension force in the cable and the bending moment in the stiffening girder, in addition to the force in the hanger rods. An examination of the most adverse arrangement of live load is also conducted. In this type of bridge the stiffening girder is modelled as being connected to the abutments by pins at each end. This is compatible with the actual fixity of the bridge deck. The structure is statically indeterminate to degree 1, and in the analysis, the flexibility method is used to determine the horizontal component H of the tension in the cable. In this analysis H is called the horizontal cable tension. To reduce the structure to a statically determinate form, a cut is placed in the cable at the lowest point, where the tension in the cable, in the indeterminate structure is H. With load applied to the bridge, this will result in the cut ends of the cable moving apart by a distance Δ. This is case 0, shown in Figure 7.10 (a), and in this case H = 0. If a unit horizontal force is applied to the cut ends, without load on the bridge, as shown in Figure 7.10(b), the cut ends will be pulled together by a small distance δ. Since δ results

from a unit force the total horizontal force needed to bring the two cut ends together again is H and is given by Eq.7.1

$$\delta H = \Delta$$

$$\Rightarrow \quad H = \frac{\Delta}{\delta} \qquad \text{Eq.7.1}$$

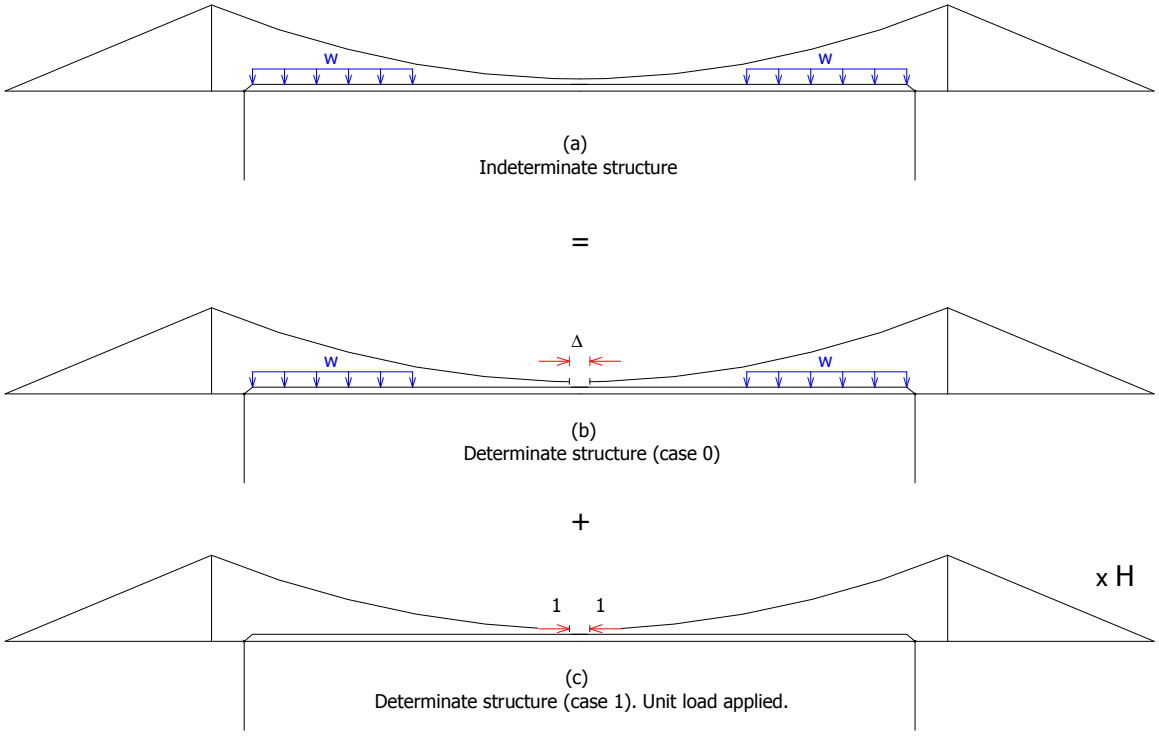

Figure 7.10 Indeterminate and determinate structural cases considered in flexibility method analysis.

Both virtual displacements, Δ and δ, may be determined by the general expressions for displacement of a point in an elastic system, as given in Eq.7.2. The stiffening girder is thought of as a beam member in this system.

$$H = \frac{\Delta}{\delta} = -\frac{\int \frac{M_s\, m}{EI} dx}{\int \frac{m^2}{EI} dx + \int \frac{t^2}{E_c A} ds} \qquad \text{Eq.7.2 (Steinman 1922)}$$

where,

M_s = bending moment in the stiffening girder under applied load, (case 0 , H = 0).

m = bending moment in the stiffening girder with unit load only applied, (case 1 , H = 1).

t = axial force in the cable, towers and hangers with unit load only applied, (case 1).

I = second moment of area of the stiffening girder.

A = cross sectional areas of the cables, towers and hangers.

E_c = modulus of elasticity for cable and E = modulus of elasticity for stiffening girder.

In the numerator of Eq.7.2 there is no axial force term because this represents the displacement Δ of the determinate structure (case 0), in which the horizontal cable tension H = 0, and all of the axial forces in the cables, towers and hangers are zero. In this case the stiffening girder carries the entire applied load as a simply supported beam.

In the denominator of Eq.7.2 both bending moment and axial force terms are present because in this case (i.e. case 1), the system contains members which carry both types of action, namely, the axial force in the cable (resulting from the applied unit tension) and the consequently present axial forces in the hangers and towers, in addition to the bending moment induced in the stiffening girder.

Further to those assumptions already mentioned the following assumptions will also apply.

1 "The cable is considered to be perfectly flexible and will assume the shape of the equilibrium polygon due to the hanger forces (see Figure A2.2).

2 The stiffening girder is modelled as a straight beam with constant second moment of area and connected to the cable uniformly throughout its length.

3 The dead load of the girder and cable is assumed uniform per unit horizontal length, so that the initial curve of the cable is a parabola (see section A2.4)

4 The form and position of the cable curve remain unaltered upon application of live load.

5 The dead load is carried entirely by the cable and causes no stress in the stiffening girder. The girder is stressed only by live load."(Steinman 1922)

The assumption that the form and position of the cable is unaltered upon application of live load is not true as shown by tests conducted on the Clifton Suspension Bridge (see Cullimore 1988). However,"in terms of the stresses within the components, the assumption of fixed cable shape is sufficiently accurate for an initial assessment analysis and it can be shown that with this assumption the calculated stresses are somewhat greater, and thus on the side of safety." (Steinman 1922)

7.6 Loading of Clifton Suspension Bridge: Numerical example

The preceding section of this chapter dealt with the theoretical background of the structural analysis of a suspension bridge form matching that of Clifton Suspension Bridge. In this section the numerical parameters of Clifton Suspension Bridge are substituted into the equations previously derived to obtain the required bending moments and forces under particular load conditions.

7.6 (a) Most adverse live load arrangement on bridge

Following an assessment carried out on the Clifton Suspension Bridge in 1953 the overall maximum load limit of 28tons (280kN), which has been in place since the bridge was opened, was maintained, and is the present day maximum overall load allowed.

For this example, the value of 28tons (280kN), is used as the total unfactored live load, which is applied as a distributed load to the bridge. The maximum bending moment in the stiffening girder is obtained by placing the distributed load over critical portions of the span. Therefore, to obtain the value of distributed load, based on a total load of 28 tons, the length of girder to be loaded may be taken from Eq.7.105, which gives the position of the critical point for maximum bending moment, as expressed by Eq.7.3.

$$M_{+} = \frac{wl}{2}\left(2k - k^2\right)x - \frac{w}{2}x^2 - \frac{wl}{10Nn}\left[2k^5 - 5k^4 + 5k^2\right]y \qquad \text{Eq.7.3 (Steinman 1922)}$$

where $$k + k^2 - k^3 = \frac{Nnx}{y} \qquad \text{Eq.7.4 (Steinman 1922)}$$

Eq.7.3 gives the positive (i.e. sagging) bending moment at any section x for a uniform load extending from x = 0 to $x = kl$ where k is given by Eq.7.4 and

$$0 \le x \le \frac{Nl}{4} \quad \text{(Steinman 1922)}$$

A diagram showing the maximum bending moments in the stiffening girder, is shown in Figure 7.12, and indicates that the maximum bending moment occurs at section x = 45m. At this section the value of k from Eq.4.105 is k = 0.42, which means that the maximum

positive bending moment is obtained by loading from x = 0 to x = 0.42(195m) = 82m. With this length of girder covered by a total live load of 14tons (140kN), (i.e. half the total load is carried by each girder), the assessment live distributed load is:

$$w = \gamma_{fl} \times \frac{140kN}{82m} = 1.5 \times 1.7 \text{ kN/m} = 2.6 \text{ kN/m} \qquad \text{(assessment live load per girder)}$$

7.6 (b) Dead load on bridge

Total weight of all chains on one side of bridge = 277 imperial tons = 2770kN.

Weight of entire suspended structure (i.e. everything except the chains) = 440 imperial tons = 4400kN. Therefore the total unfactored dead load per cable is given by:

$$\text{Dead load per chain: } p = \frac{2770kN + 2200kN}{\text{distance between towers c/c}} = \frac{2770kN + 2200kN}{214.05m} = 23.2 \text{ kN/m}$$

The design dead load per cable is: γ_{fl} (23.2 kN/m) = 1.05 (23.2 kN/m) = 24.4 kN/m

7.6 (c) Numerical bridge parameters:

From Section 7.4 the bridge parameters are:

l =195m, l_2 =93.34m, f = 17.76m, f_t = 21.405m, l' = 214.05m, $\alpha = 0.24^o$, $\alpha_1 = 24.32^o$,

$A = 0.135636 \text{ m}^2$, $I = 3362 \times 10^{-6} \text{ m}^4 = 3362 \times 10^6 \text{ mm}^4$, $n_t = f_t / l' = 0.1$,

$n = f / l = 0.0911$

where A is the cross sectional area of the cable and I is the second moment of area of the stiffening girder.

$$N = \frac{8}{5} + \frac{3EIl'}{f^2 l E_c A}\left(1 + 8n_t^2 + \frac{3}{2}\tan^2\alpha\right) + \frac{6EIl_2 \sec^3\alpha_1}{f^2 l E_c A_1} \qquad \text{Eq.7.5 (Steinman 1922)}$$

$$\Rightarrow \qquad N = 1.6 \, m^3$$

7.6 (d) Horizontal cable tension

The design horizontal cable tension due to dead load only is given by Eq.7.8.

$$H_d = \frac{pl'^2}{8 f_t} \qquad \text{Eq.7.8 (Steinman 1922))}$$

$$\Rightarrow \qquad H_d = \frac{(24.4 \, kN/m)(214.05m)^2}{8(21.405m)} = 6529kN$$

The horizontal cable tension due to live load is given by Eq.7.9.

$$H = \frac{wl}{10Nn}\left[\left(2k^5 - 5k^4 + 5k^2\right) - \left(2j^5 - 5j^4 + 5j^2\right)\right] \qquad \text{Eq.7.9 (Steinman 1922)}$$

The design live load is w = 2.6 kN/m acting over the first 82m of the span, such that in Figure 7.11 j = 0 and k = 0.42, and the horizontal cable tension due to design live load only is: H = 261.7 kN.

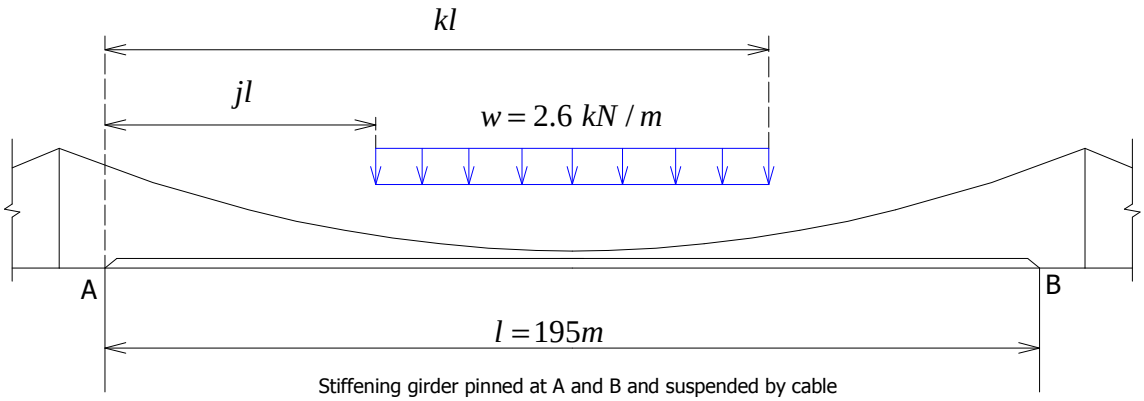

Figure 7.11 Loading of bridge to determine horizontal cable tension due to maximum live load.

Therefore, the total design horizontal cable tension is:

$$H_{total} = H_d + H = 6529kN + 262kN = 6791\ kN$$

7.6 (e) Stress in main span chains

The maximum force in the main span portion of the chains occurs at their connection to the tower saddle. However, at this point there are 12 eyebars in each chain segment, such that the tensile stress there is not the maximum value in the chain. The maximum stress in the chain occurs at a distance of 10m from the tower saddle where each chain is composed of just 10 eyebars, (i.e. at x = 10m). At this point the force in the cable is given by Eq.7.10.

$$T = H\sqrt{\left(-\frac{8f}{l^2}x + \frac{4f}{l} + \tan\alpha\right)^2 + 1} \qquad \text{Eq.7.10 (Steinman 1922)}$$

$$\Rightarrow \qquad T = 6791kN\sqrt{\left(-\frac{8(17.76m)}{(195m)^2}(10m) + \frac{4(17.76m)}{195m} + \tan 0.24^o\right)^2 + 1} \qquad = \qquad 7154kN$$

This is the force in the imaginary cable, resulting in the maximum stress, where the chain is composed of 30 eyebars, (10 eyebars per chain), with a total cross sectional area of 135636mm^2, giving a tensile stress of:

$$\sigma_{\max} = \frac{7154 \text{ x } 10^3 N}{135636 mm^2} = 53\ N/mm^2$$ (maximum stress in main span iron chain of bridge)

This is the maximum stress in a single eyebar in one of the chains. The chains are in good condition, so a condition factor of 1.0 is applied. For assessment purposes the maximum stress in the chains is given by:

$S_A^* = \gamma_{f3}\ (\sigma_{\max})$ = 1.1 (53 N/mm^2) = 58 N/mm^2 (BD 21/01 cl.3.7)

This value is used later for comparison with the design strength of the eyebars.

7.6 (f) Stress in land side chains

The tension in the land side cable is: $T_1 = \frac{H}{\cos\alpha_1} = \frac{6791kN}{\cos(24.32^o)} = 7452kN$

which produces a tensile stress of: $\sigma_1 = \frac{7452 \text{ x } 10^3 N}{135636 mm^2} = 55 N/mm^2$

For assessment purposes the maximum stress in the land side chains is given by:

$S_A^* = \gamma_{f3}\ (\sigma_{\max})$ = 1.1 (55 N/mm^2) = 61 N/mm^2 (BD 21/01 cl.3.7)

7.6 (g) Bending moment in the stiffening girder

If the bridge carries a uniform load along its entire length the bending moment in the stiffening girder is given by Eq.7.11.

$$M = \frac{w}{2}\left(-x^2 + lx\right)\left(1 - \frac{8}{5N}\right)$$ Eq.7.11 (Steinman 1922)

$$\Rightarrow \quad M = \frac{w}{2}\left(-x^2 + lx\right)(0.00036)$$ (bending moment under full uniform load)

Eq.7.11 shows that only 0.036% of the full span live load is carried by the stiffening girder. In other words, very little bending moment is induced in the stiffening girder under a

uniform live load covering the entire span, because the chains have a funicular form that relieves the stiffening girder of bending moment.

As stated at the beginning of this section, the maximum bending moment in the stiffening girder occurs when a portion of the span is covered by load. The maximum possible bending moment in the stiffening girder for every position along the span is shown in Figure 7.12(b). The values in Figure 7.12(b) were calculated using Eq.7.110. From Figure 7.12(b) the maximum bending moment is 1638 kNm and occurs at x = 45m when the load covers the span from x = 0 to x = 0.42(195m) = 82m. The bending moment diagram of Figure 7.12 (c) indicates that as load is brought onto the bridge from one side, the loaded region would tend to sag, but the far side of the stiffening girder would tend to rise up (i.e. hog). Partial loading in this manner causes the greatest bending moment in the stiffening girder.

The maximum bending stress in the stiffening girder is given by the flexure formula as follows:

$$\sigma_{\max} = \frac{My_{\max}}{I} = \frac{(1638 \text{ x } 10^6\, Nmm)(457mm)}{3368 \text{ x } 10^6\, mm^4} = 222 N/mm^2$$

The loading arrangement which produces this maximum bending stress is shown in Figure 7.12(a). This computation has ignored the presence of the parapet lattice girder and assumes that all of the 1638 kNm bending moment is carried by the 3ft deep plate-and-angle stiffening girder. Given that the characteristic yield strength for wrought iron as stated in BD21 is 220 N/mm^2 it is clear that under a load of 28 tonnes the stiffening girder is already at limit state violation. The obvious action that should be taken is to specify a lower load limit for the bridge. This is discussed further in Section 7.6(J).

It is clear that the stress in the chains is well within safe limits but for the stiffening girder it is not. This is because of the very shallow depth of the stiffening girder. In modern suspension bridges the deck is stiffened by a deep truss, but the early wrought iron suspension bridges often simply relied on a relatively shallow plate girder for deck rigidity.

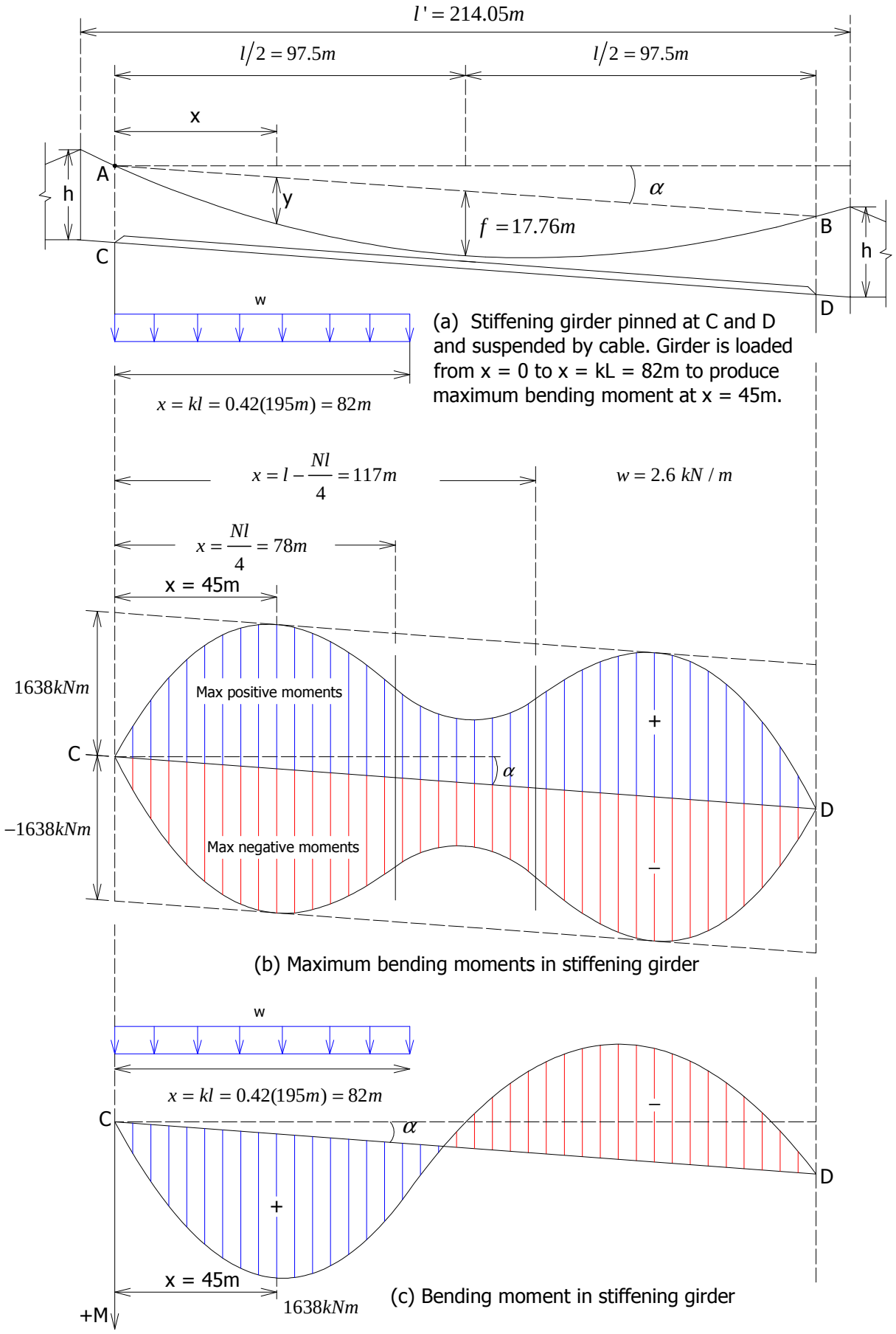

Figure 7.12 (a) Load arrangement causing maximum bending moment in stiffening girder.

α

7.6 (h) Stresses in hanger rods.

The dead load of the intact bridge is assumed to be uniformly distributed horizontally, so that the initial cable curve is parabolic. It is assumed that the dead load is carried entirely by the cable and causes no stress in the stiffening girder. According to Steinman's analysis it is assumed that the stiffening girder has sufficient flexural rigidity that it will transfer any live load that comes upon it, uniformly to the cable via the hangers, which are uniformly spaced horizontally. With a sufficient number of hangers they will effectively exert a uniform load on the cable. Thus even when live load comes upon the bridge the cable remains parabolic and the girder is stressed only by live load, as stated in Section 7.1. In reality this is not true, but these simplifying assumptions provide a means of estimating the stresses in the hanger rods..

The only loads which cause tension in the hanger rods are the dead load of the suspended structure and the live load on the bridge. The weight of the entire suspended structure (i.e. everything except the chains) = 440 imperial tons = 4400kN. Therefore, the total dead load pulling on the hanger rods on one side of the bridge is 2200kN, which as a uniformly distributed design load over the entire span is:

$$\text{Design dead load pulling on hangers} = \gamma_{fl} \times \frac{2200\text{kN}}{195\text{m}} = 1.05 \times \frac{2200\text{kN}}{195\text{m}} = 11.8 \text{ kN/m}$$

The design live load on the bridge is 2.6kN/m acting over the first 82m of the bridge. As shown earlier this value was obtained by considering a total unfactored live load of 140kN. Under the simplifying assumption that the live load is transferred from the stiffening girder uniformly to the hanger rods the equivalent uniform design live load pulling on the hanger rods is:

$$\text{Design live load pulling on hangers} = \gamma_{fl} \times \frac{140 \text{ kN}}{195\text{m}} = 1.5 \times \frac{140\text{kN}}{195\text{m}} = 1.08 \text{ kN/m}$$

Total design load on hanger rods = w_h = 11.8 kN/m + 1.08 kN/m = 12.9 kN/m

If the hanger forces (denoted by F_h) are uniformly spaced distance d apart, they are given by

$$F_h = w_h d = (12.9kN/m)(2.438m) = 31.5kN \qquad (d = 8 \text{ feet} = 2.438\text{m.})$$

The diameter of the hanger rods is $1\frac{5}{8}$ inches = 41.3mm.

Therefore the stress in the hanger rods is $\dfrac{31.5 \times 10^3 N}{\left(\dfrac{\pi(41.3mm)^2}{4}\right)} = 24N/mm^2$

In reality the chains will move slightly in response to load coming onto the bridge, and so the hanger rod stresses will fluctuate somewhat as this happens. In order to obtain a more realistic estimate of the hanger stresses a computer analysis must be performed.

7.7 (a) Application of proposed assessment method to Clifton Suspension Bridge

Of the overall proposed assessment method described in Chapter 5, the branch which applies to the bridge chains is outlined in Figure 7.13. Clifton suspension bridge is a two hinged stiffened suspension bridge and is thus statically indeterminate. According to the procedure outline shown in Figure 7.13, the first three steps have been completed, and the fourth step is to choose a member to assess. The chain eyebars will be assessed first. The stresses in the main bridge components under the maximum allowable load are summarised in Table 7.1, along with the component α factor and β factor values and characteristic yield strength values.

Component	Stress (N/mm^2)	Characteristic yield strength (N/mm^2)	α factor range	β factor
Chain eyebar	53	151	0.794 - 0.953	0.953
Stiffening plate girder	222 (max bending stress)	187	0.634 - 0.761	0.761
Hanger rod	24	151	0.794 - 0.953	0.953

Table 7.1 Summary of stresses in main bridge components under maximum allowable load.

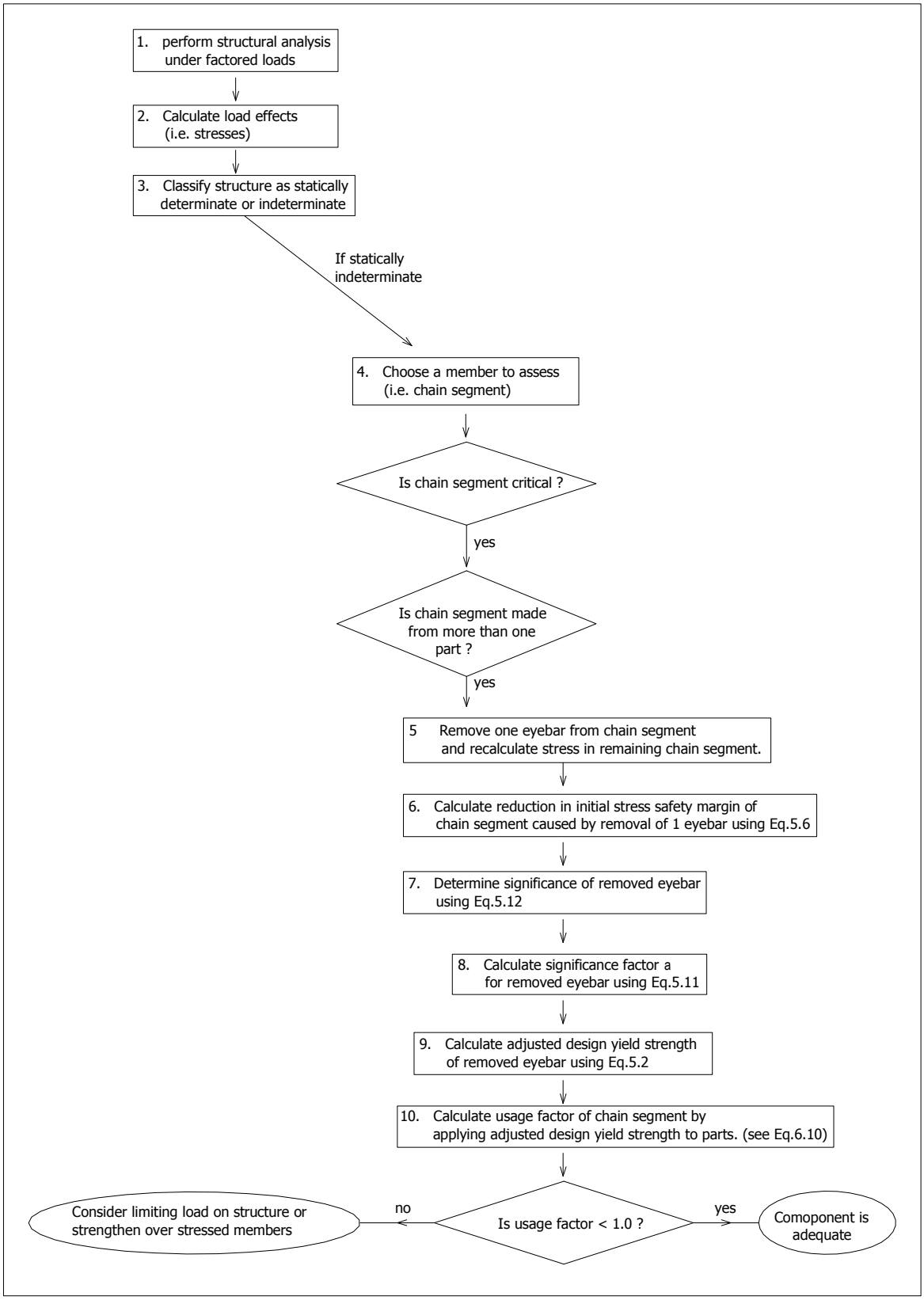

Figure 7.13 Steps in procedure for assessment of bridge chains

Clearly each segment of a chain is critical, but because it is composed of 10 eyebars arranged side-by-side, the next step in the assessment of the chain is to determine the

significance of an individual eyebar. Given the low stress in the chains under the assessment loading, a single eyebar is not critical, and therefore, the significance of the eyebars is determined by removing one at a time, and calculating the reduction in the initial stress safety margin of the remaining chain segment.

There are three rows of chains on each side of the bridge. Therefore, 30 eyebars in total make up the most highly stressed portion of the chain arrangement. In the structural analysis the three chains were modelled as one cable and the stress in this imaginary cable was calculated. A computer model of the bridge was created using this same simplification. The problem with this simplification in the proposed method, is that removal of a single eyebar will result in an increase in stress in the overall cable. It was determined that more than 10 eyebars could be removed from the imaginary cable without overstressing the cable. But removal of 10 eyebars from a single chain results in the entire collapse of the chain. Thus the stress safety margin computed on the basis of the imaginary cable would not provide a true measure of significance for an eyebar in a single chain. To overcome this problem it is proposed that the significance of a single eyebar be calculated on the basis of the removal of one eyebar for all three chains simultaneously. This will provide a more correct measure of the significance of an eyebar within a single chain.

The reduction in safety margin and increase in significance of the eyebars, after the removal of successive sets of eyebars, is summarised in Table 7.2. Removal of a set of eyebars means the simultaneous removal of one eyebar from each of the three chains, at the same location in the chain arrangement.

	Max stress in remaining eyebars (S_A^*) (N/mm^2)	Initial stress safety margin (N/mm^2)	Significance of member % And (α factor)	Adjusted design yield strength (N/mm^2)	Design safety margin (N/mm^2)	Usage factor U
Intact chain	58	93	4.3 (0.801)	150	92	0.39
1st eyebar set removed	62	89	7.5 (0.806)	149	87	0.42
2nd eyebar set removed	69	82	10.8 (0.811)	148	79	0.47
3rd eyebar set removed	79	72	14.0 (0.816)	147	68	0.54
4th eyebar set removed	92	59	20.4 (0.826)	145	53	0.63
5th eyebar set removed	111	40	73.5 (0.911)	132	21	0.84
6th eyebar * set removed	139	12	73.5 (0.911)	132	0	**1.06**
7th eyebar * set removed	185	0	73.5 (0.911)	132	0	**1.41**

Table 7.2 Variation in significance and design strength with successive loss of eyebars from a single chain. * indicates a critical component.

As an example of how the values in Table 7.2 were generated consider the removal of the first set of eyebars from the imaginary cable. Prior to the removal of any eyebars the maximum stress in the eyebars is:

$S_A^* = \gamma_{f3}$ (effects of Q_A^*) Eq.6.2 (repeated) (BD 21/01 cl.3.7)

$= 1.1\,(53 N/mm^2) = 58\ N/mm^2$

After the removal of the first set of eyebars there is an increase in stress from $58N/mm^2$ to $62N/mm^2$ in the remaining eyebars, at the location where the eyebars were removed. The initial stress safety margin of the intact member is given by Eq.5.8

Initial stress safety margin = Characteristic yield strength - stress in component (Eq.5.8)

$= 151N/mm^2 - 58N/mm^2 = 93N/mm^2$

After the removal of one set of eyebars the initial safety margin reduces to $151\ N/mm^2$ - $62N/mm^2$ = $89N/mm^2$. Therefore, the reduction in the initial safety margin of the chain associated with the loss of a single set of eyebars is $93N/mm^2$ - $89N/mm^2$ = $4N/mm^2$, and the significance of a single eyebar in the intact chain is given by Eq.5.10

$$\text{significance of eyebar} = \frac{\text{reduction in safety margin of cable}}{\text{safety margin of intact cable}} \times 100 \qquad \text{Eq.5.10 (repeated)}$$

$$\text{significance of eyebar} = \frac{4\text{N/mm}^2}{93\text{N/mm}^2} \times 100 \;=\; 4.3\%$$

Clearly the loss of a single set of eyebars has very little effect on the safety of the structure, and because a single eyebar is of such little significance the design yield strength of a single eyebar within the intact chain, under the proposed method, is distinctly greater than under the existing assessment method. For example, using a significance value of 4.3% for a single eyebar, a proportional α value for use in adjusting the design strength is calculated using Eq.5.8.

α = lowest α factor + (significance %)(size of α factor range) Eq.5.8(repeated)

The size of the α value range is given by

highest α – lowest α = $0.953 - 0.794 = 0.159$

4.3% of $0.159 = 0.00684$

$\Rightarrow$ α value corresponding to 4.3% significance $= 0.794 + 0.00684 = 0.801$

Therefore the design yield strength for this eyebar can be adjusted using Eq.5.2.

$$\text{adjusted design yield strength} = F_c . \frac{(\text{characteristic yield strength})\,\beta}{1.2\,\alpha} \qquad \text{Eq.5.2 (repeated)}$$

$$= (1.0)\frac{151\text{N/mm}^2(0.953)}{1.2(0.801)} \;=\; 150\ \text{N/mm}^2$$

Under the existing method the design yield strength would be given by Eq.5.2 as follows.

$$\text{unadjusted design yield strength} = \frac{151\ \text{N/mm}^2}{1.2} \;=\; 126\ \text{N/mm}^2$$

The design safety margin of the intact component under the proposed method is given by:

Design safety margin of intact member = adjusted design strength - stress in component

$= 150\text{N/mm}^2 - 58\text{N/mm}^2$

$= 92\ \text{N/mm}^2$

Without this adjustment in the design strength, the design safety margin of the intact component would be $126\text{N/mm}^2 - 58\text{N/mm}^2 = 68\text{N/mm}^2$. The proposed method provides a

greater safety margin, particularly for members which have a high safety margin to begin with. However, as eyebars are removed from the chain the stress in the remaining eyebars increases and so does their significance, with the consequence that the degree of adjustment to the design yield strength reduces. In other words, as members become more significant the design yield strength under the proposed method converges toward the design yield strength under the existing method.

The values in Table 7.2 were generated by considering the removal of eyebars adjacent to each other, i.e. eyebars comprising one segment of the chain. If five sets of adjacent eyebars are removed then the chain will be on the verge of limit state violation. In other words, the chain cannot sustain any further loss of eyebars. The occurrence of corrosion resulting in the loss of five sets of adjacent eyebars is highly unlikely, and therefore, the bridge is quite safe under the static loading considered in this analysis. The low stress is the chains is a result of the enforced load limit of 28 tonnes on the bridge.

7.7 (b) Assessment of hanger rods

In Section 7.6 (h) it was established that the stress in the hanger rods under the assessment loading is 24N/mm^2. Given this low stress it is clear that a single rod is not critical. Therefore the procedure to follow to assess these members is similar to that used to assess the web members of Irwell Street Bridge. The significance of the hanger rods is based on the reduction in the stress safety margin of some critical member, that would occur as a result of the loss of the hanger rods. The hanger rods relieve the stiffening girder of bending stress by being connected to the chains. Therefore, loss of some hanger rods would result in an increase in bending stress in the stiffening girder. Thus the location in the stiffening girder with the maximum bending moment should be chosen as the section on which to base the significance of the hanger rods. It is recommended that a group damage event involving the loss of a number of adjacent hangers is simulated in this investigation.

Chapter 8 Assessment of Liverpool Lime Street Station Roof

8.1 Introduction

In the later half of the 19th century the development of large roof structures was at the forefront of structural design. Ever greater spans were needed to provide unobstructed internal space for railway stations, exhibition halls and ship construction. This demand necessitated the design of lightweight trusses or framed structural forms composed of relatively slender members. Wrought iron, although not a new material, had rarely been tested over such great spans. Exceptions include the suspension bridges of Brunel and others, which is the subject of Chapter 7. Methods of structural analysis which could cope with statically indeterminate structural arrangements had to be developed in parallel with an understanding of the mechanical properties of wrought iron. This in turn drove forward the development of material testing techniques. In this Chapter the assessment method outlined in Chapter 5 is presented as a detailed example of how the method is applied to a truss. Liverpool Lime Street Station was chosen because it is still in use and because the roof consists of long span trusses composed of slender members which are critical for the stability of the structure. For this example the assessment focuses on the bottom chord eyebars and the web members.

8.2 Liverpool Lime Street Station - historic background and structural details

The present roof of Liverpool Lime Street railway station was built in 1875 by the Darlaston Iron and Roofing Company and replaced the previous roof which had been built by Richard Turner in 1849 (Swailes 2005). The 1875-present day roof is of the trussed bowstring form whose upper chord is composed of a plate and angle continuous arch and whose bottom chord forms an arched chain of eye-bar links. The truss spans a distance of approximately 57m with an overall height at mid-span of 12.3m from springing level. The bottom chord rises 6.2m at mid-span above springing level and both chords form circular arcs. (See Figure 8.1).

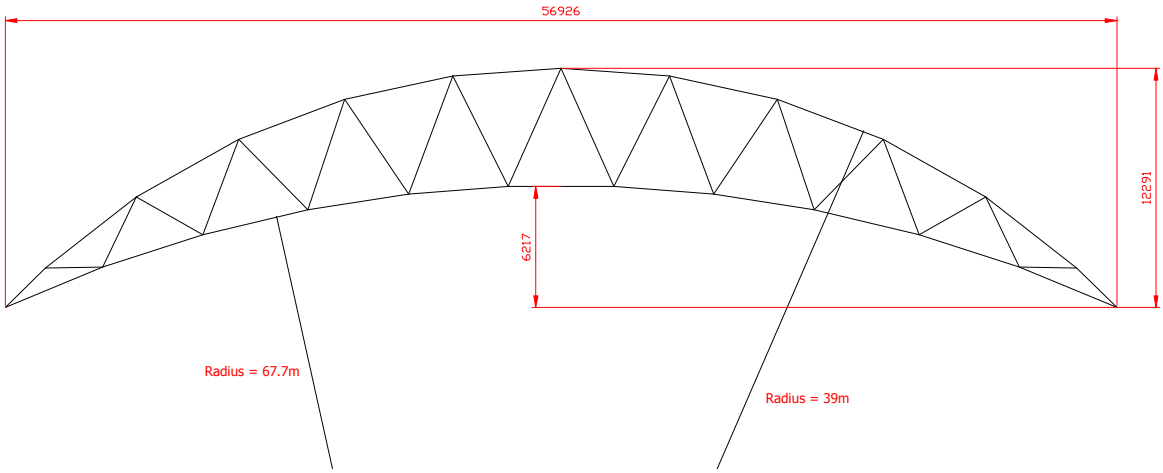

Figure 8.1 Line drawing profile of Liverpool Lime Street Station truss. All dimensions in mm unless otherwise stated. (O'Sullivan 2010)

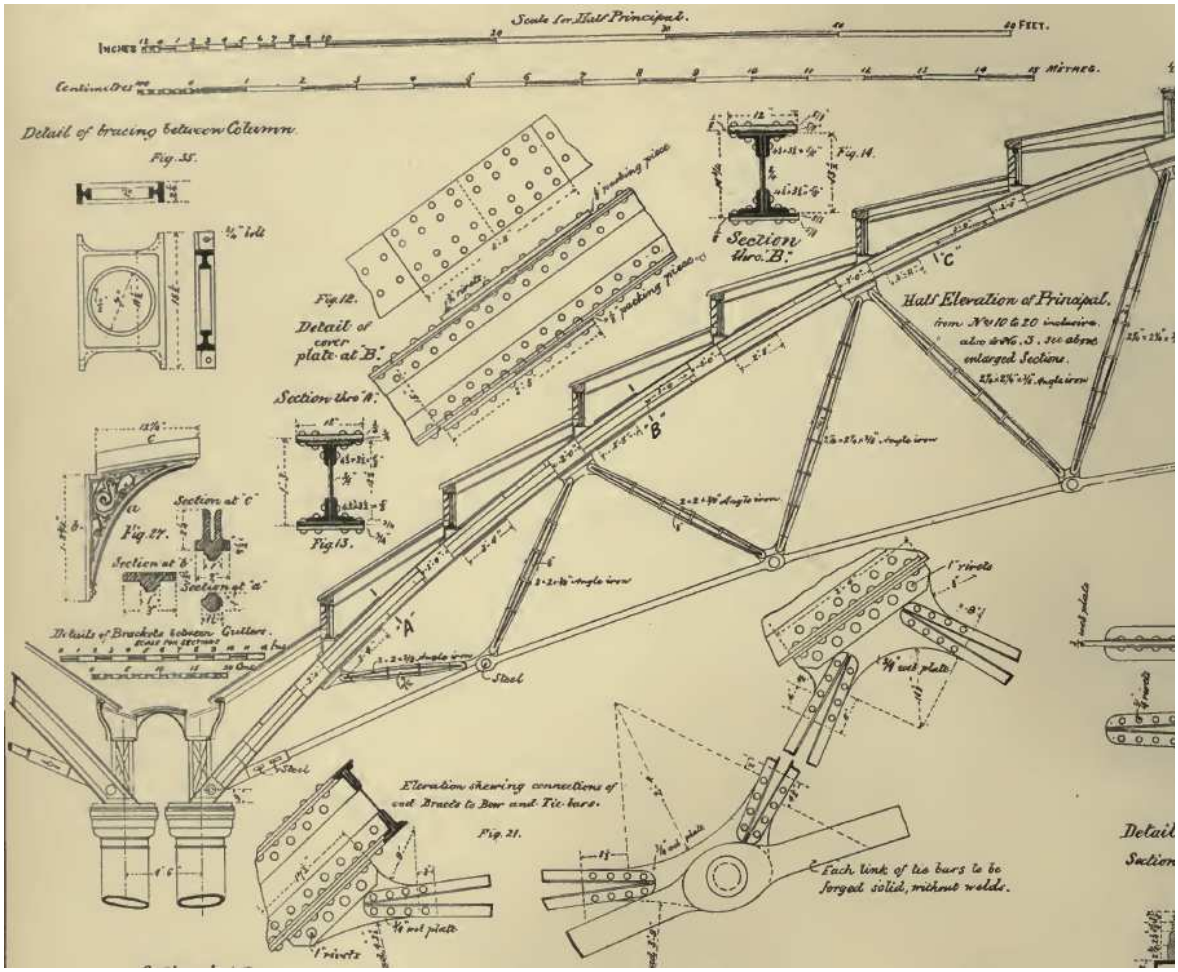

Figure 8.2 Truss details of Liverpool lime Street Station roof (Walmisley, Plate 37 1888)

The trusses are spaced 32 ft (9.75m) apart and rest on top of columns at each springing point. The web members of the trusses are each composed of four 2.25 x 2.25 x 3/8 inch angle irons, separated with cast iron distance pieces such that the angle irons are held in the

form of an open cross in cross-section, as shown in Figure 8.7, thus providing sufficient rigidity to resist buckling (Walmisley 1888).

Figure 8.3 Liverpool Lime Street Station (Swailes 2007)

8.3 Testing of Liverpool Lime Street Station roof eye-bars

Prior to erection of the structure a sample eye-bar made for the bottom chord of the roof truss was tested by David Kirkaldy in 1870. The results were published in 1871 and are summarised in Figures 8.5 and 8.6 and Table 8.1. The grade of iron of this eye-bar was described as "Thornycroft Best Best" (Kirkaldy 1871). Using his own design of testing machine, which was sensitive enough to measure the strain at yield, Kirkaldy could determine the yield strength of the iron in addition to its modulus of elasticity.

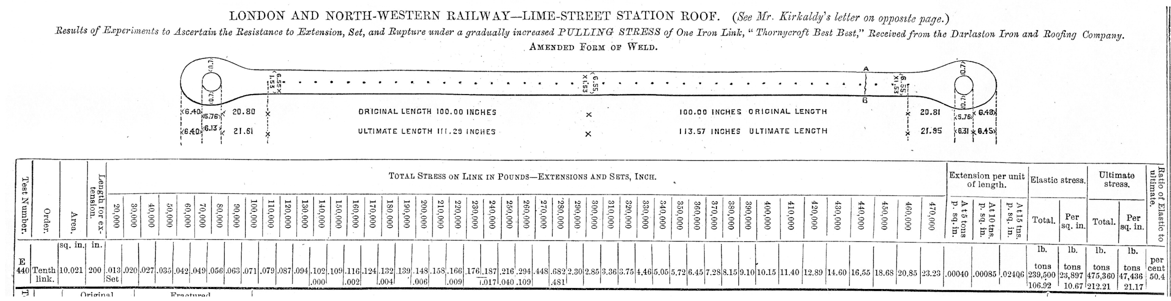

LONDON AND NORTH-WESTERN RAILWAY—LIME-STREET STATION ROOF. (*See Mr. Kirkaldy's letter on opposite page.*)

Results of Experiments to Ascertain the Resistance to Extension, Set, and Rupture under a gradually increased PULLING STRESS of One Iron Link, "Thornycroft Best Best," Received from the Darlaston Iron and Roofing Company.

AMENDED FORM OF WELD.

Test Number.	Order.	Area.	Length for extension.	Total Stress on Link in Pounds—Extensions and Sets, Inch.														
				20,000	30,000	40,000	50,000	60,000	70,000	80,000	90,000	100,000	110,000	120,000	130,000	140,000	150,000	160,000
		sq. in.	in.															
E 440	Tenth link.	10.021	200	.013 Set	.020	.027	.035	.042	.049	.056	.063	.071	.079	.087	.094	.102 .000	.109	.116 .002

Test Number.	Total Stress on Link in Pounds—Extensions and Sets, Inch.															
	170,000	180,000	190,000	200,000	210,000	220,000	230,000	240,000	250,000	260,000	270,000	280,000	290,000	300,000	310,000	320,000
E 440	.124	.132 .004	.139	.148 .006	.158	.166 .009	.176	.187 .017	.216 .040	.294 .109	.448	.682 .481	2.30	2.85	3.36	3.75

Test Number.	Total Stress on Link in Pounds—Extensions and Sets, Inch.															Extension per unit of length.			Elastic stress.		Ultimate stress.		Ratio of Elastic to ultimate.
	330,000	340,000	350,000	360,000	370,000	380,000	390,000	400,000	410,000	420,000	430,000	440,000	450,000	460,000	470,000	At 5 tons p. sq. in.	At 10 tns. p. sq. in.	At 15 tns. p. sq. in.	Total.	Per sq. in.	Total.	Per sq. in.	
																			lb.	lb.	lb.	lb.	
E 440	4.46	5.05	5.72	6.45	7.28	8.15	9.10	10.15	11.40	12.89	14.60	16.55	18.68	20.85	23.23	.00040	.00085	.02406	tons 239,500 106.92	tons 23,897 10.67	tons 475,360 212.21	tons 47,436 21.17	per cent 50.4

Figure 8.4 Kirkaldy's report of eye-bar test (Engineering 1871)

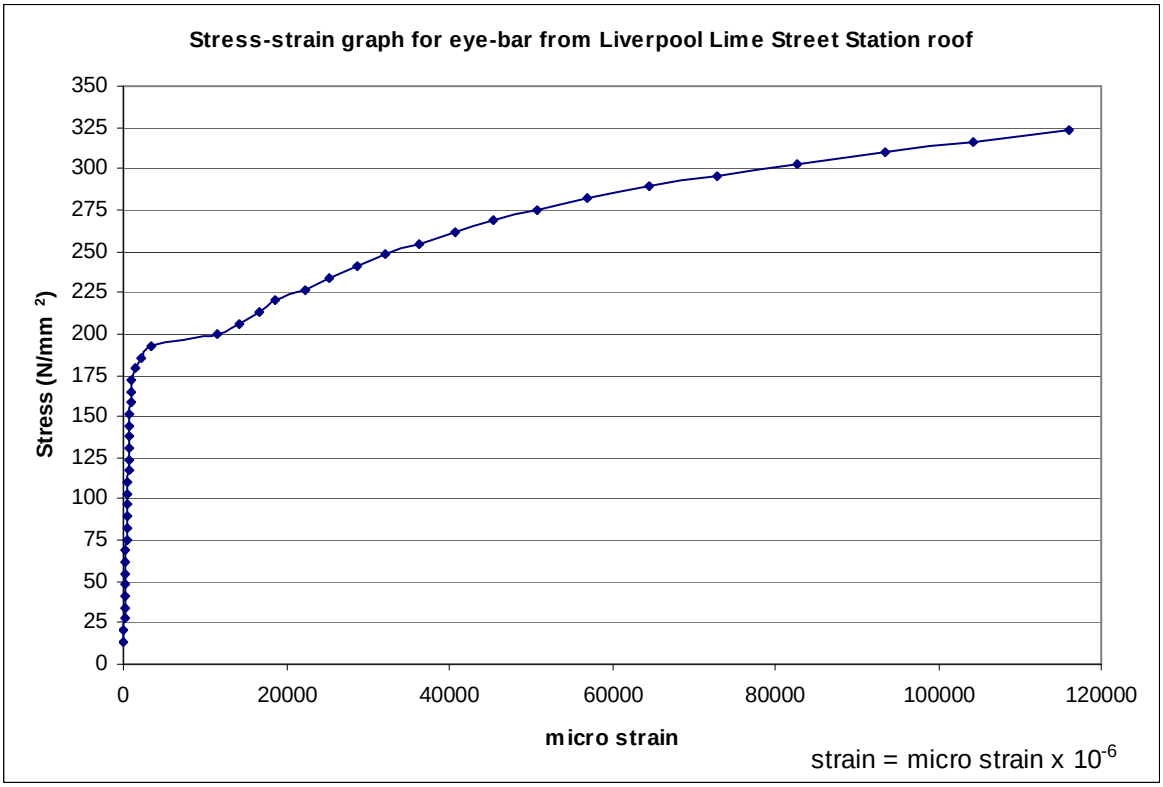

Figure 8.5 Complete stress-strain graph for Kirkaldy's tensile test of the eye-bar shown in Figure 8.4.

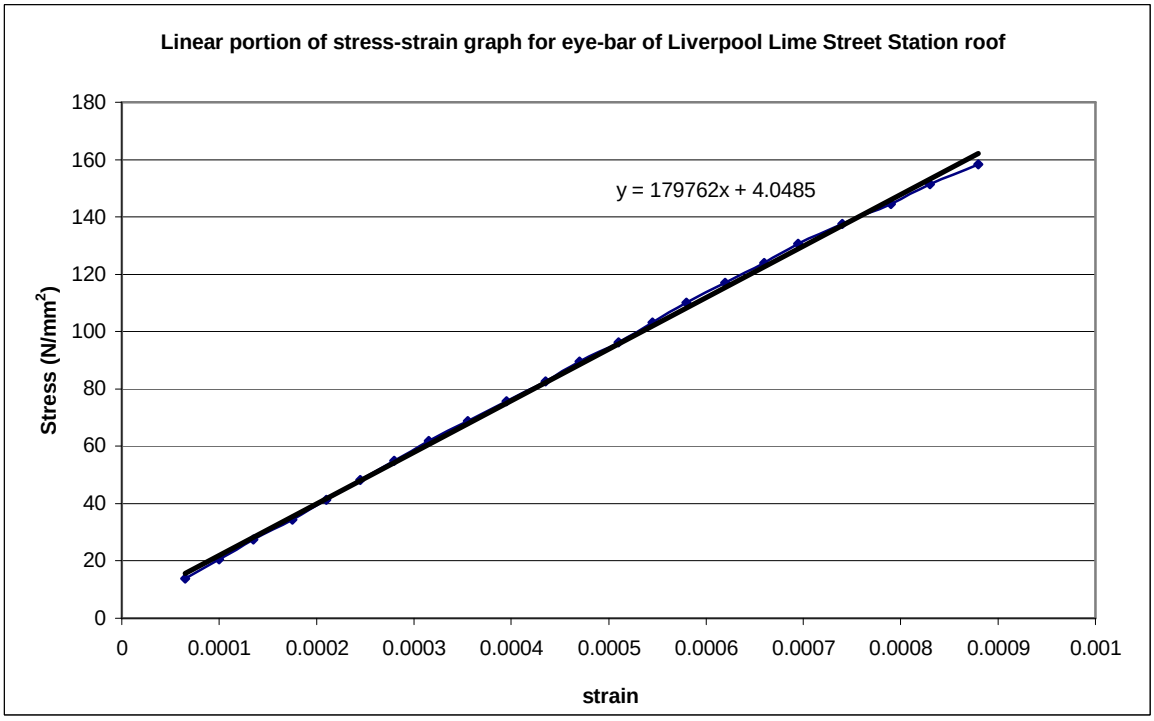

Figure 8.6 Elastic portion of stress-strain graph for Kirkaldy's tensile test of the eye-bar shown in Figure 8.4.

Elastic limit (N/mm^2)	Ultimate strength (N/mm^2)	Modulus of elasticity (N/mm^2)	Elongation at failure %
165	327	179762	11.6

Table 8.1 Summary of Kirkaldy's tensile test results for test of the eye-bar shown in Figure 8.4.

Each tie or link in the bottom chord of the roof truss is composed of four eye-bars as shown in Figure 8.7.

Figure 8.7 Bottom chord of Liverpool Lime Street Station roof truss (O'Sullivan 2009)

8.4 (a) Use of eye-bars in structures

In many of the early suspension bridges engineers used pin-connected eye-bars to form large chains as the main support to the suspended road deck. Examples include Thomas Telford's bridge of 1826 across the Menai Straits and Brunel's Clifton Suspension bridge, completed in 1864.

As shown in the case of Liverpool Lime Street Station roof, eye-bars were also used extensively for trusses. Eye-bars were very popular in 19th century USA because they allowed the construction of simple truss bridges in remote locations where the bridge parts could be assembled on site. For the construction of the Indian railways the bridge components were often made in the U.K. and shipped to India for assembly on site.

8.4 (b) Assessment of criticality of eye-bar composed structural members

In the case of suspension bridges and roof trusses tension members are critical, in that, loss of one of the links in the chain would result in total structural collapse. For example, when one of the tie bars of Charing Cross Station failed because of an undetected flaw within the bar, six people were killed in the resulting progressive collapse of the roof. "The tie had failed at a scarf weld between the plain round bar and a threaded end. Following an examination of the bar William Kirkaldy, son of David Kirkaldy, concluded that the failure of the 4.5 in. diameter bar had been the result of an internal manufacturing flaw that could not have been detected by surface examination." (Swailes 2005)

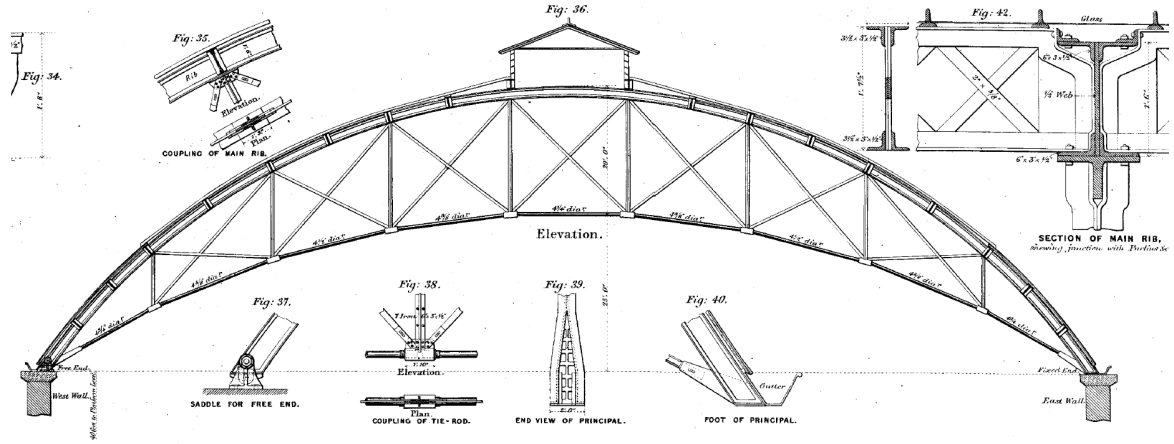

Figure 8.8 Charing Cross Station roof truss (Barry 1868)

Normally a tie member was composed of a number of eye-bars placed side-by-side, four in the case of Liverpool Lime Street Station and ten in the Clifton Suspension Bridge.

"Truss bridge members consisting of two eye-bars are considered fracture critical and lower chord members are always fracture critical unless occurring in sets of more than two" (Sparks 2004). The collapse in 1967 of the Point Pleasant Bridge in the USA resulted from a corrosion-fatigue crack in an eye-bar. The chain links which failed had only two plate eye-bars (Cullimore 1988). Where there are more than two eye-bars comprising a member the criticality of the member should be based upon an analysis of the entire structure (Sparks 2004). Firstly, an analysis is carried out to identify the most heavily loaded eye-bar-composed member, under working loads. Then a second analysis is

performed under the same loading, this time assuming loss of one of the eye-bars in the member. If the remaining members are still not overstressed then the original member may be classified as being not fracture critical (Sparks 2004). In other words the member will not fail even if one of the eye-bars is removed.

8.4 (c) Eye-bar end connections

Loss of an eye-bar may result in unbalanced loading of the pin connection and in such a case it may be necessary to assess the rotational stiffness of the pin connection to see if it can withstand the imposed torsion (Sparks 2004). In addition, the pin itself will be subjected to increased bending stresses if one or more of the eye-bars is removed .The principal failure mode of pins is in bending; shear rarely governs (Sparks 2004)

Eye-bars were shaped such that ultimate failure of the eye-bar would occur in the bar and not the head or the pin. Despite this many recorded failures occurred by rupturing of the head. When Kirkaldy tested an sample eye-bar from the manufacturers of Liverpool Lime Street Station, failure occurred in the bar, but in two other eye-bars destined for the Indian railways failure occurred in the head. Furthermore, in a larger series of tests conducted by George Berkley most of the eye-bars also failed in the head as shown in Figure 8.9.

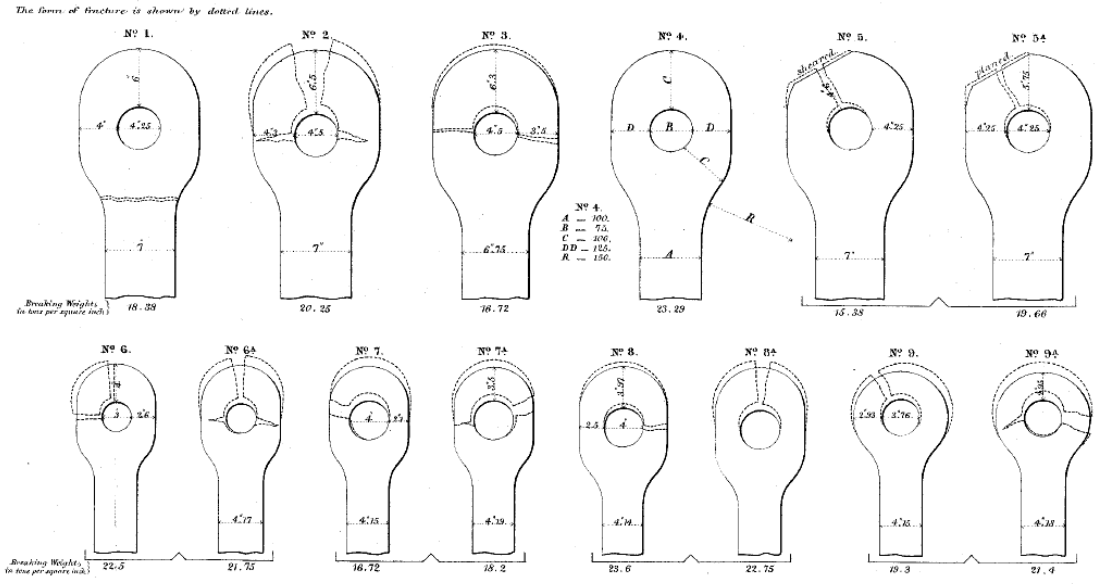

Figure 8.9 Tests on eye-bars (Berkley 1870)

A typical finite element analysis stress plot of an eye-bar under direct tension is shown in Figure 8.10. The greatest tensile stress in the head occurs at the inner surface of the hole along a diameter perpendicular to the direction of pull.

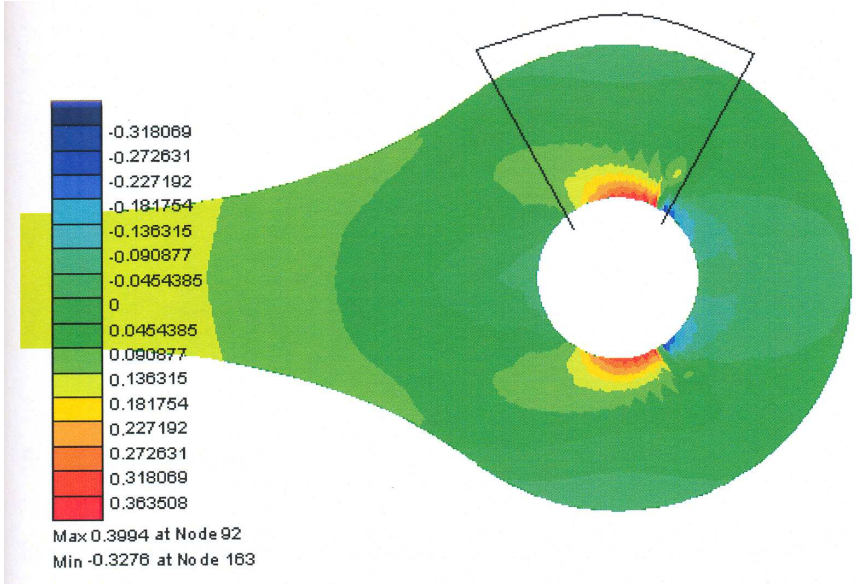

Figure 8.10 Finite element simulation of stress distribution in eye bar head resulting from interaction with pin. (He 2004)

The zones of maximum tension are shown in red and the typical stress concentration factors in these areas is about 2.7 (Sparks 2004). In the case shown in Figure 8.10 the tensile stress in the bar is 161N/mm^2, while the maximum stress in the head of the eye-bar, (the red area around the inside of the hole) is 363N/mm^2, giving a stress concentration factor of 2.25 (He 2004)

The main modes of eye-bar failure are:

1 Tensile failure in the bar or neck.

2 Tensile failure in the head around the eye (i.e. red zone in Figure 6.10).

3 Crushing of the bearing surface of the eye (i.e. blue zones in Figure 6.10).

4 Shear failure of the area bearing on the pin (i.e. tear out of the head against the pin).

5 Tension failure through the net section across the eye (i.e. red zones extend outward). (Sparks 2004)

8.4 (d) Original methods of setting out eye-bars

There was some degree of variation among engineers in the methods of proportioning eye-bar heads. "According to Shaler Smith the proportions adopted depended partly upon the mode of their manufacture." (Warren 1894). Below are some of the methods adopted for setting out the shape of an eye-bar head by various authorities.

Three eye-bar heads are shown in Figure 8.11. In (a) the form shown is a hammer forged eye-bar, "which according to Professor Burr, has stood the test of long American practice." (Warren 1894).

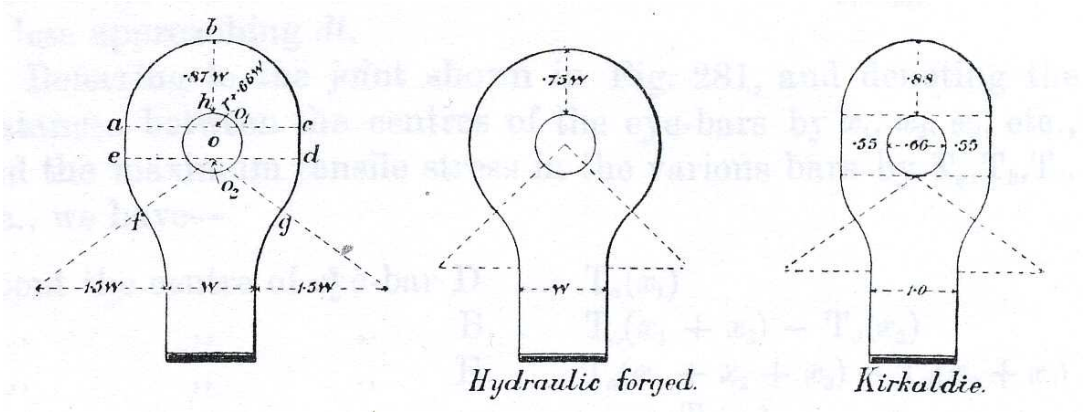

(a) (b) (c)

Figure 8.11 Proportioning of eye-bar heads (Warren 1894)

Method 1 (Hammer forged eye-bar in Figure 8.11 a)

Let *w* denote the width of the bar, and r the radius of the pin.

Make $hb = 0.87w$

Make *abc* a semicircle with o_1 as centre and radius = $r + 0.66w$, such that $00_1 = 00_2$.

The curves *ef* and *dg* are portions of a semicircle of the same radius as *abc*.

Method 2 (Hammer forged eye-bar in Figure 8.11 c)

That shown in Figure 8.11 (c) is a form of hammer forged eye-bar that was proposed by David Kirkaldy and was based on his own experimental work.

Method 3 (Hammer forged eye-bar in Figure 8.12)

George Berkley's experiments led to his proposal of the following proportions for hammer forged eye-bars. Referring to Figure 8.12 :

Width of flat bar = B, Diameter of pin: D = 0.75B

$b + b$ =1.25B, E = B, r = B, R = 1.5B

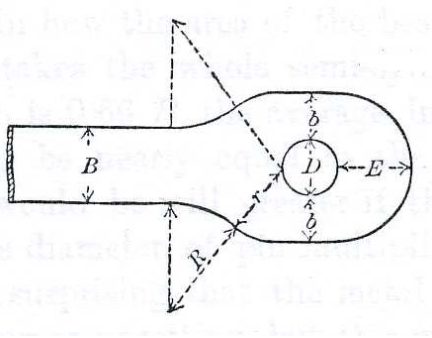

Figure 8.12 Proportioning of eye-bar head (Warren 1894)

8.4 (e) Modern method of assessing eye-bar load capacity

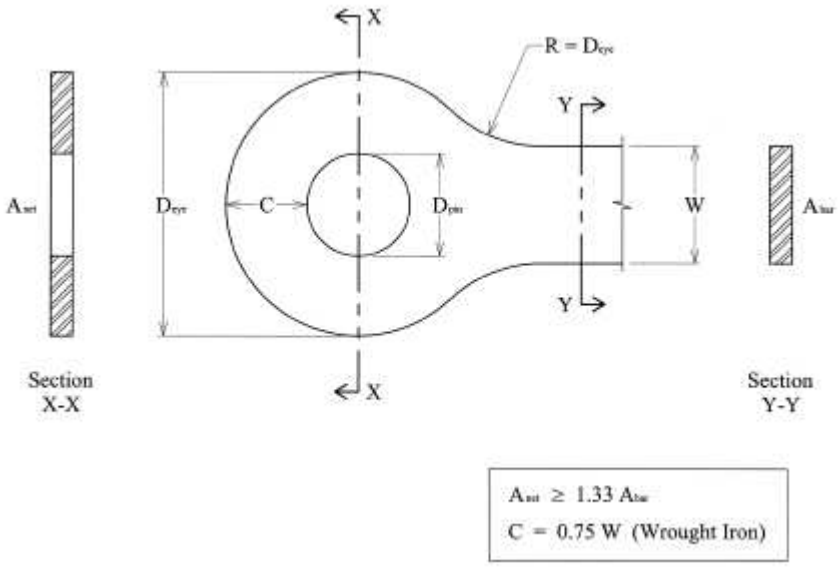

Figure 8.13 Typical eye-bar proportions (Sparks 2004)

An eye-bar with the proportions shown in Figure 8.13 should fail in the bar, and not in the head. Therefore, the load carrying capacity can be based on the sectional area of the bar, without a detailed analysis of the head (Sparks 2004). For permanent loads such as dead load the allowable stress that an eye-bar may be subjected to is $0.55\sigma_y$ where σ_y is the yield strength of the metal, and for imposed loads the allowable stress is $0.75\sigma_y$. (Sparks 2004).

8.5 Application of proposed method to Liverpool Lime Street Station

8.5 (a) 19th Century roof loading values

In the construction of wrought iron roofs different sources have quoted different design loads. For example, for the construction of the iron roofs of the workshops and ship building slips at the Royal Dockyards in Portsmouth, (circa 1841) a total weight of 40 lbs/ft^2 (1.92 kN/m^2) was used for design purposes. (Swailes 2005) However, in the design of St Pancras station roof an imposed load of 70 lbs/ft^2 was used by William Barlow, in addition to the self weight of the structure. Walmisley, stated that it was sufficient for design purposes to take a total lateral load of 45 lbs/ft^2 (2.16 kN/m^2) acting on the projected vertical area of the roof as comprising the load effect of wind and snow taken together. (Walmisley 1888).

Given these values, it would seem that an imposed load of 40 lbs/ft^2 (1.92 kN/m^2) acting both vertically and horizontally, but taken separately, was the typical design load. Given that the spacing of the roof trusses of Liverpool Lime Street Station is 9.75m, an imposed load of 1.92kN/m^2 would mean that the load per metre span would be 1.92 kN/m^2 x 9.75m = 18.7 kN/m. However, a typical modern design imposed load for this situation is 10 kN/m, and it is this value that is used in Case 1 of the analysis discussed in Section 8.5 (f). A load value of 15kN/m is considered in Case 2, (see section 8.5(g)).

8.5 (b) Load cases considered in assessment of Liverpool Lime Street Station Roof

In the following assessment procedure various "what if" damage scenarios are considered in order to identify the criticality and significance of all the truss members. In each case a member is removed that will result is some reduction of the stress safety margin of the structure.

In the first two cases considered the truss is intact and in its present condition, and is subjected to uniform vertical imposed loading (Cases 1 and 2). Thereafter, the truss is assumed to have suffered some damage as described in the following list of case details. In all cases the self weight of the truss members is included. Complete removal of a web member is considered in Cases 6 to 15. However, complete removal of any top or bottom chord member would lead to instant collapse, so their significance is based on their own stress values, as if part of a statically determinate structure, which is described in Section 6.5 (g) (Case 2). But the procedure for determining the significance of the eyebars making up the bottom chord members follows that for an indeterminate structure because loss of an single eyebar does not necessarily result in instant collapse.

Case 1 Intact truss under uniform vertical distributed loading (uvdl) = 10kN/m.

Case 2 Intact truss under uniform vertical distributed loading (uvdl) = 15kN/m.

Case 3 One eyebar in bottom chord member No.43 removed + (uvdl) = 15kN/m.

Case 4 One eyebar in bottom chord member No.43 removed + (uvdl) = 10kN/m.

Case 5 Two eyebars in bottom chord member No.43 removed + (uvdl) = 10kN/m.

Case 6 Diagonal web member No.6 removed + (uvdl) = 15kN/m.

Case 7 Diagonal web member No.7 removed + (uvdl) = 15kN/m.

Case 8 Diagonal web member No.8 removed + (uvdl) = 15kN/m.

Case 9 Diagonal web member No.9 removed + (uvdl) = 15kN/m.

Case 10 Diagonal web member No.10 removed + (uvdl) = 15kN/m.

Case 11 Diagonal web member No.11 removed + (uvdl) = 15kN/m.

Case 12 Diagonal web member No.12 removed + (uvdl) = 15kN/m.

Case 13 Diagonal web member No.14 removed + (uvdl) = 15kN/m.

Case 14 Diagonal web member No.15 removed + (uvdl) = 15kN/m.

Case 15 Diagonal web member No.13 removed + (uvdl) = 15kN/m.

The bottom chord members of Liverpool Lime Street Station roof truss are composed of four eyebars. In order to determine the significance of one of these eyebars a failure mechanism of removing one eyebar at a time should be followed. This is the procedure which is outlined in Figure 8.14 and utilises analysis Cases 1, 4 and 5, which are discussed in Sections 8.5 (f) to (j). This procedure is the same as the one applied to the chains of Clifton Suspension Bridge .

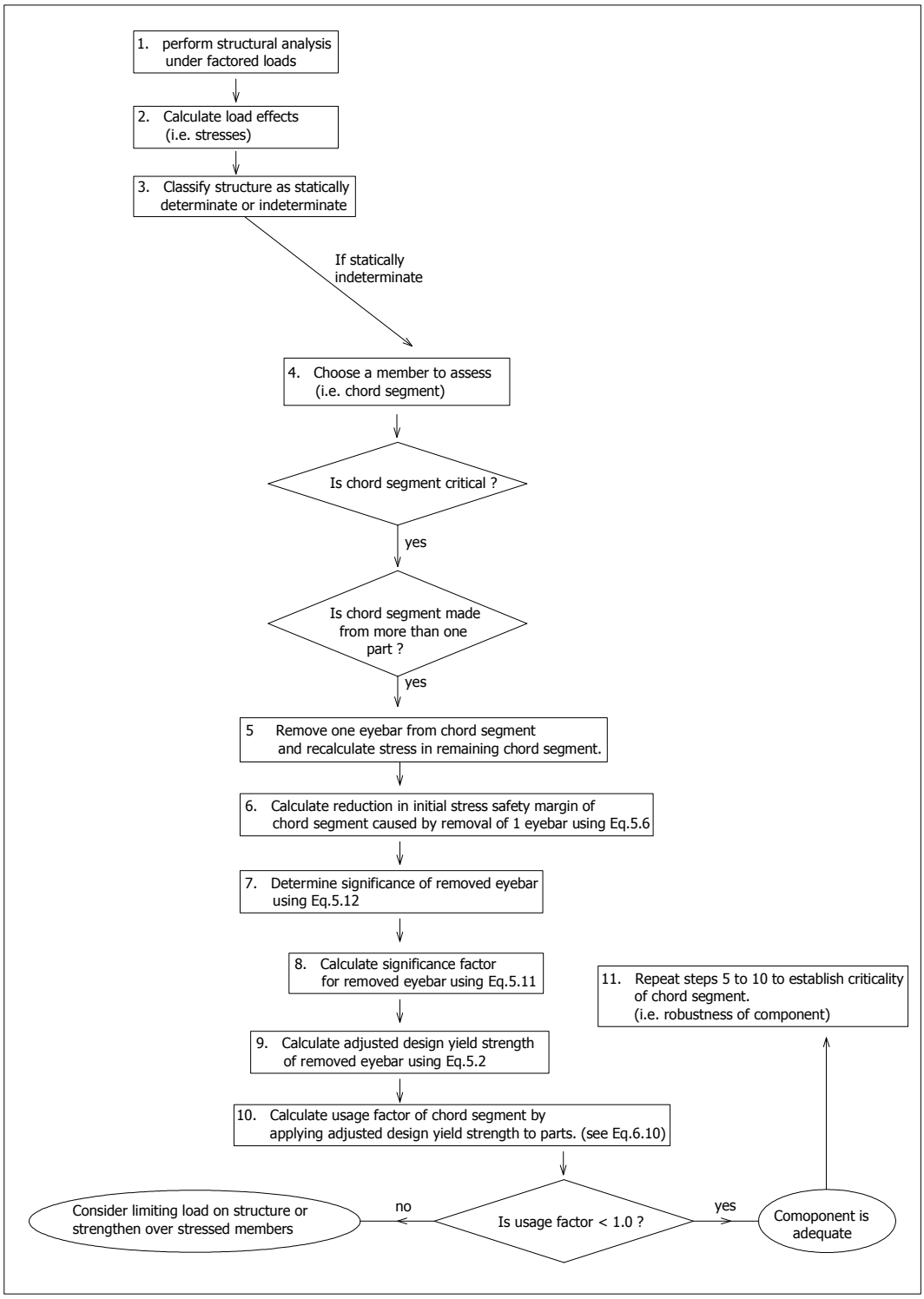

Figure 8.14 Steps in procedure for assessment of bottom chord eyebars of roof truss.

8.5 (c) Investigation of general behaviour of intact truss under uniform vertical load.

Case 1: Uniform vertical distributed load (uvdl) = 10kN/m.

The partial safety factor for imposed loading is 1.5, so the unfactored imposed load is (10 kN/m)/1.5 = 6.6 kN/m. The self weight is included in all load cases and the partial safety factor for dead load is 1.05.

From Figure 6.2 it can be seen that the roof covering attaches to the roof truss at the truss nodes and at the mid-distances between nodes. Thus the loading may be modelled as a collection of 23 point loads, as shown in Figure 8.14.

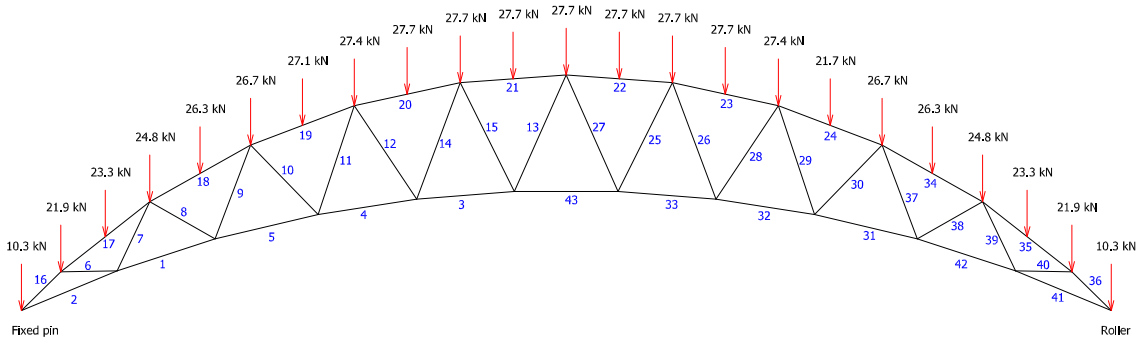

Figure 8.15 Case 1 loading of Liverpool Lime Street Station roof truss. Point loads shown are collectively equivalent to the projection of a uniform load of 10kN/m onto the curved roof surface. Numbers in blue are the member identification numbers

In the roof truss model shown in Figure 8.15 the top chord members are rigidly connected end-to-end, and thus form a continuous arch, as in the actual truss. The web members and bottom chord members are pin ended, as in the real truss. The purpose of this initial analysis is to determine which members are most critically loaded. Subsequent analyses will focus on these members in various damage scenarios. The objective is to observe how the stresses of the critical members are affected by damage to the truss. Under Case 1, the deflected shape, bending moment, shear force and axial force diagrams are given in Figures 8.16, 8.17, 8.18 and 8.19 respectively.

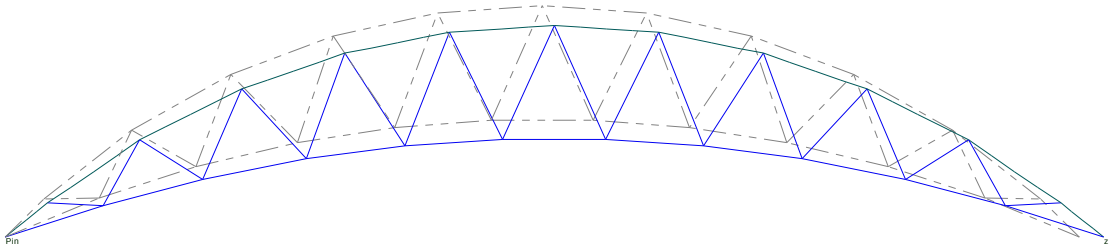

Figure 8.16 Exaggerated deflected shape of Liverpool Lime Street station roof truss under uniform vertical loading. The left end support was modelled as a fixed pin while the right support as a roller.

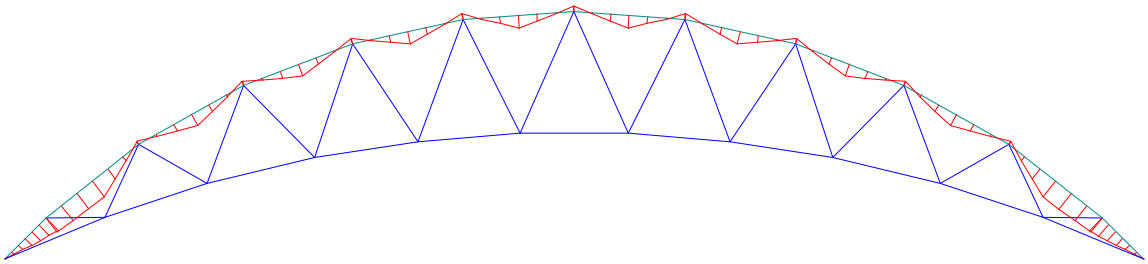

Figure 8.17 Bending moment diagram of Liverpool Lime Street station roof truss under uniform vertical loading (Case 1, see Figure 6.14). Maximum bending moment occurs in the top chord near the supports.

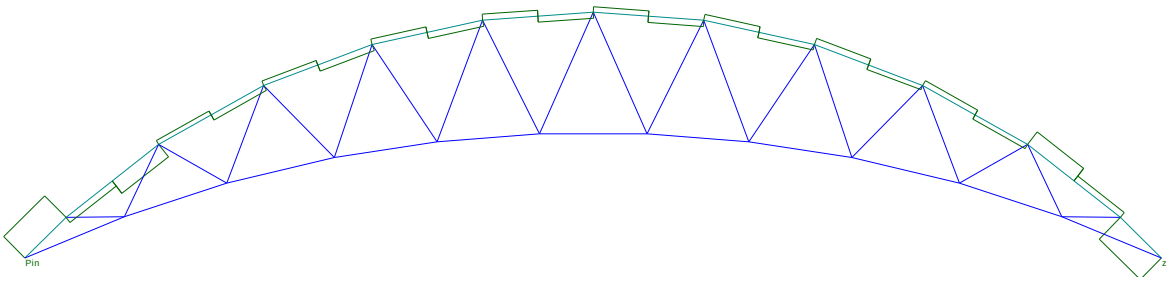

Figure 8.18 Shear force diagram of Liverpool Lime Street station roof truss under uniform vertical loading. (Case 1) Maximum Shear force occurs in the top chord near the supports.

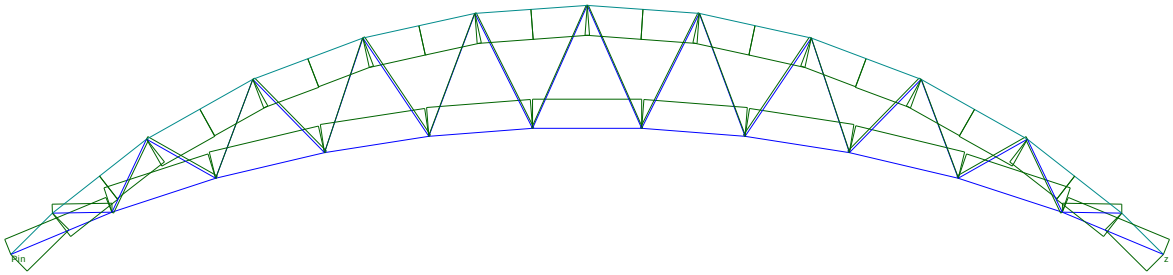

Figure 8.19 Axial force diagram of Liverpool Lime Street station roof truss under uniform vertical loading. (Case 1) Positive axial force (i.e. tension) is plotted on the upper side of a structural element while negative axial force (i.e. compression) is plotted on the underside of an element.

Clarification of the nature of the axial force (i.e. tension or compression) is given in Figure 8.20 where blue signifies tension and red signifies compression.

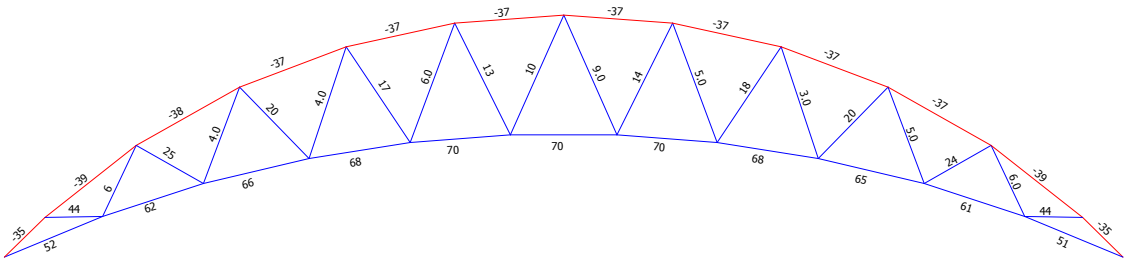

Figure 8.20 Axial stress in Liverpool Lime Street station roof truss under uniform vertical loading. (Case 1) All numerical values are the axial stresses measured in N/mm^2. (Case 1)

The truss is effectively a Warren truss, but made to assume an arched shape. Thus its basic behaviour is typical of that type of truss, except that, all of the web members are in tension. The web members with a downward and inward direction assume an increasing tensile load as one moves outward from the middle of the truss, which is typical of Warren truss behaviour, but the downward and outward pointing diagonals exhibit a decreasing tensile force as one moves outward from the middle of the truss. The compressive force in the arched upper chord does not vary significantly along the arch. But the tensile force in the bottom chord takes on a significantly greater value in the middle of the truss than at the truss ends.

8.5 (d) Case 2: Intact truss under uniform vertical distributed load (uvdl) = 15kN/m.

Imposed vertical design load per unit length of span = **15 kN/m**

The loading consists of 23 point loads, as shown in Figure 8.21. This loading is used for all cases except Cases 1, 4 and 5.

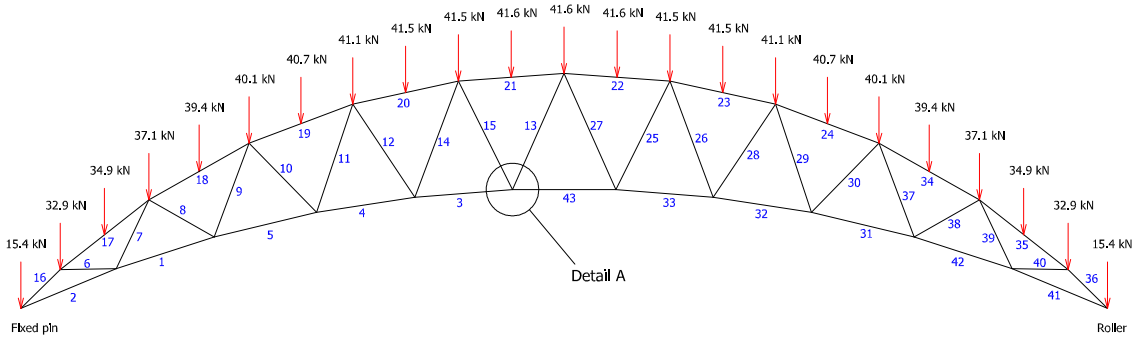

Figure 8.21 Case 2 loading of Liverpool Lime Street station roof truss. Point loads shown are collectively equivalent to the projection of a uniform load of 15kN/m onto the curved roof surface. Numbers in blue are the member identification numbers.

The procedure outlined in Figure 8.14 for the assessment of the bottom chord components is demonstrated as follows.

Step 2:

Calculate stress in components in the intact truss under the factored loading shown in Figure 8.21. Member no. 43 has the greatest stress which is 96N/mm^2. All segments of the bottom chord are critical and each is composed of 4 eyebars. A close-up view of member no.43 is shown in Figure 8.22.

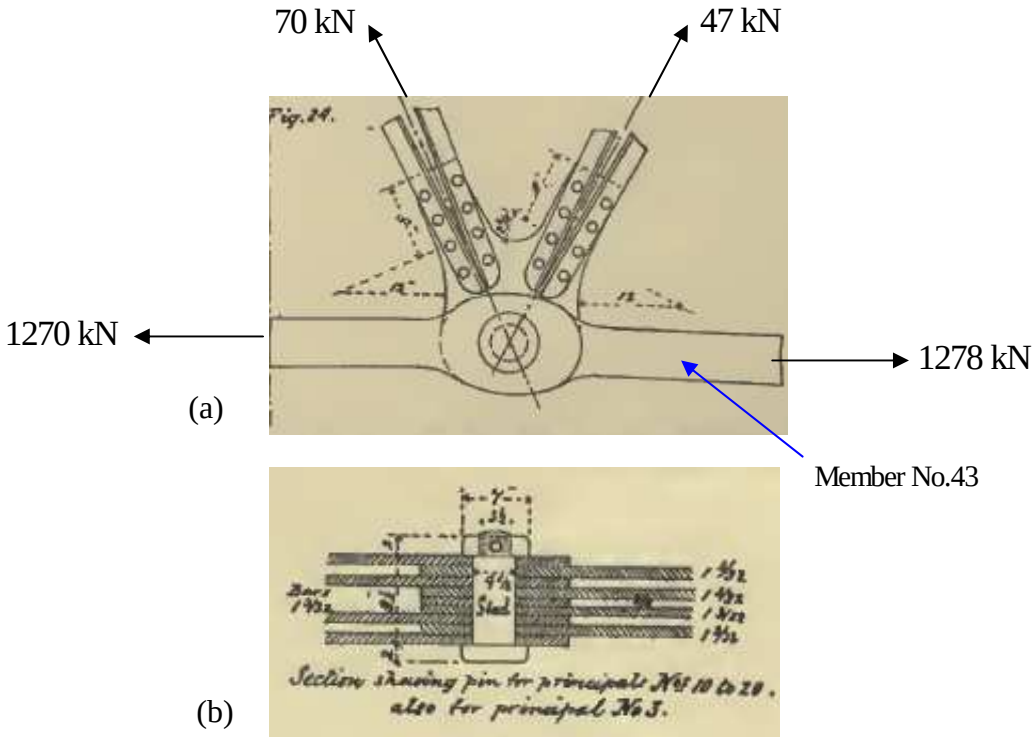

Figure 8.22 (a) Elevation and (b) plan view of bottom chord eye-bar connection in Liverpool Lime Street Station roof truss, labelled as Detail A in Figure 8.21. Case 2 loading (i.e. 15kN/m). (Walmisley 1888)

The reduction in the initial stress safety margin of member no.43 after the removal of an eyebar from this member, is given in Table 8.2

	Max stress in member no.43 (S_A^*) (N/mm^2)	Initial stress safety margin (N/mm^2)
Intact chain (Case 2)	96	55
1st eyebar removed (case 3)	128	23

Table 8.2 Reduction in safety margin due to loss of an eyebar from chord member no.43.

In this case the loss of a single eyebar results in the initial stress safety margin reducing to a small value, which means that under a load of 15kN/m all eyebars in member no. 43 may be considered critical. Therefore, the assessment of the member must proceed as if the member is part of a statically determinate structure. In other words the procedure given in Figure 8.14 should be replaced with that given in Figure 8.23.

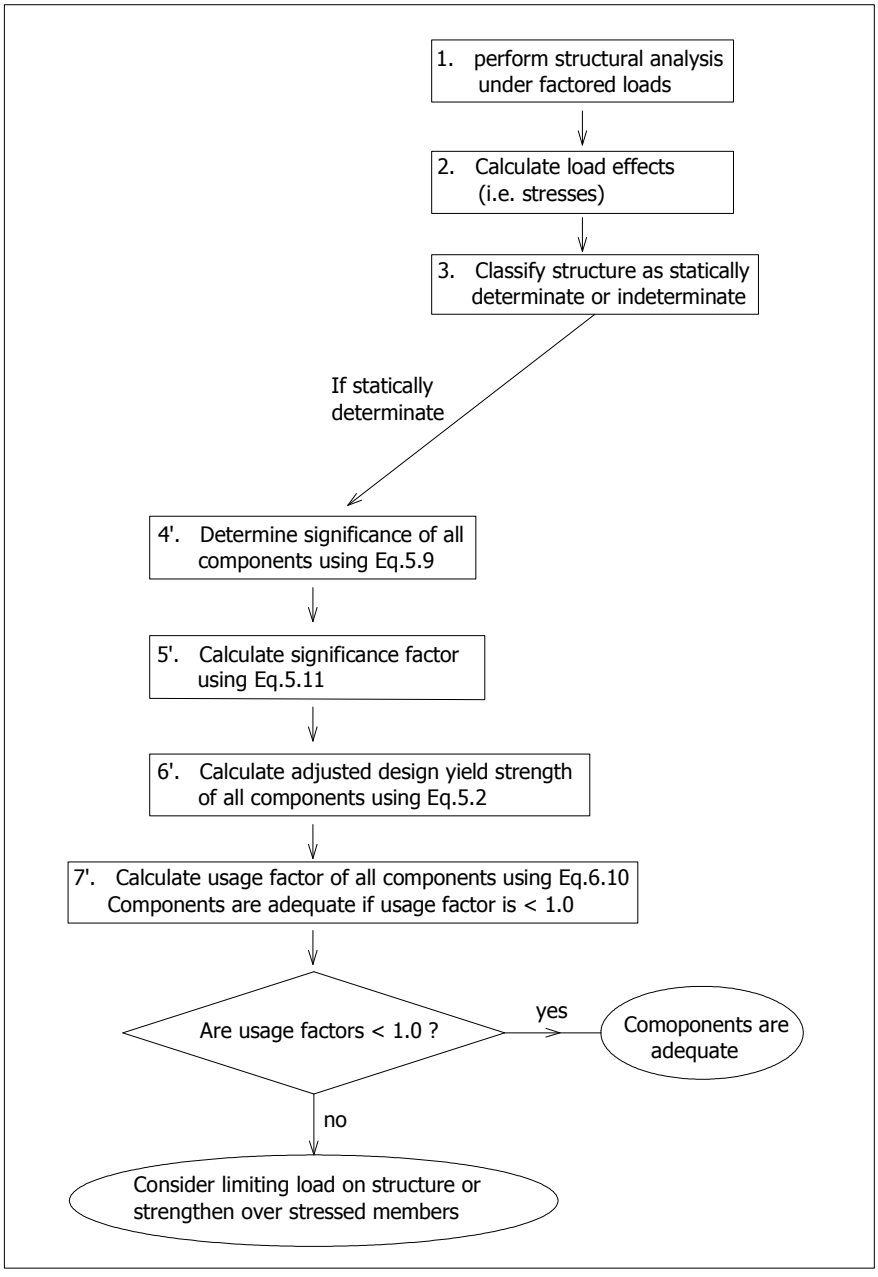

Figure 8.23 Steps in procedure for assessment of bottom chord eyebars of roof truss.

The significance values and adjusted design strengths for all the bottom chord members of the truss are given in Table 8.3.

Member type	Member No.	Axial stress (S_A^*) N/mm^2	Initial safety margin N/mm^2	significance %	Full Method design yield strength (R_A^*) N/mm^2	Full Method Usage factor	Current Method Usage factor
Bottom chord	1	84	67	55.6	136	0.62	0.67
Bottom chord	2	70	81	46.4	138	0.51	0.56
Bottom chord	3	95	56	62.9	134	0.71	0.75
Bottom chord	4	93	58	61.6	134	0.69	0.74
Bottom chord	5	89	62	58.9	135	0.66	0.71
Bottom chord	31	89	62	58.9	135	0.66	0.71
Bottom chord	32	93	58	61.6	134	0.69	0.74
Bottom chord	33	96	55	63.6	134	0.72	0.76
Bottom chord	41	70	81	46.4	138	0.51	0.56
Bottom chord	42	84	67	55.6	136	0.62	0.67
Bottom chord	43	96	34	63.6	134	0.72	0.76

Table 8.3 Details of bottom chord stresses of Liverpool Lime Street Station roof truss under uvdl = 15kN/m.

In Table 8.2, 'Full Method' denotes full application of the new proposed method and 'Current Method' denotes the current assessment method specified in BD21. Under the current method there is only one design yield strength given by (151 N/mm^2)/1.2 = 126 N/mm^2.

Clearly the proposed method provides a greater design yield strength when there is sufficient margin of safety to do so, and therefore, is a less conservative, yet safe refinement of the current assessment method.

8.5 (e) Case 4: One eyebar in bottom chord member No.43 removed + (uvdl) = 10kN/m.

If the load on the truss is 10kN/m and one eyebar is removed from member No.43 then the tensile stress increases from 70 N/mm^2, for the intact member (Case 1), to a value of

94N/mm^2 (Case 4), which is still significantly less than the characteristic elastic limit of 151N/mm^2. Therefore, under this load value a single eyebar is not regarded as critical and its significance should be calculated by determining the change in the safety margin of the component associated with the loss of this eyebar. In other words, the procedure outlined in Figure 8.15 should be followed. The analysis cases considered are Cases 1, 4 and 5.

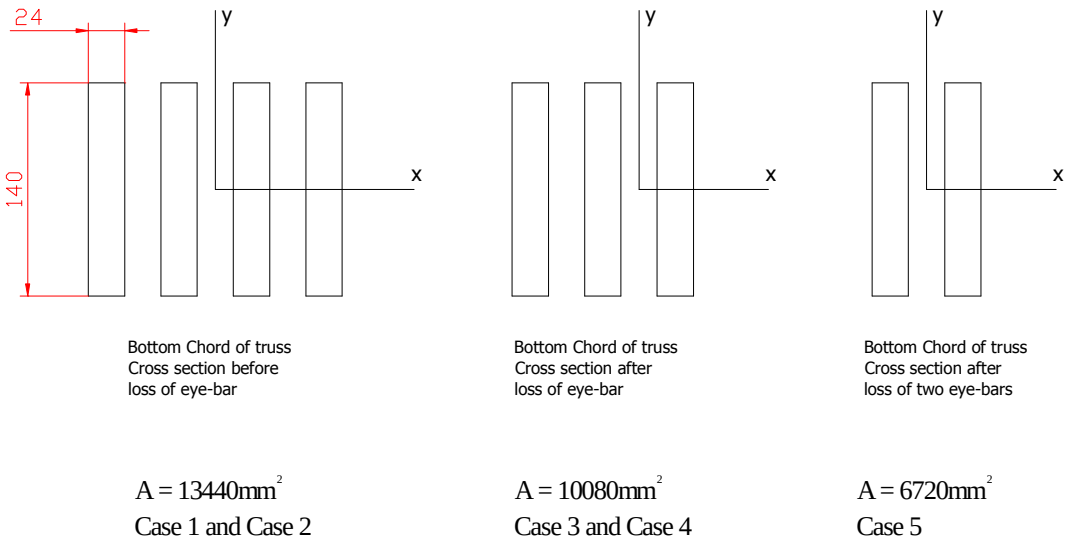

Figure 8.24 Cross section of bottom chord eye-bars in Liverpool Lime Street Station roof truss for Cases 2, 3, 4 and 5.

The reduction in safety margin and increase in significance of the eyebars, after the removal of successive eyebars, is summarised in Table 8.4.

Member no. 43	Max stress in remaining eyebars (S_A^*) (N/mm^2)	Initial stress safety margin (N/mm^2)	Significance of member % And (α factor)	New design strength (R_A^*) N/mm^2	Design safety margin (N/mm^2)	usage factor U
Intact member (case 1)	70	81	30 (0.842)	142	72	0.49
1st eyebar removed (case 4)	94	57	62 (0.893)	134	40	0.7
2nd eyebar removed (case 5)	140	11	62 (0.893)	134	0	1.04

Table 8.4 Summary of assessment of member no.43 under uvdl = 10kN/m

The values in Table 8.4 were generated as follows. The initial safety margin of the intact member is 151 N/mm^2 -70 N/mm^2 = 81N/mm^2. After the removal of one eyebar the initial

safety margin reduces to 151 N/mm^2 - 94 N/mm^2 = 57N/mm^2. Therefore, the reduction in the initial safety margin associated with the loss of a single eyebar is 81N/mm^2 - 57N/mm^2 = 24N/mm^2, and the significance of the eyebar is

$$\text{significance of eyebar} = \frac{\text{reduction in safety margin of component}}{\text{safety margin of intact component}} \times 100$$

$$\text{significance of eyebar} = \frac{24\text{N/mm}^2}{81\text{N/mm}^2} \times 100 \quad = \quad 30\%$$

Comparing cases 3 and 4 one may state that under an imposed load of 10kN/m a single bottom chord eyebar is not essential for stability and each has a significance of 30%, but under an imposed load of 15kN/m all bottom chord eyebars are essential for stability and each has an significance of 64%. (see Table 8.3). Because of the way significance has been defined a component with a significance less than 100% may be essential for stability. The decision about whether a component is essential or not is based on the existence of a non zero design safety margin for the remaining components once the initial component has been removed. In these calculations the characteristic yield strength of wrought iron was used to define significance and to determine the initial safety margin of components. However, the decision about the criticality of a component should be based on the design safety margin, which is based on the design strength of the component. This is the design strength after the adjustment for significance and quality has been made. For example, using a significance value of 30% for a single eyebar, a proportional α value for use in adjusting the design strength is calculated as follows. The size of the α value range is given by

$$\text{highest } \alpha \; - \; \text{lowest } \alpha \quad = \quad 0.953 - 0.794 \quad = \quad 0.159$$

$$30\% \text{ of } 0.159 = 0.0477$$

$$\Rightarrow \quad \alpha \text{ value corresponding to 30\% significance} = 0.794 \; + \; 0.0477 \quad = \quad 0.842$$

Therefore the design yield strength for this component can be adjusted as follows

$$\text{adjusted design strength} = \frac{(151 \text{ N/mm}^2)\beta}{1.2\alpha} \quad = \quad \frac{151\text{N/mm}^2(0.953)}{1.2(0.842)} \quad = \quad 142 \text{ N/mm}^2$$

The design safety margin of the intact component (i.e. member no. 43) is given by:

Design safety margin of intact member = adjusted design strength - stress in component

$$= 142\text{N/mm}^2 - 70\text{N/mm}^2$$

$$= 72\ \text{N/mm}^2$$

Without this adjustment in the design strength, the design safety margin of the intact component would be 126N/mm^2 - 70N/mm^2 = 56N/mm^2. Therefore, the proposed method provides a greater safety margin than the existing assessment method, in cases where members are non critical and is particularly evident when the safety margin is large to begin with.

The safety margin of the damaged member (i.e. with one eyebar missing) is dependent upon the significance of the remaining eyebars. Their significance in the damaged member is greater than in the intact member. In order to calculate the safety margin of the damaged member the design strength of the member in its damaged state must be calculated and this is determined from the significance of the remaining eyebars. Therefore, the process of determining the significance of the eyebars must be repeated, with the member in its damaged state as the starting point. In other words, a second eyebar must be removed to determine its significance.

8.5 (f) Case 5: Two eyebars in bottom chord member No.43 removed + (uvdl) = 10kN/m.

If the load on the truss is 10kN/m and a second eyebar is removed from member No.43, leaving two remaining, then the tensile stress in the member increases from 94 N/mm^2, (Case 4), to a value of 140N/mm^2 (Case 5), which is close to the characteristic yield strength value of 151N/mm^2. Therefore, the second, third and fourth eyebars are all critical components and their individual significance is the same, and is equal to the significance of the member just prior to removal of the second eyebar, and is given by:

$$\text{Component significance} = \frac{\text{stress in member after removal one one eyebar}}{\text{characteristic yield strength}}$$

$$= \frac{94\text{N/mm}^2}{151\text{N/mm}^2}$$

$$= \quad 0.623 \quad = \quad 62.3\%$$

Comparing cases 4 and 5 one may state that under an imposed load of 10kN/m a single bottom chord eyebar in the intact member is not essential for stability and each has a significance of 30%. However, if one eyebar is lost then the remaining three become critical and each has a new significance of 62%.

The design yield strength of the damaged member (i.e. with one eyebar missing) may now be determined as follows. The size of the α value range is given by

$$\text{highest } \alpha \; - \; \text{lowest } \alpha \;\; = \;\; 0.953 - 0.794 \;\; = \;\; 0.159$$

$$62.3\% \text{ of } 0.159 = 0.099$$

$$\Rightarrow \quad \alpha \text{ value corresponding to 62\% significance} = 0.794 \; + \; 0.099 \; = \; 0.893$$

Therefore the design yield strength for this component can be adjusted as follows

$$\text{adjusted design strength} = \frac{(151\ \text{N/mm}^2)\beta}{1.2\alpha} \;\; = \;\; \frac{151\text{N/mm}^2(0.953)}{1.2(0.893)} \;\; = \; 134\ \text{N/mm}^2$$

The design safety margin of the component (with one eyebar missing) is given by:

$$\text{Design safety margin of damaged member} = \text{adjusted design strength} - \text{stress in component}$$

$$= 134\text{N/mm}^2 - 94\text{N/mm}^2$$

$$= 40\ \text{N/mm}^2$$

These calculations show that by losing a single eyebar the design strength of the component drops from 142N/mm^2 to 134N/mm^2, and the design safety margin falls from 72N/mm^2 to 40N/mm^2. By losing a second eyebar the stress in the member becomes 140N/mm^2, which exceeds the design strength. Therefore, the loss of a second eyebar will place the truss at the point of limit state violation, and so, the remaining three eyebars are critical under this load value.

This example also shows that the design strength of a component and its significance are dependent upon the loads used in assessment. Greater assessment loads will result in a component registering as more significant with the consequence that the component will be given a lower design strength, thereby maintaining a safe approach to the assessment of structures.

8.5 (g) Assessment of web members

An individual web member of the truss is not critical. Therefore, the assessment of the web members should follow the procedure outlined in Figure 8.25.

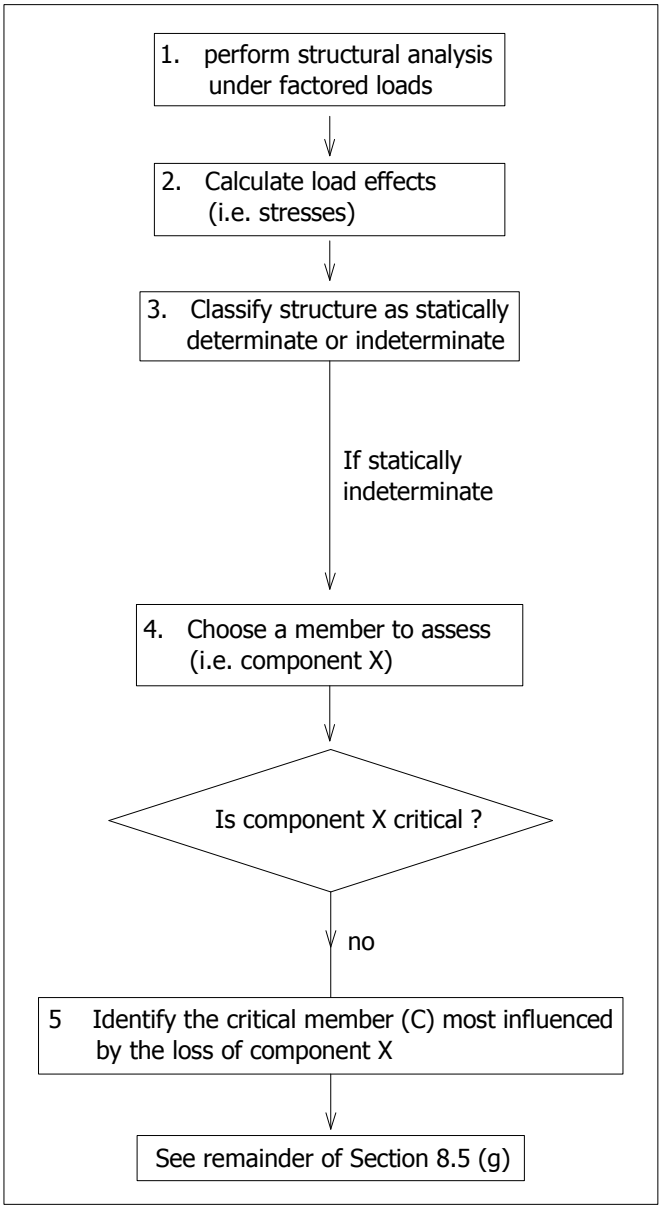

Figure 8.25 Initial steps in procedure for assessment of web members of roof truss.

Member no.43 is the most highly stressed critical member in the bottom chord. Therefore it is the logical choice on which to base the significance of the web members. If the safety margin of member no. 43 reduces because a single diagonal member is removed then the significance of the removed member is given by:

$$\text{significance of removed member} = \frac{\text{reduction in safety margin of member no.43}}{\text{safety margin of member no. 43 in intact truss}}$$

Removal of each web member was carried out and the truss analysed with just one member missing. The effect on member no.43 in each case is shown in Table 8.5

Condition of truss.	Axial Stress in member no. 43 N/mm^2
(Intact truss)	121
(member no.6 removed)	121
(member no.7 removed)	121
(member no.8 removed)	121
(member no.9 removed)	121
(member no.10 removed)	121
(member no.11 removed)	121
(member no.12 removed)	121
(member no.14 removed)	121
(member no.15 removed)	123
(member no.13 removed)	123

Table 8.5 Bottom chord axial stresses in Liverpool Lime Street Station roof truss for scenarios in which one web member is removed. Loading of truss is a udl = 20kN/m

It is clear from Table 8.5 that the removal of any single web member from the truss has no effect on the stresses within the bottom chord members. Therefore, one might at first conclude that these members have no significance, as their removal does not result in reduction of the safety margin of the most highly stressed critical members. However, this does not mean that they are unnecessary members. All of the web members in the truss act as ties within the intact truss, under a uniformly distributed vertical load of 20kN/m, as shown in Figure 8.26(a), and thus contribute to the function of the truss. Under a lateral load some of them act as struts, a function for which, they have clearly been designed, as they are broader at their middle than at their ends, so as to resist buckling. The magnitude of the stresses alternate from one web member to the next in a manner which is similar to that of a Warren truss.

However, the more important effect of the presence of the web members becomes evident in the top chord when one of the web members is removed. This is illustrated in Figure 8.26 (b), where web member no.10 has been removed. The result is that the bending moment in the top chord, at the connection point of the missing member, increases by a factor of 6, and the adjacent web member (i.e. member no. 9) goes from acting as a tie to a strut. Thus it is clear that the web members play an important role in maintaining uniformity of bending moment and force within the intact truss, and therefore they have significance.

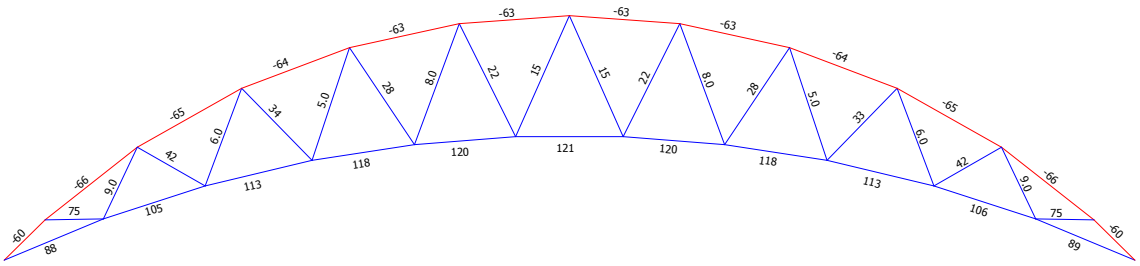

(a)

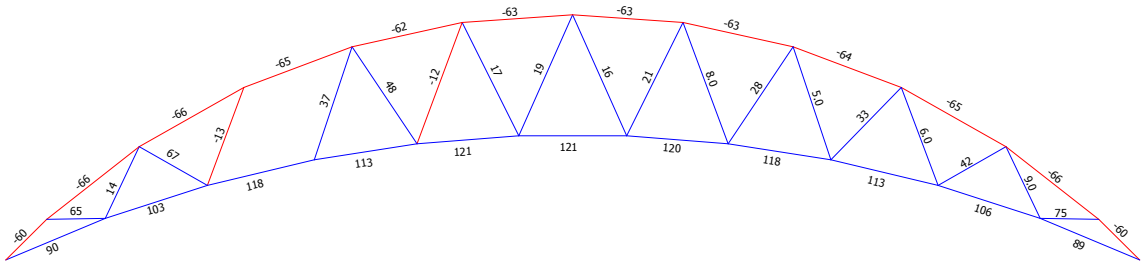

(b)

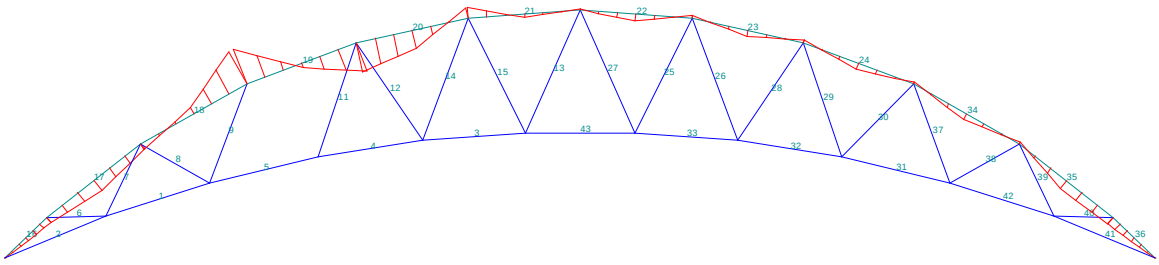

(c)

Figure 8.26 Liverpool Lime Street Station roof truss under uniform vertical loading. (a) Intact truss under udl = 20kN/m, axial stresses in N/mm^2. (b) Truss with member no.10 removed, under udl = 20kN/m, axial stresses in N/mm^2. (c) Truss with member no.10 removed, under udl = 20kN/m, bending moment diagram, numerical values are the member identification numbers.

Because the effect of losing one web member was a significant increase in the bending moment in the upper chord it is logical that one way of calculating the significance of the missing web member is to base it on the reduction in the safety margin of the top chord, rather than on that of the bottom chord. As it is a compression member, which also carries a bending moment the buckling criterion given by Eq.8.9 may be used as a way of defining the significance of the missing member.

$$\frac{F_c}{A_g p_c} + \frac{m_x M_x}{M_b} \leq 1.0 \qquad \text{Eq.8.9} \quad \text{(member buckling resistance check. source: BS5950)}$$

where F_c = compressive force in member.
A_g = cross sectional area of member.
p_c = compressive strength (i.e. buckling stress in compression. Steel data used).
M_x = maximum bending moment about major axis of member (i.e. horizontal x-x axis).
M_b = buckling resistance moment. ($M_b = p_b Z_x$ or $M_b = p_b S_x$)
m_x = equivalent uniform moment factor for major axis flexural buckling.
p_b = bending strength (i.e. buckling stress in bending and based on data for steel)
Z_x = elastic section modulus about major axis
S_x = plastic section modulus about major axis

If a measure of safety against buckling is defined as:

$$\text{safety measure} = 1.0 - \left(\frac{F_c}{A_g p_c} + \frac{m_x M_x}{M_b} \right) \qquad \text{Eq.6.10}$$

then the significance of the removed web component may be defined as the reduction in the safety measure of the critical compression member in the top chord. That is,

$$\text{significance of web member} = \frac{\text{reduction in safety measure of critical top chord member}}{\text{initial safety measure of top chord member}} \times 100$$

Eq.6.11

No information about the buckling resistance of wrought iron was available during the preparation of this project, nor is it know to exist. Most historic testing data for wrought

iron is concerned with its tensile strength. Therefore, it was necessary to use strut curve data for steel to estimate the buckling stress of wrought iron.

As an example of this assessment of significance, Case 10 may be considered as it was the removal of member no.10 that resulted in the greatest increase in the bending moment of the top chord, which occurred in member no.18. The quantities involved are summarised in Table 8.6.

	Case 2: Intact truss (Member 18)	Case 10: Member no.10 removed. (Member 18)
F_c	-1699 kN	-1684 kN
M_x	60 kNm	359 kNm
A_g	26041mm^2	26041mm^2
p_c (in plane buckling)	220 N/mm^2	220 N/mm^2
p_c (out of plane buckling)	193 N/mm^2	193 N/mm^2
M_b	662 kNm	662 kNm
m_x	0.85	0.85
p_b	215 N/mm^2	215 N/mm^2
Z_x	3.08 x 10^{6}mm^3	3.08 x 10^{6}mm^3
S_x	3.65 x 10^{6}mm^3	3.65 x 10^{6}mm^3

Table 8.6 Quantities used in assessment of buckling of top chord of Liverpool Lime Street Station roof.

For in-plane buckling of member 18 in the intact truss

$$\text{safety measure} = 1.0 - \left(\frac{F_c}{A_g p_c} + \frac{m_x M_x}{M_b} \right)$$

$$= 1.0 - \left(\frac{1699 \times 10^3 N}{(26041 mm^2)(220 N/mm^2)} + \frac{0.85(60 \times 10^6 Nmm)}{662 \times 10^6 Nmm} \right)$$

$$= 0.63$$

For in-plane buckling of member 18 in Case 10 in which member no.10 was removed.

$$\text{safety measure} = 1.0 - \left(\frac{F_c}{A_g p_c} + \frac{m_x M_x}{M_b} \right)$$

$$= 1.0 - \left(\frac{1684 \times 10^3 N}{(26041 mm^2)(220 N/mm^2)} + \frac{0.85(359 \times 10^6 Nmm)}{662 \times 10^6 Nmm} \right)$$

$$= 0.25$$

Therefore, for in-plane buckling of the top chord, the reduction in the safety measure resulting from the removal of web member no.10 is 0.63 - 0.25 = 0.38. Thus the

significance of the removed member with regard to its effect on resisting in-plane buckling of the top chord is:

$$\text{significance of web member} = \frac{0.38}{0.63}\times 100 \quad = \quad 60\%$$

The purlins of the roof help to restrain out-of-plane buckling by reducing the effective length of the top chord member, but the reduction in safety measure for out-of-plane buckling should also be calculated and compared with that for in-plane buckling. The larger the value of significance resulting from consideration of both modes of buckling should be taken as the correct significance value.

For out-of-plane buckling of member 18 in the intact truss

$$\text{safety measure} = 1.0 - \left(\frac{F_c}{A_g p_c} + \frac{m_x M_x}{M_b} \right)$$

$$= 1.0 - \left(\frac{1699\times 10^3 N}{(26041 mm^2)(193 N/mm^2)} + \frac{0.85(60\times 10^6 Nmm)}{662\times 10^6 Nmm} \right).$$

$$= 0.58$$

For out-of-plane buckling of member 18 in Case 10 in which member no.10 was removed.

$$\text{safety measure} = 1.0 - \left(\frac{F_c}{A_g p_c} + \frac{m_x M_x}{M_b} \right)$$

$$= 1.0 - \left(\frac{1684\times 10^3 N}{(26041 mm^2)(193 N/mm^2)} + \frac{0.85(359\times 10^6 Nmm)}{662\times 10^6 Nmm} \right)$$

$$= 0.20$$

Therefore, for out-of-plane buckling of the top chord the reduction in the safety measure resulting from the removal of web member no.10 is 0.58 - 0.20 = 0.38. And the significance of the removed member with regard to its effect on resisting out-of-plane buckling of the top chord is:

$$\text{significance of web member} = \frac{0.38}{0.58}\times 100 \quad = \quad 66\%$$

The correct significance value of the removed member is 66% and is governed by the increased potential for out-of-plane buckling of the top chord when web member no.10 is removed. If desired the significance of the other web members may be calculated, but since the removal of web member no.10 resulted in the greatest increase in bending moment in the top chord the significance of the other web members would be less than 66%.

The design strength of member no.10 may now be determined as follows. The member is composed of angle iron and from Table 5.10 the size of the α value range is given by

highest α – lowest α = $0.956 - 0.797 = 0.159$

66% of $0.159 = 0.105$

$\Rightarrow$ α value corresponding to 66% significance $= 0.797 + 0.105 = 0.902$

Therefore the design strength for this component can be adjusted as follows

adjusted design yield strength = $F_c . \dfrac{f_k \beta}{1.2\alpha} = (1.0)\dfrac{200\text{N/mm}^2(0.956)}{1.2(0.902)} = 177\ \text{N/mm}^2$

The design safety margin of this component (i.e. member no.10) is given by:

Design safety margin = adjusted design strength - stress in component

$= 177\text{N/mm}^2 - 34\text{N/mm}^2$

$= 143\ \text{N/mm}^2$

If the adjustment for significance and material quality is not applied then the design yield strength would be 167N/mm^2, which again shows that the proposed method provides a greater component resistance for non critical members. The outline of the procedure which specifically applies to the assessment of the web members of the truss is given in Figure 8.27.

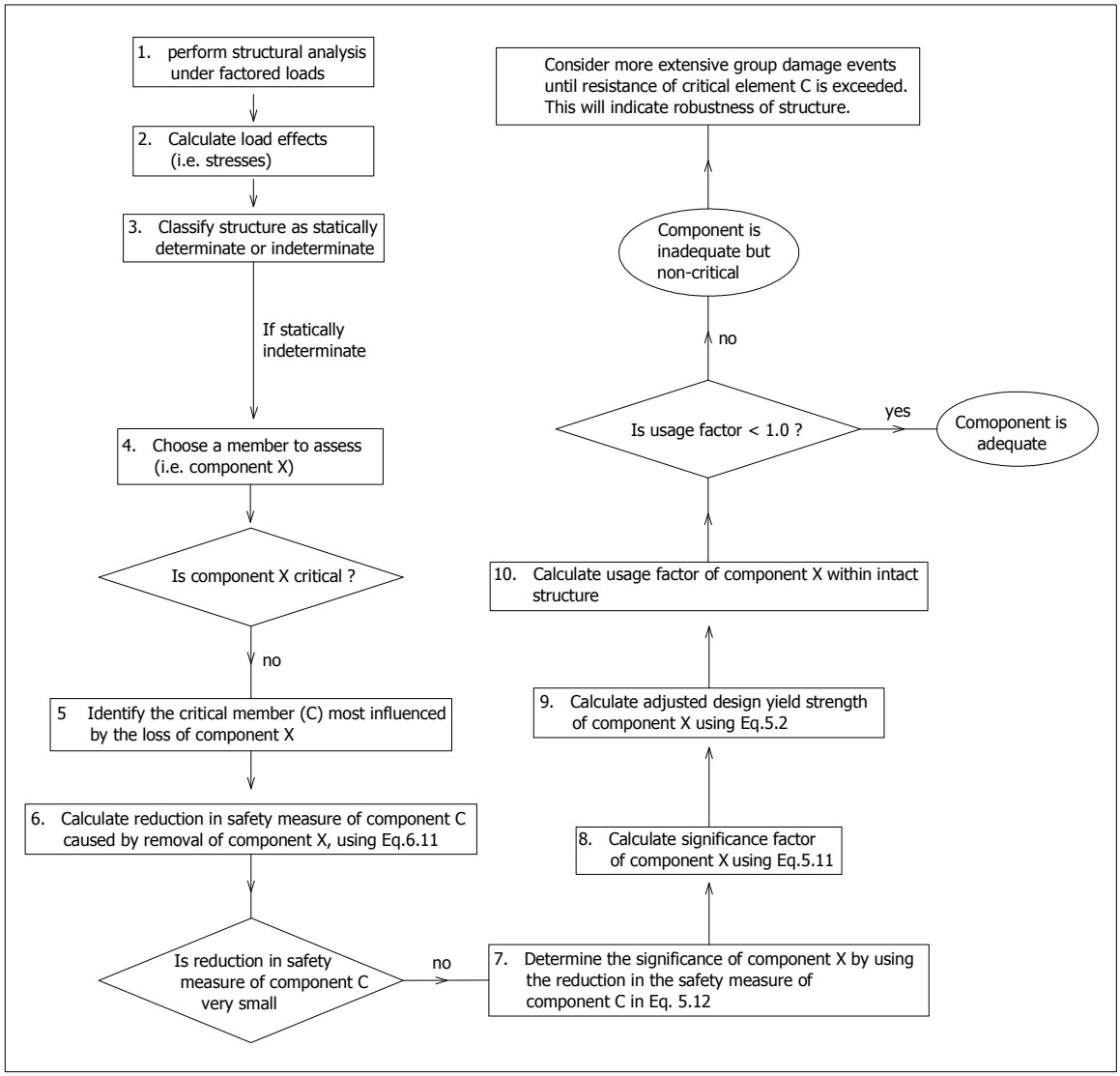

Figure 8.27 Outline of procedure for assessment of web members of roof truss.

Chapter 9 Discussion of proposed assessment method

9.1 Introduction

In this report three case studies were used to demonstrate how the proposed assessment method applies to three different structural forms. Irwell Street Bridge consists of a riveted plate and angle rigid frame, the roof of Liverpool Lime Street Station is composed of pin jointed trusses, and Clifton Suspension Bridge was built using eyebar chains. Many of the features of these structures would not be used in modern construction, simply because of better understanding of materials and structural mechanics and more efficient design practices and construction methods. Therefore, one of the objectives of the proposed assessment method is to provide a step by step path that will help the modern engineer in the assessment of what may be an unfamiliar structural form, which is built from a material that may be regarded as archaic. Structures have not been built from wrought iron for about 100 years and although eyebars were used to construct steel chains for suspension bridges in the 20th century the collapse of the Point Pleasant Bridge in 1966 effectively put an end to their use in new suspension bridges.

Point Pleasant Bridge was built in 1928 and by the middle of the 20th century cable suspension rather than chain suspension had become the norm. The failure of the Point Pleasant Bridge was due to a corrosion induced fatigue crack in the eye of one of the eyebar chain links. In this bridge each segment of the chain consisted of just two eyebars, so there was no redundancy in the chain. In contrast, Clifton Suspension Bridge has at minimum 10 eyebars in each segment of a single chain, of which there are three. Thus in the assessment of such a bridge the question of how significant are the eyebars is important, particularly since the main feature of the proposed method involves changing the current formula for the design yield strength of a structural component. The new formula for design yield strength given by Eq.5.2 is simply an adjusted form of the existing one, and its application marks the end point of the proposed assessment method, whose overall outline is given in Figure 5.8.

$$\text{Design yield strength} = F_c . \frac{(\text{characteristic yield strength})\ \beta}{1.2\ \alpha} \qquad \text{Eq.5.2 (repeated)}$$

where α is the significance factor of the component, β is the quality factor and F_c is the condition factor of the component.

Liverpool Lime Street Station provides another example of a structure built in part using eyebars. Each segment of the bottom chord of its roof trusses are composed of four eyebars. Another similar example is the roof of Piccadilly Railway Station in Manchester whose trusses have just two eyebars making up each segment of the bottom chord.

In the proposed method the significance of a component made up of parts is established and this knowledge is used to make a safe increase in the design yield strength of the component. This concept is not confined to wrought iron structures. It could just as easily be applied to any structural material, but the aim of its inclusion in the assessment procedure for wrought iron structures is to provide greater scope for preservation of these historic works. It other words, including the significance of components in assessment is a less conservative approach, although it involves more work for the assessing engineer. The main idea at the heart of the proposed method is that instead of applying a uniform safety factor to all components of a wrought iron structure larger factors of safety are assigned to more significant components while lower factors of safety are assigned to components of lower significance. In the design yield strength formula the significance of a component is represented by the α factor. Thus each component has a unique α factor that must be calculated in each case.

In addition to significance, the proposed method also incorporates a more informed understanding of the material by identifying different characteristic ductility values for different component types. In the proposed method ductility is used as a measure of quality and appears in the design yield strength formula as the β factor. The quality of the component is also reflected in the characteristic yield strength, which is also dependent upon component type.

9.2 Comparison of the proposed method with the current method

The assessment of Irwell Street bridge was performed using both the current method and the proposed method in order to provide a practical example of the usefulness of the new method. This example was chosen because it is a structure that was strengthened in 1926 in response to failure of some of its components. At some point it its history the bridge was loaded to the point that caused buckling and over stressing of some of its members. Given the modern traffic allowed on the bridge, a reassessment seemed to be justified and provided a good test of the method. The most concise set of results using three versions of assessment method are summarised in Table 9.1.

Member	Significance of member % And (α factor)	Full method usage factor U	Partial method usage factor U	Current method usage factor U
43 bar	0.5 (0.799)	0.16	0.10	0.11
44 bar	0.5 (0.799)	0.22	0.13	0.16
13 angle	1.1 (0.799)	0.14	0.13	0.16
14 angle	1.1 (0.799)	0.15	0.14	0.16
22 bar	1.1 (0.800)	0.06	0.04	0.04
23 bar	9.8 (0.814)	0.33	0.19	0.23
17 angle	2.2 (0.800)	0.16	0.15	0.17
24 bar	3.8 (0.804)	**1.20**	0.71	0.84
40 bar	12 (0.817)	**1.67**	0.98	**1.15**
28 bar	6.6 (0.809)	**1.39**	0.82	0.97
27 bar	48 (0.875)	**1.51**	0.92	**1.00**

Table 9.1 Results of assessment of Irwell Street Bridge

The 'Partial Method' set of results were obtained by retaining the characteristic yield strength of 220N/mm^2 in Eq.5.2, but by also including the proposed α and β factors. It can be seen from the usage factor results under the 'Current Method' that the bridge possesses members which are in limit state violation. Yet Manchester City Council has taken no further action to reduce the stress in those components. It is clear that a judgment of acceptability was made regarding this situation because those members which are over stressed are of little importance. Thus sensible engineering judgment was applied after the numerical assessment of the bridge. The proposed method strives to incorporate sensible engineering judgement into the workings of the assessment by the inclusion of the α and β factors. When this is done, while still retaining the value of 220N/mm^2 as the characteristic

yield strength (i.e. the 'Partial Method'), the conclusion is that no components violate the ultimate limit state. This effectively proves that the judgment of acceptability made by Manchester City Council was justified. It also demonstrates that incorporating significance into assessment is a less conservative approach that allows greater confidence in deciding upon the acceptability of old structures.

However, both the 'Partial' method and the 'Current' method ignore the findings of this research, that wrought iron has a lower characteristic yield strength that 220N/mm^2. When the lower values of characteristic yield strength are used the 'Full Method' results show that some members of the bridge are in violation of the ultimate limit state. The value of characteristic yield strength in this case was 151N/mm^2. To explain the apparent safety of the bridge one must apply some practical engineering observation, that so long as those over stressed members of little significance remain intact the critical component of the bridge (i.e. the bottom chord) will carry a stress no greater than 40N/mm^2, and thus the bridge as a whole is quite safe.

If the bridge is assessed for HB loading then this may result in higher stresses in some cases.

It would appear that, although the objective of the proposed method was to provide a means of assessment leading to greater acceptability of wrought iron structures, the proposed method is even more conservative than the current method. This is only because the newly determined characteristic yield strength is much lower than 220N/m^2 and not because of the α and β factors. In fact the α and β factors work well in allowing a less conservative, yet safe approach to assessment, but the lower characteristic yield strength dominates the final result. Although the proposed characteristic yield strength values for wrought iron may indicate that some members of existing structures are overstressed evidence of a widespread problem is lacking.

9.3 Practicalities in implementing the proposed method

The flow chart outlining the steps of the proposed method given in Figure 5.8 effectively shows how to apply the method to whatever structure is encountered by the assessing engineer. The most labour intensive part of the method involves the investigation of the significance of the component being assessed (i.e. calculating the α factor). Most structures are statically indeterminate, so the first decision to make is whether or not the component is critical. In other words, will the structure collapse if the component is lost? This is a relatively easy question to answer. For example, the bottom chord of a truss is a critical component when taken as a whole, but it may be composed from non critical parts (for example, one or more eyebars).

If the component being assessed (i.e. component X) is not critical then one must identify some other member that is critical, which is most influenced by the loss of component X. A computer model is essential at this stage of the assessment because it may be found that the loss of component X has little effect on the critical member. In that case it will be necessary to remove a group of members sufficient to induce an effect on the critical member. The significance of each member in the group may be determined my removing one after the other.

With regard to the β factor and the characteristic yield strength, it is not necessary for the assessing engineer to calculate these, as these values can be read directly from the database formulated during this research. (See Tables 5.3 to 5.8). Some engineers may prefer to take samples from the structure for testing of tensile strength and ductility. It is recommended that this practice is avoided, simply because it is unnecessary, as there is sufficient data available to furnish a good understanding of the mechanical properties of wrought iron. Also, because of the variability of the quality of wrought iron a small set of samples is unlikely to provide any more reliable information about the yield stress than the value

obtained from the database. But if one wishes to take samples for testing their results should be added to the database for recalculation of the characteristic material values.

Using the results of a small set of samples alone may be unsafe as it may lead to the conclusion that the structure is stronger than it actually is.

One exception to the above recommendation regarding the taking of samples for testing is in the case of rolled iron beams. The database for this component type is rather limited with just 24 test results. Table 5.8 contains a summary of these results, which largely came form the Royal Albert Hall floor joist, which as described in Chapter 3 was made from a grade of iron of poor quality.

Chapter 10 Conclusions

Summary of findings

The principal findings of this research project are summarised in order of presentation as follows:

1 Wrought iron was the dominant structural framing material in the period 1840 to 1890. It is a hand made metal that has sufficient ductility and tensile strength to make it suitable for the construction of long span structures.

2 The mechanical properties of wrought iron vary widely and resent research has shown that the characteristic yield strength of plate iron is 10% lower than the value of 220N/mm^2 stated by the UK Highway Standard BD21.

3 The occasional occurrence of low ductility precludes the use of plastic analysis in assessment of wrought iron structures as it would be unsafe.

4 Brittle failure of a rolled wrought iron beam was observed under static load and may have been caused by excessive phosphorus or strain hardening due to cold rolling. Thus ductile failure cannot be expected even though the metal is generally considered to be a ductile material.

5 In a small group of tensile tests it was found that bolt iron had greater ductility than either angle iron or plate iron. The characteristic ductility from a set of 6 tests of each component type was 22% for bolt iron, 15% for angle iron, and 7% for plate iron. The reason for bolt iron having a higher ductility is because bolts were made from a more refined grade of iron.

6 Using Charpy impact test data, it was found the that ductile to brittle transition temperature of wrought iron lies in the range 20 to 80^{o}C, whereas that of mild steel, is typically in the range -30 to 10 ^{o}C. Published data on the ductile to brittle transition temperature of wrought iron indicates that it lies in the range 40 to 80^{o}C (see Morgan 1996 and Green 1999).

7 Using the database of tensile test results a value of 10% elongation at failure was established as an acceptable value of ductility for wrought iron and that the quality of wrought iron should be based on two separate mechanical properties, namely ductility and characteristic yield strength.

8 A new assessment method was proposed that incorporates a 'quality factor' and a 'component significance factor' into the definition of design yield strength. The 'quality factor' measures the quality of a component based on the probability of it having a ductility greater than 10%.

9 Using the proposed method the newly obtained lower values of characteristic yield strength tend to dominate the final design strength value of a component. However, the inclusion of the quality and significance factors offset this effect and their inclusion was validated by proving that a safe yet not overly conservative design yield strength may be established by application of the proposed method.

These findings are discussed in more detail as follows.

1. (from Chapter 1)

Wrought iron was the dominant structural material in the period 1840 to 1890. It replaced cast iron as a beam material due to the brittleness of cast iron and its weakness in tension. Although cast iron is an excellent vibration damping material for machine construction, and is still used as such, its susceptibility to brittle fracture when used as a beam under the heavy vibration loads that occur in railway bridges made it unsuitable as a structural material for the emerging railways of the 1830's. In the early 1840's the development of the steam hammer and robust rolling mills facilitated large scale production of rolled wrought iron structural sections, such as I-beams, angle iron and plate iron. The much greater toughness, tensile strength and workability of wrought iron allowed structures of far greater span to be built. Beginning in the 1840's riveted plate and angle assembly emerged as the standard form of construction, ranging from simple beams to large span trusses, and arched girders.

The demand for structures of large span, such as train stations and ship building sheds, pushed forward the need for better understanding of the mechanical properties of structural iron. As a consequence of this need the discipline of materials science emerged, particularly during the 1860's. Universities, Governments, and even independent scientists set up materials testing laboratories.

Riveted plate and angle construction remained as the principal construction method even when steel began to replace wrought iron in the 1880's. Although steam powered machinery had increased the rate of production of wrought iron, by speeding the rate of working and rolling the metal, the bottle neck in the supply process was the puddling furnace, which was still a small scale craft, in that the puddling furnace was limited in size. To meet demand many puddling furnaces had to be run side by side, each being worked by hand, by a skilled operator. In addition, the quality of the wrought iron was in part dependent upon the skill of the operator. The greater uniformity of material properties of steel over that of wrought iron, and its greater strength and speed of high volume production made it more suitable for the greater demand and high rise construction of the 20th century. Yet many wrought iron structures from the Victorian period survive to this day and are subjected to modern traffic. This research project has endeavoured to add to existing knowledge about wrought iron structures so as to help in the assessment and preservation of such historic works.

2. (from Section 2.4)

A review of past and current assessment methods for wrought iron was conducted in Chapter 2. Under the current assessment method, the UK standard BD 21/01 'The Assessment of Highway Bridges and Structures', specifies a characteristic yield strength value of 220 N/mm^2 for wrought iron. A recent investigation into wrought iron strength reported a characteristic yield strength value of 198 N/mm^2 for plate iron. In addition, data

collected as part of the present research project indicates that the characteristic yield strength of wrought may be even lower than these values. In general the mechanical properties of wrought iron vary widely.

3. (from Section 2.4)

As an assessment method plastic analysis is deemed unsafe for wrought iron structures due to the sometimes low ductility of the metal.

4. (from Section 3.7 and 3.12)

The methods and results of the laboratory testing of wrought iron beams were covered in Chapter 3. Observations included the brittle failure of a rolled wrought iron floor joist from the Royal Albert Hall and the ductile failure of a riveted plate and angle floor beam from Edinburgh GPO.

4. (continued) (from Section 3.7, 3.14 and 1.9)

In wrought iron, sulphur is present as iron sulphide (FeS), but it tends to segregate from the ferrite at the grain boundaries. Because iron sulphide has a low melting point, it causes a lack of cohesion between the grains when the iron is heated to a red-hot temperature (Johnson 1939). This is the cause of 'red-shortness' in wrought iron, the condition where the metal cracks or crumbles when being hot worked. It may be possible that the metal from which the Albert hall joist was made, was red-short to some degree. Even thought red-shortness only becomes apparent when the metal is red-hot, lack of cohesion during rolling may have caused some lack of cohesion between the grains when the metal was cold, hence the brittle fracture of the joist.

Of all the possible impurity elements in wrought iron phosphorus has the most significant effect on mechanical properties. Elevated phosphorus content results in the condition known as 'cold shortness', which is exhibited by a higher yield strength and ultimate

strength, but low ductility and impact resistance at ordinary temperatures. It is possible that the Albert Hall joist possessed excessive phosphorus, as some of the tensile tests conducted on material from the beam had above average yield and ultimate strengths.

Another reason for the brittleness of the Albert Hall joist may be that it was rolled at too low a temperature. Cold rolling causes strain hardening and would make the metal more brittle.

Tests of the Edinburgh GPO beam indicated that the beam with timber attached was slightly stiffer than that without timber. However, the stiffness of the beam with timber attached was not so much greater as to indicate that the timber was added to enhance stiffness or strength. It is believed that the timber was attached simply as a means of providing housing for the timber floor joists. Buckling was the ultimate failure mode of this beam, however the beam yielded within the vertical plane prior to buckling.

5. (from Section 4.2)

The methods and results of mechanical tests on samples from the Edinburgh GPO beam were described in Chapter 4. These tests revealed that bolt iron had a noticeably greater ductility and strength than either plate iron or angle iron. Furthermore, angle iron had both greater strength and ductility than plate iron. Research on the manufacture of bolt and rivet iron has revealed that wrought iron used for these components went through further workings and thus was more refined (i.e. in general, the slag inclusions were fewer and smaller). This would explain the better results of the bolt iron.

6. (from Section 4.8)

Impact fracture tests were conducted on wrought iron samples over a temperature range of -20^{o}C to 90^{o}C. These tests revealed that, unlike steel, wrought iron may exhibit brittle fracture at ordinary environmental temperatures. Charpy impact tests are useful in providing a means of comparing the impact toughness of wrought iron from various

sources. Materials which are normally ductile, such as wrought iron, can exhibit brittle fracture under suddenly applied loads. For a given temperature Charpy impact energy values from various sources provide a scale by which the toughness and hence robustness of a structural component may be judged. Charpy impact energy values vary widely, and values in the range 20J - 140J at room temperature are typical, and may be regarded as satisfactory. Due to considerable scatter a distinct transition temperature was difficult to establish, but the tests showed that it lies in the range 20 to 80^{o}C. For comparison modern mild steel has a transition temperature in the range -30 to 10 ^{o}C. This indicates that under normal environmental temperatures wrought iron may be expected to exhibit brittle fracture. In practice the question of high transition temperature for wrought iron may not be as alarming as might be implied by these results. This is because in a Charpy test the metal is loaded much more quickly and severely than in a structure. Thus Charpy results underestimate the working toughness of structural wrought iron. For this reason authorities in the USA apply a shift of -20 ^{o}C to the transition temperature as an appropriate adjustment for intermediate rate loading (Sparks 2004). Even with this adjustment wrought iron may exhibit brittle fracture at room temperature. This was observed when the wrought iron joist from the Albert Hall was tested under a slowly applied load. The case of the wrought iron from the Albert Hall floor joists is probably a rather extreme one, as this material may be regarded as being of poor quality, compared with the wrought iron from the beams of Edinburgh GPO. Under static loading no brittleness was exhibited by the Edinburgh GPO beam material. Under a slowly applied load the Edinburgh GPO beams bent and ultimately twisted exhibiting the ductility normally expected of wrought iron, whereas the Albert Hall beams snapped and cracked suddenly under static loading. The two cases illustrate the variability of quality that may be encountered in structural assessment.

7. (from Section 5.2)

The variability in the quality of wrought iron is clearly demonstrated by tensile test data. Traditionally the two principal measures of quality are elastic limit and ductility, as expresses by the elongation at failure. The problem in judging quality is that some iron can have high strength with poor ductility, or low strength and high ductility. In order for a structure to be robust it must have good tensile toughness, which means the iron must have both good strength and good ductility. Morgan proposed the value of 10% elongation at failure as a lower bound for good ductility and this would seem quite reasonable. Using Kirkaldy's data, Morgan showed that, in a single tensile test, where the ductility was more than 10%, the measured ultimate strength would most likely lie within 10% of the mean ultimate strength value. This observation was not confirmed by the examination of a larger set of data collected during this research project. Ultimate tensile strength for wrought iron exhibits considerable scatter about the mean value and if one were to consider 10% as a lower bound for acceptable ductility, in addition to a deviation of 10% below the mean ultimate strength as a lower bound for acceptable strength, then only 65% of iron would be of acceptable quality. Although it would be convenient to have a single measure of quality based on both strength and ductility it would seem more prudent to continue to take strength and ductility as separate measures of quality and to judge whether a sample of iron is good or bad by requiring that both strength and ductility have a certain minimum value. 10% elongation at failure for ductility would seem a reasonable lower bound for this quantity. With regard to yield strength a lower bound is difficult to specify. It is recommended that the characteristic yield strength continue to be used for design and assessment purposes, but that the value of characteristic yield strength be based on a more detailed examination of a database of test results, and that it is dependent upon the component type. For example, bolt and rivet iron is generally of the best quality, so it should have its own characteristic yield strength value separate from other component types, such as plate iron or bar iron. Analysis of the database of tensile test results collected

during this research has revealed that the characteristic yield strength of plate iron, bar iron, and rivet iron is 187N/mm^2, 151N/mm^2, and 207N/mm^2, respectively.

8. (from Section 5.3)

In section 5.3 a new method was proposed for the assessment of wrought iron structures which is based on the significance of a component within a structure and upon the quality of the component. In this method a 'quality factor' and a 'component significance factor' were incorporated into the definition of design yield strength. The 'quality factor' measures the quality of a component based on the probability of it having a ductility greater than 10%.

9. (from Chapters 6, 7 and 8)

A number of examples of the assessment of wrought iron structures were considered for special attention in order to demonstrate the working of the proposed method. These structures included Irwell Street Bridge, Manchester, Liverpool Lime Street Railway Station, and Clifton Suspension Bridge. The findings of these case studies are discussed more fully in Chapter 9 but one of the main findings was that the newly obtained lower values of characteristic yield strength tend to dominate the final design strength value of a component. However, the inclusion of the quality and significance factors offset this effect and their inclusion was validated by proving that a safe yet not overly conservative design yield strength may be established by application of the proposed method.

References / Sources

Adams, H. (1903), 'Designing Ironwork. Second Series. Part IV.' Published by the author, 60 Queen Victoria Street, London.

Addis, W. (1983), 'A new approach to the history of structural engineering', History of Technology, Volume 8, pp.1-13. Mansell Publishing Ltd. London

AMSES. (1883), 'Memoirs of deceased members', Proceedings of the Association of Municipal and Sanitary Engineers and Surveyors. Vol.9, 1883, pp.206 - 207, E. & F.N. Spon. London

Anastassopoulos, A. (1997), 'Structural appraisal of old iron beams', MSc Dissertation, UMIST.

Anderson, Sir J. (1902), 'The Strength of Materials and Structures' Longmans, Green and Co. London.

Anonymous, (1928), 'Chain and cable failures', Mechanical world, Vol. 83, No. 2159, May 18th 1928, pg 363.

Anonymous, (1860), 'Admiralty experiments on the various makes of iron and steel', Transactions of the Institution of Naval Architects, Vol.1, pp. 169-170. London.

Appleby, P.V. (1883), 'On iron and steel in tension, compression, bending, torsion, and shear', Proceedings of the Institution of Civil Engineers, Vol. 74, Part 4, pp.258-269, students' paper, No. 159.

Astbury, S. J. (1923), 'Some uses and properties of wrought iron', Proceedings of the Institution of Mechanical Engineers, Vol.1, No.3, pp.511-516.

Arrol, W. (1877), 'Constructing wrought-iron girders etc. of large dimensions', Patent No. 1482, Obtained in ICE archives. London.

Bates, W. (1984), 'Historical structural steelwork handbook', British Constructional Steelwork Association, publication no. 11/84

Bardell, P.S. (1984), 'The origins of alloy steels', History of Technology, Volume 9, pp.1-29. Mansell Publishing Ltd. London

Barry, J.W. (1868), 'The City Terminus Extension of the Charing Cross Railway', Proceedings of the Institution of Civil Engineers, Vol. 27, Issue 1868, pp.410-430, Paper No. 1198.

Benson, R. (1967), 'Large forgings of wrought iron', Transactions of the Newcomen Society, Vol.40, pp.1-14.

Beardslee, L.A. (1879-82), 'Experiments on the strength of wrought-iron and of chain-cables', Report of the committees of the United States board appointed to test iron, steel and other metals, on chain cables, malleable iron and reheating and re-rolling wrought-iron; including miscellaneous investigations into the physical and chemical properties of rolled wrought-iron.' John Wiley and Sons, New York.

Bender, C. (1872), 'Historical sketch of the successive improvements in suspension bridges to the present time', American Society of Civil Engineers, Vol.1, pp.27-43.

Bell, W. (1856), 'On the laws of the strength of wrought and cast iron', Minutes of the Proceedings of the Institution of Civil Engineers, No. 945.

Berkley, G. (1870), 'On the strength of iron and steel, and on the design of parts of structures which consist of those materials', Minutes of the Proceedings of the Institution of civil engineers, Paper No. 1279, Vol. 30, Part 2, May 3rd 1870, pp215-255.

Berkley, J.J.. (1860), 'On Indian Railways', Minutes of the Proceedings of the Institution of civil engineers, Paper No.1025, Vol. 19, May 8th 1860, pp.586-610.

Bessemer, H. (1859), 'On the manufacture of malleable iron and steel', Institution of civil Engineers.

Bland, R. (1984), 'Brittle failure of wrought iron beams', (Letter to Verulam), The Structural Engineer.

Bhavnagri, V.S. (1995), 'Analysis and testing of an old lattice girder rail bridge' Australian Civil Engineering Transactions, Vol. CE.37, No.3, August 1995, pp 229-239

Birnstiel, C. (2003), 'Analysis of an early cable-stayed bridge collapse', Proceedings of the 2003 ASCE / SEI Structures Conference and Exposition: Engineering Smarter, 2003, p.1-7.

Bussel, M. (1997), 'Appraisal of Existing Iron and Steel Structures', SCI Publication 138, The Steel Construction Institute, Ascot.

Bussel, M., Wallis, G., Forsyth, M. (2008), 'Materials and skills for historic building conservation', Blackwell Publishing Ltd., Oxford.

Box, T. (1883), 'Strength of materials', E & F.N Spon, London.

Boller, A.P. (1876) 'Practical treatise on the construction of iron highway bridges, for the use of town committees', J. Wiley & Sons, New York.

Bolland, S. (1893), 'The Iron Founder, supplement. A complete illustrated exposition of the art of casting iron', Wiley, New York. Reprinted by Bradley, I.L., Lindsay Publications Inc (2001).

Brown, S. (1822), 'Description of the Trinity Pier of Suspension at Newhaven, near Edinburgh', The Edinburgh Philosophical Journal, Vol.6, pp.22-28.

Burnell, G.R. & Clark, W.T. (editors) (1853), 'Supplement to the theory, practice and architecture of bridges', John Weale, London.

Bruhwiler, E., Hirt, M.A., Morf, U. & Huwiler, R. (1989), 'Bewertung der Spontanbruchgefahr angerissener Bruckenbauteile aus Schweiβeisen (Fracture assessment of wrought-iron bridge members)', Stahlbau, Vol.58, No.1, pp.9-16.

Baker, B. (January 21st 1887). 'Some notes on the working stress or iron and steel'. The Engineer vol.LXIII.

Barlow, P. (1867) ‘A treatise on the strength of materials’, Lockwood and Co. London.

Barlow, W.H. (1867), 'Description of the Clifton Suspension Bridge', Session 1866-1867, Vol 26, January 1867, pages 243 - 257, paper No. 1156.

BS 7448-1:1991 'Fracture mechanics toughness tests' British Standards Institute. London.

BS 5950 (2002), 'BS 5950-1:2000 Structural use of steelwork in building - Part 1:Code of practice for design - Rolled and welded sections. PP7312 Extracts from British Standards for students of structural design 2002. British Standards Institute. London.

Carpenter, R.C. (1895), ‘The effect of length of specimen on the percentage of extension’, Transactions of the American Society of Mechanical Engineers, Vol. XVI, pg 904-912.

Carrington, H. (1924), ‘The strength properties of wrought iron, mild steel and nickel steel at high temperatures’, Engineering, Vol. 117, No. 3029, January 18th 1924, pg 69-71.

Chrimes, M. & Thomas, R. (1994), ‘Reading list on cast iron, wrought iron and steel frame construction prior to c.1930’, The Institution of Civil Engineers Library and Information Service.

Chrimes, M. (1985), ‘Bridges: a bibliography of articles published in scientific periodicals 1800-1829’, History of Technology, Volume 10, pp.217-257. Mansell Publishing Ltd. London

Chrimes, M. (2001), ‘Archives and Resources for Historical Engineering Structures. The Historical Treasures of the Institution of Civil Engineers, London’, International Engineering History and Heritage, Improving Bridges to ASCE’s 150th Anniversary. Proceedings of the Third National Congress on Civil Engineering History and Heritage, October 10th-13th 2001 Houston, Texas. American Society of Civil Engineers, Reston,Virginia.

Crossin, J., Marshall, G.R.D., Yeoell, D. (1998), ‘The refurbishment of Westminster Bridge: bridge strengthening’, The Structural Engineer, Vol.76, No.10, May 19th 1998. Institution of Structural Engineers, London.

Cullimore, M.S.G. (1986), ‘The Clifton Suspension Bridge – preservation for utilisation’, IABSE Proceedings P-100/86.

Cullimore, M.S.G., Fatigue and fracture investigation carried out on the Clifton Suspension Bridge’, Proc. ICE. Part 1, 84, (April 1988), pages 309-329.

Cullimore, M.S.G. (1967) ‘The fatigue strength of wrought iron after weathering in service’ The Structural Engineer vol. 45, May 1967, no. 5.

Cullimore, M.S.G. (1983), ‘Joints for Metal Structures’, Chapter 3 of ‘Engineering Structures: Developments in the Twentieth Century’, pp.49-75. University of Bristol Press. Bristol.

Curran, J.J. & Sanford, E.A. (1933), ‘Wrought iron, fact and opinion’, Metals and Alloys, Vol. 4, No. 1, January 1933, pg 1-5.

Cantrell, J.A. (1985), ‘James Nasmyth and the steam hammer’, Transactions of the Newcomen Society, vol p133-138.

Cantrell, J.A. (1985), 'James Nasmyth and the Bridgewater Foundry', The Chetham Society, Published for the Society by Manchester University Press.

Callister, W.D. (2000), 'Materials science and engineering an introduction', 5th Edition, John Wiley & Sons Inc. New York.

Carrington, H. (1924), 'The strength properties of wrought-iron, mild steel and nickel steel at high temperatures', Engineering, Vol. CXVII, January 18th 1924, pp.69-71.

Cookson, H.E. (1933), 'The development of rolls and rolling mills', The Newcomen Society, Presidential address to the Staffordshire Iron and Steel Institute, Mark & Moody Ltd., Stourbridge

Cooper, T. (1889), 'American railroad bridges', Transactions of the American Society of Civil Engineers', Vol.XXI, pp.1-58, (Paper No. 418).
Colburn, Z. (1863), 'On the relation between the safe load and the ultimate strength of iron', The Engineer, March 6th, 1863, pp.136-137.

Colburn, Z. (1863), 'American Iron Bridges', Proceedings of the Institution of Civil Engineers, vol.22, pp.540-556 and discussion pp.557-573. Paper no.1091.

Cowper, E.A. (1854), 'Description of the wrought iron roof over the central railway station at Birmingham', Proceedings of the Institution of Mechanical Engineers, Vol.5, pp.79-87.

Cowper, E.A. (1854), 'Description of the iron roof in one span over the joint railway station New Street, Birmingham', Proceedings of the Institution of Civil Engineers, Vol.14, pp.264-272.

Clark, C. (1993), 'Ironbridge Gorge', B.T. Batsford Ltd. / English Heritage, London

Cywinski, Z. (1985), 'Simplified evaluation of wrought iron bridges', Stahlbau, Vol.54, No.4 April 1985, pp.103-106.

Day, T. (1983), 'Samuel Brown: His influence on the design of suspension bridges, History of Technology, Volume 8, pp.61- 90. Mansell Publishing Ltd. London
(This article also appeared in 'Structural Iron 1750-1850' edited by R.J.M. Sutherland 1997)

Davies, T. (1857), 'Experiments on wrought iron beams', Journal of the Franklin Institute, Vol. 63. Issue 4, April 1857, pp 271-278. Taken from the London Civil Engineer and Architect's Journal, January 1857.

Davies, M.W. (1908), 'The theory and practice of bridge construction in timber, iron and steel' Macmillan and Co. Ltd., London.

DeLony, E. (1996), 'The Bollman Bridge at Savage, Maryland: Restoring America's quintessential metal truss', APT Bulletin, Vol.27, No.1/2, A tribute to Lee H. Nelson. pp.24-31

DeLony, E. (1993), 'Surviving cast- and wrought-iron bridges in America', IA: Journal of the Society for Industrial Archaeology, vol.19, no.2, pp.17-47. The Society for Industrial Archaeology, Washington, D.C.

DeLony, E. (2001), 'Documenting historic bridges', International Engineering History and Heritage, Improving Bridges to ASCE's 150th Anniversary. Proceedings of the Third National Congress on Civil Engineering History and Heritage, October 10th-13th 2001 Houston, Texas. American Society of Civil Engineers, Reston,Virginia.

Dempsey, G. D. (1857). 'The practical railway engineer'. 4th Edition. John Weale. London

Den Ouden, A. (1981), 'The production of wrought iron in finery hearths: Part 1, Historical Metallurgy, Vol. 15, No. 2, pg 63-87. Historical Metallurgy Society Limited.

Den Ouden, A. (1982), 'The production of wrought iron in finery hearths: Part 2, Historical Metallurgy, Vol. 16, No. 1, pg 29-32. Historical Metallurgy Society Limited.

Dept. of Transport (2001), 'The assessment of highway bridges and structures, Departmental standard BD 21/01'.

Diestelkamp, E.J. (1982), 'Richard Turner and the palm house at Kew Gardens', Transactions of the Newcomen Society, Vol. 54. pp.1-26.

Doran, D.K. (ed) (1992), 'Construction Materials Reference Book', Butterworth-Heinemann.

Driver, C.H. (1874), 'On iron as a constructive material', Transactions of the Royal Institute of British Architects, pp 165-168.

Ebbing, D.D. (1996), 'General Chemistry', 5th Edition, Houghton Mifflin Company, Boston.

Edwards, L.N. (1932), 'The evolution of early American bridges', Transactions of the Newcomen Society, Vol. 13,

Elban, W.L., Borst, M.A., Roubachewsky, N.M., Kemp, E.L. & Tice, P.C. (1998), 'Metallurgical assessment of historic wrought iron: U.S. Custom House, Wheeling, West Virginia', APT Bulletin, Vol. 24, No. 1, pg 27-34.

Epps, F.A. & Jones, E.O. (1917), 'Influence of high temperature upon the elastic and tensile properties of wrought iron', Metallurgy and Chemical Engineering, Vol. XVII, July 15th 1917, pg 67-71. McGraw-Hill Publishing Company, New York.

Fairbairn, W. (1850), 'An experimental inquiry into the strength of wrought-iron plates and their riveted joints as applied to ship-building and vessels exposed to severe strains', Philosophical Transactions of the Royal Society, Vol. 140, pp 677-725.

Fairbairn, W. (1864), 'Iron its history, properties, & processes of manufacture', Adam and Charles Black, Edinburgh

Fairbairn, W. (1864), 'Experiments to determine the effect of impact, vibratory action and long continued changes of load on wrought iron girders', Philosophical Transactions of the Royal Society, Vol. 154, pp 311-325.

Fairbairn, W. (1870), 'On the application of cast and wrought iron to building purposes', 4th Edition, Longmans, Green & Co., London.

Fairbairn, W. (1857), ‘On the tensile strength of wrought-iron at various temperatures’, From the Report of the British Association for the Advancement of Science for 1856. Taylor and Francis, London.

Flint, A.R. & Pugsley, A.G. (1955), 'Some experiments on Clifton Suspension Bridge. Correlation between calculated and observed stresses and displacements in structures'. Institution of Civil Engineers, London, Paper No.8. pp124-134.

Gale, W.K.V. (1977), ‘Historic Industrial Scenes Iron and Steel’, Moorland Publishing Company, Buxton.

Gale, W.K.V. (1969), ‘Iron and Steel’, Longmans, Green and Co. Ltd. London.

Gale, W.K.V. (2002), ‘Ironworking’, Shire Album 64, Shire publications Ltd., (First published in 1981)

Gale, W.K.V. (1966), ‘The Black Country iron industry a technical history’, The Iron and Steel Institute, London.

Gale, W.K.V. (1963), ‘Wrought iron –A Valediction’, Transactions of the Newcomen Society, vol 36

Gale, W.K.V. (1964), ‘The rolling of iron’, Transactions of the Newcomen Society, vol.37, pp.35-46.

Gasparini, D.A. & Provost, C. (1989), ‘Early Nineteenth Century developments in truss design in Britian, France and the United States’, Construction History, Vol. 5, pg 21-33.

Gere, J.M. & Timoshenko, S.P. (1999), 'Mechanics of Materials' 4th SI Edition, Stanley Thornes Ltd. Cheltenham.

Gibbons, C.H. (1934), ‘History of testing machines for materials’, Transactions of the Newcomen Society, Vol.15, pp.169-184

Goodwyn, H. (1844), ‘Memoir on wrought-iron roofing’, G.H. Huttmann, Bengal Military Orphan Press, Calcutta.

Gordon. R.B. (1996), ‘American Iron 1607-1900’, The Johns Hopkins University press, Baltimore

Gordon. R.B. (1984), ‘The quality of wrought-iron evaluated by microprobe analysis’, Microbeam Analysis 1984 – Proceedings of the 19th annual conference of the microbeam analysis society, Bethlehem, Pennsylvania, 16-20 July 1984. Edited by A.D. Romig and J.I. Goldstein, San Francisco press, Inc. San Francisco.

Gordon. R.B. (1988), ‘Strength and Structure of Wrought Iron’, Archeomaterials Vol. 2, No. 2, pp 109-137.

Gordon. R.B. & Knopf, R. (2005), ‘Evaluation of wrought iron for continued service in historic bridges’, Journal of Materials in Civil Engineering, Vol. 17, No. 4, August 2005, pg 393-399. American Society of Civil Engineers.

Gough, H.J. & Murphy, A.J. (1931), ‘The nature of defective laminations in wrought-iron bars and chain links’, The Journal of the Iron and Steel Institute, Vol. CXXIII, No.1, pg 285-311, published at the offices of the Institute, London.

Gough, H.J. & Murphy, A.J. (1928), 'The causes of failure of wrought-iron chain and cable', Proceedings of the Institution of Mechanical Engineers', No.2, April 1928, pp.293-352.

Green, P.S., Connor, R.J., Higgins, C. (1999), 'Rehabilitation of a nineteenth century cast and wrought iron bridge' Proceedings of the 1999 Structures Congress, pp.259-262.
See also the website: http://users.ce.ufl.edu/~historic/WSB_HomePage/walnutframe.htm for an good account of the restoration work.

Griggs, F.E. (2001), 'Restoration of cast and wrought-iron bridges', International Engineering History and Heritage, Improving Bridges to ASCE's 150th Anniversary. Proceedings of the Third National Congress on Civil Engineering History and Heritage, October 10th-13th 2001 Houston, Texas. American Society of Civil Engineers, Reston,Virginia.

Grundy, P. (1986), 'Capacity of a wrought iron lattice girder bridge after 117 years of service', Transactions of the Institution of Engineers, Australia, Civil Engineering, Vol. CE28, No.2, April 1986, pp.195-200.

Hackney, W. (1884) 'The adoption of standard forms of test-pieces for bars and plates', Proceedings of the Institution of Civil Engineers, Vol.76, Part 2, pp.70-90.

Hall, J.W. (1927), 'The making and rolling of iron', Transactions of the Newcomen Society, vol.8, pp.40-55.

He, F. (2004), 'An investigation into structural wrought iron and wrought iron eye-bars', MSc Dissertation, UMIST.

Hendry 1998 (see section 6.12a)
Hertzberg, R.W. (1996), 'Deformation and fracture mechanics of engineering materials', 4th Edition, John Wiley & Sons, New York.

Higgins, J.H. (1930), 'Investigation of the effect of phosphorus in wrought iron', Contained in Appendix II of the report of committee A-2 on wrought iron, Proceedings of the annual meeting of the American Society for Testing Materials, Part 1, June 23-27, 1930, pp.159-186.

Holley, A.L. (1879), 'The strength of wrought iron as affected by its composition and its reduction in rolling', Transactions of the American Institute of Mining Engineers, Vol. 6, pp. 101-124.

Hopkins, H.J. (1970), 'A span of bridges', David and Charles Ltd., Newton Abbot.

Howard, J.E. (1883), 'Reports of tests on the strength of structural material made at the Watertown Arsenal, Mass., during the fiscal year ending June 30, 1883',

Humber, W. (1870), 'A complete treatise on cast and wrought iron bridge construction including iron foundations', 3rd Edition, Vol.1. Lockwood & Co. London.

Hume, I.J. (1997), 'The structural engineer in conservation', The Structural Engineer, vol. 75, No. 3, 4th February, p 33-37.

Hum-Hartley, (1978), 'Nondestructive testing for heritage structures, APT Bulletin, Vol.10, No.3, pp.4-20. Department of Indian and Northern Affairs, Canada. Association for Preservation Technology (APT).

Hunt, A.E. (1891), 'The tests and requirements of structural wrought-iron and steel', Transactions of the American institute of mining engineers'

Hutchinson, E. (1879), 'Girder making and the practice of bridge building in wrought iron', E. & F.N. Spon, London.

Jackson, A.A. (1998), 'The development of steel framed buildings in Britain 1880-1905', Construction History, Vol. 14, pp 21-40.

James, J.G. (1980), 'The evolution of iron truss bridges to 1850', Transactions of the Newcomen Society, Vol. 52, pp.67-101.

James, J.G. (1986), 'The origins and worldwide spread of warren-truss bridges in the mid-nineteenth century. Part 1. Origins and early examples in the UK', History of Technology, Vol.11, pp.65-123, Mansell Publishing Limited, London

James, J.G. (1982), 'Russian iron bridges to 1850', Transactions of the Newcomen Society, Vol.54, pp.79-104.

Jameson, A.H. (1897), 'Testing the strength of materials', Proceedings of the Institution of Civil Engineers, Vol.134, Part 4, pp.352-362, Student's Paper No. 400.

Jeffrey, R., Seager, J. & Woodhead, J.H. (1959), 'The mechanical properties of wrought iron', Safety in Mines Research Establishment, Research report No. 154, Ministry of Power.

Johnson, W.R. & Reeves, B. (1837), 'Report of the Committee of the Franklin Institute of the State of Pennsylvania on the explosion of steam boilers, of experiments made at the request of the Treasury Department of the United States, Part II, containing the report of the Subcommittee to whom was referred the examination of the materials employed in the construction of steam boilers', Journal of the Franklin Institute, Vol.19. February - pp. 75-109, March - pp157-193, April - pp241-277, May - pp325-361, June - pp409-451. Vol. 20. July - pp.1-31, August - pp73-113.

Johnson, W.R. (1839), 'Experiments on two varieties of iron manufactured at the Adirondack Works, directly from the magnetic ore of McIntyre, Essex County, New York', American journal of science, Vol.66, pp.94-105.

Johnson, J.B. (1939), 'Johnson's materials of construction' Rewritten and revised by M.O. Withey & J. Aston, 8th Edition, John Wiley & Sons Inc. New York.

Jones, S.K. (1981), 'A link with the past. History of Newbridge Works of Brown, Lenox and Co, Pontypridd', Glamorgan Historian vol. 12, 1981, p27-45, edited by Stewart Williams.

John, A.H. & Williams, G., editors (1980), 'Glamorgan County History', Vol V, Industrial Galmorgan from 1700 to 1970, Glamorgan County History Trust Limited, University of Wales Press, Cardiff. (Page 232 gives a brief reference to the early work of Brown and Lenox).

Kemp, E.L. (1973), 'Ellet's contribution to the development of suspension bridges', Engineering Issues, Vol.99, No.PP3, pp.331-351. The American Society of Civil Engineers.

Kemp, E.L. (1979), 'James Finley and the modern suspension bridge, Long span suspension bridges: History and performance. Sessions 70 & 78, ASCE National Convention, Boston, Massachusetts, April 2-6 1979, pp.1-38.

Kemp, E.L. (1979), 'Links in a chain: The development of suspension bridges 1801-70', The Structural Engineer, Vol.57A, No.8, August 1979. Institution of Structural Engineers, London.

Kemp, E.L. (1977), 'Samuel Brown: Britain's pioneer suspension bridge builder', History of Technology, Vol.2, pp.1-37, Mansell Publishing Limited, London

Kennedy, A.B.W. (1880), 'Mild steel and its applications to building purposes', Transactions of the Royal Institute of British Architects, p162-172.

Kennedy, A.B.W. (1886), 'The use and equipment of engineering laboratories', Minutes of the proceedings of the Institution of Civil Engineers, Vol.88, Part 2, pp.1-80. Session 1886-1887, (Paper No.2204). (This paper gives a list of the principal university engineering laboratories in Europe and America at that time).

Keating, P.B., Fisher, J.W., Yen, B.T. & Frank, W.J. (1984), 'Fatigue behaviour of welded wrought-iron bridge hangers', Transportation research record, Vol.2, pp.113-120

Kohn, F. (circa 1868), 'Iron and steel manufacture', Published by William Mackenzie, London.

Kontos, N. (1996), 'Investigation of wrought iron as a structural material', MSc Dissertation, UMIST.

Kirkaldy, D. (August 8th 1873) 'Riveting' The Engineer, vol. 36. pg 86

Kirkaldy, D. (1866), 'Results of an experimental inquiry into the tensile strength and other properties of various kinds of wrought iron and steel', 2nd Edition, Hamilton Adams & Co., London and Simpkin, Marshall & Co., London.

Kirkaldy, D. (1876), 'Results of an experimental inquiry into the relative properties of wrought-iron plates manufactured at Essen, Rhenish Prussia, and Yorkshire, England', Kirkaldy Testing and Experimenting Works, London.

Kirkaldy, W. G. (1891), 'Illustrations of David Kirkaldy's system of mechanical testing as originated and carried on by him during a quarter of a century'. Obtained from the Institution of Civil Engineers archives.

Kirkaldy, D. (1875), 'David Kirkaldy, Testing and Experimenting Works, 99 Southwark Street, London' (Publicity Brochure)
Gives information on the kind of work carried out, and details of the contents and layout of the building.

Kirk, H. (May 11th 1877). 'On Homogeneous iron, and the degree of homogeneity to be expected in iron produced by various systems of puddling and subsequent working'. The Engineer vol. 43 pg 329.

Knapton, J., Johnson, M. & Leach, T. (1993), 'An investigation into the iron bridge, Cragside, Northumberland', Construction Repair, Vol. 5, No. 5. Sep/Oct. Palladian Publications.

Lanza, G. (1887), 'Notes on the Engineering Laboratories of the Massachusetts Institute of Technology', Minutes of the Proceedings of the Institution of Civil Engineers, Part 1, Volume 91, Session 1887-1888, pp 347-365, (Paper no. 2245).

Latham, J.H. (1858) 'The Construction of wrought iron bridges' Macmillan and Co. London.

Lamb, R.H. (2008), 'The use of riveting in the refurbishment of Hercilio Luz Bridge, Brazil', The Structural Engineer, November 4th 2008, Vol 86, No. 21, p33-36. Institution of Structural Engineers, London.

Love, G.H. (1852), 'Memoire sur la resistance du fer et de la fonte et l'emploi de ces metaux dans les constructions', Carilian-Goeury et V. Dalmont, Paris.

Magaziner, H.J. (1986), 'The rebirth of an engineering Landmark' , APT Bulletin, Vol.18, No.4, pp.52-64. Association for Preservation Technology.

Manchester Corporation (1907), Old bridge record ledger, 'Bridges over the Irwell Book 1 of 2' dated 1907).

Marshall, C.A. (1887), 'Compressive strength of steel and iron', Transactions of the American Society of Civil Engineers, Vol. XVII, paper no.364, August 1887, American Society of Civil Engineers, New York.

Marine, (1938), 'Physical properties of welds in wrought iron', Marine Engineering and Shipping Review, Vol. 43, No.6, June 1938, pp. 270-275.

Marine, (1937), 'Welding wrought iron', Marine Engineering and Shipping Review, Vol. 42, No.7, July 1937, pp. 377-379.

M.I.T. (1894), 'Tests of engineering materials made at the Massachusetts Institute of Technology, 1887-1894, Technology Quarterly and Proceedings of the Society of Arts, Vol. VII, July, 1894. This book is located in the archives of the Institution of Civil Engineers, London.

Matheson, E., (1873) 'Works in Iron: Bridge and Roof Structures', E. & F. N. Spon, London.

Matheson, E., (1882) 'Steel for structures', Minutes of Proceedings of the Institution of Civil Engineers, paper no. 1851, Vol. 69, Part 3, 28th February 1882, pp 1-23.

Maw, W.H. & Dredge, J. (1872), 'Modern examples of road and railway Bridges', Published at the offices of 'Engineering', London
(Full text available at http://bridges.lib.lehigh.edu/BookListpage.html)

Mckibben, F.P. (1912), 'Tests of wrought iron girders- A study', The Engineering Record, Building Record and Sanitary Engineer, Vol. 66, No. 8, 24th August 1912, pg 200-204.

Miller, G. (2006), ‘Union Chain Bridge: Linking engineering’, Proceedings of the Institution of Civil Engineers, Civil Engineering vol.159, May 2006, pp.88-95, Paper No.13981.

Mills, A.P. (1911), ‘The Old Essex-Merrimac Chain Suspension bridge at Newburyport, Massachusetts, and tests of its wrought iron links after 100 years in service’, Engineering News Vol 66, No. 5 pp.129-32. Also see Cornel Civil Engineer.

Mitchell-Baker, D., Cullimore, M.S.G. (1988), 'Operation and maintenance of the Clifton Suspension Bridge', Proceedings of the Institution of Civil Engineers, Part 1, vol. 84, Issue 2, April 1988, p291-308, paper No. 9216.

M.I.T. (1897), ‘Tests of engineering materials made at the Massachusetts Institute of Technology, 1887-1897, Compiled from *Technology Quarterly*, Society of Arts, Massachusetts Institute of Technology. This book is located in the archives of the Institution of Civil Engineers, London.

Mott, R. A. (1978), ‘Dry and wet puddling’. Transactions of the Newcomen Society, vol. 49, p153-158.

Morgan, J.E. (1996), ‘The wrought-iron of the S.S. Great Britain’, Royal Institute of Naval Architects, conference proceedings, Historic Ships Design, Restoration & Maintenance.

Morgan, J.E. (1999), ‘The strength of Victorian wrought iron’, Proceedings of the Institution of Civil Engineers (Buildings and Structures), November, v34, p295-300.

Moreland, R. (1884), ‘Constructional ironwork for buildings’, Minutes of Proceedings of the Institution of Civil Engineers, Students paper no. 176, Vol. 77, Part 3, pp281-296.

Moreno, J. & Valiente, A. (2004), 'Stress intensity factors in riveted steel beams', Engineering Failure Analysis, Vol.11, Issue 5, October 2004, pp.777-787

Morton, G.R. & Birt, R.G. (1974), ‘The present day production of wrought iron’, Historical Metallurgy: Journal of the Historical Metallurgy Society, Vol. 8, pg 96-102.

Moy, S.S.J., Clarke, H.W.J., Bright, S.R. (2009), 'The engineering properties of Victorian structural wrought iron', Proceedings of the Institution of Civil Engineers (Construction Materials 162), February 2009, Issue CM1, p1-10. Paper No. 800031.

Moy, S.S.J., Clarke, H.W.J., Bright, S.R., Bussell, M. (2012), 'Disscussion: The engineering properties of Victorian structural wrought iron', Proceedings of the Institution of Civil Engineers (Construction Materials 165), August 2012, Issue CM4, p255-257. Paper No. 1000050.

Mumford, W.T. (1860), ‘Lloyd’s experiments upon iron plates and modes of riveting applicable to the construction of ships’, Transactions of the Institution of Naval Architects, Vol 1, pp. 99-104. London

Napier, Robert & Sons (1859), ‘Description of experiments on the comparative strength, &c., of steel and wrought iron, Transactions of the Institution of Engineers in Scotland, vol. 2, 1858-9, p 134-163 + plates.

Nasmyth, J. (ed. Smiles, S.) (1883), ‘James Nasmyth, Engineer: an autobiography’, John Murray, London.

Nasmyth, J. (1842), ‘Experiments on the tenacity of wrought iron’, The Civil Engineer and Architect’s Journal, Vol.5, 1842, pp 285-287.

Needham, J. (1971), ‘Science and Civilization in China Vol.4’, Cambridge University Press. Cambridge.

Nicholson, P.(1828), ‘Nicholson’s New Carpenters Guide’, Jones & Co., London.

Nieuwmeijer, G.G. (2003), ‘The maintenance of historic iron and steel structures: Repair techniques, Advances in Architecture, Vol.15, Structural studies, repairs and maintenance of heritage architecture, VIII 2003, pp.697-704

O'Sullivan, M. & Swailes, T. (2008), 'A study of historical test data for better informed assessment of wrought iron structures', Proceedings of the sixth international conference on structural analysis of historic construction, 2-4 July 2008, Bath, U.K. Structural analysis of historic construction: Preserving safety and significance, Vol 1, pp.207- 215 ,CRC Press, Taylor & Francis Group, London.

Pallant, J. (2010), 'SPSS survival manual: a step by step guide to data analysis using SPSS', 4th Edition, McGraw-Hill, Maidenhead.

Popplewell, W.C. (1901) ‘Experimental Engineering : a treatise on the methods and machines used in the mechanical testing of materials of construction, Vol.2, Testing and strength of materials of construction’, The Scientific Publishing Company, Manchester.

Paget, F.A. (1864), ‘Iron and how it is affected’, The Engineer, May 14th 1864, pp.353

Parmenter, M. (1996), ‘An investigation of the strength of cast iron beams’, PhD Thesis, UMIST.

Pankowski, R. (1959), ‘Contribution a l’etude du crochet et du palier a la limite elastique dans les fers vieillis apres la deformation (Contribution to the study of yield point in wrought irons aged after deformation)’, ATB Metallurgie, Vol.1, No.8, pp.207-216.

Paxton, R.A. (1978), ‘Menai Bridge (1818-1826) and its influence on suspension bridge development’, Transactions of the Newcomen Society, Vol. 49, pp.87-110.

Picton, J.A. (1880), ‘Iron as a material for architectural construction’, Transactions of the Royal Institute of British Architects, pp.149-161.

Pite, B., Baggallay, F.T., Searles-Wood, H.D., & Sprague, E. (1910), ‘Building Construction’ Volume 1, Longmans, Green and Co. London.

Petroski, H. (1992), ‘The Britannia Tubular Bridge’ American Scientist, Vol. 80 May/June (1992) pp 220-224. Published by Sigma Xi
Peterson, C.E. (1980), ‘Inventing the I-beam: Richard Turner, Cooper & Hewitt and Others’, Bulletin of the Association for Preservation Technology, Vol.12, No.4, pp.3-28.

Peterson, C.E. (1993), ‘Inventing the I-beam, Part II: Richard William Borrow at Trenton and John Griffen of Phoenixville, Bulletin of the Association for Preservation Technology, Vol.25, No.3/4, pp.17-25.

Platt, J. & Hayward, R.F. (1887), 'Experiments on the strength of iron and steel in shear and torsion', Minutes of Proceedings of the Institution of Civil Engineers, Students' paper no. 227, Vol. 90, Part 4, pp 382-413.

Prichard, H. S. (1916), 'The effects of straining structural steel and wrought iron', Transactions of the American Society of Civil Engineers, Paper No. 1370.

Pope, T. (1811), 'A treatise on bridge architecture', printed by Alexander Niven, New York.

Porter, G. (1974), 'Brunell and the design of the Clifton Suspension Bridge', Proc. ICE, Vol. 56, Issue 3, August 1974, pages 303 - 321, Paper No. 7724.

Pugsley, A.G. (1944), 'The history of structural testing', The Structural Engineer, Dec 1944. pp 492-505.

Rankine. W.J.M. (1872), 'A manual of Civil Engineering', 8th Edition, Charles Griffin and Company, London

Rankine. W.J.M. (1895) 'A Manual of Applied Mechanics' 14th Edition, Charles Griffin and Company Ltd., London.

Rankine. W.J.M. (1869) 'A Manual of Machinery and Millwork', Charles Griffin & Co., London.

Rankine, W.J.M. & others (1863) 'Discussion of paper by David Kirkaldy', Transactions of the Institution of Engineers in Scotland, Vol. 6, pp. 27-51.

Rawdon, H.S. (1917), 'Some unusual features in the microstructure of wrought iron', Bulletin of the American Institute of Mining Engineers, No. 129, September 1917, pp1345-1363.

Rawdon, H.S. & Epstein, S. (1924), 'The nick-bend test for wrought iron' Technological papers of the Bureau of Standards No. 252, part of Vol.18. Dept. of Commerce, Government printing office. Washington.

Rennie, G. (1818) 'Account of experiments made on the strength of materials', Philosphical Transactions of the Royal Society of London, Vol. 108. pp. 118-136. The Royal Society.

Rees, A. (c.1800), 'The Cyclopaedia; or Universal dictionary of Arts, Sciences and Literature', Longman, Hurst, Rees, Orme & Brown, Paternoster Row.

Richards, C.B. (1874), 'Experiments on the tensile strength of bar-iron and boiler plate' Transactions of the American Society of Civil Engineers, Vol. LXXIV, pp.339-348.

Richardson, L.T. (1920), 'Influence of enclosed slag on the corrosion of wrought iron', Transactions of the American Electrochemical Society, Vol. 37, pp 529-541.

Rodionov, D.P., Schastlivtsev, V.M., Filippov, Yu.I. (2004), 'Structural and mechanical properties of Ural wrought iron', Physics of Metals and Metallography, Vol. 97, No. 1, pp. 82-88.

Roe, J.P. (1913), 'The manufacture of wrought iron', Iron Trade Review, February 6th 1913, pg 353-360.

Rowlandson, T.S. (1864), 'History of the steam hammer: a lecture with illustrations', reprinted from the *Eccles Advertiser* of 17th December 1864. Shuttleworth, Stationer & Co.

Ruddock, Ted (2002), 'Some iron suspension bridges in Scotland 1816-1834 and their origins', The Structural Engineer, Vol.81, Issue 5, March 4th 2003. Institution of Structural Engineers, London.

Salmon, E.H. (1945), 'Materials and Structures. Volume 1. The elasticity and strength of materials', Longmans, Green and Co. London.

Salvadori, M., Levy, M. (1981), 'Structural Design in Architecture', 2nd Edition, Prentice-Hall, Englewood Cliffs, New Jersey

Sauveur, A. (1907), 'The structure of wrought iron', Electrochemical and metallurgical industry, Vol. V, No. 4, April 1907, pg 119-120.

Scoffern, J. & others. (1866), 'The useful metals and their alloys', Houlston and Wright, London

Skelton, H.J. 1924. Economics of iron and steel. 2nd Edition. London

Smith, S. (1992), 'The design of structural ironwork 1850-1890: Education, Theory and Practice', Construction History: Journal of the Construction History Society, Vol. 8, 1992, pp 89-108.

Smith, C.A.M. (1911), 'A handbook of testing materials', Constable & Company Ltd., London.

Smith, D. (1980), 'David Kirkaldy (1820-1997) and Engineering Materials testing', Transactions of the Newcomen Society, Vol. 52.

Smith, D. (1976), 'Structural model testing and the design of British railway bridges in the Nineteenth Century', Transactions of the Newcomen Society, Vol. 48.

Smith, D. (1977), 'The use of models in nineteenth century British suspension bridge design', History of Technology, vol.2, pp.169- 214 , Mansell Publishing Ltd. London.

Smith, S. (1992), 'The development and use of the tubular beam', History of Technology, Volume 14, pp.100-134. Mansell Publishing Ltd. London

Steude, T. (2000), 'The strength of wrought iron and early mild steel beams', MSc Dissertation, UMIST

Steele, J.D. (1873), 'Test of bridge irons', Transactions of the American Society of Civil Engineers. Vol. LVIII, pp.223-227.

Stevenson, R. (1821), 'Description of bridges of suspension', The Edinburgh Philosophicaal Journal, Vol.5, No.10, October 1821, pp.237-256.

Steinman, D.P. (1922), ‘A practical treatise on suspension bridges, their design construction and erection', John Wiley & Sons Inc. New York.Stillman, H. (1894), ‘Structural changes in wrought iron’, The Practical Engineer, June 22 1894, pg 479-480.

Swailes, T. & de Retana, E. (2004), ‘The strength of cast iron columns and the research work of Eaton Hodgkinson (1789-1861)’, The Structural Engineer, 20th January 2004.

Swailes, T. (2006), ‘Guide for practitioners, Scottish Iron Structures’, Historic Scotland, Edinburgh.

Swailes, T. & Marsh, J. (2005), ‘Development of long-span iron roof structures in Britain’, Proceedings of the Institution of Civil Engineers, Structures and Buildings 158, pp.321-339, Paper No.13908.

Scrivenor, H. (1967), ‘History of the iron trade’, Frank Cass & Co. Ltd., London. (This is a reprint of the second edition of the book which was published in 1854 by Longman, Brown, Green, and Longmans. London)

Schubert, H.R. (1957), ‘History of the British iron and steel industry’, Routledge & Kegan Paul, London.

Badoux, M.E. & Sparks, S.P. (1998), ‘Non-destructive evaluation of a historic wrought-iron truss bridge in New Braunfels, Texas’, APT Bulletin, Vol. 24, No. 1, pg 5-10.

Sparks, P. (2004), ‘Guide to evaluating historic iron & steel bridges’ Report prepared for the Texas Department of Transportation, Sparks Engineering Inc.

Sproule, G. (1933), ‘Primitive wrought iron manufacture’, Metals and Alloys, Vol. 4, pg 144-146.

Styffe, K. (1869), ‘Iron and steel : the elasticity, extensibility, and tensile strength of iron and steel’, John Murray, London.

Sutherland, R.J.M. (ed), (1997), ‘Structural Iron, 1750-1850’, Ashgate Publishing Ltd. Aldershot

Sutherland, R.J.M. (1992), ‘Wrought iron’ Chapter 4 of Construction Materials Reference Book’, Butterworth-Heinemann, Edited by D.K. Doran.

Sutherland, R.J.M. (1964), ‘The introduction of structural wrought iron’, Transactions of the Newcomen Society, v36, p67-84.

Sutherland, R.J.M. (1990), ‘The impact of structural iron in France’, The Structural engineer, vol.68, No.14, 17th July, p279-282.

Sutherland, R.J.M. (1994), ‘Active engineering history’, The Structural engineer, vol.72, No.13, 5th July, p205- 216.

Sutherland, R.J.M. (1988), ‘Shipbuilding and the long-span roof’, Transactions of the Newcomen Society, vol.60, pp.107-126..

Tesche, O.A. (1941), ‘Wrought iron viewed as an iron-phosphorus alloy’, Metal Progress, Vol. 39, No.3, March 1941, pg 338-339.

Timoshenko, S.P. (1953), 'History of strength of materials', McGraw-Hill Publishing Company, London.

Tipper, C.F. (1962), 'The brittle fracture story', Cambridge University Press, Cambridge.

Tredgold, T. (1842), 'Practical Essay on the strength of cast iron and other metals', 4th Edition, John Weale, London

The Tech. (1925), Professor-Emeritus Gaetano Lanza. *The Tech*. Monday. September 28th. 1925. Cambridge: Massachusetts Institute of Technology.

The Tech. (1928), Obituary of Gaetano Lanza. *The Tech*. Friday. March 23rd. 1925. Vol. XLVIII. No.19. Cambridge: Massachusetts Institute of Technology.

Trinder, B. (1974), 'The Darbys of Coalbrookdale', Phillimore & Co. Ltd., Chichester.

Thurston R.H. (March 7th 1873). 'Tensile strength of American and English iron and steel'. The Engineer, vol. 35. pg 138. (Extract from the Journal of the Franklin Institute, Oct 1871)

Thurston R.H. (1874), 'On the mechanical properties of materials of construction', Journal of the Franklin Institute, Vol. 97, issue 6, June 1874, pp 419-430 continued in Vol. 98, Issue 1, July 1874 pp 47-66.

Thurston R.H. (1894), 'A treatise on Iron and Steel. Part II Materials of Engineering' 6th Edition, John Wiley & Sons, New York.

Thorneycroft, G.B. (1850), 'On the manufacture of malleable iron; with the results of experiments on the strength of railway axles', Proceedings of the Institution of Civil Engineers, Vol.9, pp.294-300, Paper No. 828.

Tilly, G. (2002), 'Conservation of Bridges', Spon Press, London

Todhunter, I. (1960), 'A history of the Theory of Elasticity and of the strength of Materials', vol II, Part 1, Dover Publications Inc. New York. (This is a reprint of the volume which originally appeared in 1893 and published by Cambridge University Press)

Traill, T.W. (1890) 'Boilers, marine and land: their construction and strength', Charles Griffin and Company, London.

Turner, T. (1908), 'The Metallurgy of Iron' 3rd Edition, Charles Griffith & Company Ltd. Strand.

Twelvetrees, W.N. (1900), 'Structural iron and steel', Whittaker & Co. London.

Unwin, W.C. (1910), 'The testing of materials of construction', Longmans, Green & Co., London, 3rd Edition.

Unwin, W.C. (1869), 'Wrought iron bridges and roofs', E. & F.N. Spon, London.

Unwin, W.C. (1887). 'A new view of the resistance of materials'. The Engineer vol LXIII. January 7th 1887, pp.2.

Vogel R.M. & Shayt, D. (1981), ‘Creusot steam hammer: an international historic mechanical engineering landmark’. American Society of Mechanical Engineers, commemorative brochure.

Walker, R. (2002), ‘The production, microstructure and properties of wrought iron’, Journal of Chemical Education, Vol. 79, No. 4, April 2002

Walmisley, A.T. (1888), 'Iron Roofs', 2nd Edition, E. & F.N. Spon, London

Wallis, G. & Bussel, M. (2008), 'Materials and skills for historic building conservation', Edited by Forsyth, M., Blackwell Publishing Ltd., Oxford.

Warburton, B. (1971), ‘Eaton Hodgkinson (1789-1861) and the science of strength of materials’, PhD thesis, UMIST.

Warren, W.H. (1894), ‘Engineering construction in iron, steel and timber’, Longmans, Green & Co. London

Watertown Arsenal (1883-1893), ‘Report of tests on the strength of structural material made at the Watertown Arsenal, Massachusetts. (Reports appeared as annual volumes). The ICE library has volumes for 1883 to 1896 inclusive.

Watkins, J.E. (1890), 'Development of the American rail and track', The Engineer, October 17th 1890, pp.319-322.

Williams, G & John, A.H. (1980), ‘Glamorgan County History. Volume V: Industrial Glamorgan from 1700 to 1970’, Glamorgan County History Trust Limited and University of Wales Press.

Whipple, S. (1899) ‘An elementary and practical treatise on bridge building: an enlarged and improved edition of the author’s original work’, Van Nostrand, New York.

Wood, D.V. (1895), ‘The strength of iron as affected by tensile stress while hot’, Transactions of the American Society of Mechanical Engineers, Vol. XVI, pg 739-741.

Worsley, J., Lee, L., Lee, H., Nicoletti, J.P. (1988), ‘Structural upgrading: Managing construction on the California Capitol’, APT Bulletin, Vol.20, No.1, pp.17-26. Association for Preservation Technology.

The Builder (1848), ‘The new palm house, Kew Gardens’, The Builder, Vol. VI. Jan. 15th, 1848, pp.29-31.

The Builder (1863), ‘Details of the Suspension Bridge, Clifton', The Builder,. Aug 8th, 1863,

The Engineer (1877). ‘The strength of riveted joints’. The Engineer. Vol. 43, Feb 23rd 1877, pp.125.

The Engineer. (1890), ‘Testing machine in Professor Kennedy’s laboratory’, The Engineer, July 18th 1890, pp.54.

The Engineer. (1888), ‘The Watertown Arsenal Testing Machine’, The Engineer, Jan 20th 1888, pp.54-55.

The Engineer. (1890), ‘Hot piling puddle bars’, The Engineer, November 21st 1890, pp.422.

The Engineer. (1890), ‘Hot charging trolley for rolling mills’, The Engineer, October 10th 1890, pp.299.

The Engineer. (1884), ‘Testing laboratory, Coopers Hill Engineering College’, The Engineer, July 25th, 1884, pp.70.

The Engineer. (1888), ‘Railway bridge near Cordova, Alabama’, The Engineer, August 3rd 1888, pp.92.

The Engineer. (1890), ‘The development of the American rail and track’, The Engineer, October 17th 1890, pp.319-322.

Engineering, (1871), ‘Wohler’s experiments on the fatigue of metals’, Engineering, April 7th 1871, 243-244.

Engineering, (1871), ‘The steel Committee, (letter by Kirkaldy), Feb. 24th 1871, pp.146 - 148

The Engineer. (1862), ‘American iron bridges’, The Engineer, January 3rd , pp.9-10.

The Engineer. (1863), ‘The elastic limit of iron’, The Engineer, March 6th 1863, pp.139-140.

The Engineer (1868), 'Bridge over the Spree, Berlin and Gorlitz Railway', The Engineer, September 18th 1868, pp.218 & 222.

The Engineer (1867), 'Midland Railway Extension - St Pancras Terminus Hotel', The Engineer, June 14th, 1867, pp.540.

The Engineer (1877),’Irwell Street Bridge, Manchester’ April 6th, pages 232-236.

Manchester Corporation. (1907),’Bridges over the River Irwell, Book 1 of 2’, (Manchester Corporation old bridge record ledger).

Manchester City Council. (1994), ‘Irwell Street Bridge Assessment’

The Scotsman, (1858), ‘Designs for the New Post Office of Edinburgh’, The Scotsman, Wednesday, May 12th.

The Scotsman, (1865), ‘The New General Post Office’, The Scotsman, Monday, Dec. 18th.

Internet references and sources

RCAHMS website: www.rcahms.gov.uk

Figure 1.1 www.tate.org.uk

Figure 1.24
http://www.bbc.co.uk/tyne/content/image_galleries/union_chain_bridge_gallery.shtml?10

Figure 7.1 (http://devonvisitor.blogspot.com/2011/02/clifton-suspension-bridge.html)

Figure 7.3 http://commons.wikimedia.org/wiki/File:On_the_Clifton_Suspension_Bridge_-_DSC05756.JPG

Figure 7.6 http://bristol.cityseekr.com/clifton-suspension-bridge-interpretation-center/tourist-attractions-sightseeing/venue/15849